DEVELOPMENT OF ULTRAHIGH PERFORMANCE CHIRAL PHASES

FOR SEPARATIONS APPROACHING THE SPEED OF SENSORS

by

DARSHAN C. PATEL

Presented to the Faculty of the Graduate School of

The University of Texas at Arlington in Partial Fulfillment

of the Requirements

for the Degree of

DOCTOR OF PHILOSOPHY

THE UNIVERSITY OF TEXAS AT ARLINGTON

August 2017

"There is no such thing as a self-made man. We are made up of thousands of others. Everyone who has ever done a kind deed for us, or spoken one word of encouragement to us, has entered into the make-up of our character and of our thoughts, as well as our success" -George Matthew Adams

This dissertation is dedicated to my wife Megha.

Acknowledgements

It has been a great honor and a privilege to have worked for my mentor Professor Daniel W. Armstrong. Through his teachings on all aspects of analytical chemistry, he taught me to become a better problem solver and a better scientist. Under his tutelage, I had the opportunity to learn on subjects ranging from fundamentals of separation science to fundamentals of wine tasting and even the proper form on weight lifting. He is ever inspiring and always there to commend me on positive research outcomes while motivating me on discouraging ones. He taught me to constantly strive to improve my understanding of topics and aim for more than what appears possible and I cannot thank him enough. I want to thank Dr. Saiful Chowdhury, Dr. Kevin Schug, Dr. Krishnan Rajeshwar, and Dr. Peter Kroll for taking their valuable time to be part of my graduate committee.

I am thankful to Dr. Jimmy Rogers for being an amazing undergraduate advisor and encouraging me to pursue undergraduate research which led me to this path. I would like to express my deepest gratitude for Dr. Zachary Breitbach, Dr. M. Farooq Wahab, and Dr. Ross M. Woods for being outstanding mentors and colleagues. They showed great interest in tutoring me and satisfied my innate curiosity as a budding analytical chemist. Working alongside them and learning new things was the most joyful part of my graduate research. I want to thank the entire Armstrong research group as well as many peers throughout the department for their support and inspiration. I dearly thank Mrs. Barbara Smith for all her help.

I am eternally thankful to my dear family and friends who have always been at my side through this journey. This endeavor was only made possible with their constant support and motivation. I especially thank my mother who has selflessly and tirelessly worked to provide me with a better future. I am forever indebted to my grandparents for

iv

instilling in me the value of hard work and resilience in life. Lastly, I want to thank my dear wife Megha who has constantly supported me and motivated me to keep going. She has been very patient through my long work hours and has been the constant source of optimism and happiness in my life.

July 31, 2017

Abstract

DEVELOPMENT OF ULTRAHIGH PERFORMANCE CHIRAL PHASES

FOR SEPARATIONS APPROACHING THE SPEED OF SENSORS

Darshan C. Patel, PhD

The University of Texas at Arlington, 2017

Supervising Professor: Daniel W. Armstrong

Chromatography using chiral stationary phases is the most effective and popular technique for qualitative and quantitative analysis of enantiomers in the pharmaceutical, agricultural, and food industry, among many others. Given the prevalence of chirality in nature, creation of new technologies for improving the speed and performance of chiral separations can provide immediate and significant benefits. This dissertation focuses on development of ultrahigh performance chiral phases which can provide separations at speeds that approach the speed of typical sensors and thereby enable chromatography as a real-time analysis tool. A variety of chiral selectors namely macrocyclic glycopeptides (teicoplanin, teicoplanin aglycone, vancomycin), cyclic oligosaccharides (derivatized cyclofructans, derivatized cyclodextrins), and cinchona anion exchangers (derivatized quinine) are utilized for their high-selectivity and versatility in operating under different chromatographic modes. Effects of bonding chemistry on selector performance is also studied.

Superficially porous particles were chosen as stationary phase supports to exploit their high-efficiency, modest backpressure, and reduced retention in high-throughput separations. Once synthesized, stationary phase packing must be optimized

to obtain high-efficiency columns. Fundamental studies on high-pressure slurry packing revealed the effects of non-Newtonian fluids and their impact on packed bed homogeneities. Several metrics were developed to qualitatively analyze the behavior of suspensions and successfully predict the type of bed that is likely to be formed. Effective and general slurry optimization techniques were developed to obtain high efficiencies and symmetric peak shapes. A novel peak shape analysis was also developed to identify and quantify concurrent fronting and tailing of peaks in order to optimize packing methods for modern high-efficiency stationary phase supports.

Also studied were instrumental optimizations such as extra-column band broadening, detector artifacts and peak shape distortions, and frictional heat when operating at high flow rates. With high-efficiency and high-selectivity stationary phases and an optimized instrument, a plethora of sub-minute and sub-second separations were developed for chiral and achiral analytes. Further, application of resolution enhancement techniques such as segmented peak sharpening based on derivatives and extra-column band broadening correction through Fourier transform is demonstrated. For showcasing the ultimate capability of ultrahigh performance chiral phases, a sub-second separation of 10 peaks also is shown.

Table of Contents

List of Illustrations

List of Tables

Chapter 1

Introduction

1.1 Prevalence of Chirality in Nature

Chirality is deeply embedded in all biological systems and chiral analysis is prevalent in fields of pharmaceutical, agricultural, food, environmental, and forensic science among others. Chiral auxiliaries and catalysts play important role in asymmetric synthesis.[1] Chiral separations can help determine enantiopurity, such as existence and levels of non-prevalent D-amino acids in living systems, which could be important to biological processes.[2] For drug molecules that possess stereocenters, each enantiomer can exhibit a different efficacy, toxicity, and pharmacokinetic profile and therefore must be evaluated individually as well as in their racemic form before being administered.[3,4] Separation and characterization of chiral compounds is critical to the drug development process since more than 80% of the new drugs introduced this century contain at least one stereocenter. Further, for more than 70% of those drugs, a single enantiomer is the active pharmaceutical ingredient (API).[3,4] Presence of a non-active enantiomer in the drug may enhance, suppress, or have no effect on the efficacy and toxicity of the active pharmaceutical ingredient (API).[4,5] High performance liquid chromatography (HPLC) or supercritical fluid chromatography (SFC) coupled with a chiral stationary phase (CSP) is a highly selective and effective method of chiral analysis and, accordingly, the most widely used technique.[4] Development of ultrahigh performance chiral phases that can provide cost-effective and rapid separations can help in all areas of chiral analysis.

Chromatographic separations are primarily governed by the selectivity, retention factors, and efficiency.[6] Resolution of species relates to these three important parameters as described in Equation 1-1, derived based on work of J. H. Purnell,[7]

1

$$R_S = \left(\frac{\sqrt{N_2}}{4}\right)\left(\frac{\alpha-1}{\alpha}\right)\left(\frac{k_2}{1+k_2}\right)$$

(1-1)

where R_S = resolution, N_2 = efficiency of the second peak, α = selectivity, and k_2 = retention factor of the second analyte. A graphical representation of this equation can be seen in Figure 1-1. The operating region required for each parameter for ultrafast (< 60 s) separations are highlighted.[8] Each contributing factor to the resolution is considered at length below.
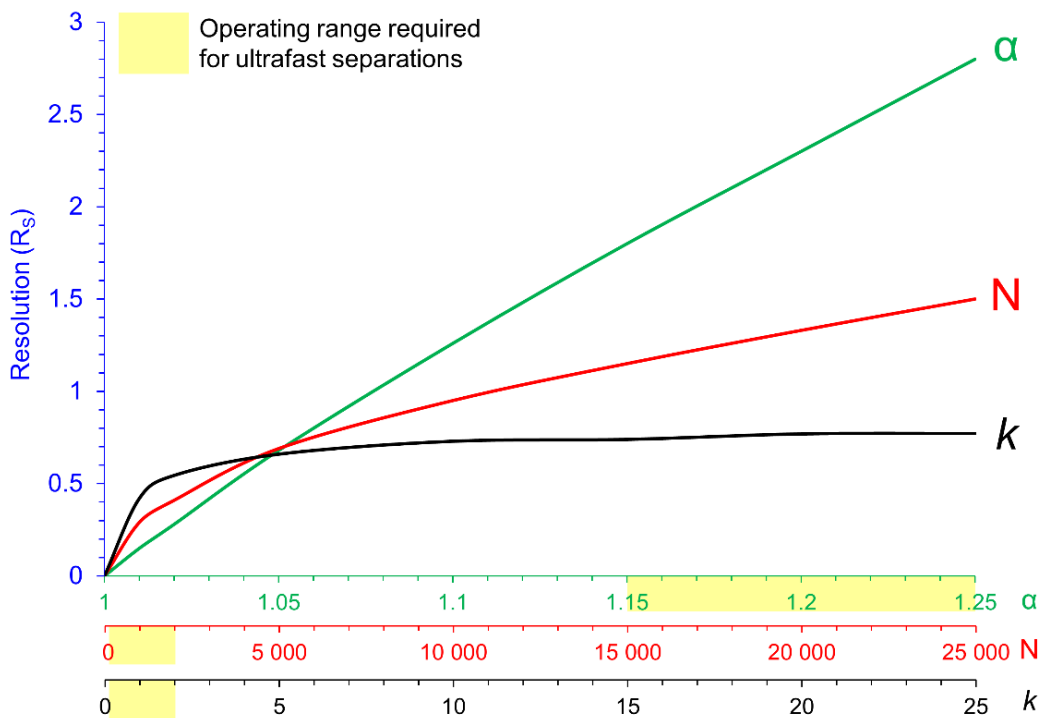
Figure 1-1. A graphical representation of the impact of selectivity (α), efficiency (N), and retention factor (k) on resolution. The operating range for parameters required for ultrafast separation has been highlighted in yellow. Data source: reference 8.

1.2 Selectivity (α)

Selectivity α is the ratio of retention factors of two analytes k_2/k_1. Figure 1-1 shows that a change in selectivity has the greatest impact on the resolution. Logically,

2

since its inception, the advances in the field of chiral separations have primarily focused on development of new or improved selectivity through design of novel chiral selectors.[9-20] Obtaining selectivity for chiral discrimination of enantiomers is particularly difficult due to multiple different interactions required.[21] These interactions can be ionic, π-π stacking, dipole-dipole, hydrogen bonding, electron donating/accepting, steric, and others.[21] A mature technique, chiral separations are still among the most challenging of all chromatographic separations as chiral interactions still cannot be completely predicted and require a trial-and-error approach.[22] The highlighted region for selectivity x-axis in Figure 1-1 indicates that selectivity value of 1.15 or greater are typically necessary for ultrafast separations. Based on this, high-selectivity chiral selectors namely derivatized cyclodextrins, derivatized cyclofructans, macrocyclic antibiotic, and cinchona based anion-exchangers, were utilized in Chapters 5-7 to obtain rapid chiral separations with analysis times ranging from 40 seconds to sub-second for a large number of analytes of varying polarities. The separations were obtained in normal phase mode (NPLC), reversed phase mode (RPLC), polar organic mode (POM), and polar ionic mode (PIM). Compatibility of polar organic and reversed phase mode with mass spectrometry (MS) makes these chiral selectors attractive for chiral LC-MS.

1.2.1 Recent Developments in the Selectivity of Chiral Phases

Chiral crown ethers were first utilized as chiral selectors by Cram and co-workers in the late 1970's.[23,24] In the early 1980's, Armstrong and coworkers introduced cyclic oligosaccharide cyclodextrins and functionalized cyclodextrins (Figure 1-2) which provided separations of a wide variety of analyte classes in different modes. Hydroxypropyl derivatized-β-cyclodextrin selector bonded to superficially porous particles (SPPs) was used in Chapter 6 of this dissertation for ultrafast chiral separations in RPLC

3

mode. Pirkle and co-workers demonstrated π-complex type *N*-derivatized amino acid based chiral stationary phases (Figure 1-3).[12,13,15,25] These stationary phases work primarily in normal phase mode as well as SFC. Being synthetic chiral molecules, π-complex chiral selectors can provide reverse elution orders by switching to the opposite enantiomer configuration of the selector.[25] Concurrently, protein based chiral selectors were reported followed by introduction of derivatized cellulose and amylose based coated or immobilized polysaccharide stationary phases.[20,26,27]
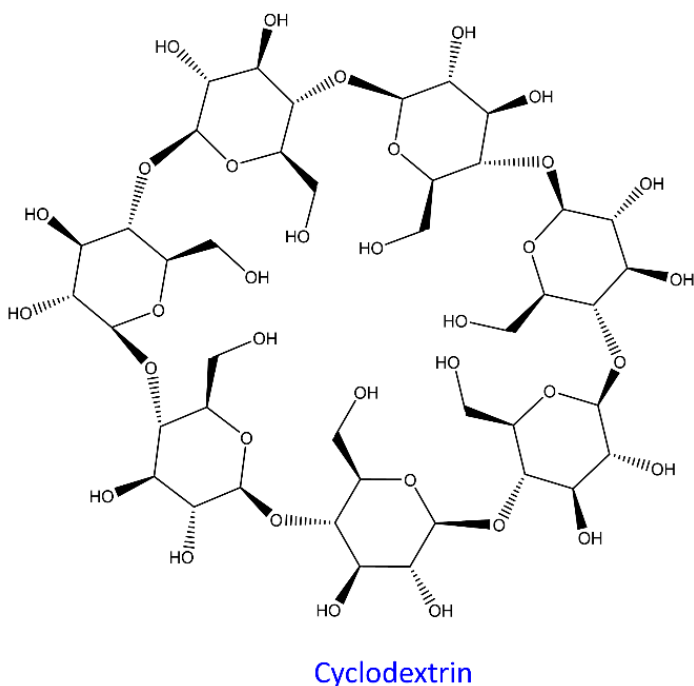
Cyclodextrin

Figure 1-2. Structure of cyclodextrin, a cyclic oligosaccharide used as a chiral selector in its native and functionalized form.

4
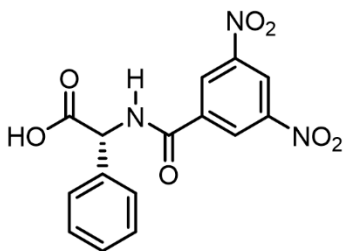
DNB-D-Phenylglycine

Figure 1-3. Structure of 3,5-dinitrobenzoyl-D-phenylglycine, a Pirkle-type π-complex chiral selector.

In the early 1990's, the strength of macrocyclic glycopeptides, namely teicoplanin, vancomycin, and teicoplanin aglycone, as chiral recognition media was demonstrated.[10,28] See Figure 1-4 for structure of these chiral selectors. They were shown to be particularly advantageous for separation of native and *N*-derivatized amino acids in addition to many other functional groups. Chapter 6 shows the performance of these chiral selectors when bonded to SPPs for ultrafast separations. Teicoplanin bonded to SPP was further utilized in Chapter 7 for sub-second separations.

(A)

Teicoplanin

(B)

Vancomycin

(C)

Teicoplanin aglycone

Figure 1-4. Structures of macrocyclic antibiotics (specifically, glycopeptides) used as chiral selectors. (A) Teicoplanin, (B) Vancomycin, (C) Teicoplanin aglycone.

6

In the mid-1990's, derivatized cinchona alkaloids were used as anion-exchangers for separation of chiral acids by Lindner and coworkers.[16,17] They showed enhanced selectivity in particular for *N*-blocked amino acids. Interestingly, quinine and quinidine selectors can also produce reversed elution order in many cases. The performance of derivatized quinine (Figure 1-5) bonded to SPPs, via two different chemistries, is discussed in Chapter 5 of this dissertation. Hydrosilated quinine is further used in Chapter 7 for sub-second separations, including a sub-second separation of two different chiral analytes in a single sample.
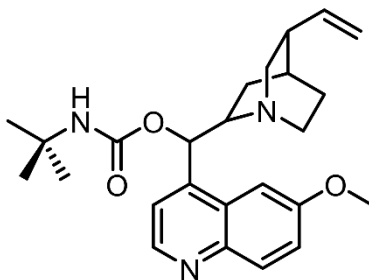
tert-butyl carbamoylated Quinine

Figure 1-5. Structure of *tert*-butyl carbamoylated quinine, an anion-exchanger.

A recent new class of chiral selectors in the form of cyclic oligosaccharide cyclofructan and its derivatives was introduced in 2009.[9,29,30] The cyclofructans are cyclic fructofuranose oligomers and have a unique crown ether core which forms complexes with a number of cations including ammonium (NH_4^+) and potassium (K^+). These selectors show particular affinity towards primary amines. Structures of cyclofructan 6 and cyclofructan 7 are shown in Figure 1-6. Chapter 2 of this dissertation shows performance of three derivatized cyclofructan stationary phases for the first reported chiral separations of 30 novel atropisomers (axially chiral), many of which are important in asymmetric synthesis as well as potential anti-bacterial agents.[31,32] These selectors

7

were bonded to SPPs and utilized for ultrafast separations in Chapter 6 of this dissertation.

(A)   (B)

Cyclofructan 6   Cyclofructan 7
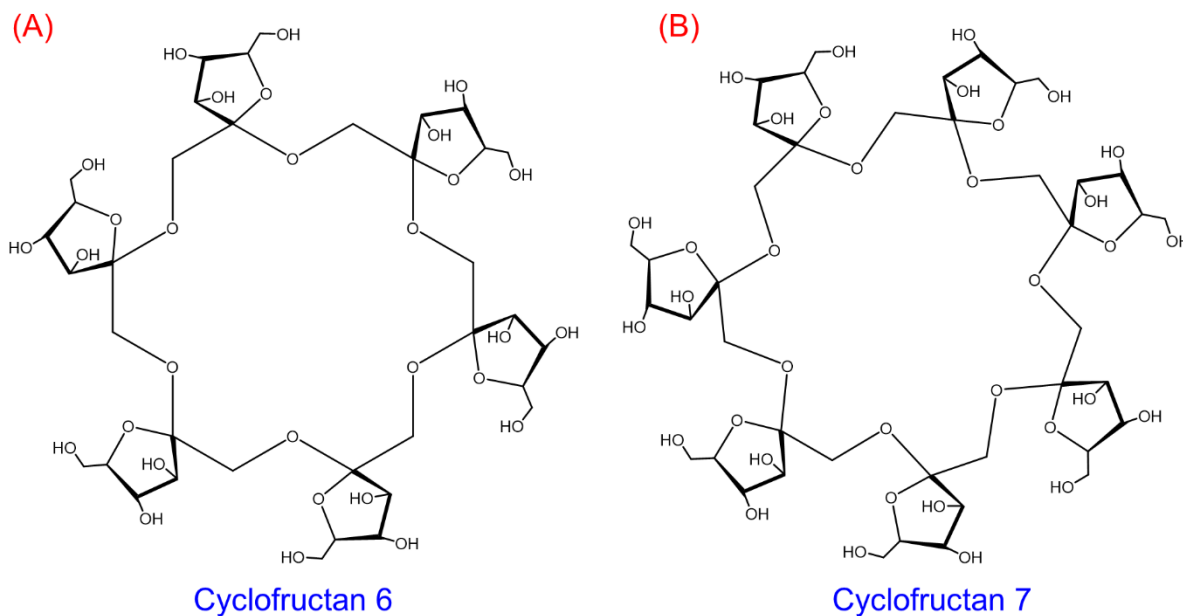
Figure 1-6. Structure of cyclic oligosaccharide chiral selectors (A) Cyclofructan 6 and (B) Cyclofructan 7.

1.3 Efficiency (N)

Since the dawn of chiral HPLC, a strong focus on devising new and improved selectors to enhance the principal separation factor, selectivity, led to neglect of improvements in areas such as efficiency and kinetic performance for HPLC columns. Few researchers focused on developing more efficient stationary phases while the field of column packing remained largely empirical in nature.[33-35] In an effort to improve efficiencies, the concept of superficially porous particles (SPPs) originated in 1967 with work of Horváth and Lin who coated thin polymer layer on glass beads.[34] In 1970s, J. J. Kirkland first developed the 50 μm diameter silica version of the SPP and 10 μm diameter

in 1990s.[36] However, these advances remained a niche academic interest and unfortunately did not garner widespread interest or adoption at the time.[36] Turn of the century saw advances in high-throughput chemistry, combinatorial synthesis, and automated laboratory instrumentation which enabled researchers to perform thousands of small-scale reactions routinely.[37-42] This created an incentive to develop high-throughput screening and separation methods and high-efficiency columns packed with sub-2 μm FPPs and new generation of 2.7 μm SPPs rose in popularity.[43,44] Higher efficiencies result in faster analysis, improved separation of species, better sensitivity, a more robust method, and easier quantitation of low-abundant species such as trace level impurities.

1.3.1 Superficially Porous Particles (SPPs)

Superficially porous particles (SPPs) have a solid, impermeable core surrounded by a porous layer. The new generation of 2.7 μm SPPs introduced in 2007 quickly gained widespread popularity due to their high-efficiency at modest backpressures compared to sub-2 μm FPPs which allowed their use on normal 400-600 bar pressure limit HPLCs.[43] The 2.7 μm SPPs provide efficiencies comparable to sub-2 μm FPPs on normal HPLC instrument which are ubiquitous in research laboratories and more cost-effective compared to UHPLCs. When packed well, SPP based stationary phases provide very high efficiencies (up to 250,000-350,000 N/m for 2.7 μm SPP based commercial C18 columns) at modest backpressure and perform better than their FPP counterpart of equivalent size.[45,46] SPPs bonded to conventional reversed phase non-polar C18 or C8 stationary phases can routinely yield reduced plate heights (h = H/dp, where H = height equivalent to theoretical plate, dp = particle size) in range of 1.4-1.7.[47,48] The high efficiency of SPPs comes from reduced contribution to band broadening, especially the

eddy dispersion (A term), along with minor improvements from longitudinal diffusion (B term) and resistance to mass transfer (C term) in van Deemter equation.[49] The obstruction factor of the packed bed determines the longitudinal diffusion of the analyte band.[50] The solid core of SPPs has a greater obstruction factor and, consequently, has a lower contribution to the band broadening.[50] The shorter diffusional path length of SPPs lead to lower trans-particle diffusion.[39,40] The shorter porous path length can also improve the mass transfer kinetics and reduce the contribution to the band broadening for large molecules with small diffusion coefficients as well as small molecules with slow adsorption-desorption kinetics.[49,51] This reduced contribution is very important for high-throughput separations which will utilize higher flow rates and likely operate in C-term dominant area of the van Deemter curve.[52] Note that the primary reason for efficiency improvement for SPPs is the reduced contributions from eddy dispersion term (A term), and contribution from potential improvements in B and C terms are secondary.[49]

Indeed, the SPP silica has reduced surface area compared to FPP silica. However, the selectivity of FPP can be obtained on SPP silica by maintaining a similar surface coverage of the selector on the surface of the silica, allowing roughly the same number of interactions per surface area to the analyte.[53,54] The reduced surface area of SPP also leads to reduced retention of analytes (up to 40% lower compared to FPP of equivalent size) which is beneficial for reducing analysis times. In retrospect, relatively modest backpressure, high-efficiency, and reduced retention of SPPs make them particularly attractive for creating ultrahigh performance phases for high-throughput separations.

1.3.2 High-Pressure Slurry Packing

Column packing is an essential step, perhaps the most difficult one, when creating new stationary phases. To effectively evaluate a new stationary phase, it must be properly packed to form a high-efficiency column which is a multidisciplinary science transcending fields of chemistry, fluid mechanics, rheology, and high-pressure engineering. Column packing has long been considered an art and there is a striking lack of published literature on this crucial topic.[55] Relatively few studies have paid attention to the phenomena behind the behavior of non-Newtonian suspensions under high-pressure and their effect on packed bed homogeneity.[56-58] Wahab et al. described an important and general phenomena for analytical columns in that dispersed slurries pack better than agglomerated slurries.[57] Jorgenson and coworkers have found the agglomerated slurries to work well for capillary columns packed with C18 particles.[56] Microscopy of a stationary phase suspension in a chosen slurry solvent can reveal the behavior of the slurry and its impact on column packing. Over the years, researchers have placed greater emphasis on reducing the particle size of the stationary phase over improving their packing methodologies to obtain higher efficiencies.[59] Reducing the particle size does not necessarily provide the theoretically expected improved efficiencies. As particle sizes get smaller, the columns become increasingly more difficult to pack. For example, an attempt of creating sub-1 μm FPP based cyclodextrin column resulted in 50,000-70,000 N/m,[60] which would have provided a column performance roughly equivalent to one packed with 5 μm particle along with drawbacks of high backpressures of sub-1 μm particles. Examples of poor efficiency columns packed with 1.5 μm diameter SPPs have also been reported.[61] A clear understanding of particle rheology, predicting the behavior of slurries under high-pressures, and a logical approach to method optimization is necessary to repeatedly obtain near intrinsic efficiencies of smaller particle sizes.

11

From Figure 1-1, it is clear that efficiency, N, has the second greatest impact on resolution, and Equation 1-1 shows that R$_S$ ∝ $\sqrt{N}$. For example, doubling the efficiency would only improve resolution by factor of 1.4. When considering the ultrafast separations, efficiency plays a critical role. The highlighted region in Figure 1-1 for N shows that short columns (0.5-3 cm length) used for ultrafast separations typically provide 250-2000 plates at high flow rates. It becomes increasingly difficult to obtain baseline resolutions for species when the efficiency of short columns is further affected by extra-column band broadening. As mobile phase elution strengths are adjusted to reduce the retention factor of analytes and, possibly, the selectivity, the efficiency must be sufficiently high to negate the negative impact of decreased α and k to maintain baseline resolution (Equation 1-1). Optimizing the packing of short columns, use of high-efficiency SPP or sub-2 µm FPP, optimizing the system for low extra-column volume, and using detector with high sampling frequencies and low response times are essential to obtaining baseline ultrafast separations. Chapter 4 of this dissertation will delve into the intricacies of new-Newtonian suspensions and their vital role in packed bed homogeneity in high-pressure slurry packing.

1.3.3 Recent Developments in the Efficiency of Chiral Phases

Chiral separations are thought to be inherently less efficient due to multiple simultaneous interactions required for enantiomeric discrimination and widespread use of 5-10 µm diameter FPP silica stationary phase that produce 40,000-50,000 N/m and 10-30 min analysis times. being standard. Researchers have started to exploit the higher efficiencies of sub-2 µm FPPs and 2.7 µm SPPs in chiral separations. In 2010. Gasparrini and coworkers demonstrated the first major successful example with π-complex type stationary phase diaminocyclohexane derivative followed by Whelk-O selector on sub-2

μm FPPs, showing a few examples of ultrafast chiral separations.[62,63] Lindner and coworkers first sought to take advantage of high-efficiency of 3 μm SPPs in a cinchona-type anion-exchanger quinidine stationary phase for chiral separation of derivatized amino acids.[64] Soon after, coated polysaccharide based SPP CSP and brush-type covalently bonded cyclic oligosaccharide SPP CSPs were reported.[53,65,66] From these reports, it is clear that high-efficiency sub-2 μm FPPs and SPPs can help bring chiral separations to the high-throughput regime and enable rapid screening and analysis of a plethora of compounds. Fast separations can be used as 2nd dimension of two-dimensional liquid chromatography (2DLC) as well for on-line liquid chromatography. The focus of this dissertation is to develop ultrahigh performance chiral phases with high-selectivity, high-efficiency, and high stability to perform sub-second separations which can approach the speed of common sensors.

1.4 Green Chiral Separations Using Supercritical Fluids

Supercritical fluid chromatography is analogous to normal phase LC as it uses a polar stationary phase with non-polar mobile phases, with an important exception of the mobile phase being a super/subcritical fluid, typically CO_2 with a modifier. Consequently, SFC is a "greener" alternative to HPLC and can significantly reduce the operating cost and toxic waste produced.[67] In recent years, SFC has gained popularity for chiral separations, especially for preparative applications in pharmaceutical industry.[22,68-71] SFC has several distinct advantages when it comes to chromatography. The lower mobile phase viscosity allows higher flow rates while faster diffusion of analytes into the mobile phase can reduce the resistance to mass transfer (C term in van Deemter equation), making it possible to obtain higher-efficiencies, reduced analysis times, and improved peak shapes.[22,70] Additionally, for preparative applications, SFC is particularly

advantageous because of reduced solvent consumption and necessity to only evaporate the modifier from collected fractions to obtain desired analytes.[68] SFC can also be used for fast method development of chiral analytes.[22] Quinine based SPP CSPs prepared in Chapter 5 are evaluated in SFC and their capability to produce ultrafast SFC separations is shown.

<div align="center">1.5 Hydrophilic Interaction Liquid Chromatography (HILIC)</div>

Hydrophilic Interaction Liquid Chromatography (HILIC) is an alternative to RPLC for separation of polar analytes that do not have sufficient retention in the RPLC mode. HILIC utilizes a polar stationary phase and an aqueous-organic mobile phase with particularly high organic content. The HILIC stationary phase can be bare silica or silica derivatized with a polar selector and typical mobile phases consisting of acetonitrile and 1-40% v/v of aqueous content. The primary mode of separation is partitioning of polar analytes between the organic rich mobile phase and the water-rich layer solvated on the stationary phase surface in addition to interactions such as hydrogen bonding, dipolar interactions, and electrostatic interactions. As a rule of thumb, analytes can be considered suitable for HILIC analysis if their Log P (lipophilicity or analyte partition coefficient between octanol-water) < 0 or they elute before caffeine in RPLC mode. HILIC is MS compatible and a popular technique in proteomics and metabolomics research. In later parts of this dissertation (Chapter 7), sub-second HILIC separations are presented for important classes of compounds such as nucleosides, plant hormones, and salicylic acid related analytes as well as a sub-second separation of 10 peaks to demonstrate the ultimate capability of ultrahigh performance phases developed in this work.

1.6 Research Objectives and Organization of the Dissertation

The primary motivation behind the research described in this dissertation is to elevate chiral separations to the high-efficiency regime and enable chromatographic separations that approach the speed of common sensors. Studies include synthesis of high-selectivity stationary phases, optimization of surface derivatization of high-efficiency SPPs, devising novel packing methods, and developing fast separations ranging from sub-minute to sub-second in analysis time. Chapter 2 compares the selectivity and performance of cyclofructan derivatives for chiral separations of 30 novel atropisomers. A new total peak shape analysis approach is demonstrated in Chapter 3 along with its application in column packing optimizations. The effectiveness of the new automated approach in detecting concurrent fronting and tailing on chromatography peaks is demonstrated. Chapter 4 is an account of fundamental studies on high-pressure slurry packing for modern high-efficiency columns using sub-2 µm FPPs and 2.7 µm SPPs. Generalized tests to predict packing behavior as well as practical examples are shown along with a flow chart for packing optimization.

Chapter 5 shows performance comparison of a quinine derivative anion-exchanger bonded to SPPs with its FPP silica based commercial counterpart using geometry-independent kinetic plots. Different bonding chemistries and their effects on selectivity and kinetic performance are studied while capability of SPP phases in ultrafast separation is evaluated. Chapter 6 focuses on fundamental studies on ultrafast (< 60 s) chiral separations where six chiral selectors were bonded to SPPs to produce more than 60 separations under 40 seconds. Also shown are the effects of extra-column band broadening, instrumental artifacts from detector parameters, and the effect of frictional heating on the kinetic performance of the columns. In Chapter 7, sub-second separations of achiral and chiral analytes using SPPs are shown including a separation of 10 analytes

within a second. Several example applications of sub-second separations of structurally and functionally related molecules are shown. The utility of high-throughput separations in real-time monitoring of reaction kinetics also is demonstrated. Finally, Chapter 8 presents a general summary of this dissertation.

Chapter 2

Enantiomeric Separation of Biaryl Atropisomers Using Cyclofructan Based Chiral

Stationary Phases

2.1 Abstract

Normal phase chiral HPLC methods are presented for the enantiomeric

separation of 30 biaryl atropisomers including 18 new compounds recently produced *via*

a novel synthetic approach. Three new cyclofructan based chiral stationary phases were

evaluated. Separations were achieved for all but six analytes and the LARIHC™ CF6-P

alone provided 15 baseline separations. Effects of polar modifiers and temperature

effects also were studied. Apparent thermodynamic parameters were determined by van't

Hoff plots. Preparative scale methods were developed and employed resulting in the first

ever isolation of these novel atropisomers in their pure enantiomeric form. Insights into

the mechanism of retention and chiral discrimination are presented.

2.2 Introduction

Substituted biaryls in which the rotation around the aryl–aryl single bond is

hindered are referred to as atropisomers. They represent a major class of axially chiral

molecules that have found use in many applications including privileged ligands in

asymmetric synthesis,[72-75] chiral resolving agents,[76] and as pharmaceutical

compounds.[77,78] Recently, a variety of novel 2,2′-diamino-1,1′-binaphthalenes[32] as well as

2,2′-aminohydroxy-1,1′-biaryls were synthesized using a transition metal free direct

arylation method.[31] These new compounds have the potential to be used as chiral ligands

in asymmetric synthesis and may possess unique biological activities including antitumor

and antimicrobial activities.[79] The chiral analytes considered herein are 1,1′-biaryls and

17

fall into one of three groups: 2,2′-diol, 2-amino-2′-ol and 2,2′-diamine. Probe analytes also differ in aryl type and type/position of substituents on the aryl groups.

Chiral molecules are often needed as pure enantiomers for evaluation in the aforementioned applications and thus the need for methods to determine the enantiomeric excess (%ee) of newly synthesized molecules is ever present.[80-84] There is also a need to develop preparative HPLC methods to purify milligram to gram scale amounts of enantiomerically pure compounds.[85,86] HPLC combined with chiral stationary phases (CSP's) has proven to be an excellent technique for the separation of axially chiral molecules.[14,87] A wide variety of CSP's have been used to separate biaryl atropisomers including bonded cyclodextrins,[88] 1,3,5-triazine based CSP's,[89] quaternized brucine-based CSP's,[90] derivatized cyclofructans[91,92] and immobilized polysaccharide-based CSP's.[93] Chiral HPLC is also useful for preparing single enantiomers as instrumental methods and HPLC column dimensions are easily scaled from analytical to semi-preparative and preparative capacities.[85]

A new class of CSP's based upon derivatized cyclofructans, which are cyclic oligosaccharides consisting of six or more β(2→1)-linked D-fructofuranose units has recently been introduced.[94] In this study, three functionalized cyclofructan CSPs were evaluated for use as HPLC CSPs. The first, the LARIHC CF6-P (isopropylcarbamate derivatized cyclofructan-6) has shown exceptional selectivity for racemates with a primary amine moiety[30] while the LARIHC CF6-RN (R-naphthylethylcarbamate derivatized cyclofructan-6) and LARIHC CF7-DMP (dimethyphenylcarbamate derivatized cyclofructan-7) CSPs have shown broad selectivity and applicability for a variety of classes of molecules.[95-99]

In this paper, 30 biaryl atropisomers were screened with three CSPs under normal phase and polar organic HPLC conditions to elucidate potential interactions

18

governing retention and enantioselectivity on cyclofructan based chiral selectors. The three commercially available binapthyl analytes, BINAM, BINOL and NOBIN as well as 1-(2-aminophenyl)naphthalen-2-amine were selected for further analysis to study the effect of the three different 2,2′-substituents and type of aryl groups on retention and enantioselectivity. For normal phase separations, the effects of both the type and composition of the polar modifier was investigated as well as the effect of column temperature on enantioselectivity. The effect of acidic and basic additives also was investigated. A preparative separation of 1-(2-amino-3,4,5-trichlorophenyl)naphthalen-2-ol is presented allowing the pure enantiomers of this novel molecule to be evaluated for antimicrobial/antibiotic activity (data not reported), showing the separations reported herein are both scalable and necessary for future applications involving these new biaryls. This is the first report on the enantiomeric separation of many of these important analytes which, in turn, provides insights into the mechanism of retention and chiral recognition for cyclofructan based CSPs.

2.3 Experimental

2.3.1 Materials

HPLC grade heptane, ethanol, acetonitrile and ACS grade hexanes (5% methylpentanes) were purchased from Fisher Scientific (Waltham, MA). HPLC grade 1-propanol, 2-propanol 1-butanol, ACS grade trifluoroacetic acid and triethylamine were purchased from Sigma–Aldrich (St. Louis, MO). 1,1′-binaphthyl-2,2′-diamine (BINAM, Table 2-1 no. 1), 1,1′-bi-2-naphthol (BINOL, no. 2), 2-amino-1,1′-binaphthalen-2′-ol (NOBIN, no. 3), 6,6′-dibromo-[1,1′-binaphthalene]-2,2′-diol (no. 23), 3,3′-bis(3,5-dimethylphenyl)-5,5′,6,6′,7,7′,8,8′-octahydro-[1,1′-binaphthalene]-2,2′-diol (no. 24), 3,3′-diphenyl-[2,2′-binaphthalene]-1,1′-diol (VANOL, no. 25), 3,3′-dibromo-5,5′,6,6′,7,7′,8,8′-

19

octahydro-[1,1′-binaphthalene]-2,2′-diol (no. 26), 3,3′-dibromo-[1,1′-binaphthalene]-2,2′-diol (no. 27), 3,3′-bis(triphenylsilyl)-[1,1′-binaphthalene]-2,2′-diol (no. 28), 3,3′-di(anthracen-9-yl)-[1,1′-binaphthalene]-2,2′-diol (no. 29), and 2,2′-dimethoxy-1,1′-binaphthalene (no. 30) were purchased from Sigma–Aldrich (St. Louis, MO). LARIHC CF6-P, CF6-RN and CF7-DMP were obtained from AZYP L.L.C. (Arlington, TX). Analytes 4-22 (Table 2-1) were synthesized as reported.[31]

2.3.2 HPLC Methods

All analyses were performed on an Agilent 1260 Infinity HPLC system utilizing a degasser, quaternary pump, autosampler, column thermostat and diode array detector. Data analysis was carried out using OpenLAB CDS ChemStation Edition Rev. C.01.04. Samples were prepared at approximately 0.5 mg/mL in ethanol. Analytical column dimensions were 250 mm × 4.6 mm with 5 μm particle diameter. All injections were 5 μL unless otherwise noted. Flow rates were held at 1 mL/min unless otherwise noted. Wavelengths monitored were 254 nm and 280 nm. Separations were performed at ambient temperature unless otherwise noted. Normal phase mobile phases consisted of heptane with a polar modifier. Ethanol, 1-propanol, 2-propanol and 1-butanol were evaluated as polar modifiers in the range of 1–50% (v/v). Polar organic mobile phases consisted of acetonitrile with 0–10% w/v methanol as a modifier. Void volumes were determined by the first disturbance in the baseline resulting from unretained diluent. Resolutions (Rs) and peak symmetries (PS) were calculated using ChemStation software.

Thermodynamic experiments were carried out at 25 °C, 29 °C, 33 °C, 37 °C and 41 °C to determine the enthalpic and entropic contributions using the equation: $\ln k = -(\Delta H°/RT) + (\Delta S°/R) + \ln \phi$ where $\Delta H°$ and $\Delta S°$ represent the change in standard

molar enthalpy and entropy, respectively, R is the universal gas constant and T is the absolute temperature (K) of the column, ϕ is the ratio of stationary phase and mobile phase volumes, V_s and V_m, respectively. $\Delta S°^*$ is used in place of ($\Delta S°/R$) + ln ϕ as the chromatographic phase ratio is not easily determined. All thermodynamic values are stated as apparent rather than absolute due to the inability to distinguish between enantioselective and non-enantioselective interactions. Thermodynamic values were calculated using Microsoft Excel.

Preparative scale analyses were conducted on a Shimadzu preparative LC system consisting of an LC-20AP pump, SPD-20AV detector, SIL-10AP autosampler and FRC-10A fraction collector. Data analysis was conducted using LabSolutions Ver. 5.54 SP1. The LARIHC CF6-P preparative column dimensions were 250 mm × 21.2 mm with 5 µm particle diameter (AZYP, LLC). Sample 19 (Table 2-1) was dissolved in 50:50 hexanes: ethanol at 60 mg/mL. The mobile phase consisted of 98:2 hexanes: ethanol with a flow rate of 30 mL/min. Stacked injections of 200 µL (12 mg) were performed at 15 min intervals. The wavelength used was 254 nm. Fractions containing each enantiomer were pooled and solvent removed under reduced pressure. For determining enantiomeric excess of the collected fractions, detector linearity was confirmed at 0.4– 20 µg (on column, R^2 = 0.998, n = 5). Samples were prepared at 1 mg/mL. S/N for the minor enantiomer peak was >100 with the major enantiomer peak < 0.5 A.U.
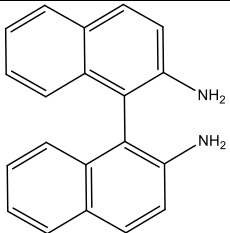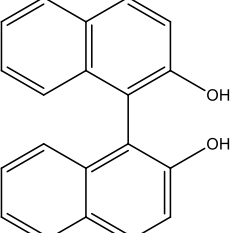
2.4 Results and Discussion
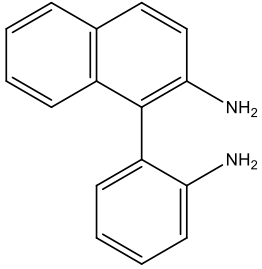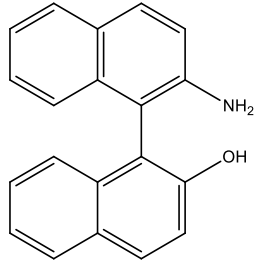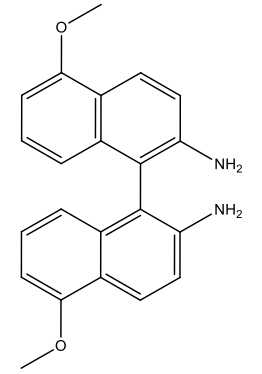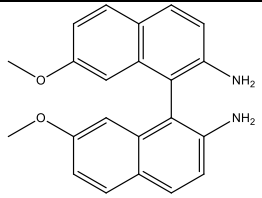
2.4.1 Separations Obtained and Insights to Retention and Chiral Recognition
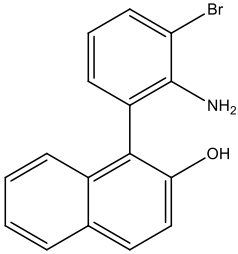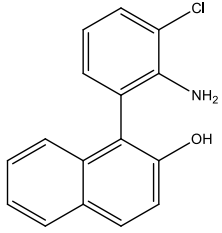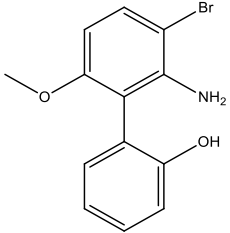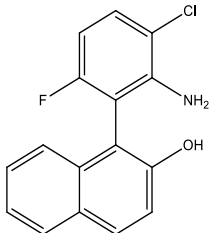
Table 2-1 shows the analyte structures, optimized separation conditions and chromatographic data for 30 biaryl atropisomers. Under normal phase conditions, the LARIHC CF6-P stationary phase showed enantioselectivity toward 22 out of the 30

21
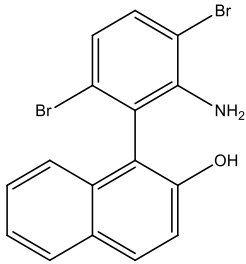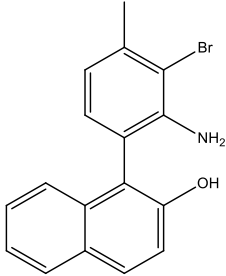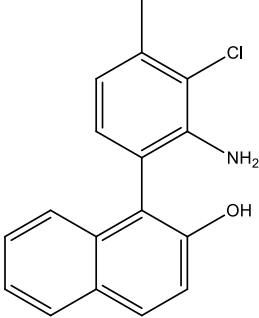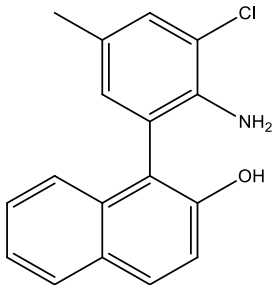
analytes with 15 baseline separations ($R_s \geq 1.5$). The CF6-RN and CF7-DMP showed

enantioselectivity for 15 analytes each with 8 and 10 baseline separations, respectively.

The CF6-RN column best complemented the CF6-P column in that it was able to provide

two unique separations (Table 2-1), compounds 9, 24) which were not obtained on the

CF6-P column. Further, the CF6-RN provided one additional baseline separation (Table

2-1, compound 26) which was only partially separated by the CF6-P. Though the CF7-

DMP phase did not provide any unique separations, it did on occasion yield excellent

resolutions such as a R_s value of 7.6 (Table 2-1, compound 6). In all, enantioselectivity

was observed for 24 of 30 analytes with 17 baseline separations using a heptane mobile

phase with ethanol as a polar modifier. Clearly, the CF6-P is the most useful CSP studied

in the separation of this set of atropisomers.
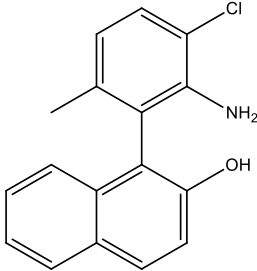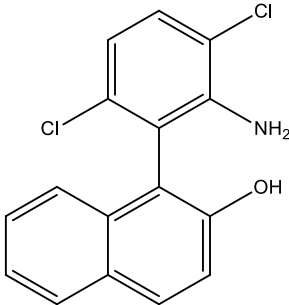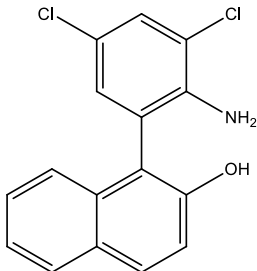
Table 2-1. Structures and Chromatographic Data for Enantiomeric Separations.
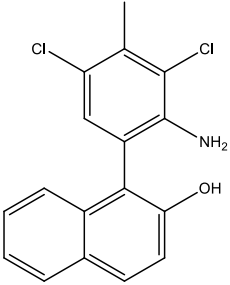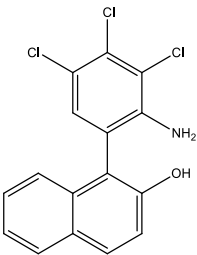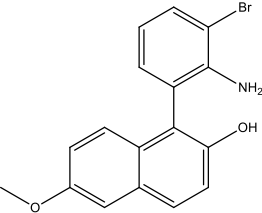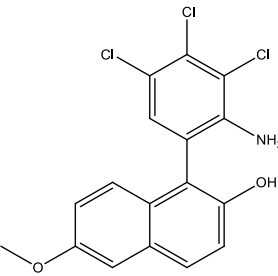
Analyte #	Structure	Column	Hept: EtOH	α	R_S	$k`_1$	$k`_2$
1	[1,1'-binaphthalene]-2,2'-diamine	CF6-P	90:10	1.26	4.8	4.1	5.2
		CF6-RN	90:10	1.21	4.6	5.0	6.1
		CF7-DMP	70:30	1.35	6.8	3.1	4.2
2	[1,1'-binaphthalene]-2,2'-diol	CF6-P	90:10	1.10	2.6	2.8	3.1
		CF6-RN	95:5	1.06	1.0	5.5	5.9
		CF7-DMP	95:5	1.09	1.5	5.2	5.7
3		CF6-P	90:10	1.10	2.7	3.0	3.4
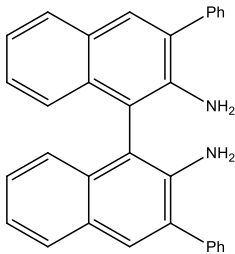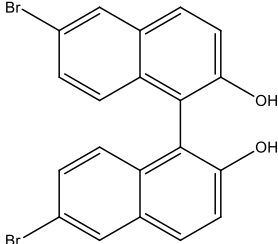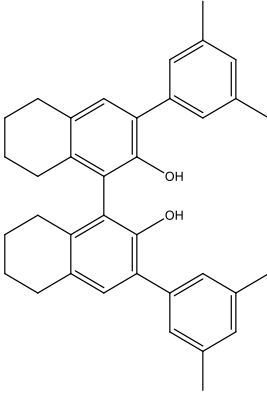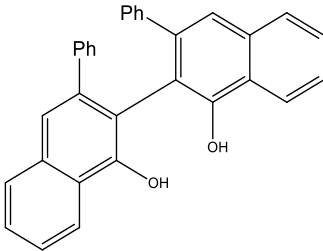
Analyte #	Structure	Column	Hept: EtOH	α	R_S	$k\dot{}_1$	$k\dot{}_2$
	1-(2-aminophenyl)naphthalen-2-amine	CF6-RN	95:5	1.14	1.6	5.5	6.3
		CF7-DMP	90:10	1.27	5.5	5.8	7.4
4	2'-amino-[1,1'-binaphthalen]-2-ol	CF6-P	90:10	1.16	2.9	3.5	4.1
		CF6-RN	90:10	1.10	2.6	4.0	4.5
		CF7-DMP	95:5	1.2	5.3	4.5	5.5
5	5,5'-dimethoxy-[1,1'-binaphthalene]-2,2'-diamine	CF6-P	90:10	1.15	3	5.1	5.9
		CF6-RN	90:10	1.1	2.7	7	7.8
		CF7-DMP	50:50	1.27	3.2	2.6	3.3
6	7,7'-dimethoxy-[1,1'-binaphthalene]-2,2'-diamine	CF6-P	95:05	1.1	1.7	8	9
		CF6-RN	95:05	1.1	1.9	8.6	9.4
		CF7-DMP	70:30	1.5	7.6	5	7.5
7		CF6-P	90:10	1.06	1.0	1.5	1.7

23
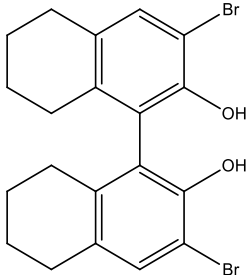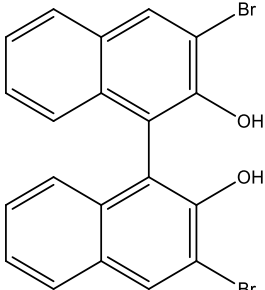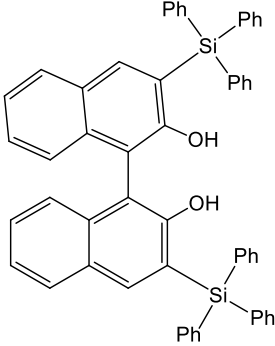
Analyte #	Structure	Column	Hept: EtOH	α	R_S	$k`_1$	$k`_2$
	1-(2-amino-3-bromophenyl)naphthalen-2-ol	CF6-RN	90:10			1.7	
		CF7-DMP	99:1			3.7	
8	1-(2-amino-3-chlorophenyl)naphthalen-2-ol	CF6-P	90:10	1.06	1	1.55	1.67
		CF6-RN	90:10			1.8	
		CF7-DMP	99:1			3.7	
9	2'-amino-3'-bromo-6'-methoxy-[1,1'-biphenyl]-2-ol	CF6-P	90:10			5.1	
		CF6-RN	99:1	1.07	1.9	8.3	8.9
		CF7-DMP	99:1			5.6	
10	1-(2-amino-3-chloro-6-fluorophenyl)naphthalen-2-ol	CF6-P	99:1	1.03	1.1	17	17.6
		CF6-RN	90:10			2.7	
		CF7-DMP	95:05	1.04	1.0	7.4	7.7
11		CF6-P	90:10	1.13	2.3	2.1	2.4

24
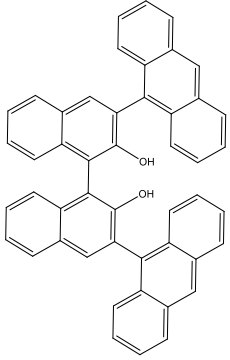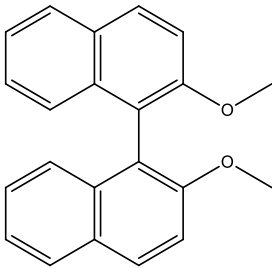
Analyte #	Structure	Column	Hept: EtOH	α	R_S	k`1	k`2
	1-(2-amino-3,6-dibromophenyl)naphthalen-2-ol	CF6-RN	99:01			13.6	
		CF7-DMP	99:01	1.04	1.5	7.4	7.8
12	1-(2-amino-3-bromo-4-methylphenyl)naphthalen-2-ol	CF6-P	99:1			4.8	
		CF6-RN	90:10			1.5	
		CF7-DMP	99:1			3	
13	1-(2-amino-3-chloro-4-methylphenyl)naphthalen-2-ol	CF6-P	90:10	1.03	0.4	3.5	3.6
		CF6-RN	90:10			1.5	
		CF7-DMP	99:1			3	
14	1-(2-amino-3-chloro-5-methylphenyl)naphthalen-2-ol	CF6-P	90:10			1.2	
		CF6-RN	90:10			1.5	
		CF7-DMP	75:25			1.9	

25

Analyte #	Structure	Column	Hept: EtOH	α	R_S	$k`_1$	$k`_2$
15	1-(2-amino-3-chloro-6-methylphenyl)naphthalen-2-ol	CF6-P	99:1	1.01	0.3	5.32	5.39
		CF6-RN	90:10			1.5	
		CF7-DMP	99:1			3.1	
16	1-(2-amino-3,6-dichlorophenyl)naphthalen-2-ol	CF6-P	95:5	1.10	2.1	4.5	4.9
		CF6-RN	90:10			2.5	
		CF7-DMP	99:1	1.04	1.2	7.1	7.4
17	1-(2-amino-3,5-dichlorophenyl)naphthalen-2-ol	CF6-P	95:5	1.1	2.3	3.7	4.1
		CF6-RN	90:10			2.1	
		CF7-DMP	99:1	1.03	1.1	6.5	6.8
18		CF6-P	95:5	1.09	2	3	3.3
		CF6-RN	90:10			1.8	

Analyte #	Structure	Column	Hept: EtOH	α	R_S	$k`_1$	$k`_2$
	1-(2-amino-3,5-dichloro-4-methylphenyl)naphthalen-2-ol	CF7-DMP	1.05	1.6	5.4	5.7	1.05
19	1-(2-amino-3,4,5-trichlorophenyl)naphthalen-2-ol	CF6-P	1.15	3.6	4.8	5.6	1.15
		CF6-RN	1.02	0.5	5.8	5.9	1.02
		CF7-DMP	1.09	2.5	9.1	9.9	1.09
20	1-(2-amino-3-bromophenyl)-6-methoxynaphthalen-2-ol	CF6-P	90:10			5.4	
		CF6-RN	90:10			2.4	
		CF7-DMP	99:1			10	
21	1-(2-amino-3,4,5-trichlorophenyl)-6-methoxynaphthalen-2-ol	CF6-P	90:10	1.3	5.8	2.9	3.9
		CF6-RN	90:10	1.06	2.2	7.9	8.4
		CF7-DMP	95:5	1.2	3.6	4.4	5

27

Analyte #	Structure	Column	Hept: EtOH	α	Rs	k`1	k`2
22	 3,3'-diphenyl-[1,1'-binaphthalene]-2,2'-diamine	CF6-P	99:1	1.13	1.5	1.1	1.2
		CF6-RN	95:5			0.8	
		CF7-DMP	95:5			0.5	
23	 6,6'-dibromo-[1,1'-binaphthalene]-2,2'-diol	CF6-P	95:5	1.15	2.7	7.3	8.4
		CF6-RN	95:5	1.12	2.2	8.3	9.3
		CF7-DMP	95:5	1.07	1.5	5.8	6.2
24	 3,3'-bis(3,5-dimethylphenyl)-5,5',6,6',7,7',8,8'-octahydro-[1,1'-binaphthalene]-2,2'-diol	CF6-P	95:5			0.1	
		CF6-RN	99:1	1.07	0.6	0.8	0.9
		CF7-DMP	95:5			0.18	
25	 3,3'-diphenyl-[2,2'-binaphthalene]-1,1'-diol	CF6-P	95:5	1.18	2.1	1.7	2
		CF6-RN	99:1	1.09	1.3	5.6	6.1
		CF7-DMP	95:5	1.17	2	1.2	1.4

Analyte #	Structure	Column	Hept: EtOH	α	R$_S$	k`$_1$	k`$_2$
26	3,3'-dibromo-5,5',6,6',7,7',8,8'-octahydro-[1,1'-binaphthalene]-2,2'-diol	CF6-P	95:5	1.07	0.8	1.4	1.5
		CF6-RN	99:1	1.19	1.7	4.7	5.6
		CF7-DMP	95:5			1.14	
27	3,3'-dibromo-[1,1'-binaphthalene]-2,2'-diol	CF6-P	95:5	1.05	0.9	4.4	4.6
		CF6-RN	95:5	1.06	0.9	4.9	5.2
		CF7-DMP	95:5	1.03	0.9	2.9	3.0
28	3,3'-bis(triphenylsilyl)-[1,1'-binaphthalene]-2,2'-diol	CF6-P	95:5			0.1	
		CF6-RN	95:5			0.95	
		CF7-DMP	95:5			0.42	
29		CF6-P	95:5			2.3	
		CF6-RN	99:1			0.34	

29

Analyte #	Structure	Column	Hept: EtOH	α	R$_S$	k`$_1$	k`$_2$
	3,3'-di(anthracen-9-yl)-[1,1'-binaphthalene]-2,2'-diol	CF7-DMP	95:5			2.0	
30	2,2'-dimethoxy-1,1'-binaphthalene	CF6-P	95:5			0.57	
		CF6-RN	99:1			1.5	
		CF7-DMP	95:5			0.8	

The common normal phase additives triethylamine (TEA) and trifluoroacetic acid (TFA) were evaluated at various concentrations. Peak symmetry was improved by using TEA but retention and selectivity were decreased. No significant increase in resolution was observed when TEA concentrations ranged from 0.05% to 0.2%. A large decrease in retention was observed when using 0.2% TEA. Using TFA in the mobile phase caused a decrease in retention and no significant improvement in resolution.

Both retention and selectivity varied considerably for different analyte and CSP combinations. The lack of aromatic functionality on the CF6-P column indicates that π–π interactions play no role in either retention or enantioselectivity when using this CSP. The potential exists for π–π interactions when using the aromatic functionalized CF6-RN and

CF7-DMP CSP's. However, no pronounced trend showing increased retention was observed under similar mobile phase conditions for these CSP's *vs.* the CF6-P. Under polar organic conditions, no retention was observed for any analyte when using 100% acetonitrile indicating that retention due to hydrogen bonding between the analyte and CSP is not substantial in the presence of that solvent. The potential exists for hydrogen bonding to play a role in chiral recognition, but only under conditions that favor analyte retention, *i.e.* high heptane content in the mobile phase. Given the apparent lack of strong π–π and H-bonding interactions, the primary mechanism for analyte retention is proposed to be dipole–dipole interactions between the polar 2,2′ moieties of the biaryls and the polar groups present on the derivatized cyclofructans. Previous studies using linear free energy relationship (LFER) models have shown that dipolarity/polarizability plays an important role in both retention and chiral recognition when using derivatized cyclofructans under normal phase conditions.[97] This is further validated by the lack of retention observed for analytes with steric hindrance at the 2,2′ positions (Table 2-1, compound 28, 29, 30). This indicates that retention is highly dependent on the ability of the polar 2,2′ moieties to form a strong interaction with the CSP.

The retention and selectivities observed for the various analytes varied considerably depending on both the type of aryl groups present as well as the type and location of substituents on the aryl rings. As can be seen in Table 2-2, when using the CF6-P CSP with 10% ethanol in heptane, the binapthyl diamine BINAM retained longer and showed greater enantioselectivity ($k_1 = 3.4$, $\alpha = 1.22$) than the 2,2′-diol BINOL ($k_1 = 2.6$, $\alpha = 1.12$), with the 2-amino-2′-ol (NOBIN) showing intermediate retention and selectivity ($k_1 = 2.7$, $\alpha = 1.14$). This indicates that the amine group plays an integral role in both retention and enantioselectivity on this CSP. When comparing BINAM ($k_1 = 3.4$, $\alpha = 1.22$) to 1-(2-aminophenyl)naphthalen-2-amine ($k_1 = 3.0$, $\alpha = 1.12$), retention and

31

selectivity were also increased indicating that selectivity is greatly improved when both aryl groups are napthyl.

Table 2-2. Effect of polar modifier on retention and enantioseparation.

Modifier	ethanol				1-propanol				1-butanol			
Analyte no.	k_1	α	R_s	PS	k_1	α	R_s	PS	k_1	α	R_s	PS
1	3.4	1.22	4.1	0.82	4.5	1.27	4.2	0.66	5.7	1.27	3.4	0.59
2	2.6	1.12	2.2	0.85	2.8	1.14	2.1	0.77	3	1.12	1.6	0.72
3	2.7	1.14	2.6	0.93	3.2	1.21	3.2	0.66	3.9	1.28	3.5	0.6
4	3	1.12	2.6	0.76	4	1.17	2.5	0.58	5.4	1.17	1.7	0.54

Conditions: column, CF6-P; mobile phase, 90:10 heptane: modifier (v/v); detector, UV 254 nm; column temperature, 25 ◦C.

With respect to the types of substituents on the aryl groups, the general trend was that increasing the number of electron withdrawing substituents had the effect of increasing retention and selectivity. As can be seen in Figure 2-1, a pronounced increase in selectivity is observed (1.15 *vs.* 1.01) on the CF6-P stationary phase when comparing 1-(2-amino-3,4,5-trichlorophenyl)naphthalen-2′-ol (Table 2-1, compound 19) *vs.* 1-(2-amino-3-chlorophenyl)naphthalen-2′-ol (Table 2-1, compound 8) with the dichloro substituted analyte showing intermediate selectivity. Possible explanations for the enhanced chiral recognition include altering of the dihedral angle of the aryl–aryl bond as well as induced differences in the hybridization of the amine group. The majority of analytes that showed poor selectivity were either of the napthyl–phenyl type with only a single substituent present on the phenyl ring or had the 2,2′ moieties hindered by bulky substituents at the 3,3′ positions. Modeling studies to determine the effect of substituents on the dihedral angle and to elucidate the types of interactions between the derivatized cyclofructans and biaryl analytes is ongoing.
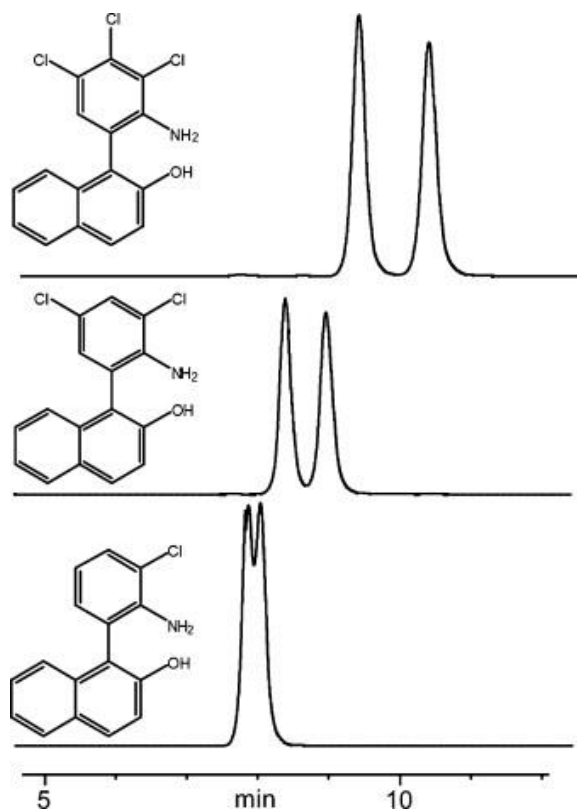
Figure 2-1. Effects of additional halogen substituents on retention and selectivity. Conditions: column CF6-P; mobile phase 95:5 (v/v) heptane:ethanol; detector, UV 254 nm.

2.4.2 Effect of Polar Modifier

By increasing the alkyl chain length of the polar modifier in the mobile phase, retention was increased. Minor improvements in selectivity were observed when going from ethanol to 1-propanol or 1-butanol (Table 2-2). However, both efficiencies and peak symmetries were diminished. Significant tailing was observed when using 1-butanol as a polar modifier and observable band-broadening occurred when switching away from ethanol in all cases. This provides further evidence for a dipolarity/polarizability mechanism of retention as using lower polarity solvents increased retention and slowed on/off kinetics between analyte and CSP. The effect of varying the composition of polar

33

modifier was an increase in retention and selectivity when the % ethanol was changed

from 16% to 4% (Table 2-3). Based upon the combined results, a mobile phase

composition of 10% ethanol in heptane is recommended for screening new biaryl

atropisomers in the normal phase mode.

Table 2-3. Effect of polar modifier composition on retention and enantioseparation.

% Ethanol	16%			13%			10%			7%			4%		
Probe	k_1	α	R_s	k_1	α	R_s	k_1	α	R_s	k_1	α	R_s	k_1	α	R_s
1	2.1	1.19	3.3	2.6	1.22	3.7	3.4	1.22	4.1	4.6	1.24	4.9	7.1	1.27	6.1
2	1.5	1.11	1.8	1.9	1.12	2	2.6	1.12	2.2	3.7	1.13	2.4	6.2	1.12	2.6
3	1.7	1.12	1.9	2.1	1.13	2.2	2.7	1.14	2.6	3.7	1.16	3.2	5.7	1.2	4.2
4	1.9	1.12	1.8	2.3	1.14	2.3	3	1.12	2.6	4	1.15	3	5.8	1.17	4

Conditions: column, CF6-P; mobile phase, heptane: ethanol (v/v); detector, UV 254 nm; column temperature, 25 ∘C.

2.4.3 Temperature Effect

Excellent linearity was observed for van't Hoff plots in the range of 25–41 °C

indicating that the CSP was not altered significantly in this temperature range. All $\Delta\Delta S°*$

values were negative suggesting enthalpy-driven enantioselectivity (Table 2-4). The

absolute $\Delta H_2°$ values were in the range of 14–19 kJ mol^{-1} indicating a strong interaction

with the CSP. The trend in absolute values for the $\Delta H_2°$ energies of the 1′,1-binapthyls

matches the trend in retention and selectivity observed for the three types of 2′,2

substituents, *i.e.* 2,2′-diamine > 2-amino-2′-ol > 2,2′-diol. This indicates that analyte

adsorption to the CSP is more exothermic for 2,2′-diamines and 2-amino-2′-ol analytes

than for 2,2′-diols. Absolute values for $\Delta\Delta H°*$ ranged from 1.5 to 2.5 kJ mol^{-1} *vs.* 14 to

19 kJ mol^{-1} for $\Delta H_2°$, indicating much of the analyte–CSP interaction is common to both

enantiomers. However, the differences in $\Delta\Delta H°*$ were of sufficient magnitude to provide

adequate selectivity at room temperature. No significant differences in thermodynamic

parameters were observed when switching from ethanol to 1-propanol or 1-butanol (data

34

not shown). Previous studies utilizing the immobilized polysaccharide CSP Chiralpak IA have reported thermodynamic parameters for BINOL using 90:10 hexane:propanol (v/v).[93] Under those conditions, BINOL showed entropy driven enantioselectivity *vs.* enthalpy driven for the CF6-P using 90:10 heptane: ethanol. Clearly the driving forces for enantiomeric separation on these two CSP's are different with respect to BINOL, with the CF6-P showing enthalpy driven enantioseparation and the Chiralpak IA showing entropy driven enantioseparation.

Table 2-4. Thermodynamic parameters for enantiomeric separations.

Probe	ΔH°_1 (kJ/mol)	$\Delta S^{\circ *}_1$ (J/mol*K)	R^2	ΔH°_2 (kJ/mol)	$\Delta S^{\circ *}_2$ (J/mol*K)	R^2	$\Delta\Delta H^{\circ}$ (kJ/mol)	$\Delta\Delta S^{\circ}$ (J/mol*K)
1	-16.1	-39.7	0.999	-18.6	-45.9	0.999	-2.5	-6.2
2	-12.1	-31.6	0.999	-14.6	-38.8	0.999	-2.4	-7.2
3	-17.4	-44.3	0.999	-18.8	-47.6	0.999	-1.4	-3.4
4	-15.2	-40.3	0.999	-16.9	-44.1	0.999	-1.7	-3.8

Conditions: column, CF6-P; mobile phase 90:10 heptane:ethanol (v/v); detector 254 nm.
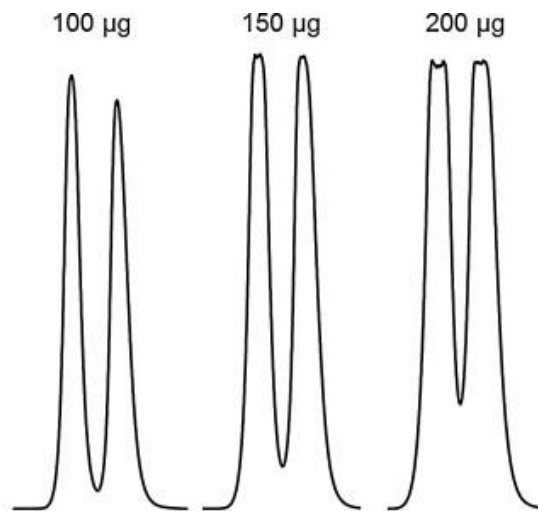
Figure 2-2. Analytical loading study of CF6-P. Conditions: probe no. 19 prepared in 1:1 heptane:ethanol at 10 mg/mL, injection volumes, 10,15,20 μL; mobile phase, 95:5 heptane:ethanol; flow rate, 2 mL/min; UV 254 nm.

Analyte no. 19 (1-(2-amino-3,4,5-trichlorophenyl)naphthalen-2-ol) was initially

selected for antimicrobial/antibiotic activity screening (data reported elsewhere) and was

needed in an enantiomerically pure form. A preliminary loading study was conducted on a

250 mm × 4.6 mm CF6-P column with a flow rate of 2 mL min^{-1} and a resolution of 1.4

was obtained when injecting 100 µg at a concentration of 10 mg mL^{-1} (Figure 2-2). By

switching from heptane to hexanes, significant cost savings were realized without a loss

of selectivity. Acceptable selectivity was observed at a flow rate of 30 mL min^{-1} using 2%

ethanol in hexanes. Injection volume was increased until baseline resolution was lost.

Acceptable resolution was observed on the preparative column when injecting 200 µL at

a concentration of 60 mg mL^{-1} (Figure 2-3). By stacking injections every 15 min, a total of

24 mg of each enantiomer was collected per hour at a cost of 1.8 L of hexanes. After

combining fractions and removing solvent, the %ee of each sample was determined to be

≥98%.
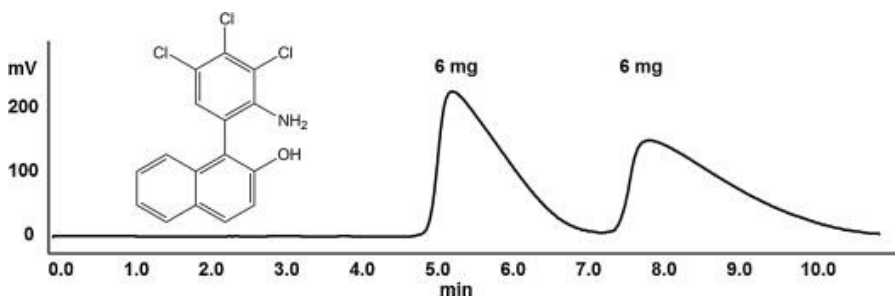
Figure 2-3. Preparative scale enantioseparation on CF6-P. Conditions: sample no. 19 prepared in 1:1 hexanes:ethanol at 60 mg/mL; column dimensions, 250 mm x 21.2 mm; mobile phase, 98:2 (v/v) hexanes:ethanol; flow rate, 30 mL/min; UV 254 nm; stacked injections of 200 µL every 15 min.

2.5 Conclusions

New chiral HPLC methods were presented for the enantiomeric separation of a

variety of biaryl atropisomers using heptane with ethanol as a polar modifier. The primary

36

mechanism of retention is likely dipolarity/polarizability interactions between the 2,2′

functionalities of the biaryls and polar groups present on the derivatized cyclofructans.

Selectivity was observed for 24 out of 30 probe analytes with 17 baseline separations

using three different CSP's. The CF6-P CSP was the most successful with 15 baseline

separations using simple mobile phases without the need for additives. When ethanol

was used as a polar modifier, high efficiencies and good peak symmetries were

observed. When propanol and butanol were used, selectivity was improved but band

broadening and peak tailing were increased. All probes studied showed enthalpy-driven

patterns and the trend in absolute enthalpies of the second eluting enantiomer matched

the trend in selectivities observed for the three types of 2′,2-binapthyls. Future work will

involve determining the energy barriers to racemization as well as modeling studies to

determine the effects of different substituents on molecular hybridization and chiral

recognition.

Chapter 3

Total Peak Shape Analysis Approach: Detection and Quantitation of Concurrent Fronting,

Tailing, and their Effect on Asymmetry Measurements

3.1 Abstract

Most peak shapes obtained in separation science depart from linearity for various

reasons such as thermodynamic, kinetic, or flow based effects. An indication of the

nature of asymmetry often helps in problem solving e.g. in column overloading, slurry

packing, buffer mismatch, and extra-column band broadening. However, existing tests for

symmetry/asymmetry only indicate the skewness in excess (tail or front) and not the

presence of both. Two simple graphical approaches are presented to analyze peak

shapes typically observed in gas, liquid, and supercritical fluid chromatography as well as

capillary electrophoresis. The derivative test relies on the symmetry of the inflection

points and the maximum and minimum values of the derivative. The Gaussian test is a

constrained curve fitting approach and determines the residuals. The residual pattern

graphically allows the user to assess the problematic regions in a given peak, e.g.,

concurrent tailing or fronting, something which cannot be easily done with other current

methods. The template provided in MS Excel automates this process. The total peak

shape analysis extracts the peak parameters from the upper sections (> 80% height) of

the peak rather than the half height as is done conventionally. A number of situations are

presented and the utility of this approach in solving practical problems is demonstrated.

3.2 Introduction

Separation scientists rely on peak shapes for extracting basic chromatographic

performance parameters such as number of theoretical plates, peak height, area,

resolution, and thermodynamic/ kinetic information of the processes taking place in the

column.[100] Apart from visual judgment, two common chromatographic figures of merit, namely, theoretical plate numbers and asymmetry are used for peak shape assessment. In addition, there are more than 20 theoretical or semi-empirical models for fitting experimental peak shapes with mathematical functions mainly from the family of Gaussians, such as polynomial modified Gaussian, bi-Gaussian, Gaussian-Lorentzian Sum, Exponentially Modified Gaussian (EMG), Giddings, Half Gaussian Modified Gaussian (GMG), Haarhoff-Van der Linde, Pearson IV, and Log Normal 4 or 5 Parameter to fit chromatographic peaks.[101-103] Most chromatographic peaks under analytical conditions will invariably fit one of the above mentioned models with a reasonable goodness of fit (R^2 > 0.98-0.999). Many commercial softwares such as PeakFit[TM] or MATLAB[TM] help in modeling of a variety of peak shapes from which the peak moments can be extracted. By achieving a good fit, the chosen model still may not present a physical reality. For instance, none of these models specifically incorporates packed bed heterogeneities or the effect of digital filters into peak shapes.

The Gaussian distribution is one of the most useful functions because it is a limiting case of many statistical distributions (Equation 4-1).[103] For most separations in chromatography and electrophoresis, it is desired to have Gaussian peaks as they give the highest detection sensitivity as compared to other asymmetric peak shapes, as well as allowing convenient integration. Obtaining Gaussian peaks also is an indication that the separation system is well behaved (*i.e.* linear chromatography). Although separation scientists prefer to use asymmetry/tailing factors and efficiencies, it should be borne in mind that these single values are insufficient to describe the whole peak shape e.g. a USP tailing factor will ignore a peak shoulder arising from a poorly packed column. A careful analysis of many chromatographic peaks can reveal that tailing might be coupled with fronting; an Eiffel Tower effect (*vide infra*) can occur but goes unnoticed when the

"front" or "tail" is in excess as is commonly the case. In chromatography, peak tailing can originate from slow sorption-desorption kinetics, thermodynamic factors,[104] or from a *RC* digital filter in the data acquisition software.[105] Peak asymmetry may also be seen in packed beds due to the non-ideal arrangement of particles in the column near the walls.[106,107] Similarly, peaks are distorted in electrophoretic separations due to buffer mismatch among other reasons.[106] For these purposes, it is important to understand *which region(s) of the peak reflect the problem*. There are several statistical distribution comparison methods that can test whether a distribution is normal or not.[108] Rigorous methods for peak shape analysis require calculating moments, e.g. skew or kurtosis, of a given peak. Such calculations result in a single number by taking the overall properties of a distribution.[109] Both skew and kurtosis are extremely sensitive to the choice of peak start and end-points- a slight change in end-points results in a different answer. To the best of our knowledge, no column manufacturer reports the chromatographic peak shape (and even efficiency) by the methods of moments for their quality control tests since the precision is quite low. Statistics also allows graphical tests such as the "Distribution Function Method"[110] and "Lévy distances"[111] for comparing peak shapes. These methods require a mathematical model of the real peak to begin the peak shape assessment. Interested readers can consult a summary of statistical methods for peak shape assessment in reference.[112]

Herein a very simple and visual approach is proposed for total peak shape analysis. It is based on the properties of the Gaussian function to assess a real peak shape, and its departure from a perfect Gaussian shape. Also demonstrated is a more simple and objective measure of peak asymmetry as a way to quantify the contributions of concurrent fronting and tailing to non-Gaussian peaks. In this work, we demonstrate complete and visual analysis of peak asymmetry using the method of derivatives as well.

Unlike the conventional way of *fitting* a Gaussian model using the method of least squares, the method introduced in this work uses superimposition with specific constraints to help identify the problematic regions of the peak. The Gaussian test is not a statistical distribution comparison test; rather it is a visual and quantitative tool to assess problems in a chromatographic peak such as concurrent fronting or tailing, shouldering, etc. It enables qualitative and quantitative assessment of individual contributions from concurrent fronting and tailing to the overall peak distortion, which is quite common, but rarely noticed and never quantified.

3.3 Theory

A Gaussian chromatographic peak $g(t)$ with an amplitude A, retention time of t_r, and a standard deviation of σ can be described by:

$$g(t) = A \, exp\left(-\frac{(t - t_r)^2}{2\sigma^2}\right) \quad\quad (\text{3-1})$$

The nth derivative of the Gaussian is also a Gaussian function multiplied by a Hermite polynomial.[113] Thus, for the first derivative, the zero crossing of the derivative of a peak appears at the same time as the retention time since $t\text{-}t_r$ becomes zero in Equation (4-2).

$$\frac{dg(t)}{dt} = -A\frac{(t - t_r)}{\sigma^2} exp\left(-\frac{(t - t_r)^2}{2\sigma^2}\right) \quad\quad (\text{3-2})$$

Given that the chromatographic data is digitized with very small time intervals on modern detectors e.g. Δt of <0.0125 s (or data sampling frequencies of > 80 Hz), we can estimate this derivative with

$$\frac{dg(t)}{dt} = \frac{y_2 - y_1}{t_2 - t_1} \quad\quad (\text{3-3})$$

where y is the instrument signal and t is the time. This derivative is plotted with respect to the original time scale. The property of Gaussian (or any peak shaped functions) derivative allows a *very sensitive test for symmetry* of any peak shape without relying on the choice of peak start or end. If the magnitude of maximum and minimum values $\frac{dg(t)}{dt}$ is not identical, it reveals the presence of asymmetry about the y-axis.

Secondly, we can approach the peak shape analysis from the upper section of the peak. It is possible to determine the standard deviation of a Gaussian peak from any height rather than the conventional half height (Equation 4-4). The width of a peak normalized to unity w_H at any height H, is related to the standard deviation as follows:

$$\sigma = \frac{w_H}{2\sqrt{2\ln\left(\frac{1}{H}\right)}} \qquad (\,3\text{-}4\,)$$

The derivation of this equation is provided below. An ideal chromatographic peak $g(t)$ with an amplitude A, retention time of t_r, and a standard deviation of σ can be described by

$$g(t) = A\,exp\left(-\frac{(t-t_r)^2}{2\sigma^2}\right)$$

For g(t) at height equivalent to fraction H of amplitude A

$$\Rightarrow H*A = A\,exp\left(-\frac{(t-t_r)^2}{2\sigma^2}\right)$$

Taking natural log on each side

$$\Rightarrow \ln(H) = -\frac{(t-t_r)^2}{2\sigma^2}$$

Multiply each side with (-1)

$$\Rightarrow -\ln(H) = \frac{(t-t_r)^2}{2\sigma^2}$$

Since -ln x = ln 1/x

$$\Rightarrow \ln\left(\frac{1}{H}\right) = \frac{(t-t_r)^2}{2\sigma^2}$$

$$\Rightarrow 2\sigma^2\ln\left(\frac{1}{H}\right) = (t-t_r)^2$$

42

$$\Rightarrow t - t_r = \sigma \sqrt{2 \ln\left(\frac{1}{H}\right)}$$

Full width at height fraction h for an ideal Gaussian

$$w_H = 2(t - t_r)$$

Substituting the values from Equation S7

$$\Rightarrow w_H = 2\sigma \sqrt{2 \ln\left(\frac{1}{H}\right)}$$

$$\Rightarrow \sigma = \frac{w_H}{2\sqrt{2 \ln\left(\frac{1}{H}\right)}}$$

By modeling a peak from the standard deviation extracted at 85% of the peak height or above, one can easily visualize the departure of the real peak from the Gaussian shape by superimposition with certain constraints followed by analysis of the residuals (discussed in the the Gaussian Test Approach), unlike the standard peak fitting procedure. Herein, this process will be referred to as the Gaussian test.

The Pearson IV (Area) Model used was simulated based on equation below[114,115]

$$y = \frac{a_0 a_3 \, exp\left[a_3 tan^{-1}\left(\frac{x + \frac{a_2 a_3}{2} - a_1}{a_2}\right)\right]}{a_2 \left[exp\left(\frac{a_3 \pi}{2}\right) - exp\left(-\frac{a_3 \pi}{2}\right)\right]\left[1 + \left(\frac{x + \frac{a_2 a_3}{2} - a_1}{a_2}\right)^2\right]} \qquad (3\text{-}5)$$

Where a_0 = amplitude, a_1 = center, a_2 = width, a_3 = shape.

3.3.1 The Gaussian Test Protocol

The Gaussian Test referred herein uses a Microsoft Excel based template to automate the process. The template is available elsewhere.[48] The following is the protocol to perform the Gaussian Test using the template.

1. Getting the X and Y data for the peak of interest

    a. Export the X (retention-time) and Y (absorbance/ Instrument Signal) coordinates of a chromatogram to an Excel sheet. For example:

        i. For Agilent ChemStation: File > Export > CSV

    b. Open the file in Excel, select both X and Y data, and plot a scatter plot

    c. Visually estimate time points that cover a single peak of interest and copy the corresponding X and Y data points for the peak. (e.g., X and Y points for retention time 1.0 to 1.4 min can be selected if the peak of interest starts at 1.1 min and ends at 1.3 min.). It is important to select points that only cover a single peak.

2. Getting the peak of interest in Microsoft Excel Gaussian Test Template

    a. Download the Gaussian Test Excel template provided elsewhere[48] and open it.

    b. Choose the "Values" sheet, right click in cell A2 and paste X and Y points copied above in step 1c. The formulas already included (columns C to M) have been extended up to row 20,000 and can be extended further by user if needed.

    c. The built-in Excel formulas will calculate peak parameters for the normalized peak and display them to the right. The retention time, peak height, and sigma of normalized peak extracted at 85% peak height will be used to model initial Gaussian. See the section 3 of the manuscript for details on the approach.

44

  d. The normalized peak will be superimposed with a Gaussian model which can be seen on "Peak and Model" tab of the Excel sheet.

3. The Derivative Test

  a. The 1st derivative of the normalized peak will be calculated and displayed on the "Derivative" tab of the Excel sheet.

  b. The minima and the maxima of the 1st derivative are also calculated in column O.

4. The Gaussian Test

  a. For Windows, in the Excel's ribbon interface on the top, go to "Data" tab, "Analyze" section, and click "Solver".

    i. If you cannot find "Solver", you must enable it first. Go to File menu > Options > Add-ins > In the manage dropdown, select "Excel Add-ins" and click "Go". Check the boxes next to the "Solver" add in, and click OK. It should appear in Data tab now.

  b. For Mac, in the Excel's Tools menu, click on "Solver"

    i. If you cannot find "Solver", you must enable it first. Go to Tools menu > Excel add-ins > Check "solver" and click OK. It should appear in Tools menu now.

  c. In the "Solver Parameters" window, set objective should be set to cell V22

    i. The differences between the points on the peak of interest and the model at 85% peak height are squared and the sum of squared differences is calculated in cell V22 that is to be minimized using solver to fit. See the section 3 of manuscript for details.

d. In the "Solver Parameters" window, "By Changing Variable Cells" should be set to cell S8 which is the σ calculated at 85% peak height (set in cell S4) for the model.

e. In the "Solver Parameters" window, "Subject to the Constraints" should have the following entries for constraints.

    i. O5 ≤ S5 (point on the leading edge of the peak and the model at 85% peak height)

    ii. O6 ≥ S6 (point on the tailing edge of the peak and the model at 85% peak height)

f. Click "Solve" and let solver complete. Solver should find an exact solution.

    i. For verification, user can fill cell S8 with a different value, run the steps a-f again, and compare the values. Click "Ok".

g. Go to "Peak and Model" sheet to inspect the Gaussian model superimposition on the normalized peak and the residuals.

5. Individual contribution from fronting and tailing to the peak distortion

a. The individual contributions to the total peak distortion will be calculated automatically based on built-in formulas and displayed in column S.

3.4 Experimental

The core-shell (2.7 µm diameter) silica particles were provided by Agilent Technologies (Santa Clara, CA). The columns were packed using the dispersed slurry technique using a Haskel DSHF-202 pneumatic pump (Haskel, Burbank, CA). A given amount of the stationary phase was dispersed in a solvent which dispersed the particles such as in ethanol-cylohexanol or methanol-cyclohexanol mixture. The particles were sonicated and then transferred to a slurry chamber. The chamber was pressurized up to

10,000 psi. For the section packing experiment, three 5 cm x 0.46 cm i.d. modular

columns (IDEX, Corporation) were connected in series by custom made unions at the

UTA machine shop. The unions had modular adapter connections at both ends and the

same internal diameter as the column. The columns were packed in the same fashion.

However, after packing, the three columns were disconnected and capped. The top,

middle and bottom sections were tested. Only the bottom section is reported here. The

15 x 0.46 cm i.d. C18 2.7 μm core-shell column was purchased from Agilent

Technologies. All solvents including acetonitrile (ACN), methanol (MeOH), and analytes

were from Sigma Aldrich. DI water was obtained from Milli-Q purification system (EMD

Millipore, Billerica, MA, US).

Chromatography was performed with an Agilent C18 Poroshell Column (15 x0.46

cm i.d., 2.7 μm particle size) on a Vanquish UHPLC instrument (Thermo Fisher Scientific,

Waltham, MA) controlled using Chromeleon 7.2 SR4 software (Thermo Fisher Scientific

2009-2016). For all other separations, an Agilent 1290 Infinity Series UHPLC instrument

(Agilent Technologies, Santa Clara, CA) controlled by OpenLAB CDS ChemStation

software (Rev. C.01.06 [61], Agilent Technologies 2001−2014) was used. The column

thermostat compartment was bypassed to reduce any peak shape distortion by plumbing

in both UHPLCs. The USP tailing factors are based on the equation $T = \frac{W_{0.05}}{2f_{0.05}}$; where

$W_{0.05}$ = peak width at 5% peak height and $f_{0.05}$ = distance from the leading edge of the

peak to the peak maximum at 5% peak height.

3.5 The Gaussian Test Approach

The Gaussian Test can be easily performed in Microsoft Excel (2007 and higher).

Solver add-in should be installed (see "The Gaussian Test Protocol" above). A

screenshot shows the labels on the columns for convenience in Figure 3-1. The Microsoft

Excel Gaussian Test template (provided elsewhere[48]) is used for explanations below on the approach to superimpose a Gaussian Model. The template includes all formulas necessary to automate the Gaussian test. There are several steps which take place after the raw data (time vs. signal) is pasted. A straight forward protocol to performing a Gaussian test is provided above. Note that only a single peak data (or a section of a chromatogram containing a single peak) must be analyzed in this template, at a time.

	A	B	C	G	K	L	M	N	O	P	Q	R	S	T
1	Time (min)	Peak (mAU)	Normalized Peak (mAU)	Gaussian Model	Residuals	Abs Residuals	Derivative	Normalized Peak				Gaussian Model		
2	1.0000	1.5E-02	8.0E-05	1.9E-161	8.0E-05	8.0E-05		Max Height (a)	1	mAU		Max Height (a)	1	mAU
3	1.0001	1.7E-02	8.9E-05	2.8E-161	8.9E-05	8.9E-05	1.1E-01	Ret time b	1.156	min		Ret time b	1.156	min
4	1.0002	1.5E-02	7.9E-05	4.2E-161	7.9E-05	7.9E-05	-1.2E-01	Peak Height L	85%	mAU		Peak Height fraction L	85%	mAU
5	1.0003	1.0E-02	5.2E-05	6.2E-161	5.2E-05	5.2E-05	-3.3E-01	x1 at peak height L	1.152	min		x1 at peak height L	1.15232272	min
6	1.0003	5.6E-03	2.9E-05	9.2E-161	2.9E-05	2.9E-05	-2.8E-01	x2 at peak height L	1.159	min		x2 at peak height L	1.15884328	min
7	1.0004	2.6E-03	1.4E-05	1.4E-160	1.4E-05	1.4E-05	-1.8E-01	FW at height L	0.00661628	min		FW at height L	0.00652056	min
8	1.0005	-1.5E-03	-8.0E-06	2.0E-160	-8.0E-06	8.0E-06	-2.6E-01	Sigma from L	0.00580252	min		Sigma from L	0.00571871	min
9	1.0006	-5.6E-03	-2.9E-05	3.0E-160	-2.9E-05	2.9E-05	-2.5E-01							
10	1.0007	-4.8E-03	-2.5E-05	4.5E-160	-2.5E-05	2.5E-05	4.4E-02	Peak Height fraction M	90%			Peak height fraction M	90%	mAU
11	1.0008	1.4E-03	7.4E-06	6.6E-160	7.4E-06	7.4E-06	3.9E-01	x1 at peak height M	1.15287752			x1 at peak height M	1.15295812	min
12	1.0008	1.0E-02	5.3E-05	9.8E-160	5.3E-05	5.3E-05	5.5E-01	x2 at peak height M	1.15819873			x2 at peak height M	1.15820788	min
13	1.0009	1.9E-02	9.7E-05	1.5E-159	9.7E-05	9.7E-05	5.1E-01	FW at height M	0.00532121			FW at height M	0.00524976	min
14	1.0010	2.4E-02	1.3E-04	2.2E-159	1.3E-04	1.3E-04	3.5E-01	Sigma from M	0.00579598			Sigma from M	0.00571815	min
15	1.0011	2.7E-02	1.4E-04	3.2E-159	1.4E-04	1.4E-04	1.8E-01							
16	1.0012	2.8E-02	1.5E-04	4.8E-159	1.5E-04	1.5E-04	6.4E-02	Peak Height fraction N	80%			Peak Height fraction N	80%	mAU
17	1.0013	2.8E-02	1.4E-04	7.0E-159	1.4E-04	1.4E-04	-3.6E-02	x1 at peak height N	1.1516471			x1 at peak height N	1.1517627	min
18	1.0013	2.7E-02	1.4E-04	1.0E-158	1.4E-04	1.4E-04	-4.6E-02	x2 at peak height N	1.1594186			x2 at peak height N	1.1594033	min
19	1.0014	2.9E-02	1.5E-04	1.5E-158	1.5E-04	1.5E-04	1.3E-01	FW at height N	0.00777149			FW at height N	0.0076406	min
20	1.0015	3.6E-02	1.9E-04	2.3E-158	1.9E-04	1.9E-04	4.2E-01	Sigma from N	0.00581657			Sigma from N	0.00571861	min
21	1.0016	4.5E-02	2.3E-04	3.4E-158	2.3E-04	2.3E-04	5.9E-01							
22	1.0017	5.3E-02	2.7E-04	5.0E-158	2.7E-04	2.7E-04	4.7E-01	1st Derivative				Residuals sum	15.5768619	
23	1.0018	5.5E-02	2.9E-04	7.4E-158	2.9E-04	2.9E-04	1.6E-01	Maxima	100.395158			Abs residuals sum	15.7776646	
24	1.0018	5.3E-02	2.7E-04	1.1E-157	2.7E-04	2.7E-04	-1.7E-01	Minima	-103.84705					
25	1.0019	4.6E-02	2.4E-04	1.6E-157	2.4E-04	2.4E-04	-4.1E-01					Abs Fronting side residuals	11.394	
26	1.0020	3.6E-02	1.9E-04	2.4E-157	1.9E-04	1.9E-04	-6.0E-01					% Abs front contribution	72%	
27	1.0021	2.5E-02	1.3E-04	3.6E-157	1.3E-04	1.3E-04	-6.9E-01					Abs Tailing side residuals	4.384	
28	1.0022	1.5E-02	7.6E-05	5.3E-157	7.6E-05	7.6E-05	-6.6E-01					%Abs tail contribution	28%	

Figure 3-1. A screen shot of a Gaussian test in Excel template with all column labels. The user has to fill in the time and signal data only followed by Solver Analysis to obtain derivative results and the analysis from the Gaussian test. The template is provided elsewhere.[48]

3.5.1 Normalization of Peak to Unity

The experimental peak is normalized to unity (amplitude of 1) by dividing the y-axis absorbance data by the peak maximum value.

3.5.2 The Derivative Test

The first derivative of the normalized peak is generated based on equation 3 and shown in the derivative sheet of the Excel template. The minima and maxima of the derivative are calculated as well on the "values" tab.

3.5.3 Extraction of the Standard Deviation

The σ or standard deviation value remains constant when obtained at various peak heights of an ideal Gaussian peak (Equation 4). However, for peaks that are not completely Gaussian, the σ obtained at various peak heights will differ. We choose to obtain the standard deviation from the upper region of the peak since, even for severely distorted peaks, the upper region (80% of peak height or above) generally follows an ideal Gaussian profile. As such, the Gaussian test template determines the x-axis values that correspond to 80, 85, and 90% peak heights (can be altered by the user) to calculate the peak width at these heights.

3.5.4 The Gaussian Model

To assess the departure of chromatographic peak from an ideal Gaussian shape, the real peak is superimposed with a Gaussian model generated based on equation 4. Amplitude A of unity and retention time of experimental peak is chosen as t_r. The standard deviation of experimental peak calculated at 85% peak height is used to model the initial Gaussian. This is a constrained fitting of a peak. The y-axis values for the Gaussian model are calculated in a column and plotted against x-axis time values and the superimposition can be seen in "Peak and Model" tab.

3.5.5 The Gaussian Test

Once a Gaussian model is generated, it is refined by the method of least squares to improve the model's superimposition and visualize the residuals. A constraint in Solver is imposed that the points corresponding to the 85% peak height of the model either lie

49

on the experimental peak or be encompassed by it. The peak height of 85% or 90% for superimposition worked well when put to test on a variety of peak shapes produced from a variety of stationary phases. The user can easily modify the peak height chosen (85% peak height is used by default) for the superimposition in the template and re-run the solver add-in to minimize residuals at new peak height. Once done, the resulting superimposition and the residuals can be seen on the "Peak and Model" sheet.

3.5.6 Quantifying the Contributions to Peak Distortion

To assess the individual contribution from the peak fronting and tailing to the overall peak distortion, a sum of absolutes of the residuals is calculated. A sum of absolute residuals only to the left of the peak maxima expressed as a fraction is considered the contribution from fronting to the total peak distortion. A similar value is calculated for contribution from tailing by taking the sum of residuals to the right of the peak maxima and expressing it as a fraction of the total absolute residual sum.

3.6 Results and Discussion

3.6.1 Proposed Derivative and Gaussian Tests on Simulated Peak Shapes

A facile approach that allows visual detection of the departure of real peaks from the perfect Gaussian is proposed. In Figure 3-2(A) and (B), two idealized simulated peaks sampled at 160 Hz in the absence of noise are shown. Figure 3-2(A) is a Gaussian peak ($\sigma = 0.300$ s) and Figure 3-2(B) is a Pearson (IV) area peak (Equation 4-5, $a_0=1.0999$, $a_1=30$, $a_2=$width$=0.350$, $a_3= 0.001$).[102,114] The latter shows nearly equivalent elements of fronting as well as tailing giving it an Eiffel Tower like shape (a.k.a. excess

kurtosis in statistical terms).[1] Visually, both of the peaks are symmetric (USP tailing of

1.0000 and 1.0006 at 5% height respectively). The extra significant figures are retained to

show the sensitivity of the proposed tests. However, the USP tailing for the latter does

not provide any information on the almost equal fronting element of the peak seen in

Figure 3-2(B). The derivative test confirms the perfect symmetry for the Gaussian model

in Figure 3-2(C) (max. 2.0215 and min. -2.0215). However, a derivative test for Figure

3-2(B) peak detects a slight asymmetry in Figure 3-2(D) (max. 1.8568, min.=- 1.8556)

very sensitively. This implies that the slope on the left is slightly different from the right.

Note that actual experimental peaks showing analogous behavior will be discussed in the

subsequent sections.

---

[1] There are other distributions with broad bases and narrow apices (e.g. Laplace, Lorentzian or other Pearson types etc.). The derivative of the Laplace distribution is discontinuous. Pearson (IV) equation is included in PeakFit^{TM} and used here for demonstration purposes for an equally fronting or tailing peak.
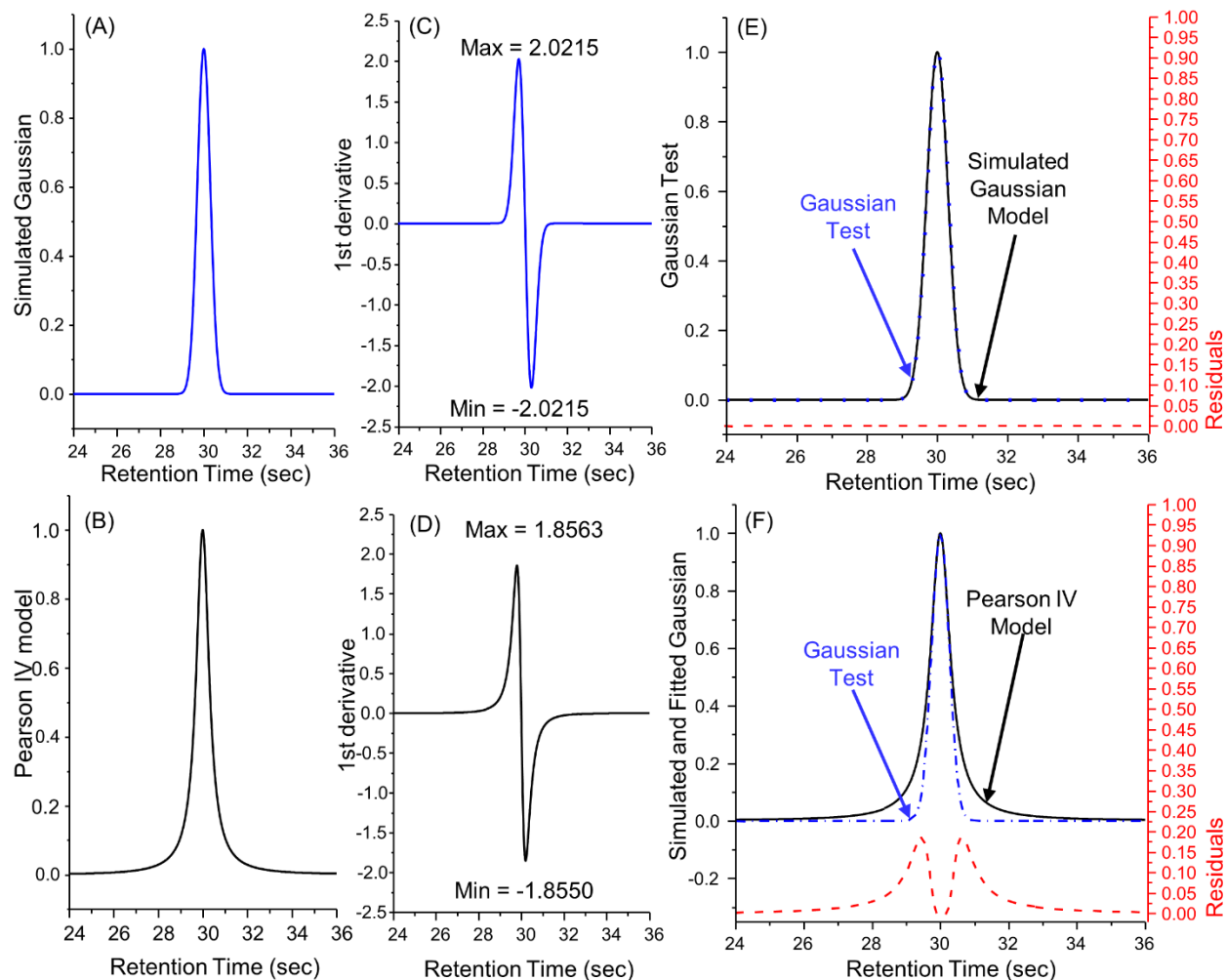
Figure 3-2. A graphical comparison of (A) a simulated Gaussian model and (B) a Pearson IV (area) model. (C) The 1st derivative of simulated Gaussian (D) 1st derivative of Pearson IV area model. Note the differences in the positive and negative intensity of the derivatives. The Gaussian test with set of constraints described in this work is applied on (E) simulated Gaussian model and (F) Pearson IV area model.

The Gaussian test can now be applied to obtain information on the tailing and fronting contributions with the set of constraints discussed below. A Gaussian model can be of two types: matching the area or the amplitude. The amplitude Gaussian (equation 4-1) is superimposed after normalizing the peak height to unity since the interest is not in quantitation by area but rather the analysis of peak profile and its departure from the

52

Gaussian shape. This Gaussian test is *not* meant to obtain a best fit of the whole peak by

the method of least squares (as is conventionally done); rather the model is overlaid on

the peak with a set of constraints. The constraints are that the superimposed Gaussian

model (i) have an amplitude of unity; (ii) have identical retention time as the real peak,

and (iii) the residuals between the real peak and the ideal peak are minimized *at well*

above the full width at half maximum by the method least squares rather than the whole

peak. Excel Solver add-in is utilized for this purpose (See the Gaussian Test Protocol

above). In Figure 3-2(E), the Gaussian test, with the aforementioned constraints, is

applied on the simulated Gaussian peak with a σ = 0.30000 s. We approach the peak

shape analysis from the upper section of the peak rather than the bottom as is

conventionally done. The Gaussian test predicts a standard deviation of 0.29999 at 90%,

85% and 80% of peak height using the equation 4-4. The error in prediction is negligible

(7.4×10^{-5} %), which confirms the validity of the Gaussian test approach along with its set

of constraints. The analysis of the residuals shows that there is no departure from the

perfect Gaussian shape of this peak. The approach for extracting standard deviation at

heights well above the full width at half maximum (FWHM) such as 85% or 90% peak

height is based on the observation that the upper regions of real chromatographic peaks

are nearer to perfect Gaussian function even for severely distorted peaks. The idea was

validated by testing more than ten tailing, fronting, or peaks with shoulder obtained on

several stationary phases. For the peak in Figure 3-2(B), the Gaussian test (Figure

3-2(F)) clearly shows that there is a fronting as well as tailing element. If we wish to

express the individual contributions from fronting and tailing to the overall peak distortion,

one can sum the absolute residuals and calculate the fraction of fronting and tailing

residuals. Doing so, we get a 49.95% distortion contributed by fronting and 50.05%

contributed by tailing in the simulated peak (Figure 3-2B). Since there is a very slightly

larger contribution from tailing, the USP tailing factor turns out to be 1.0006, which would have been significantly higher, had the tailing not been masked by the fronting portion. Alternatively, one can also measure the area difference between the perfect superimposed Gaussian and the real peak from the line of symmetry.

3.6.2 Peak Shape Analysis of an Ultrahigh Efficiency Commercial Core-Shell C18 Column

It is important to ensure that there is no peak distortion from the data acquisition software for real separations. All data was sampled at > 80, 160 or 200 Hz to fulfil this criterion with the smallest possible response times (0.016-0.063 s). The Agilent software employs a Gaussian weighted centered moving average as a smoothing algorithm which makes all peaks perfectly Gaussian under slow response times. This property is based on the concept of Central Limit Theorem, therefore all the true peak shape information is lost under those conditions.[105] Similarly, Thermo Fisher Scientific's Chromeleon software employs a Savitsky-Golay type filter which can produce "dips" near the peak ends.[105] A commercial C18 column was tested as a bench mark for peak shape analysis on an optimized UHPLC instrument. The manufacturer reports the efficiency of the column as 38,000 plates as a quality control test. This implies that the reduced plate height of the column is 1.46 (assuming a nominal particle size of 2.7 μm). These efficiencies are extremely high and can only be obtained after taking special steps to optimize the instrument as detailed in previous studies.[52,105] The question arises as to whether these ultrahigh efficiency columns produce perfect Gaussians or not? Figure 3-3 shows the result for a 1,3-dinitrobenzene peak with an efficiency of 38400 plates for a data collected at 200 Hz with 0.02 s rise time. The instrument reported USP tailing factor of the peak is 0.92. The derivative test shows a lack of symmetry (max. 100.395 vs. -103.847).

54

Although derivatives also can enhance the noise, but herein we show that the data collected at 200 Hz (considered a very high sampling rate) the derivative test is still useful in predicting asymmetry. However, it is recommended to have a high signal to noise ratio (e.g. peak height of > 150 mAu). In our case for three replicates, < 1% RSD was observed on the minima and the maxima of the first derivative. If there is excessive noise on the derivative, one can use a centered moving average or a Savitsky-Golay smoothing on the derivative. Most users rarely need a sampling rate above 80 Hz even for sub-minute separations.[52] Classical peak fronting can be interpreted in terms of derivatives as a condition where the inflection point maximum of the left side is lower than the right side. As will be shown, this is not the only type of fronting peaks that column developers encounter. The Gaussian test shows the fronting contribution as well as a smaller tailing contribution. By doing the residual analysis, we obtain 72% and 28% contribution to peak distortion from fronting and tailing, respectively. This observation is consistent with the USP tailing factor of 0.92, however the information on the tailing is absent from the traditional calculation.
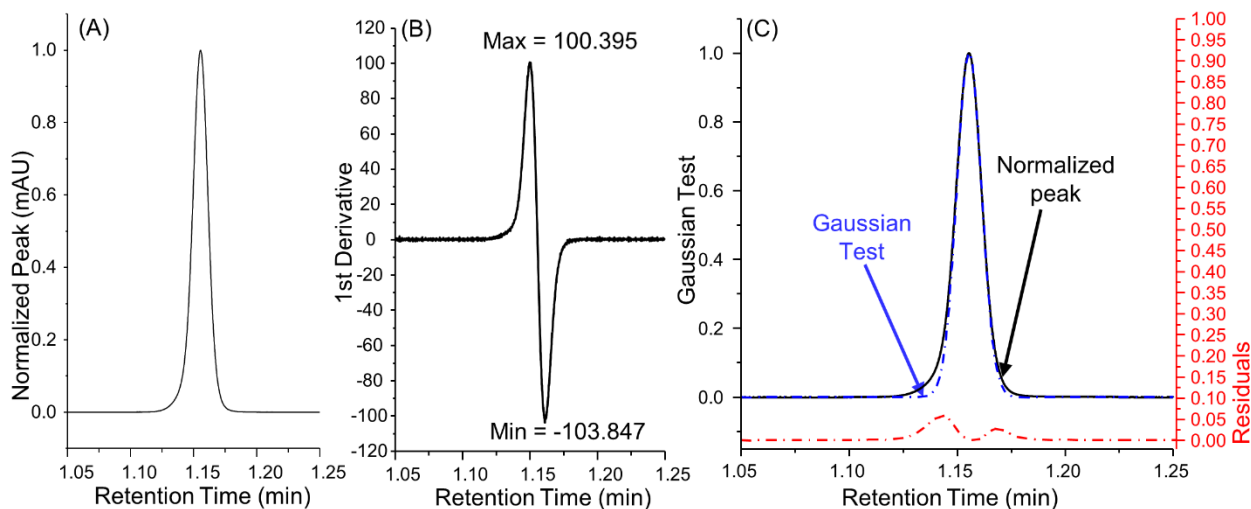
Figure 3-3. (A) A high-efficiency peak on a commercial C18 column. (B) 1st derivative of the peak. (C) the Gaussian Test. For experimental peak, column: C18 Poroshell 2.7 μm

superficially porous particles (15 x 0.46 cm i.d.). Analyte: 1,3-dinitrobenzene. Method: 70/30 ACN/DI water at 1.8 mL/min flow rate. UV detection at 254 nm with 200 Hz detector frequency and 0.02 s response time.

The Gaussian test also indicates that there is a departure from perfect Gaussian at peak heights 20% and below. The rest of the peak conforms to a pure Gaussian profile. Most fronting and tailing for unretained or low retention factor peaks originates from a velocity bias (wall effects) due to packed bed heterogeneities.[106] In general, fronting peaks have very high efficiencies if calculated at the half height. For instance, the peak efficiency calculated by second moments in Figure 3-3, are 25,000 as compared to 38,000 (assuming Gaussian shape). This is a loss of 13,000 plates simply because the peak is not a perfect Gaussian.

3.6.3 More Prominent "Eiffel Tower" Effects

In many cases, the degree of fronting and tailing on a given peak is not equivalent but still may be present to a significant extent. Figure 3-4 is a case in point for a teicoplanin bonded core-shell column in a 2.1 mm i.d. format. The separation of 5-methyl 5-phenylhydantoin is a QC test on this column using methanol as a mobile phase. The USP tailing of the peak is 1.22. However, a visual judgement (Figure 3-4A) shows that there is departure from Gaussian at the peak bottom, coming from some fronting and more tailing. The derivative test shows asymmetry (max. = 61.2132, min= -44.8111), showing significant peak distortion which is not apparent with the USP tailing factor. However, a total peak shape analysis shows the problematic regions of this peak. On the front side, the departure from Gaussian function is at 30% peak height whereas the distortion of tailing side, starts from 70% peak height and continues below until it meets the baseline. Thus, the Gaussian test shows that the total peak is distorted by 22% from a fronting element and 78% percent from a tailing element. This tailing arises not from

56

packing but by slow desorption kinetic effects in chiral chromatography,[52] however, the

front is purely a packing artifact.
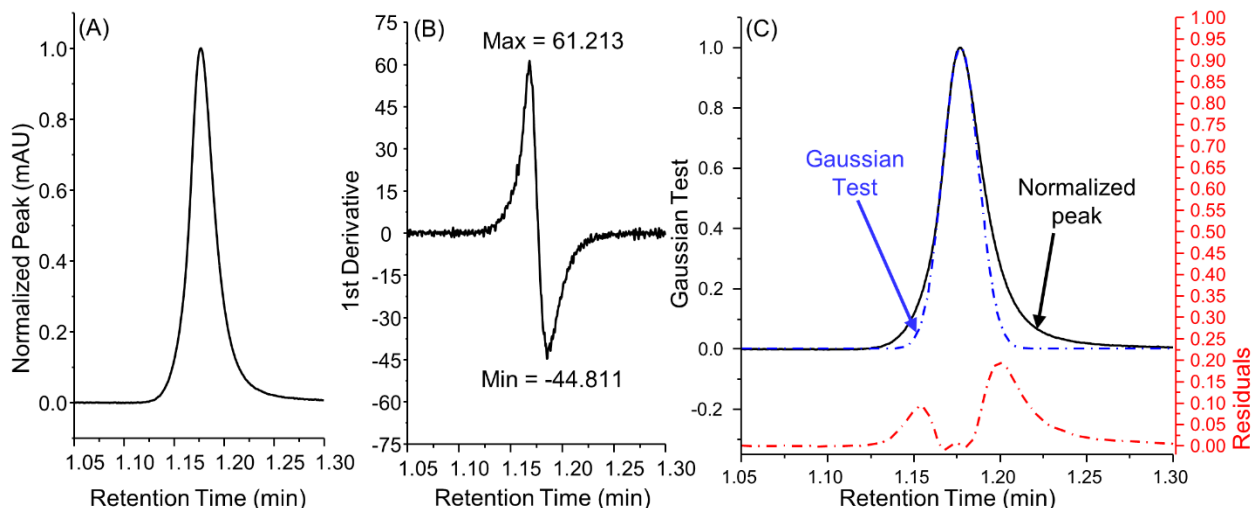
Figure 3-4. (A) A peak that demonstrates a visually apparent "Eiffel Tower Effect", i.e. concurrent fronting and tailing. (B) 1st derivative of the peak showing much shorter negative peak indicating tailing. (C) the Gaussian test. For experimental peak, column: teicoplanin bonded to 2.7 μm superficially porous particles (15 x 0.21 cm i.d.). Analyte: 1st eluting enantiomer of 5-methyl 5-phenylhydantoin. Method: pure MeOH mobile phase at 0.35 mL/min flow rate. UV detection at 220 nm with 80 Hz sampling frequency and 0.0631 s response time.

In the previous example, visually perceptible fronting and tailing were present. In

many cases, the Gaussian and the derivative test must be used to detect even more

subtle fronting or tailing in the peak that might be obtained during column development.

More specifically, determining the problematic section of a poorly packed column is

imperative to the fundamental understanding of the role of suspension rheology under

extreme pressures (~ 10,000-16,000 psi). For that purpose, a 15 cm x 0.46 cm i.d.

column was prepared with 2.7 μm core-shell silica (See Experimental). The column

consisted of three detachable 5 cm columns connected via unions. We intentionally

chose 2-propanol (to make a viscous slurry) to obtain non-optimal results. The question

of interest is whether the whole column is bad along its length or only certain sections

57

have a poor bed structure. It turns out that when a non-optimal slurry is chosen; all

sections of the column perform poorly with the same peak profiles. In Figure 3-5, the

lowest efficiency bottom 5 x 0.46 cm section of this column is analyzed. The column

produces reduced plate height h = 3.1 (6000 plates), which is higher than the expected

reduced plate height of 2. The USP tailing of the peak is 1.08. From a visual analysis, the

peak shape appears to be symmetrical. Without a proper whole peak shape analysis, it is

difficult to arrive at any conclusion about the nature of the 2-propanol slurry, whether it

produces fronting, shoulders or tails etc. The derivative test, confirms that asymmetry is

present (max 80.738, and min -79.888). The Gaussian test at 85% peak height is

performed (Figure 3-5). The residuals clearly show that the poor performance of 2-

propanol as a slurry solvent is not only due to a tailing element (visually clear) *but a

subtle fronting element also is present.* This fronting element would not have been

detectable by any tailing factor, skew or kurtosis. The residual analysis shows 29%

fronting contribution and 71% tailing contribution. Slurry solvents, which produce fronting

and tailing with broad peaks, should not be further optimized and a new solvent system

should be used altogether. Thus total peak shape analysis can save time by reducing the

number of choices for suspension solvents. The following section will clarify how to solve

these problems.
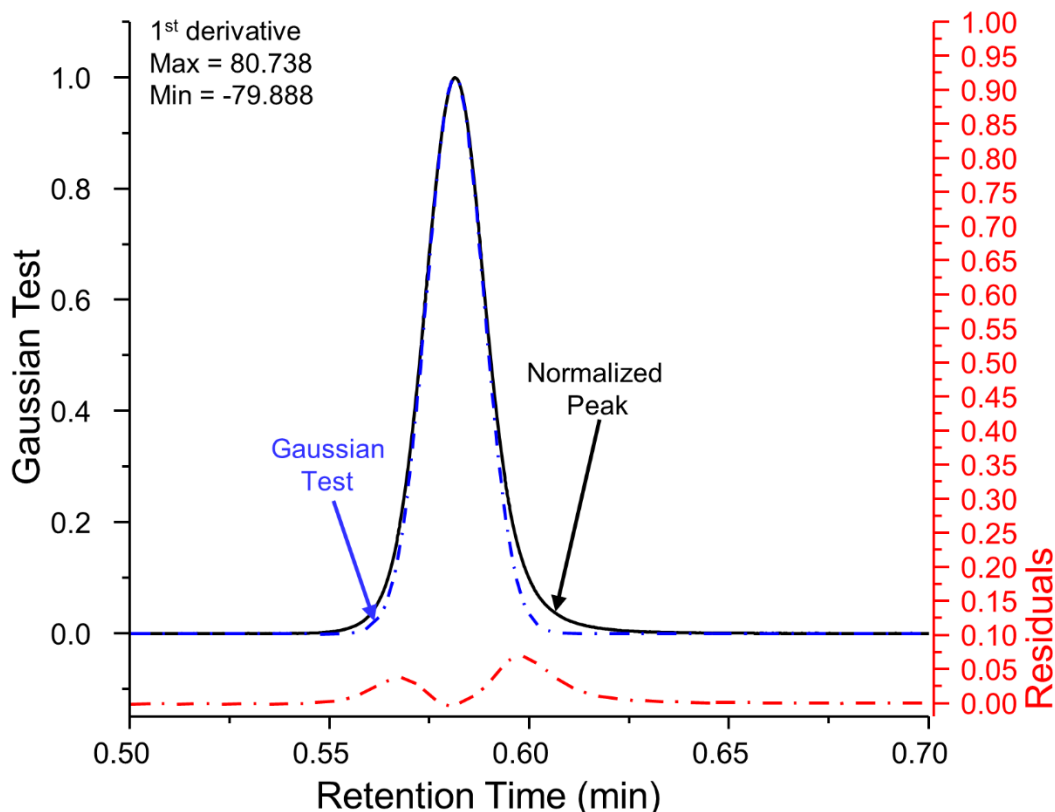
Figure 3-5. The Gaussian test applied on a peak that demonstrates a subtle case of the "Eiffel Tower Effect", i.e. fronting and tailing in a single peak. For experimental peak, column: bottom 5 cm section of a 15 x 0.46 cm long packing of native 2.7 μm superficially porous particles. Analyte: uracil. Method: 50/50 MeOH/DI water at 1.0 mL/min. UV detection at 254 nm with 160 Hz sampling frequency and 0.016 s response time.

3.6.4 Utility of the Proposed Tests in the Analysis of Peak Shapes

Narrow bore columns (2.1 mm i.d. to 3 mm i.d.) save significant amounts of solvents because the same linear velocity as 4.6 mm i.d. columns is obtained at lower volumetric flow rates. It is known that narrow bore columns can show significantly lower plate numbers, usually up to 40 % reduction, than their 4.6 mm i.d. counterparts due to wall effects.[116,117] We show how the total peak-shape analysis can help in tuning peak shapes during column packing. Herein, we chose ethanol-cyclohexanol system as a dispersing medium for core-shell silica particles in 5 x 0.3 cm i.d. columns. Using low concentration of silica slurry (~ 2.3% w/v), the derivative test confirms the presence of

59

asymmetry (max. = 84.839 and Min =-82.822) as shown in Figure 3-6(A). For reference,

the USP tailing for the 2.3% slurry is 0.93, showing that the peak is fronting. The peak

shape is not acceptable in practice. It is also not clear if this suspension produces tailing

or not from a single USP number. Only the full peak shape analysis identifies the

problematic regions of the total peak. The presence of residuals shows significant regions

of fronting plus tailing elements despite an indication from USP tailing factor that the peak

only fronts. The contribution to peak distortion is 58% percent from fronting and 42% from

tailing. Such departures from ideality on the fronting side are easily cured by increasing

the slurry concentration. As shown in Figure 3-6(B), just by increasing the slurry

concentration to 16% w/v, the fronting element has become negligible and the left side of

the peak has a perfect Gaussian character. The value of the derivative still detects

asymmetry (max. =86.598, min.=-80.282). The peak shape distortion from the Gaussian

test shows 10% contribution from fronting and 90% from tailing. Note that since uracil is

an early eluting analyte on a narrow bore column, the persistent presence of tailing has

its origins in extra-column connections for narrow bore columns. A later eluting peak on

the same column has negligible tailing. As a result, of slurry concentration increase, the

peak shape has been tuned by the packing process only. This is a generalization of peak

shape optimization with slurry concentration that will be discussed in the next chapter.[47]

Alternatively, another approach on peak shape analysis which can detect fronting, tailing,

and peak purity has recently appeared.[118]
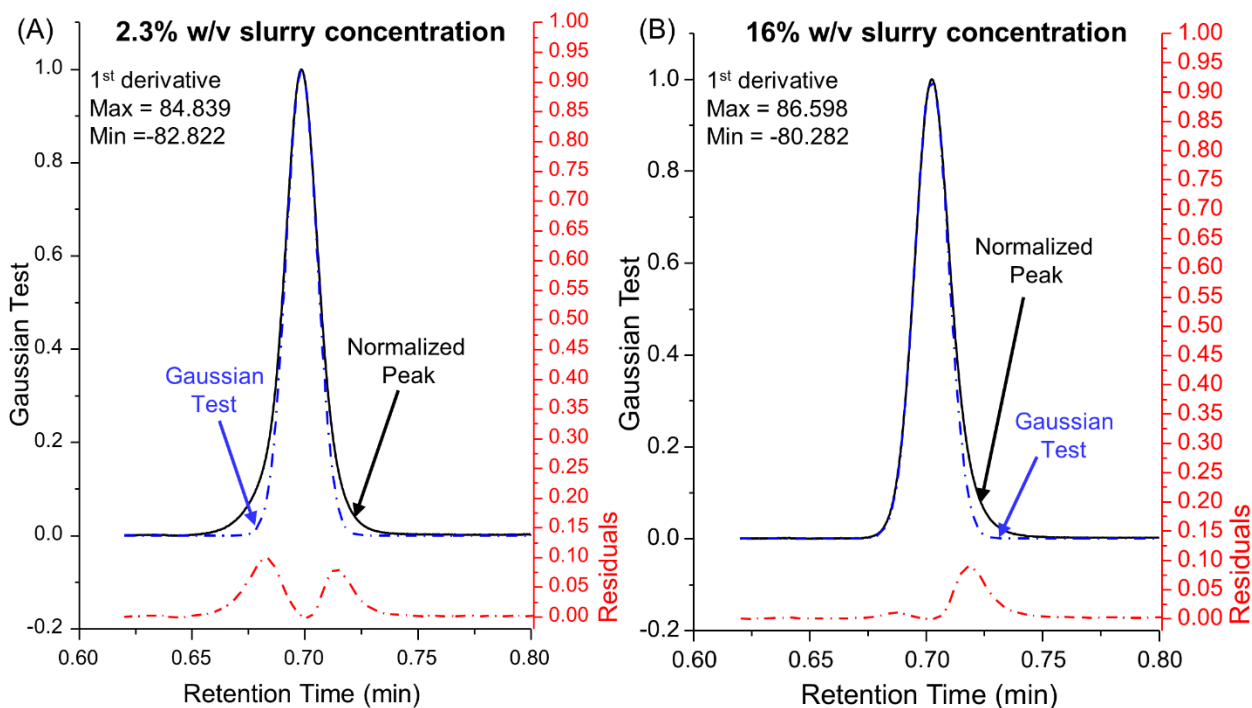
Figure 3-6. The Gaussian test applied on examples of (A) asymmetric peak emerged from use of a non-optimal (2.3% w/v) slurry concentration and (B) improvement of peak asymmetry by using an optimal (16% w/v) slurry concentration. For experimental peaks, columns: native 2.7 μm superficially porous particles (5 x 0.3 cm i.d.) packed using different slurry concentrations. Analyte: uracil. Method: 80/20 ACN/25 mM NH$_4$OAc at 0.425 mL/min flow rate. UV detection at 254 nm with 160 Hz sampling frequency and 0.016 s response time.

3.7 Conclusion

Simple objective means to analyze total peak shapes and their departure from symmetry and Gaussian profile are proposed. An Excel^{TM} template is provided which automates the entire analysis. Assessment of peak shapes by single valued descriptors of peak shape such as USP tailing, skew, or kurtosis are inadequate because they do not give a complete picture of the overall peak shape. The derivative test is based on the concept that if a peak is symmetric, their inflection points will be mirror images. The derivative test is a very sensitive test for the "presence" of asymmetry on *any* peak

shape, even when the data is sampled at very high sampling rates up to 200 Hz. The

signal to noise ratio should be high for the proposed tests (as is usually the case). The

Gaussian test superimposes a Gaussian model on a normalized peak with its set of

constraints and shows the problematic regions of the peak. The standard deviation is

extracted from the upper section of the peak rather than the conventional half height

approach. The proposed methods will be useful for researchers engaged in stationary

phase development, column packing, or hardware design to achieve better peak shapes.

The approach used in the Gaussian test is general and, in fact, can be used for testing

the departure of any peak shape from the expected mathematical model.

Chapter 4

Fundamental and Practical Insights on the Packing of Modern High Efficiency Analytical

and Capillary Columns

4.1 Abstract

New stationary phases are continuously developed for achieving higher efficiencies and unique selectivities. The performance of any new phase can only be assessed when the columns are efficiently packed under high pressure to achieve a stable bed. The science of packing columns with stationary phases is one of the most crucial steps to achieve consistent and reproducible high resolution separations. A poorly packed column can produce non-Gaussian peak shapes and lower detection sensitivities. Given the ever larger number of stationary phases, it is impossible to arrive at a single successful approach. The column packing process can be treated as science whose unified principles remain true regardless of the stationary phase chemistry. Phenomenologically, the column packing process can be considered as a constant pressure or constant flow high pressure filtration of a suspension inside a column with a frit at the end. This process is dependent on the non-Newtonian suspension rheology of the slurry in which the particles are dispersed. This chapter lays out the basic principles and presents examples for researchers engaged in stationary phase development. This chapter provides an extensive set of slurry solvents, hardware designs, and a flow chart - a logical approach to optimal column packing, thus eliminating the trial and error approach commonly practiced today. In general, non-aggregating, but high slurry concentrations of stationary phases tend to produce well packed analytical columns. Conversely, C18 packed capillary columns are best packed using agglomerating solvents.

4.2 Introduction

Stationary phase development in separation science is an active and prolific research area. Once the stationary phase has been developed, the particles must be packed into columns to perform separations. A frustrating situation for a researcher arises when the desired selectivity is achieved but the column efficiency, measured as the reduced plate height h (plate height H/particle diameter d_p), turns out to be greater than 2 along with a non-Gaussian peak shape. A range of chromatographic materials have been developed such as bare silica, modified silica, non-porous or macroporous polymers, inorganic oxides (TiO_2, Al_2O_3, and ZrO_2),[119-121] carbon coated silica,[122,123] diamonds, boron doped diamonds,[124] and porous graphitic carbon.[125,126] In Figure 4-1, the scanning electron micrographs (SEM) of several particle morphologies namely, fully porous sub-2 μm silica (FPP), 2.7 μm superficially porous silica (SPP), latex coated sulfonated polymer, and 5 μm porous graphitic carbon are shown.[57] To overcome packing challenges, a thorough understanding of the properties of suspensions and hardware design is required. Several properties are desirable for a packed column such as Gaussian peaks with $h \leq 2$, and a mechanically stable bed which can survive 500-1000 injections. This chapter highlights the current scientific understanding along with our own experience with 20 different stationary phases (Table 4-1), provides insights in packing small particles of various polar and non-polar chemistries from the literature and from other practitioners. These approaches were developed over the course of packing several hundreds of columns in various dimensions.

64
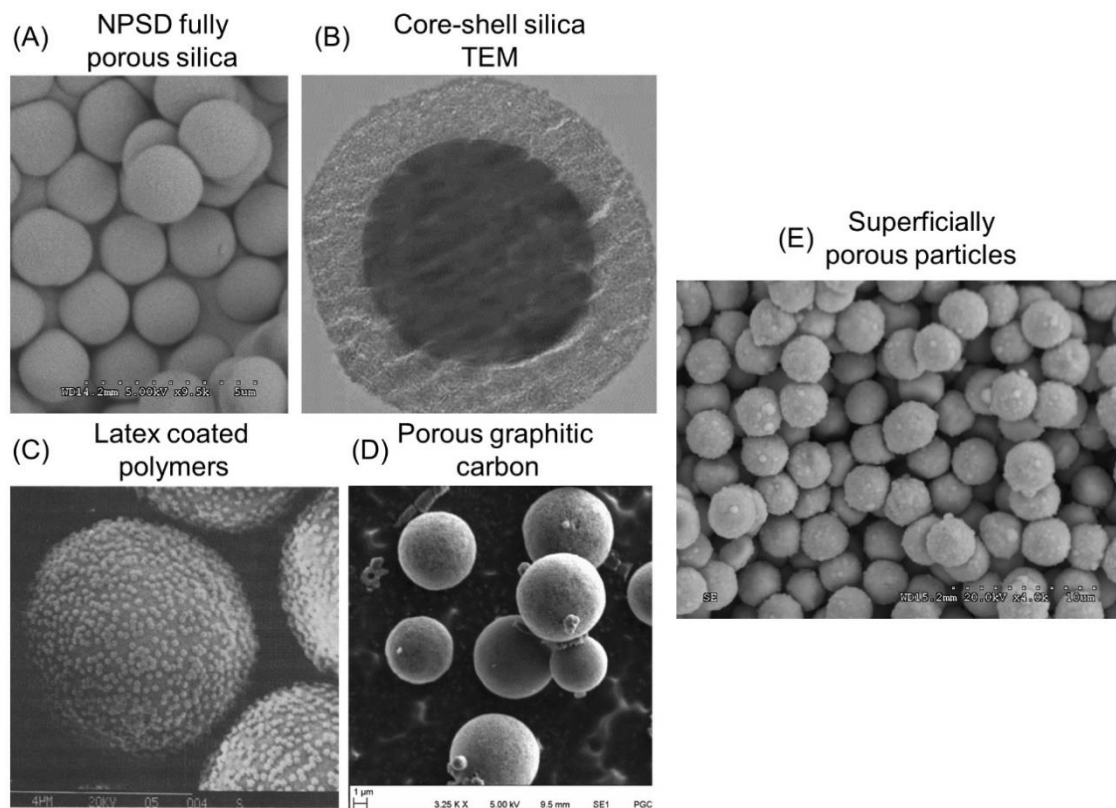
Figure 4-1. Scanning (SEM) and transmission (TEM) electron micrographs of various stationary phases (A) SEM of narrow particle size distribution (NPSD) 1.9 µm fully porous silica (9500x), (B) TEM of 3.6 µm superficially porous silica (shell thickness 0.5 µm) (C) 5 µm latex coated sulfonated styrene divinylbenzene (9000x) (D) 5 µm porous graphitic carbon (3250x) (E) SEM of 2.7 µm superficially porous particle silica (4000x). (A) and (E) were obtained on a Hitachi S-3000N SEM instrument. Sample was sputter coated with Ag using CrC 100 sputter system prior to imaging.

Table 4-1. List of stable bonded chemistries successfully packed in our laboratory and evaluated in HPLC and SFC. The phenomena discussed in this chapter have been developed through experience of packing of these stationary phases.

Teicoplanin (FPP and SPP)[52,127]	Hydrosilated quinine[128]
Teicoplanin aglycone[52,127]	Carboxylated cyclofructan [129]
Vancomycin (FPP and SPP)[52] [127]	Fully porous bare silica 1.9 µm (this work)
Zwitterionic phosphonium based phases (unpublished work)	Superficially porous bare silica 1.5, 2, and 2.7 µm (this work)
Hydroxypropyl-β-cyclodextrin[52]	Fully porous C18 silica 1.9 µm (this work)

65

Cyclofructan 6 isopropyl carbamate[52]	Fully porous C18 silica 5 μm (unpublished results)
Carbon clad zirconia[130]	Mercapto-linked quinine[128]
Carboxylated porous graphitic carbon[131]	Cyclofructan 7 dimethylphenyl carbamate[52]
Sulfonated EVB-DVB particles 4.4 μm[57]	DNB-Phenylglycine (unpublished work)
DNB-Diphenylethylenediamine C_{10} linker (unpublished work)	DNB-Diphenylethylenediamine C_3 linker (unpublished work)
DNB-Leucine derivative (unpublished work)	

4.3 Phenomenological Understanding of the Slurry Packing Process

The column packing process is a pressure filtration of a suspension into a cylindrical mirror polished tube with a frit at the end (Figure 4-2). The force of filtration is obtained from a pump which can operate in a constant pressure or constant flow mode. The current understanding of the slurry packing process of columns is far from complete because it is difficult to model suspension rheology, particle to wall friction, and behavior of the particle solvent interface under extreme pressures ranging from 4000 to 30,000 psi. As the bed of particles is formed, the secondary consolidation processes take place to make a tighter bed under pressure.[132] The pressure is such that it is 2-3 times the expected pressure on the chromatograph. After the column is packed, the pressure is removed and the column is capped. There are numerous column geometries with the options of construction materials such as stainless steel, polyether ether ketone (PEEK), and PEEK or glass lined stainless steel tubes. The column nomenclature is typically classified as capillaries (20 μm to < 1 mm i.d.), microbore (1 - < 2.1 mm i.d.), narrow bore (> 2.1 - 3.9 mm i.d.), and normal bore columns (3.9 - 5 mm i.d.). Preparative columns employ slurry packing or mechanical approaches such as dynamic axial packing or radial compression to obtain high efficiency preparative columns and will not be considered here.[133]

66
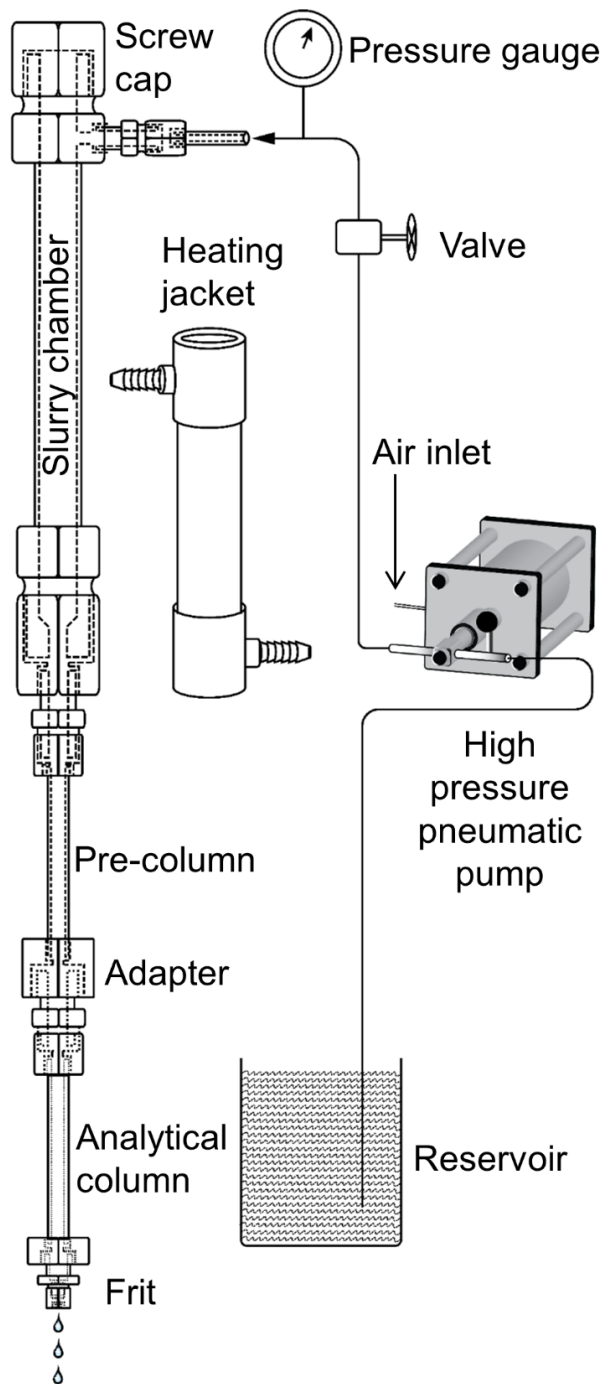
Figure 4-2. A downward slurry packing system for packing analytical columns (up to 20,000 psi). The connection tubings are connected by a collar and gland type or

Swagelok fittings. The pre-column should be at least 5-10 cm long with the same i.d. as the column being packed (real pictures published elsewhere[47]).

4.4 Hardware Design Considerations

Well-designed column packing hardware is critical to achieve high efficiency columns in any format. Figure 4-2 is a schematic of the hardware: a solvent reservoir connects to an ultrahigh pressure pump which pushes the suspension of particles held in a slurry chamber attached to a pre-column and an empty column. Under pressure, a tightly packed bed builds up in a dynamic fashion (with an axial density gradient of particle concentration). We prefer pneumatically driven pumps (30,000 psi max.) which operate in a constant pressure mode. The main drawback of penumatic pumps is the large pressure pulsations during the "breathing cycle" of piston strokes. Electrically driven piston pumps (up to 18,000-25,000 psi) can also used either in constant flow or constant pressure mode. If accurate flow rates are required, up to 30,000 psi, specially designed syringe pumps can be used. Typically 10, 20, 40, and 80 mL slurry chambers with 1.4 cm (or narrower) i.d. are employed for 2.1 to 4.6 mm i.d. columns. Verzele[134] achieved maximum efficiency when the geometries of the slurry chamber and the column matched. It is important to match the pre-column diameter extending from the slurry chamber with the column for a smooth transition of the suspension into the column. Any disturbance by a poor design/bent tubing, damaged seals usually leads to a failed column. The slurry chamber can be externally heated by circulating hot water as shown in Figure 4-2 using a heating jacket.[57] For the slurry chamber design, the pushing liquid can be made to enter the chamber at a 90° angle, rather than vertically. If vertical entrance is preferred, a flow distributor which distributes the liquid in horizontal directions (images of a real setup are published elsewhere[47]) is used. The logic behind this design is to prevent rapid mixing of the suspension with the pushing solvent.

68

The outlet frit retains the stationary phase inside the column during packing. Frits should be chosen to withstand pressures (4000-30,000 psi) during column packing. Figure 4-3 shows SEM of a metal based and a PEEK based frit. The stainless-steel based frit in Figure 4-3A shows visible metal filings possibly retained from manufacturing process. The PEEK based frit in Figure 4-3B was attached to a column outlet and the column was packed at 10,000 psi. After packing, the frit was removed and examined (Figure 4-4) using high-resolution digital microscope (Keyence VHX digital microscope, Keyence Corporation, Osaka, Japan). It was found that the frit was damaged during the packing leaving a 56.13 µm wide hole on the surface. A more detailed depth analysis (Figure 4-5) revealed the depth to be 10.60 µm. A hole of this size could easily retain several particles of 5 µm or smaller size and cause the bed to be uneven, leading to band broadening. The theoretical importance of frit designs and flow distribution properties is discussed elsewhere and it should be ensured to use high quality frits made from small sintered particles.[135]

(A) Stainless steel column frit from MFR. A
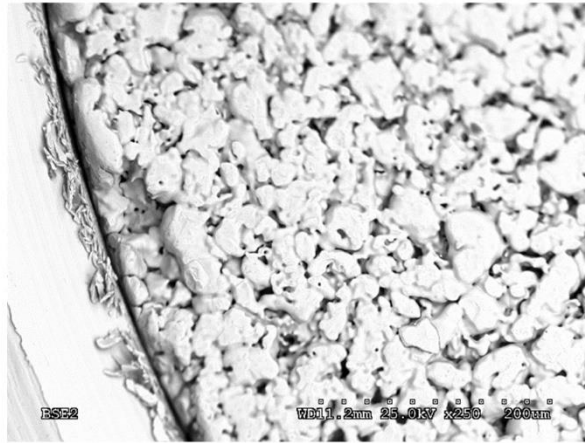
(B) PEEK based column frit from MFR. B
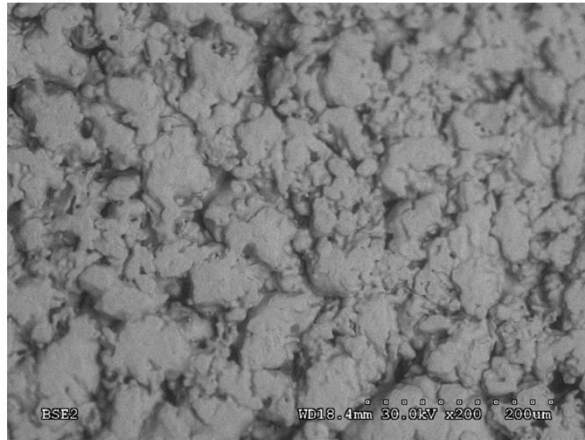
Figure 4-3. SEM of column frits obtained on a Hitachi S-3000N SEM instrument. (A) SEM of an unused stainless-steel based frit from manufacturer A is shown at 250x magnification. The left region shows possible metal filings left from machining while the right shows the porous region of sintered particles. (B) SEM of the porous region of an unused PEEK based frit from manufacturer B is shown at 200x.

Figure 4-4. A high-resolution image of the PEEK based frit from Figure 4-3(B) after it had been exposed to 10,000 psi during a packing. A 56.17 μm diameter hole appeared on the surface when the damaged frit was removed from the column. The manufacturer lists the specification of the frit to be above 10,000 psi. Image taken using Keyence VHX digital microscope using Z20 lens with 200x magnification.
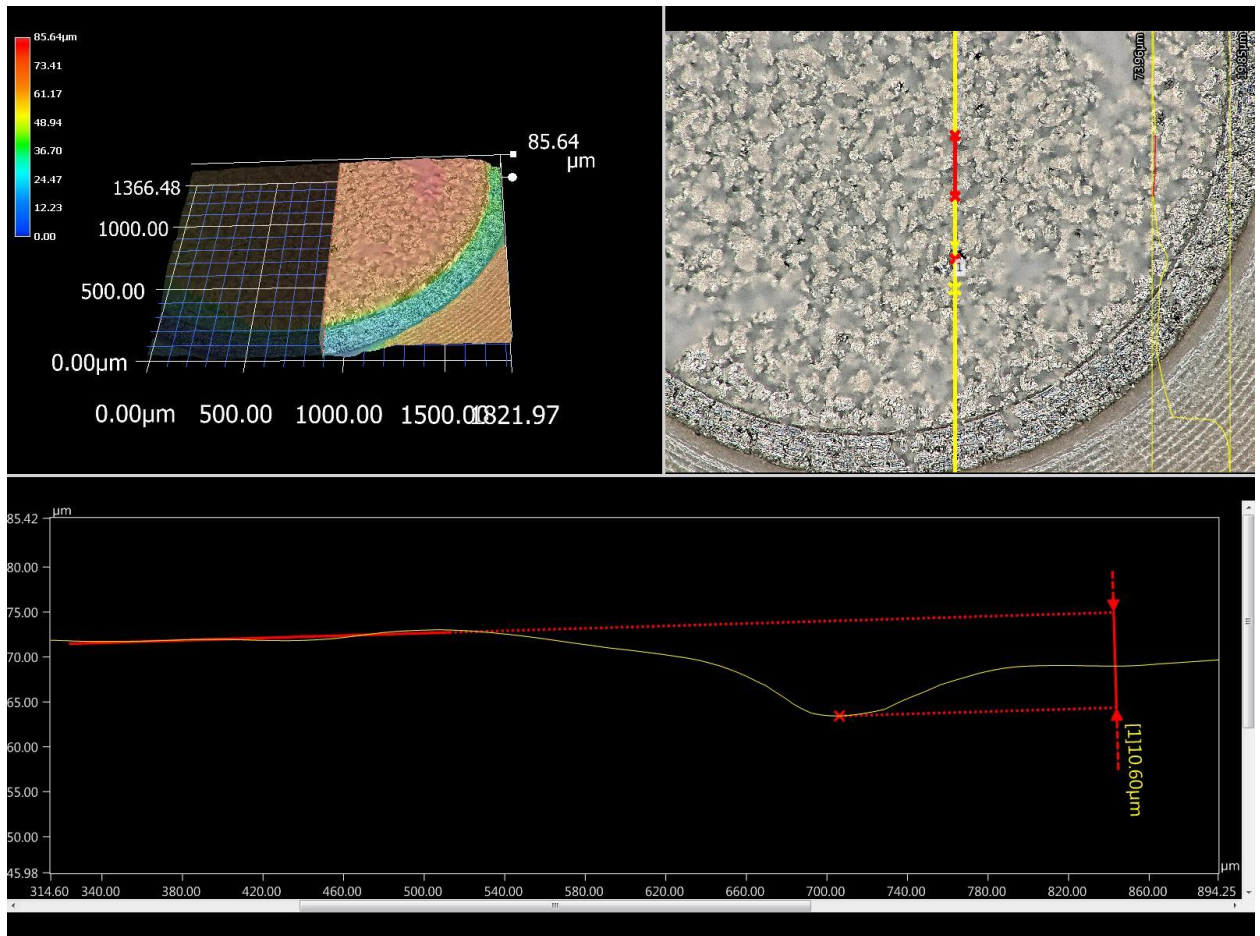
Figure 4-5. Surface depth analysis of the damaged frit pictured in Figure 4-4 using the Keyence VHX digital microscope with lens Z20. The bottom half shows the graph of depth revealing the hole to be 10.60 μm deep, large enough to fit a few silica particles 5 μm or smaller in size.

The packing methods for capillaries usually involves high pressures (5,000-40,000 psi) using pneumatically driven pumps.[136] Alternatively, for capillary packing, a high pressure generator is a manually operated piston screw pump can also be employed (High Pressure Equipment Company, PA). These pumps can compress small volumes of liquids (< 100 mL) to extremely high pressures without producing pressure pulses. A schematic of a custom designed system is shown in Figure 4-6 which is based on the system designed by Jorgenson (see elsewhere for real images[47]).[137] The capillary is

72

placed in a small suspension chamber (stirred with a small magnetic bead), and high

pressure is applied from a pneumatic pump directly to a bolted chamber. The packing

behavior can be monitored by an optical microscope. For packing capillary columns, the

column frits are often prepared in-house by the Kasil frit method and other techniques.[138]

Additionally, the capillaries can also be packed in a downward fashion without a stir bar

just like an analytical column. The key requirement in such design is to have a precision

engineered bore in the outlet, matching the i.d. of the capillary. This allows smooth

transition of the suspension of the particles into the capillary rather than clogging the

capillary head (a common problem). Capillaries are often sonicated during packing.

Several commercial slurry chamber designs have pressure limitations of 9000 psi and

utilize He gas to push the solvent through capillaries. The readers can consult the classic

work on high pressure hardware design by Spain and Paauwe.[139]
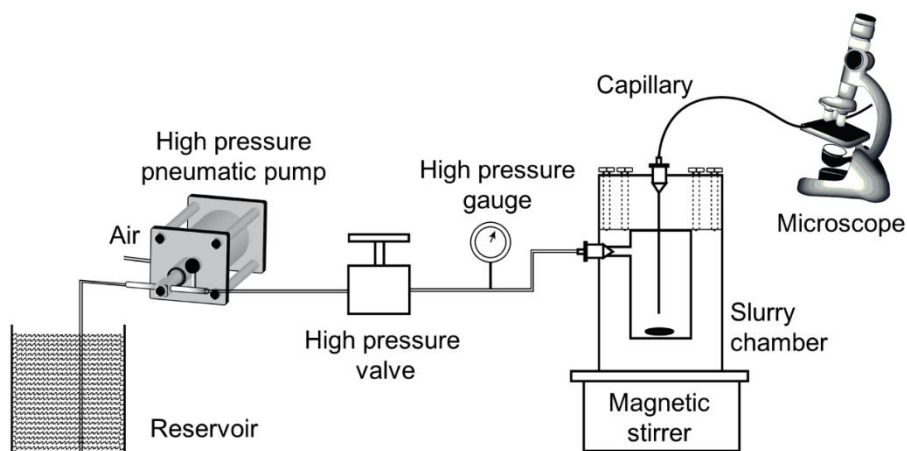
Figure 4-6. A high-pressure upward slurry packing system for capillaries (up to 30,000-60,000 psi). The microscope can be used for examining the bed as the capillary is being packed. See external publication for real images.[47]

4.5 Fundamental Insights into the Slurry Packing Process

The following sections describe the theoretical considerations in the column

packing process to achieve good results.

4.5.1 Particle Size Distribution and its Role in Column Performance

The concept of "reported" particle diameter is rather complex and there are several ways to express the particle size. To theoretically estimate h, the true particle diameter must be known for making any judgements on the packing procedure. The Sauter diameter d_{Sauter} is commonly used for quoting chromatographic particle sizes. It represents the diameter of a sphere that has the same volume to surface area ratio as a particle and it is defined as:[140]

$$d_{Sauter} = \frac{\sum n_i d_{p,i}^3}{\sum n_i d_{p,i}^2}$$

(4-1)

where *n* is the number of particles and d_p is the particle diameter. The Sauter diameter is easily determined by Coulter-counter techniques.[140] One may also employ laser diffraction particle size analyzer or scanning electron microscopy (SEM) and measure the particle diameter, e.g., by using ImageJ software for SEM images for n > 500 followed by using equation (1).[141] It will be clear from Figure 4-1 that there is no "unique" particle size and, at times, there is a significant departure from the nominal particle size. Another specification for size distribution is the percentile ratio, $\frac{d_{90}}{d_{10}}$; where d_{90} and d_{10} are the particle diameter at 90th and 10th percentile of the particle size distribution (PSD), respectively. The closer the value of $\frac{d_{90}}{d_{10}}$ is to unity, the narrower is the particle size distribution. Commercial stationary phase particles rarely come close to $\frac{d_{90}}{d_{10}}$ of unity. Titan particles (1.9 µm, Supelco, Sigma-Aldrich) marketed as "monodisperse" silica have a $\frac{d_{90}}{d_{10}}$ ~ 1.3, while other suppliers for sub-2 µm silica have even higher ratios.[127] The larger size distribution can have a very significant effect on the bed density and affect the efficiency in deleterious ways (as per recent reports)[142,143] or beneficial ways (e.g. having a small percentage of large particles).[144] Sometimes adding 5-10% of

larger particles than the nominal size being packed implemented in practice to ease the packing process.[137]

4.5.2 Role of Stationary Phase Fines in a Column Performance

Fines refer to very small spherical or irregular particles found in particulate materials (e.g. in Figure 4-1D). The problems in particle size distribution mainly arise if smaller particles (and fines) are the major cause of size distribution rather than larger particles. Higher back-pressure than expected from the nominal size is observed in such cases. A study on fines concluded that "*it is not so much the width or span of the particle size distribution, but rather the presence of fines that greatly determines the chromatographic performance of particulate columns.*"[142] SEM will reveal the quality of the particles, presence of debris or foreign material before and after synthesis. If magnetic bars are used for small scale synthesis, some particles may be crushed by mechanical/grinding forces. This is true for soft materials or silica of low mechanical strength, porous graphitic carbon, or coated particles such as carbon clad zirconia etc.

4.5.3 Picking Suspension Solvents for a Given Stationary Phase

Choosing the right and stable suspension medium for given particles is very important for successful packing. The term "stable" suspension refers to the fact that the critical suspension properties do not change significantly in a given time-frame of the column packing process. All suspensions are thermodynamically unstable but may be kinetically resistant to settling (compare the stability of colloids).[145] Table 4-2 shows an extensive summary of slurry solvents utilized in packing for various surface chemistries. It is also useful to consider wettability, dispersion state, viscosity, density of the solvent, and shear thickening/ thinning properties before finalizing the choices (*vide infra*).

75

Table 4-2. A guide to choosing slurry solvents for capillary and analytical columns. Suspension with chosen solvent should be examined by optical microscopy.

(a)	**Silica**: MeOH,[56,146] IPA,[147-149] Acetone,[147,150,151] 70:30 IPA:MeOH, 1:1 5% Tween 20:ethylene glycol,[152] 50/2.5/47.5 ethylene glycol/Tween 20/Water,[152,153] IPA:CCl$_4$
(b)	**Cyano Silica Phases**: Anhydrous EtOH,[147] (50:50) → (90:10) Toluene:IPA,[147]
(c)	**Reversed Phase Silica Phases (C18 type)**: 50:50 MeOH:IPA,[154,155] 1:1 paraffin:CCl$_4$,[155-157] Acetone,[158-161] 1:2 acetone:hexane,[162] CHCl$_3$,[159,163] 80:20 CHCl$_3$:MeOH (with acidic additives), 95% EtOH:n-propanol:toluene 1:1:1(v/v) **Reversed Phase Silica Phases (C4/C8 type)**: Anhydrous EtOH,[147] Anhydrous IPA,[147,156,159] 50:50 Acetone: IPA,[147] (50:50) → (90:10) THF:IPA[147]
(d)	**Silica based HILIC Phases including Amino Silica and Sugar Bonded Phases**: 98:2 ACN: 1M NH$_4$NO$_3$, 70:30 Dichloromethane:MeOH, (50:50 → 90:10) Toluene/IPA[147]
(e)	**Polymeric Ion-Exchangers/ Stationary Phases**: Pure deionized water (heated slurries),[57,164] 2:1 Acetone:H$_2$O,[165] Acetic acid/ethylene diamine/polyethylene glycol/mono(nonylphenyl)ether in DI water,[166] Note: *Polymeric phases usually swell in organic solvents unless highly cross-linked*
(f)	**Carbon Based Phases including Porous Graphitic Carbon**: MeOH,[167] dichloromethane,[168] neutral surfactants such as Igepal in water **Modified hydrophilic PGC**: Pure deionized water[167]
(g)	**Hybrid Materials:** Carbon coated zirconia (IPA), Carbon coated silica (N-methylpyrrolidone), Polymer coated zirconia (IPA, 50:50 IPA:THF), Core-shell diamonds (50:50 acetone:water)
(f)	**Additional Successful Blends for Dispersing Stationary Phases**: 50:50 IPA:THF, 50:50 IPA:acetone, 50:50 MeOH:acetone, 50:50 IPA:chloroform with organic acid additives such as formic acid, 80:20 MeOH:cyclohexanol, 80:20 MeOH:glycerol, 80:20 EtOH-cyclohexanol, 80:20 1-butanol cyclohexanol, 80:20 EtOH-anhydrous dimethylsulfoxide, 50:50 MeOH:dioxane, 85:15 Dichloromethane: MeOH, acetone:dichloromethane, butanol:dimethylsulfoxide, pure acetone (the ratios can be varied depending on achieving a dispersed state)

4.5.4 Wettability and Surface Energies

One of the most obvious requirements is to choose a solvent which will wet the stationary phase surfaces. An incorrect match leads to "creaming" i.e. the stationary phase rises to the surface. For example, water will not wet C18 silica, or a carbonaceous phase (see Figure 4-7); the stationary phases keeps floating on the surface despite having higher densities than water. This example of "creaming" occurs when the solvent is unable to wet the stationary phase such as 1.9 µm C18 stationary phase dispersed in absolute ethanol and water. Water is unable to wet a C18 phase; hence it is not a useful

slurry for packing this particle chemistry. By adding surfactants in water, one can still disperse the particles.

Figure 4-7. 1.9 µm C18 phase dispersed in ethanol (left) and water (right). This is an example of creaming. Although ethanol is able to wet the phase, it is highly agglomerating; therefore, not a suitable suspension medium.

The wetting process originates from a balance of surface forces. Thermodynamically, if the spreading coefficient S, as defined in equation 5-2,[169,170] is positive, then wetting will occur spontaneously. Here γ represents surface energies, the subscripts S refers to solid and L refers to liquid phases, and LS represents the liquid-solid interface.

$$S = \gamma_S - (\gamma_L + \gamma_{LS}) \qquad (4\text{-}2)$$

Harkins and Feldman[170] noted that free surface energy of solids is usually larger than liquids e.g. silica has a surface energy (γ_S) of 287 mJ/m^2, whereas water has surface energy of 72.2 mJ/m^2, the spreading coefficient is likely to be positive assuming γ_{LS} to be small.[171] Silica is indeed thoroughly wetted by water. Organic materials such as

polymeric phases have usually lower surface energies than inorganic materials. In other cases, especially for aqueous dispersions, wetting agents such as neutral, cationic, or anionic surfactants will usually lower γ_L and γ_{LS}. For instance, porous graphitic carbon phase (PGC), which is not wettable by water at all, forms a stable suspension in the presence of neutral surfactants such as Igepal. As Table 4-2 shows, surfactants such as Tween 20 (polyoxyethylene-sorbitan monolaurate), Igepal DM-970, sodium lauryl sulfate, and polyethyleneglycol mono(nonylphenyl) ether have led to significant improvement for packing C18 silica, bare silica, and ion-exchange resins in narrow bore tubes as well as capillaries.[152,153,166] Note that adding the surfactants may not be the first priority, since wetting agents not only affect the surface tension and viscosity but can also lead to an unstable suspension. Kirkland pointed out a very interesting solvent: hexafluoro-2-propanol (HFIP) which he termed as a "universal" slurry medium.[55] He postulated that the reason for the capability of HFIP to handle a wide variety of stationary phase types is that the molecule has low surface energy at one end from the halogen atoms, and high surface energy (hydroxyl groups) at the other side of HFIP. Thus, HFIP can "energy match" various stationary phase chemistries. Thus, Kirkland concluded "*high surface energy, polar unmodified silica requires methanol or some other high surface energy or polar solvent. Modified particles with much lower surface energy, such as C8 or C18 (which still contains many polar unreacted silanol groups), should be packed with a lower surface energy, less polar solvent such as tetrahydrofuran, methyl-t-butyl ether, or mixtures such as acetonitrile/chloroform.*"[55]

4.5.5 Viscosity and Density Considerations of Solvents and the Suspension

The viscosity and density of the solvent(s) both contribute to the suspension stability as predicted by the Stokes law on settling velocity v. For a suspension of porous particles of finite concentration, the settling velocity v is:

$$v = \frac{(1-\varphi)^{-\kappa} d_p^2 \{\varrho_p(1-\varepsilon_i) + \varrho_l(\varepsilon_f - 1)\} g}{18\eta} \qquad (\text{4-3})$$

where $(1-\varphi)^{-\kappa}$ is a hindered settling function of particles in suspension of volume fraction φ, ϱ_p and ϱ_l are the densities of the particle skeleton and the liquid, η is the viscosity of the liquid, and g is the gravitational constant. The ε_i is the particle porosity and ε_f is the fraction of a total particle volume.[172] The particle skeleton densities can be measured with a He based stereopycnometer.[172] The skeleton density of porous silica is 1.98-2.19 gm/cm^3.[172] From an examination of the modified Stokes law (equation 5-3) for the settling of porous particles, it is clear that a lower particle density and a higher solvent viscosity will prevent settling. This concept led to use of balanced density methods (now obsolete because of toxicity concerns of brominated solvents). A better metric for choosing solvents systems is their kinematic viscosity $\frac{\eta}{\rho}$ rather than individual density or viscosity values e.g. acetone, chloroform, methanol, and isopropanol (IPA) have kinematic viscosities of 0.41, 0.38, 0.745, and 2.7 cSt, respectively. Thus, a suspension made in pure IPA will settle very slowly, but it will also be very viscous and will pack extremely slowly with small particles. Often peak shoulders are observed in very viscous suspensions when packed at medium pressures of 10,000 psi. Binary solvent mixtures offer greater flexibility in tuning the density, viscosity and surface energies of the slurry system. For example, adding acetone to IPA in 1:1 ratio would bring its viscosity from 2.6 down to ~ 0.6 cSt which can offer higher flow rates under constant pressure packing. Perhaps, the "universal" nature of hexafluoro-2-propanol (HFIP) as a

suspension medium is due to its high density 1.596 g/mL which is closer to silica and low viscosity 1.03 cP (compare from water 1 cP).

4.5.6 Non-Newtonian Behavior of Suspensions

In the previous section, the physicochemical properties of neat solvents or their mixtures were highlighted. The particle concentration affects the surface tension as well as the viscosity of the suspension.[173] If we express volume fraction ϕ of particles in a suspension as the *volume occupied by particles/total supension volume* , then the relative viscosity η_{rel} (compared with the pure solvent system), as the particle concentration increases, the relative viscosity of suspension becomes a higher order polynomial function as shown in equation 5-4.[174]

$$\eta_{rel} = 1 + B\phi + B_1\phi^2 + \dots \qquad (\text{4-4})$$

where, B is a constant. This relationship shows a faster viscosity increase as the particle concentration is increased. In reality, most suspensions are non-Newtonian which implies that their viscosity is dependent on the flow rate (or shear rate). One can estimate the shear stress τ and the wall shear rate $\dot{\gamma}$ under constant velocity conditions with a pressure drop ΔP in a tube of radius *r* and flow rate of *V/t.*:[175]

$$\tau = \frac{\Delta P r}{2L} \qquad\qquad \dot{\gamma} = \frac{4}{\pi r^3}\left(\frac{V}{t}\right) \qquad (\text{4-5})$$

Only three papers have paid attention to practical rheology, in detail, in column packing and with non-Newtonian suspension behavior.[57,153,175] The suspensions which become very viscous with flow rate are shear thickening and the ones which drop the viscosity are shear thinning (Figure 4-8). Paradoxically, *all* non-aggregating solid suspensions, which often produce the highest plates, display reversible shear thickening under the right conditions.[176] These conditions are dependent on particle properties (size

80

distribution, shape, particle-particle interactions), continuous phase viscosity and the

nature of suspension deformation (extensional or shear type).[176] On the other hand,

agglomerated suspensions can have permanent clusters (flocculates), and are typically

shear thinning. Light scattering experiments (using Bragg diffraction) have shown that

there is microstructural changes when suspensions make transitions from Newtonian to

non-Newtonian behavior; these changes are referred to flow induced order-disorder

transitions (Figure 4-8).[174] The term hydroclusters is used to describe this localized flow

induced suspension density variations (which can form in protic/aprotic solvents). These

rheological ideas are summarized by Barnes.[176]
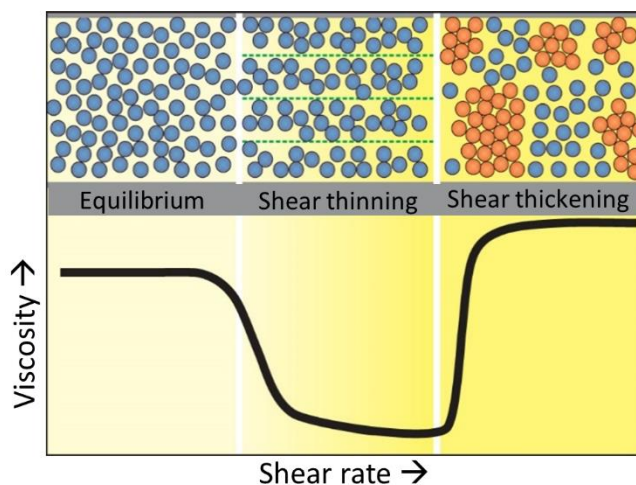
Figure 4-8. The change in the microstructure of a suspension explains the transition to shear thinning and shear thickening. In equilibrium, random collisions among particles make them naturally resistant to flow. But as the shear rate increases, particles become organized in the flow, which lowers their viscosity (shear thinning). At yet higher shear rates, hydrodynamic interactions between particles dominate over random collisions and the viscosity increases significantly (shear thickening).

4.5.7 Fundamental Problems with Narrow Diameter Columns

Herein a fundamental issue with narrow diameter columns is highlighted, which

are increasingly becoming popular because of LC-MS compatibility. Improved detection

sensitivity (less dilution of the injected band) when operated at the same linear velocity as

a wider bore column, saving of solvent and expensive stationary phase are additional benefits. Unfortunately, narrow bore columns present significant theoretical and practical challenges. From the following equation 5-6 obtained from solving the diffusion problem in 3 dimensions in an empty tube, two critical problems in narrow bore columns are discussed.[177]

$$C(r,z,t) = \frac{M}{(4\pi t)^{3/2} D_t \sqrt{D_a}} \exp\left[\frac{-(z-ut)^2}{4D_a t} - \frac{r^2}{4D_t t}\right] \qquad (\text{4-6})$$

where C is the analyte concentration, r, z are radial and axial coordinates at time t, M is injected mass, D_t is the dispersion coefficient in the radial direction and D_a is the dispersion coefficient in the axial direction, u is the linear velocity. The first problem pertains to the limiting case of the last term in the equation 6, $(4D_t * dead\ time) \ll r_c^2$, where r_c is the column radius. This situation corresponds to the elution time being smaller than the time to "see and explore" the total radius of the column. Herein, the influence of packing heterogeneities near the wall is negligible but the flow path distribution at the inlet and the outlet of the column is not (hence the importance of frits). The problem is clearly illustrated in Figure 4-9, where the low retention band traveling in center has a separate velocity as well as a separate band shape compared to the wall. It is now well established as to why a non-Gaussian peak shapes arise due to velocity bias around the column walls.[178] It can be shown that there is significant velocity bias in the center and the wall by implanting electrochemical detectors at radial positions on the column outlet.[177] Such wall effects were well known in chemical engineering 50 years ago.[179] The "wall region" extends to 30-50 particle diameters. Conversely, if $(4D_t * dead\ time) \gg r_c^2$, this implies that solute spends enough time in the column to reach radial equilibration and "see and explore" the walls. This case pertains to narrow (capillary like) columns.

82

Counterintuitively, one rarely sees fronting or tailing in packed capillaries, rather the peaks are symmetrically broad.[137] Any distortion introduced by the heterogeneity near the walls is compensated by the trans-column diffusion. Two types of wall effects were recognized and understood much later in chromatography.[180] The first is the geometrical wall effect just because the particles cannot penetrate the walls; the second wall effect is the oscillation in the porosity of the bed as one goes from wall towards the center.[181,182]
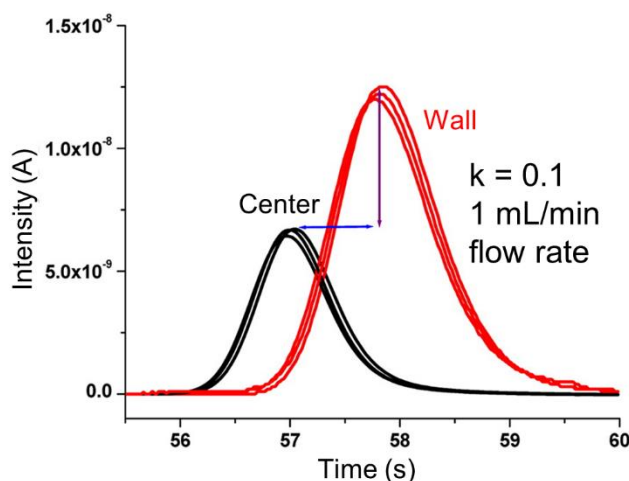
Figure 4-9. The velocity bias between the wall region and the center of a radially heterogeneous packed bed (packed by the manufacturer). Sample: p-benzoquinone, recorded by electrochemical detection at the center and the wall of the outlet frit. Column: 10x0.46 cm i.d. Kinetex-C18 2.6 μm SPP. MP: 30/70 water/methanol, k = 0.1.

4.6 Practical Insights into Packing High Efficiency Analytical and Capillary Columns

This section will discuss the practical considerations in slurry packing of capillary and analytical columns while providing a useful set of guidelines. These concepts have been developed after an experience of packing of over 17 different surface chemistries (see Table 4-1). The chemistries comprise chiral, HILIC, polymeric, reverse phases, silica based ion-exchangers, zwitterionic phases, porous graphitic carbon, π-complex phases, and carbon clad zirconia particles in analytical/narrow bore formats. The flow chart in Figure 4-10 is a general outline for packing when starting with a new stationary phase. If prior information on the packing procedure is not available, one can start by picking 5

slurry solvents (use HPLC grade/anhydrous solvents) from Table 4-2 after thoroughly

cleaning, defining, and drying (if applicable) the stationary phase and the hardware. It

may be useful to determine the charge on the stationary phase, if dealing with hydrophilic

chemistries or polar chemistries by zeta potential measurements. Fines, if visible in the

SEM, can be removed by suspending the stationary phase in a low viscosity solvent in a

container such as a 1 L Schott bottle. Solvents such as hexane, methanol, or water (if

polymeric particle is used) can be cleaned of light debris, and colloidal particles if used to

suspend the material. If one sees signs of flocculation, another solvent must be chosen

since all large and small particles will settle together. It is better to use a dispersing

suspension. The suspension is sonicated and allowed to settle for few hours or overnight.

The supernatant is carefully discarded by suction with a Teflon tube connected to a

vacuum flask. The process can be repeated again. Decantation can disturb the bed and

should be avoided. *There can be significant loss of material* and the number of steps

should be kept to a minimum for removing fines. ***A note of caution***: Presence of

moisture in the stationary phase, high humidity, or moisture in the hardware can result in

poor efficiency especially with halogenated solvents because of particle aggregation.[183]

For some charged polymeric phases, organic solvents cannot be employed (because of

swelling), there even pure deionized water as suspension medium can produce reduced

plate heights of < 2.[57]

Clean, remove fines and dry* the stationary phase

Prepare 5 solvent systems based on the surface chemistry (see Table 1 for examples)

Perform optical microscopy of suspensions (0.1-0.5% w/v) and classify the dispersion
Each particle separate → fully dispersed, Few particles clumped → partially agglomerated, All particles clumped → fully agglomerated
Additional tests: settling in Wintrobe tubes, vial settling test, filament test, shear thickening test

2.0 to 4.6 mm i.d. columns | 30 to 400 μm i.d. capillaries

Left branch (2.0 to 4.6 mm i.d. columns):

Choose a fully dispersed and a slow settling suspension

Begin trial pack with initial conditions choose 7-10% w/v suspension, apply ~1000 psi/cm bed length, pack for 1 hour

Test an unretained and a retained analyte

Perform total peak shape analysis (Figure 7)

Low N (h>>3) | High N (2≤h<3)

Broad Gaussian or tailing peaks

Fronting, shoulders on left, Minimal tailing

Tailing, minimal fronting

Change slurry concentration

Choose another slurry system, ensure moisture removal in solvents, particles, and hardware*

+5% w/v increment

-5% w/v reduction

Optimize until peaks are assessed to be symmetric via the total peak shape analysis

Study the effect of pressure increase (increments of 100-200 psi per cm bed length)

Expose the column to its maximum intended flow rate for 30 min and study bed stability

Right branch (30 to 400 μm i.d. capillaries):

Choose partially or fully agglomerated suspension for reversed phases. For other phases, try both agglomerated and dispersed suspension medium

30 to 75 μm i.d. | 100 to 400 μm i.d.

1-2% w/v suspension, apply 2000-3000 psi/cm bed packed

Begin trial pack with initial conditions

2-5% w/v suspension, apply 1000-2000 psi/cm bed packed

Test an unretained and a retained analyte

Perform total peak shape analysis (Figure 7)

High N (2<h<2.5) | Low N (h>>2)

Study slurry concentration effect until h ≤ 2 (up to 20% w/v)

Choose a different suspension system

Study the effect ultrasonication on capillary during packing with high slurry concentrations

Expose column to its maximum intended flow rate for 30 min and study bed stability

*Drying is not important if aqueous slurries are used

Figure 4-10. The flow chart for logical optimization of slurry packing.

Once a suitable choice of the solvent system is made from preliminary judgements of density, viscosity, and wettability; optical microscopy of the suspensions should be performed. It is the most useful qualitative predictor of packed column's performance. Figure 4-11 shows a comparison of microscopic images of two silica and a polymeric stationary phase in dispersed and agglomerated forms. To perform optical microscopy, place few drops of a dilute suspension and observe the suspension near the edges of the cover slip. The evaporating liquid (at the air interface) causes motion in the suspension and one can easily see how the particles would travel during the column packing process. One major problem occurs when the solvent's refractive index matches

85

with that of silica (e.g. CCl_4 + silica). In such cases, small amounts of other solvents can be added until the particles are visible. A slurry that promotes dispersion of particles would pack in a "layer by layer" fashion forming a random closed packed structure and resulting in a tightly packed high-efficiency column at high flow rates. Oppositely, an agglomerated slurry can induce packing of stationary phase particles in clusters leading voids in the beds. For capillaries, we wish to point out a stark difference for C18, where agglomerated suspensions followed by sonication have produced the best results.[56,136] Unfortunately, there are very few packing details published on other stationary phase chemistries in capillaries. For now, it may be useful to keep the "world" of capillaries separate from the narrow bore and analytical columns.
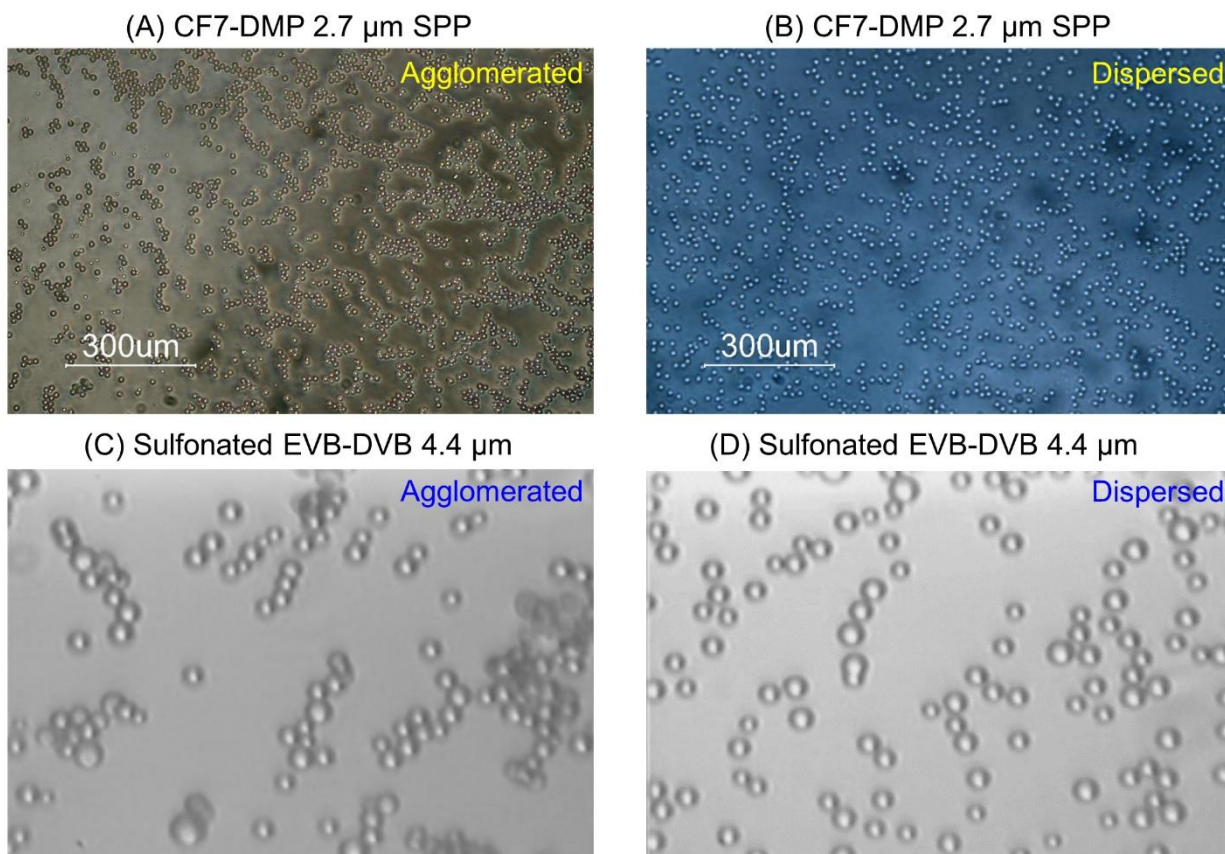
Figure 4-11. Optical microscopy of stationary phase suspensions. Derivatized cyclofructan-7 bonded to 2.7 µm SPP in (A) 98:2 methanol:1M NH4OAc – agglomerated slurry and (B) 1:1 CHCl$_3$:IPA – dispersed slurry. A suspension of 4.4 µm non-porous sulfonated ethylvinylbenzene-divinylbenzene in (C) 0.1M MgCl2 – agglomerated slurry and (D) Deionized water – dispersed slurry.

A settling test or vial test,[57] should be performed by letting a sonicated suspension settle and monitoring the nature of the bed so formed in small vials or better in Wintrobe tubes (narrow test tubes with a length scale). A vial test example is shown in Figure 4-12 for sub-2 µm FPP C18 silica. After settling, the vial can be tilted and rotated for bed examination.[57,130] Note: Very low viscosity suspensions, such as those made in acetone and dichloromethane, can settle very fast (e.g. 2 µm SPP silica) and the settled bed may appear to be loose, but the microscopic examination will reveal that the

suspension is still very dispersed. A loose bed (or lager height in a Wintrobe tube) is an excellent test of a poor solvent system. As a caveat, very dispersive suspensions but in a low viscosity solvent (acetone/dichloromethane system) may settle very fast yet yield excellent columns.

Figure 4-12. 1.9 µm C18 fully porous particles (Titan) suspended in ethanol. The particles are allowed to settle after sonication (preferably overnight) and the bed is examined by tilting the vial. Note how the bed slides down the base of the vial. A loose bed (shown above) is an indicator of a bad slurry. Indeed, EtOH produced very poor columns regardless of the slurry concentration (80,000 N/m plates vs. 210,000 N/m plates using a dispersive suspension).

Settling speed alone is not a good predictor. An excellent review for shear thickening in non-aggregating suspensions is given by Barnes.[176] The phenomenon itself is very complex, perhaps not fully understood to date. Although in future studies, suspension rheology will eliminate many problems in column packing. However, currently, one can propose only qualitative tests. Shear thickening and its effects on column packing was first demonstrated by Wahab et al. in ion-chromatography.[57] The phenomenon of shear thickening can be observed easily with concentrated corn starch dispersed in water. If concentrated enough, when force is applied to the surface, the corn starch surface becomes solid and difficult to break through. However, surface can be easily manipulated with hands. A simple rheological test to determine shear thickening in

a given solvent, referred as "the filament test" or "test on a spatula", can be done as follows. One can make a very concentrated suspension by adding few drops of slurry solvent on the stationary phase in a vial. Quickly moving a thin spatula, one can notice the resistance offered by suspension in the motion of the spatula, followed by drying/cracking. As the motion is stopped, the suspension becomes *wet and shiny* (from the so-called dilatancy effect)*.* Lifting the spatula from such suspensions forms a flowing filament (an indication of shear thickening system) as seen in Figure 4-13.

Figure 4-13. A thick suspension of C18 1.9 μm FPP silica showing a filament formed when picked up with a pipette.

After choosing the slurry, carefully pour the sonicated suspension into the slurry chamber (*e.g.* with a syringe), the top-up solvent should be very carefully trickled into chamber without disturbing the slurry concentration. The first column can be packed as a trial based on the initial parameters suggested in Figure 4-10. The criteria for choosing a push solvent are given in Table 4-3. It should not be very compressible at the packing pressures nor denser than the slurry itself. For instance, if hexane is chosen, at 10,000

psi, it will be compressed as 158×10^{-6}/bar. We prefer a pressure ramp starting from 0 psi to the final pressure (in 10-20 seconds) for safety and improved reproducibility. The packing pressure is typically chosen to be at least twice (or thrice) the operating pressures. We consistently see a significant efficiency loss, if the packing pressure is similar to the operating pressure especially in short columns. In general, for 4.6 mm i.d. columns, 10,000 to 12,000 psi is sufficient, whereas narrow bore columns are typically packed at 16,000 psi to 30,000 psi for particle sizes < 5 μm silica or other inorganic oxides. Polymeric/carbonaceous materials cannot handle this pressure. Once the column is packed, the system should be allowed to come to the atmospheric pressure and the column should be removed as soon as possible, flattened with a blade knife, and fitted with a frit. An unretained solute peak and a well retained solute peak should be analyzed for plate count and a total peak shape assessment should be performed.[48]

Table 4-3. Criteria for choosing push solvents

(a) Degassed solvents with relatively low compressibility at high pressures (> 10,000 psi) and low viscosity e.g. acetonitrile, MeOH, isooctane, toluene, hexane, acetone, hexane:IPA, or in some cases with aqueous slurries, pure water can be used.
(b) Ideally, agglomerating solvent for the stationary phase
(c) Density should be lower than the solvent blend used in the chamber so that the push solvent floats on the suspension

4.6.1 Total Peak Shape Analysis after Packing Experiments

During packing experiments, one may obtain non-Gaussian peak shapes. The departure from Gaussian shape of an unretained analyte is a manifestation of flow heterogeneity problems from poor velocity distribution in the packed bed (Figure 4-14). In Figure 4-14A, a peak with concurrent fronting and tailing is shown, the asymmetry of which is not identifiable by asymmetry factors such as USP tailing factor As.[48] However, with use of Gaussian superimposition at the peak top, one can detect concurrent fronting

and tailing. The example shown in Figure 4-14B is a seemingly symmetric peak which only shows its concurrent slight fronting in addition to tailing when analyzed with Gaussian superimposition.
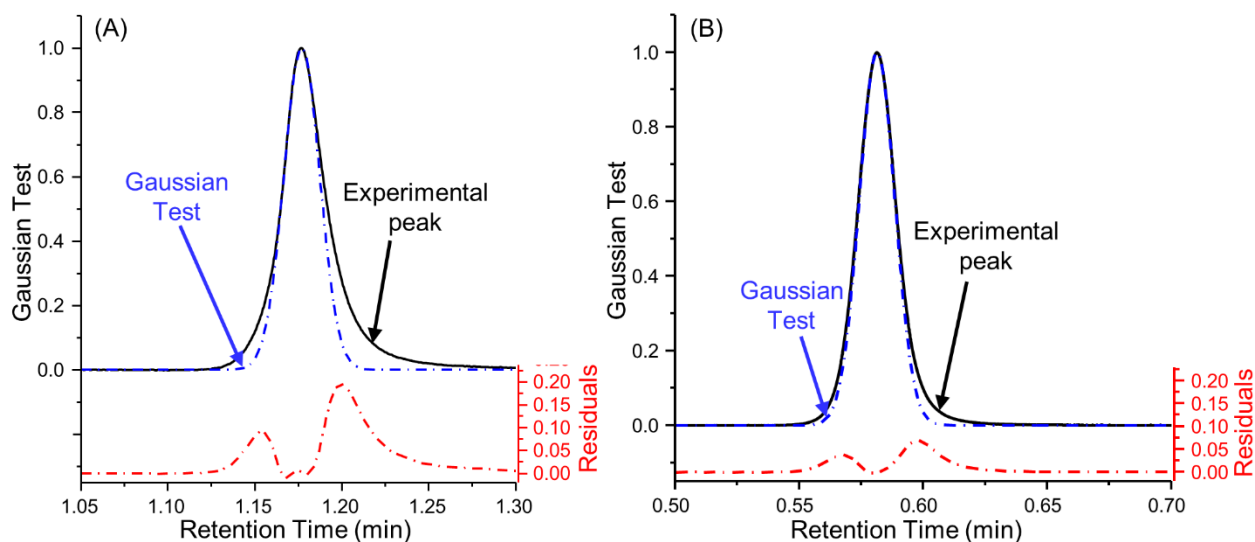
Figure 4-14. Gaussian test applied to experimental peaks for testing a peak shape after column packing. The peaks show concurrent fronting and tailing which remain undetected by the USP tailing factor. The residuals here show the problematic regions of the peaks (A) Column: teicoplanin bonded 2.7 μm SPP (15x0.21 cm i.d.). Analyte: 1st eluting enantiomer of 5-methyl-5-phenylhydantoin, (B) the bottom 5 cm section of a long column packed with 2.7 μm SPP silica in IPA slurry. Analyte: uracil. Retrieve the total peak shape analysis template from ref [48].

4.7 Practical Insights with Illustrative Examples

Illustrative examples based on fundamentals discussed above will be demonstrated below. The general principles are straightforward and applicable to virtually all stationary phases. All columns were packed with a pneumatically driven Haskel (DSHF-202) pump using slurry chambers (10, 20, 40, 80 mL) from Scientific Systems Inc. (USA) and pushed with either methanol or acetonitrile. The packing hardware utilized in all experiments was similar to that shown in Figure 4-2, except that the push solvent entered vertically through a flow distributor. The glassware/ apparatus was oven dried

91

and disposable Norm-Ject syringes (Henke Sass Wolf) were used for volume measurements of solvents. All slurry concentrations reported in this work are %w/v as g/mL. Chromatography was performed on an optimized Agilent 1290 Infinity series UHPLC.[52,184] As suggested in the flow chart, the SEMs revealed the absence of fines or broken/cracked particles in the silica used in the following experiments. The efficiencies of the peaks were calculated by the half-height method whereas distorted peak efficiencies were determined by the second moments (Agilent OpenLab). The peak asymmetries (As) are based on the USP tailing $W_{0.05}/2f_{0.05}$, where $W_{0.05}$ is the width at 5% peak height and $f_{0.05}$ is the distance from the leading edge to the peak maximum at 5% peak height. The results and phenomena discussed below were found to be reproducible (data not shown).

4.7.1 Dispersed Slurries Produce Better Columns

Figure 4-15 shows a very important and general phenomenon that has a profound effect on the column performance. It is postulated that dispersed suspensions should pack "layer by layer" producing a uniform bed without channeling or voids resulting in high-efficiency columns. On the other hand, agglomerated suspensions can pack as "loose clumps" piling up on each other resulting in a loose bed. Intuitively, one would expect to have more voids in such a bed structure. These concepts are shown using a 2.7 μm SPP dimethyl phenyl cyclofructan-7 bonded chiral (polar) stationary phase and a 1.9 μm FPP bonded C18 silica (Figure 4-15). Additionally, two different column geometries were chosen to illustrate the key differences between agglomerated and dispersed suspensions. As pointed out earlier, a dispersed and agglomerated suspension will have the opposite rheological behaviors, shear thickening and shear thinning, respectively.[185] To obtain a dispersed suspension, various combinations of several organic solvents (chosen from Table 4-2) were assessed via microscopy (Figure

92

4-11A,B), sedimentation, and shear thickening test. It was found that a mixture of 1:1 chloroform/IPA provided a dispersed slurry and 98:2 MeOH/H_2O (ammonium acetate) agglomerated the particles. The kinematic viscosities of 1:1 chloroform/IPA and 98:2 MeOH/H_2O are 0.58 and 0.76 cSt, respectively.[186,187] A trial packing was performed with 5% w/v concentration at 10 000 psi in a 5 cm × 0.46 cm i.d. column. Figure 4-15A,B shows the peak profiles from a dispersed and agglomerated slurry, respectively. Although identically packed otherwise, a change of slurry dispersion state provided more symmetric peaks with 178 000 N/m and $h = 2$ (Figure 4-15A), while the agglomerated slurry produced only 77 400 N/m (Figure 4-15B) and $h = 4.8$ which is a ~60% decrease in efficiency.[52] The lower backpressure of the agglomerated slurry column also indicates a more loosely packed bed.

5 x 0.46 cm i.d. CF7-DMP 2.7 µm SPP

(A) 178,000 N/m A_S = 1.12 — Dispersed ΔP = 116 bar

(B) 77,400 N/m A_S = 1.27 — Agglomerated ΔP = 112 bar

10 x 0.21 cm i.d. C18 1.9 µm FPP

(C) 105,000 N/m A_S = 1.79 · 217,000 N/m A_S = 1.18 · 206,000 N/m A_S = 1.02 — Dispersed ΔP = 218 bar

(D) 41,500 N/m A_S = 1.72 · 97,300 N/m A_S = 1.37 · 142,000 N/m A_S = 1.18 — Agglomerated ΔP = 208 bar
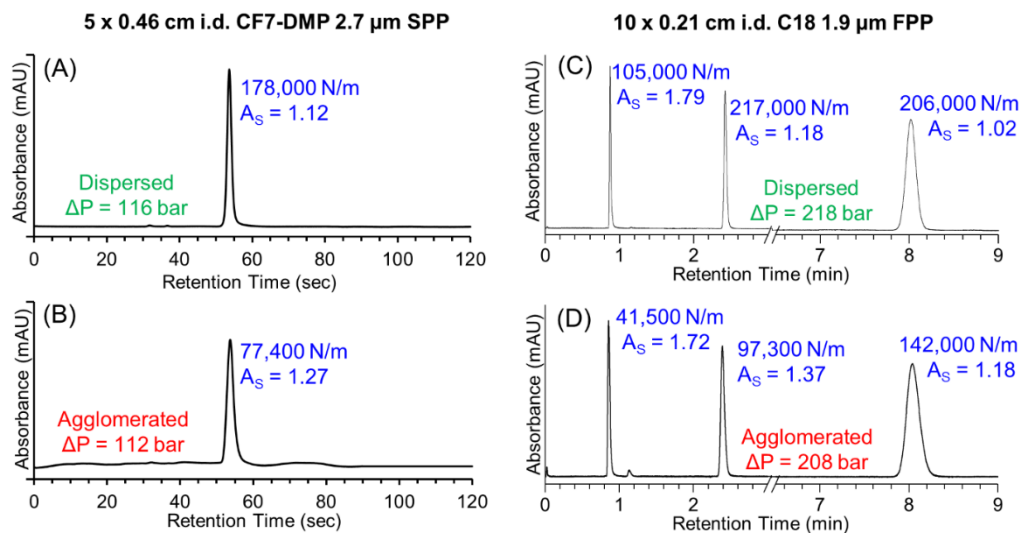
Figure 4-15. Performance comparison of dispersed vs. agglomerated slurries on analytical and narrow bore columns with different surface chemistries. (A) and (B) show the 5x0.46 i.d. columns packed with 2.7 µm SPPs bonded to cyclofructan-7 dimethylphenyl carbamate (CF7-DMP) analyzed with 1,3-dinitrobenzene using 70/30 heptane/EtOH at 1.0 mL/min. (C) and (D) show the 10x0.21 cm i.d. columns packed with

C18 bonded 1.9 µm FPP silica analyzed using a mixture of uracil, 1,3-dinitrobenzene, and biphenyl (in order of elution) using 60/40 ACN/Water at 0.2 mL/min.

For an achiral example, a 1.9 µm FPP silica C18 was packed in 10 cm × 0.21 cm i.d. columns. Using a procedure similar to that described for 4.6 mm i.d. columns, two slurry mediums were used that provided a dispersed slurry (85/15/0.1 $CHCl_3$/MeOH/formic acid; literature value of kinematic viscosity of 85/15 $CHCl_3$/MeOH[188] is 0.38 cSt) and an agglomerated slurry (absolute EtOH, kinematic viscosity 1.51 cSt) under an optical microscope. Using 8% w/v slurries, two 10 cm × 0.21 cm i.d. columns were packed at 12 000 psi, and their performance comparison is shown in Figure 4-15C and D. The dispersed slurry produced far greater number of plates (217 000 N/m) as compared to the agglomerated slurry (142 000 N/m, a ~35% decrease). Also apparent are the significantly enhanced peak symmetries for dispersed slurries while the agglomerated slurry shows more tailing. The remarkable efficiencies seen in Figure 4-15C far outperform the specifications of many 10 cm × 0.21 cm i.d. C18 columns from major manufacturers (170 000 N/m). Consistent with our postulate on agglomerated suspensions forming a loose bed, the agglomerated slurry column showed a 10 bar lower (~5%) backpressure.

Note that in each successful case of dispersed suspensions, the *additional benefit* comes from the low kinematic viscosities of chloroform-IPA and chloroform methanol (<1 cSt) with relatively high densities, which is consistent with our discussion on choosing appropriate solvent systems. In contrast, simply choosing a low kinematic viscosity solvent such as hexane/pentane/acetone will not produce a good column. Additionally, our previous experience with Hypercarb, polymeric cation exchangers, fully porous (1.9–5 µm) and core-shell particles of various sizes (1.5–2.7 µm) convincingly

94

illustrate the advantages of using dispersed suspensions producing near theoretical plate height of two particle diameters.[52,57,127,128,130,131]

4.7.2 Can Agglomerated Slurries Ever Produce Good Columns in Analytical or Narrow Bore Formats?

In our experience[52,57] and that of others,[35] analytical and narrow bore columns packed with agglomerated suspensions of particles have invariably performed poorly (as shown in Figure 4-15), regardless of the stationary phase chemistry. The failure rate is very high but occasionally one might obtain acceptable efficiency. However, reproducibility of such experiments is very low. For example, aqueous slurries of 4.4 μm sulfonated ethylvinylbenzene-divinylbenzene in the presence of Al^{3+}, Mg^{2+}, and Na^+ ions which caused particle agglomeration (Figure 4-11C) always produced very low efficiency columns. When pure DI water was used, it dispersed the particles because of their high negative zeta potential (−52 mV) and produced high efficiencies.[57] Silica has a very negative zeta potential in water (−56 mV) implying a highly charged surface; hence, it is difficult to agglomerate. For the native 1.9 μm FPP silica, no suitable slurry solvents could fully agglomerate the silica particles except toluene, which produced permanent flocculates. Similarly, 1.9 μm fully porous silica when packed using pure THF (∼23% w/v slurry concentration, agglomerated) into 5 cm × 0.3 cm i.d. columns produced very low plate counts (83 800 plates/m). A mixture of oleylamine and hexadecyl-trimethylammonium bromide, when added in EtOH, *partially* agglomerated the silica particles. The adsorption of the surfactant and amine on the surface can produce a pseudo-C18 like phase. A 5 cm × 0.21 cm i.d. column packed with this 18% w/v slurry at 8 000 psi produced 200 000 N/m in a 2.1 mm i.d. column with slight tailing (see Figure 4-16). A similar attempt for a positively charged phase hydrosilylated quinine (2.7 μm

95

SPPs) failed in agglomerated suspensions. This stationary phase provided high efficiencies (180 000 N/m), when packed with a dispersive suspension of chloroform/IPA.[128] Our recommendation is to start with dispersed slurries for quickly optimizing column packing processes. Partially agglomerated suspensions, especially of ion-exchangers, may produce good columns. For the capillaries, researchers have shared with us[137] that partially dispersed or high concentration suspensions produce very high efficiencies with theoretically expected plate heights $H = 2d_p$ (see more discussion in the following sections) especially with C18 phases.
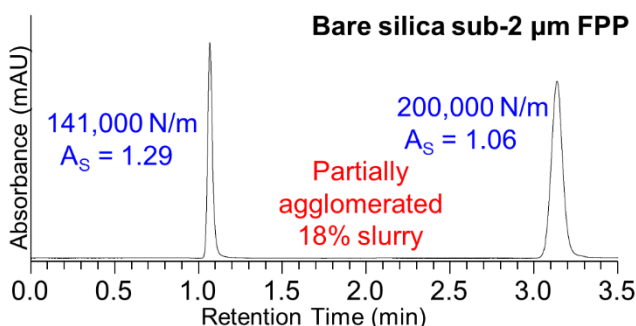
Figure 4-16. Performance of agglomerated slurries for polar 1.9 μm bare silica packed in 5 x 0.21 cm i.d. column with 18% w/v/w 100/0.1/0.075 EtOH/oleylamine (assay: 80-90% C18 content)/hexadecyl-trimethyl-ammonium bromide slurry. Analyzed using a mixture of uracil and cytosine (in order of elution) with 90/10 ACN/100mM NH$_4$OAc at 0.2 mL/min.

4.7.3 No Column is Axially or Radially Homogeneous

Figure 4-17 shows interesting examples of a long 0.46 cm i.d. column packed with 2.7 μm bare SPP silica. The IPA slurry was chosen because it dispersed the particles; however, it does have a high viscosity to density ratio (2.6 cSt). Three 5 cm × 0.46 cm i.d. columns, connected in series, with unions were packed at 10,500 psi using a 4.3% w/v suspension. In general, high viscosity and dispersive suspensions are shear thickening and often produce fronting peaks due to high shear rate at the column walls.

96

Qualitatively, IPA suspension of SPP particles displays shear thickening effect when a dense suspension is with a spatula. The question arises if a column performs poorly, is the entire column bad or are only certain sections of it. Figure 4-17 shows the chromatographic performance of three sections. There are several remarkable features in the figure: (a) the bottom column section shows the highest back-pressure and poorest column efficiency (b) and the top column shows (generally lower pressure) and comparable efficiency (within error) to the middle section. We also observed that the top section is metastable i.e. high efficiency but the bed settles with time. This is consistent with the fact that the top column section experiences the least force under constant pressure mode. In fact, the total column length dictates which sections of a column will perform the best, e.g., for a 15-cm column, the bottom and the middle sections were the best as shown previously.[158] However, the authors employed 10 μm C18 silica particles using acetone suspensions and no detail on column interfacing was provided. Our studies with 2.7 μm SPPs (bonded or nonbonded) showed that bottom sections always perform poorly regardless of chosen slurry solvent than the middle or top sections for 15 cm formats. In the constant pressure mode, the initial flow is very fast but drastically decreases as the hydraulic resistance increases from the packed bed. In a constant flow mode, the pressure builds up as the bed is formed while the flow remains constant. In each case, the entire column does not experience the same pressure drop. The smaller asymmetry of the bottom section (A_s = 1.24) is *deceptive* because the peak is both fronting and tailing as revealed by the total peak shape analysis (Figure 4-14B).[48] Performing the total peak shape analysis reveals interesting properties of the sections. The bottom section, which packs the fastest in the constant pressure mode, has the highest contribution from fronting to the overall peak distortion. This contribution decreases with middle section and is the lowest for the top section. This trend is

consistent with Equation(4-5 ($\dot{\gamma} = 4V/\pi r^3 t$), which shows that the shear rate will be highest at the walls and high shear rate (high flow) will produce shear thickening effects in a viscous suspension, such as IPA. This implies that the wall region is different from the bulk packed region making it radially heterogeneous as well. Alternatively, instead of section packing, one can do peak parking experiments to assess which part of a column is "bad" along its entire length from the shape of the distorted peak.[189]
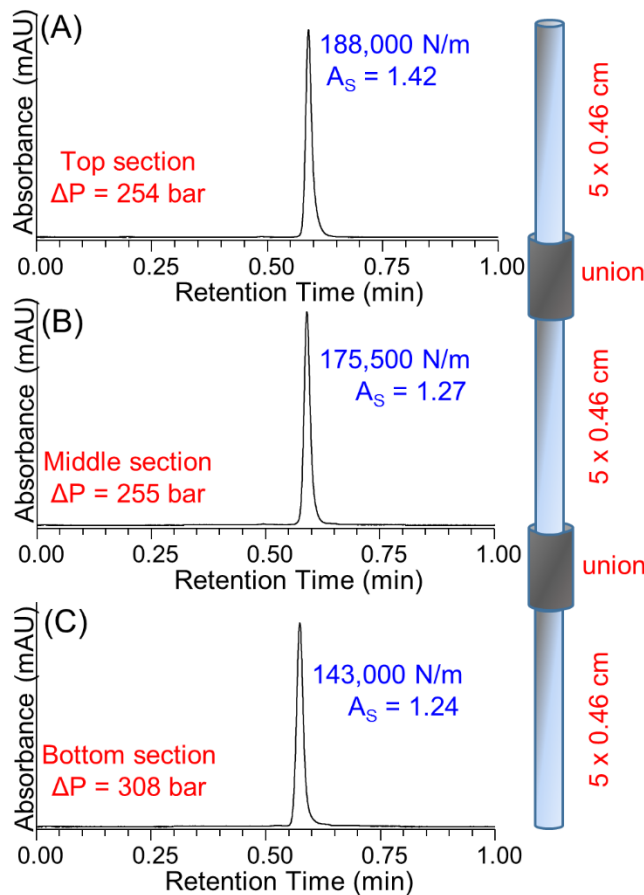
Figure 4-17. Packing homogeneity of various parts of a column investigated through packing of 2.7 μm SPPs in 5x0.46 cm i.d. columns in series using a 4.4% w/v IPA slurry at 0-10,500 psi final pressure and evaluated chromatographically individually. Sample: uracil. Mobile phase: 1:1 MeOH:Deionized Water, 1.0 mL/min, 254 nm.

4.7.4 Narrow Bore Columns are Not Easy to Pack

In narrow bore columns, the wall effects can easily affect the column efficiency resulting from the proximity of the column wall to the injected band. One can roughly estimate the time it takes for radial equilibration as ($d_c^2/4D_t$). It can be shown,[177] with L/u of <50 s, in a 2.1 mm i.d. column, it will take 1000 s for an analyte to reach the walls, whereas for a 4.6 mm i.d. column, it will take 5000 s. Since the wall region is "different or heterogeneous" in the packing structure than the rest of the bulk, narrow bore columns usually offer lower plates than their 4.6 mm i.d. counterparts.

From a practical perspective, narrow bore columns typically show two major problems, namely, higher permeability (which implies loose packing) and up to 40% lower plates as compared to their wider bore counterparts (3 or 4.6 mm i.d.), even in the absence of extra-column effects. Note that all the packing phenomena in going from a 4.6 i.d. to 2.1 mm i.d. remain the same. As we decrease the diameter, for the same pressure, the *absolute* force decreases since force = pressure × area. Not only the absolute force but linear velocity changes with the column diameter. Thus, narrow bore columns with sub-2 μm particles are often packed at 15 000–30 000 psi in industrial settings. However, this might be an "overkill" situation since medium pressures with the right slurry choice may be adequate to form a random closed packing and further pressurizing may simply decrease the permeability. Figure 4-18 shows the difference in peak shape distortion as the column diameter changes from 4.6 mm to 3 mm i.d. after being packed with 1.9 μm FPP silica using the same conditions (3.4–3.5% w/v, 80:20 IPA/CHCl$_3$). It is clear, that the 3 mm i.d. column shows significantly more distortion (what we refer to as a "foot" in the chromatographic peak) as seen from lower efficiency and USP tailing.
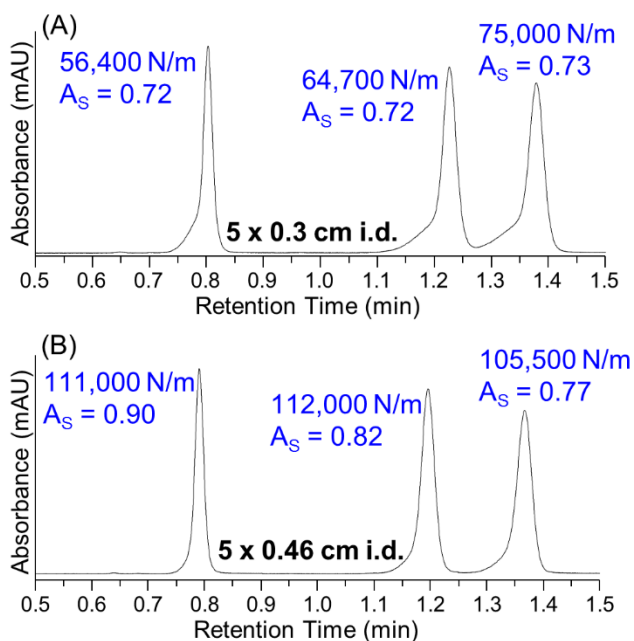
Figure 4-18. Enhancement of wall effects in a narrow and analytical bore columns packed identically with bare 1.9 µm FPP silica at 11,000 psi final consolidation pressure. (A) 5x0.3 cm i.d. column, 0.425 mL/min. (B) 5x 0.46 cm i.d. column, 1.0 mL/min. Mobile phase for both chromatograms was 80/20 ACN/25mM NH$_4$OAc. Sample: uracil, adenine, and cytosine (in the order of elution). Efficiency is calculated by statistical moments to account for peak shapes that strongly depart from the Gaussian profile.

Note that in this case, although the slurries were fully dispersed, the kinematic viscosity of 80:20 IPA/CHCl$_3$ is 1.9 cSt.[187] The density of the solvent system is 0.83 g/mL. As we stated in the theory section, high kinematic viscosity solvents can lead to fronting or peaks with "foot" on the leading edge. This is a consistent effect seen with many stationary phases and it is most likely a rheological phenomenon rather than stationary phase chemistry related issue. The cure is described in the next section.

4.7.5 Shear Thickening as a Kinetic Process: The Influence of Slurry Concentration on

Column Performance

Often dispersed suspensions produce a so-called "foot" on the front side of otherwise narrow peaks which probably arises from the shear thickening effects. The

100

peak efficiency in such cases, if calculated by half-height method in Figure 4-18, gives

226 000 N/m (h = 2.3). Shear thickening suspensions (dispersed) may lead to channeling

(thick suspension tend to crack), if given sufficient time during packing. Figure 4-19

shows a comparison of three different slurry concentrations on the performance of 5 cm ×

0.3 cm i.d. columns packed with 1.9 μm FPP silica using a dispersed slurry. It is apparent

that the lower slurry concentrations (3.5 and 10% w/v) led to low efficiencies (75 000–

89 200 N/m) along with a distinct foot on the leading edge of every peak. This systematic

behavior is an indication of channeling or cracks in the packed bed. Increasing the slurry

concentration is known to prevent formation of large voids in the packed bed and,

accordingly, as the slurry concentration is increased to 23% w/v, significantly higher

efficiencies (206 000 N/m) along with improved peak symmetries are noted. Our

hypothesis is that since shear thickening has a kinetic aspect, a 23% w/v suspension

packs the column very fast as compared to more dilute slurry concentrations, thus

mitigates the non-Newtonian behavior. This phenomenon is reproducible and general

rather than stationary phase specific. As indicated in the flowchart, Figure 4-10, it is

recommended to start with a 7–10% w/v slurry concentration for columns and further tune

the peak shape to make it symmetrical. If tailing is seen instead of fronting, the slurry

concentration can be lowered to prevent particle agglomeration. A question often brought

up is that whether by increasing slurry concentration in a dispersive medium, are we

essentially agglomerating the particles? This is a misconception because even with high

slurry concentration, optical microscopy shows that the particles are indeed separate

from each other. The particles are close but not flocculated (clumped); this criterion still

differentiates this concentrated suspension in a dispersive medium from an agglomerated

one.
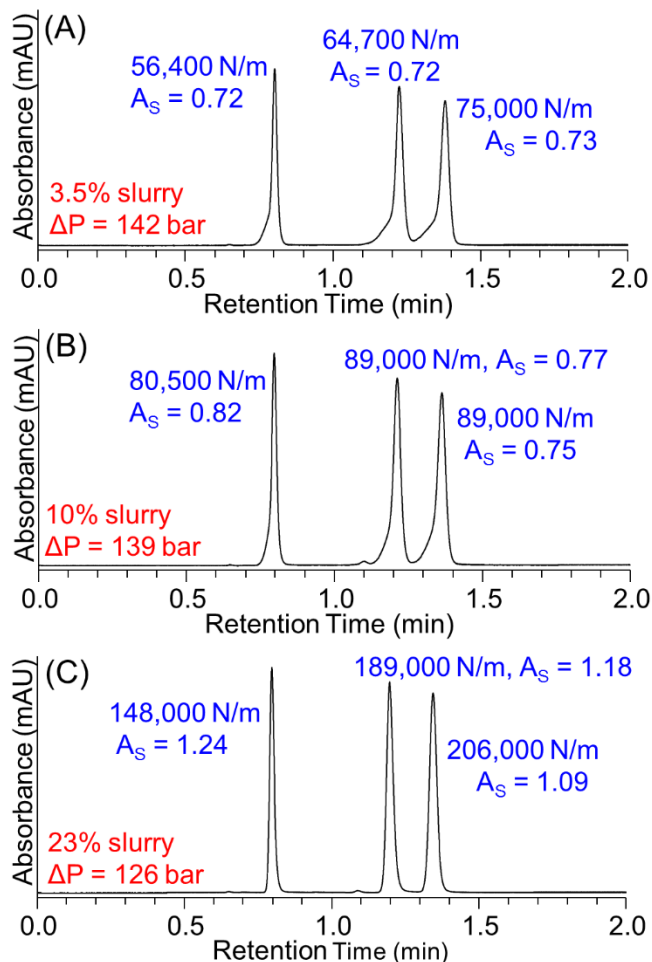
Figure 4-19. Effect of varying slurry concentrations on 5x0.3 cm i.d. columns packed with 1.9 μm fully porous native silica using a dispersed slurry of CHCl3/IPA using a pressure gradient 0-8,000 psi followed by 8,000-11,000 psi for 15 min each. Sample: mixture of uracil, adenine, and cytosine (in the order of elution). Mobile phase: 80/20 ACN/25 mM NH4OAc, 0.425 mL/min, 254 nm. (A) 3.5% w/v slurry concentration (B) 10% w/v slurry concentration (C) 23% w/v slurry concentration, N obtained using statistical moments.

4.7.6 Influence of Packing Pressure in Short Analytical Columns

The packing pressure is a factor that can be altered to affect the rate of bed

formation and the performance of the column as indicated in Figure 4-10. Besides

column efficiency, a packed bed should be stable to >1000 injections and the pressure

shocks it receives at every injection from valve switching. A dispersed slurry of 1:1

acetone/IPA (found using the approach in Figure 4-10 and solvents from Table 4-2) was

102

used to pack bare 2.8 μm SPP silica in 5 cm × 0.3 cm i.d. column at 5 000, 8 000, 10 000, and 12 250 psi, respectively. The column packed at 5 000 psi performed the best with 194 000 N/m followed closely by the columns packed at 10 000 and 12 250 psi which produced about 175 000 N/m (Figure 4-20). This experiment shows that very high packing pressures may not be necessary for packing narrow-bore columns, and even pressures as low as 5 000 psi can be adequate for a 5-cm column, since pressure drop per unit length is what matters rather than the absolute pressure value. However, if the short column is to be used at high flow rates, higher packing pressure should be employed. For example, a 5000 psi packed column should not be employed if the working pressures are ≥5000 psi. One practical exception for very high pressure packing is the guard columns (0.5–1 cm) which we still pack at 10 000 psi for 2 μm silica SPP or FPP (considering the length including the bed packed in the precolumn).
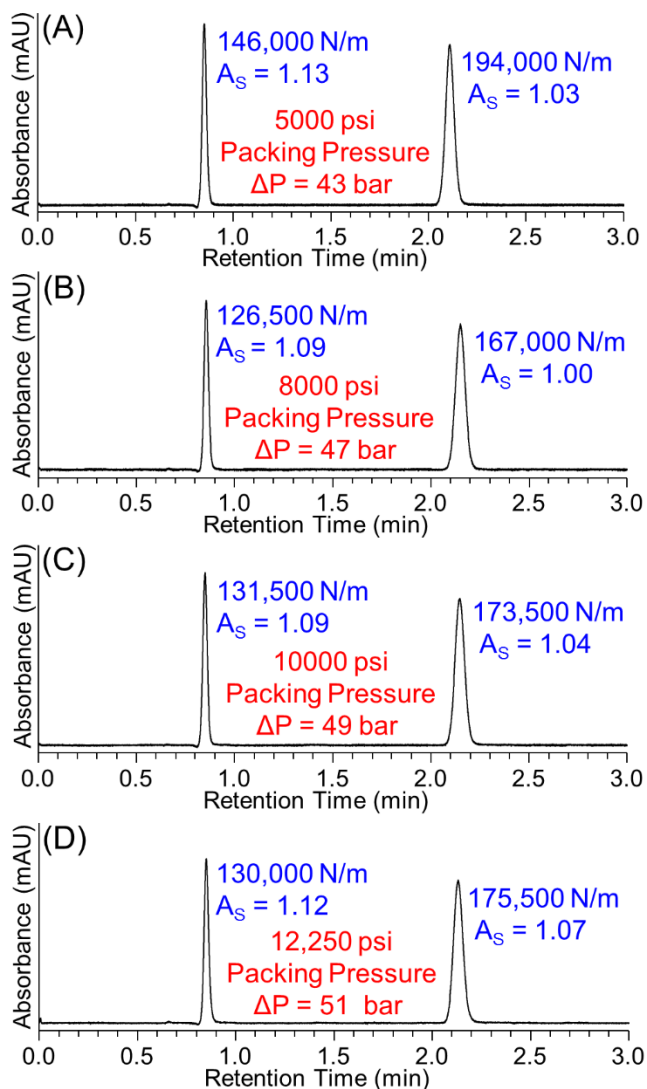
Figure 4-20. Effect of packing pressure on the chromatographic performance of 5x0.3 cm i.d. columns packed with 2.8 µm native SPP silica using dispersed slurry 1:1 acetone: IPA slurry (ca. 16% w/v concentration). Sample: uracil and cytosine (in order of elution). Method: 90/10 ACN/100mM NH4OAc, 0.425 mL/min, 254 nm. (A) 5000 psi, (B) 8000 psi, (C) 10,000 psi, and (D) 12,250 psi packing pressure. Pressure ramp was from 0 to the final pressure.

4.8 Packing of Capillary Columns: It is a Separate World

Capillaries, like narrow bore columns, save solvent and expensive stationary

phase and provide high detection sensitivity. Unlike the analytical bore columns, there is

104

no fronting or tailing in capillaries because of fast lateral diffusional relaxation provided

the capillaries are long enough to satisfy the Aris-Taylor dispersion requirements.[137]

Capillaries have produced phenomenal efficiencies (h as low as 1.0) which have never

been observed in analytical or narrow bore columns.[136] As the trend of moving to smaller

particle size continues, this work only covers packing methods for capillary packed with

sub-2 μm SPP and FPP, largely derived from the work of Jorgenson on C18

chemistries.[56,136,137,162,190-194] When choosing to pack a capillary column, the same

principles apply; optical microscopy is still the best predictor of the packed capillary.

Figure 4-21A shows a comparison of slurry solvents on the performance of capillary

columns packed with 1.1 μm C18 SPPs. The proprietary solvent is very dispersive,

whereas acetone and hexane are partially agglomerating and MeOH produced large

aggregates. It is clear from the van Deemter curve that a flocculated suspension is

beneficial in producing higher efficiencies for reversed phases in capillaries. The logic

behind choosing agglomerated suspension is that snow-ball effect, where a clump

containing large number of particles simply piles up on the bed reducing the size

discrimination between the wall and the central region.[137] Microscopy videos of capillaries

being packed clearly show this effect, whereas dispersed dilute suspensions pack in the

center as a pile and the particles roll-off toward the walls.[56,137] Following the guidelines in

Figure 4-10, next the slurry concentration should be optimized. Figure 4-21B shows that

increasing the slurry concentration from 0.3 to 2.5% w/v drastically enhances the capillary

performance (173 000 to 318 000 N/m). Through studies of capillary bed structure with

confocal laser scanning microscopy, it was discovered that the bed heterogeneity

between the capillary column's wall region and the bulk packed region is the key

contributor to poor performance and so is the presence of voids.[182,195,196] This

heterogeneity can be influenced with changes in slurry concentration as increasing the

105

slurry concentration leads to an even distribution of voids across the bed improving its

uniformity.[181,192]
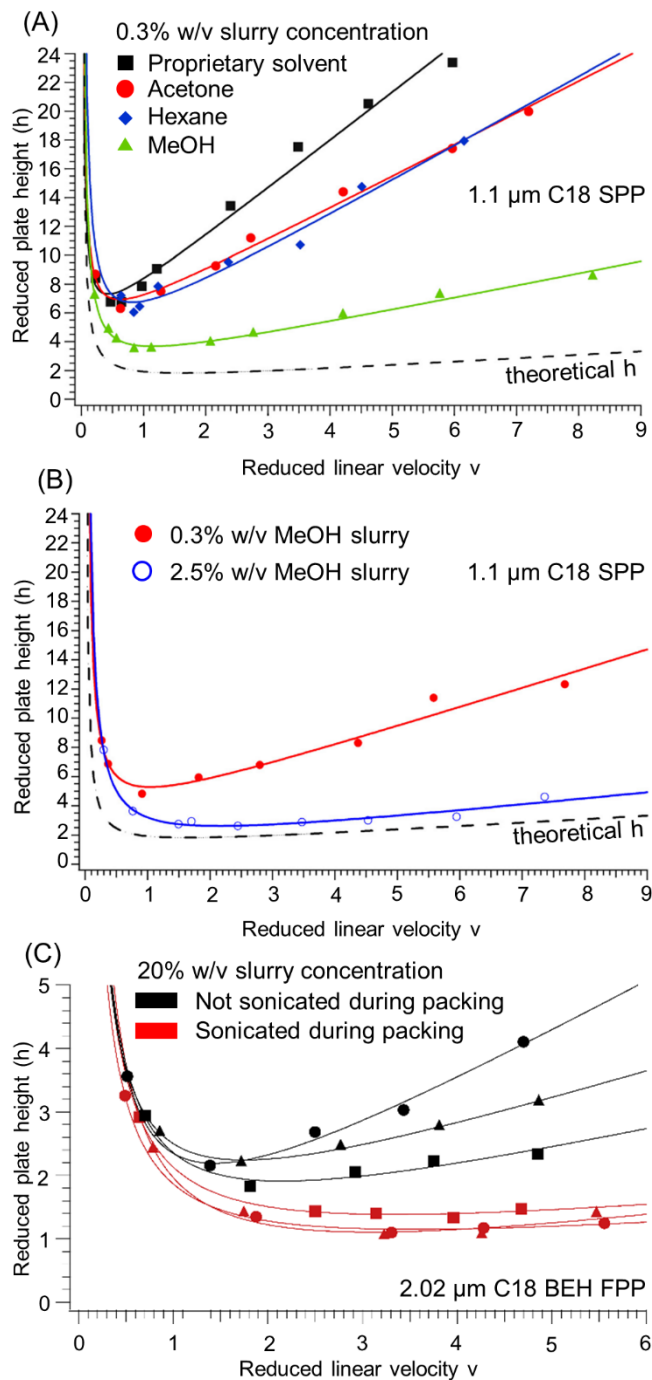
Figure 4-21. The van Deemter plots (h vs. reduced velocity v) of packed capillaries which show the effect of packing C18 SPP particles in (A) various slurry solvents and (B) various slurry concentrations in an agglomerating solvent in 30 μm i.d. capillaries. Dashed black lines represents ideal limits in (A) and (B). The effect of ultrasonication

107

during packing with high slurry concentration (20% w/v) with C18 FPP in 1 mx75 µm i.d. is shown in (C).

Increasing the slurry concentration also leads to an increased number of voids in the packed bed, eventually resulting in diminishing returns.[181,192] Figure 4-21C shows a recent study that demonstrated performance improvement from ultrasonication during packing with concentrated slurries (20% w/v) and achieved an impressive reduced plate height of 1.05 for capillary packed with 2.0 µm C18 bridged ethyl hybrid (BEH) FPPs.[136] Compared to this, the columns not sonicated during packing but packed identically otherwise produced h in the range of 1.8–2.2. It was reported that the use of ultrasonication (at 80 kHz) during packing prevented formation of large voids typically formed when using high concentration slurries.[136] To the best of our knowledge, first use of ultrasonication during packing of analytical and capillary columns was reported by Light[156] and Novotny,[197] respectively. For metallic analytical columns, the metal can absorb the ultrasonic energy (typical sonic bath), and we have seen poor packing results in doing so. It is highly desirable to learn whether there are any drawbacks of ultrasonication on column stability and lifetime. In this publication and many others from the past decade, there are no systematic results on long-term bed stability with agglomerated slurries, because such beds may be metastable because of their high permeability. In packing a capillary using supercritical fluids, stable beds have been reported after 6 months of use.[198]

4.9 Future Directions for Column Packing and Improving Chromatographic Efficiency

It is apparent that emerging techniques in improving column efficiencies will try to circumvent the problems of axial and radial heterogeneities of the packed beds, which are main causes of poor column performance.

4.9.1 Colloidal Crystals as Chromatographic Beds

One of the most interesting directions is enhancing column efficiencies using monodisperse colloids which organize themselves in long-range-ordered crystals.[199] This arrangement is excellent for any chromatographic columns since simulations have shown that a crystalline bed can provide extremely high efficiencies ($h < 1$).[200] The authors tested simple cubic (sc), body-centered cubic (bcc), and face-centered cubic (fcc) arrangement of particles and concluded that zone broadening is less for the fcc structure than the sc and bcc structures at the van Deemter minimum. Surprisingly, the random packed bed outperformed at higher flow velocities. It is known that uniformly sized silica particles can self-assemble into highly ordered fcc crystals. [201] Reproducible packing studies and packing procedures are yet to be demonstrated for making crystalline packed capillaries from colloidal crystals.

4.9.2 3D Printing of Columns and Wall Patterning

Three dimensional (3D) printing can possibly bring a paradigm shift in separation science, where 3D printed columns will circumvent many packing problems and wall effects. It is possible to obtain crystalline packing in simulations which can be 3D printed to obtain an ideal packed bed. In the first proof of concept of a 3D printed column, the researchers simulated perfectly ordered beds with octahedral beads (115 μm apothem) packed in a simple cubic configuration.[202] The models were then printed by UV curing of acrylonitrile-butadiene-styrene powder layers. A complete column including a bed, flow connectors, and flow distributors were printed. An interesting capability of 3D printing is the possibility to embed the particles in the wall. This approach will break the geometrical discontinuities which occur near the walls of all existing capillary and analytical columns. In 2016, Agilent Technologies (Santa Clara, CA) patented a technology of creating spiral

109

patterns on the column walls referred to as "structured walls" to potentially circumvent these geometrical constraints.[203] However, no supporting chromatography was provided. Of course, for chromatographic purposes, a 3D-column must be able to withstand high pressures and provide high surface area. Other alternatives such as pillar-array columns have emerged as ordered separation media which can also provide very high efficiencies.[204]

4.9.3 Nonconventional Column Packing Approaches

Although the slurry packing at high pressures has remained a preferred method of packing columns, other methods such as packing using supercritical fluids,[198,205,206] electro-kinetic packing,[207] and packing by centripetal forces have been tested with mixed results.[205,208,209] Packing capillaries using supercritical CO_2 has also been considered a viable alternative to the traditional slurry packing.[198] Packing capillaries using centripetal forces uses acceleration of particles with an in-house designed apparatus that can spin the columns during packing.[208,209] This approach could significantly improve the productivity due to the possibility of packing multiple columns simultaneously as well as rapid speed of packing.[210]

4.9.4 Active Flow Management (AFM)

AFM is not a column packing approach; however, it is a clever way to circumvent the radial heterogeneities of the packed bed as highlighted in the limiting cases of Equation(4-6. In AFM, the analyte is introduced into the center of the column. A "curtain flow" of mobile phase prevents the solute from seeing and exploring the wall region of the column.[211] A segmented outlet fitting is designed to allow sampling of the central region of the band. With this approach, significantly higher efficiencies are obtained because of the elimination of the wall effects (a virtually infinite diameter column) as well as

110

concentrating the sample in the central zone. The sample from the central section is passed through a detector as a plug. Note that in this column technology, only the inlet and outlet ports have been altered. A traditional main body of the column (cylindrical tube) is utilized. It was shown that for a 5 μm C18 column (100 mm × 4.6 mm), which the reduced plate heights of butyl benzene decreased from 2.9 to 2.3, just by the curtain flow approach. Significant improvement in peak is also observed.

4.10 Conclusions

Herein a unified approach toward the science of making high efficiency reproducible packed columns was presented. Theoretical considerations and non-Newtonian properties of suspensions were shown. The nonlinear viscosity behavior of suspensions can govern the nature of the packed bed (e.g., jammed state, shear thickened state etc.). Therefore, column packing can be considered as an ultrahigh pressure filtration process of a non-Newtonian suspension. After gaining experience from a range of nonpolar to polar stationary phases with modern SPP and FPP of narrow particle size distribution, a flowchart was developed to provide a logical progression of packing stationary phases of any chemistry. Illustrative examples were shown showing different packing phenomena and suspension properties. Results indicate that relatively concentrated nonaggregating suspensions usually produce better packed analytical and narrow bore columns regardless of the stationary phase chemistry. The best packed reversed phase capillaries usually require aggregating solvents. More studies are needed for capillary columns using different stationary phases to generalize this phenomenon. New directions in colloidal crystals, 3D printing are laid out and the use of nonconventional approaches such as 3D printing and active-flow management are highlighted. Future work on quantitative suspension rheology is needed to understand

111

and model the dynamics of the column packing process, a technology which will continue

to evolve for several decades to come.

Chapter 5

Quinine Bonded to Superficially Porous Particles for High-Efficiency and Ultrafast Liquid
and Supercritical Fluid Chromatography

5.1 Abstract

Two new anion-exchange columns were prepared by bonding tert-butyl
carbamoylated quinine to 2.7 μm superficially porous particle (SPP) silica to create chiral
stationary phases for high-efficiency and ultrafast chromatography. Performance and
retention parameters of these new columns are compared with an analogous 5 μm fully
porous particle (FPP) based Chiralpak QNAX column and a 3-4 fold increase in efficiency
was observed. Ultrafast separations ranging from 12 seconds down to sub-second are
shown using 2.7 μm SPP bonded via hydrosilation to the selector. Potential benefits of
2.7 μm SPP based columns for increased LC-MS compatibility were investigated. A van
Deemter plot comparison showed 2.7 μm SPP based columns provided a lower reduced
plate height and a higher optimal linear velocity compared to the 5 μm FPP based
column. With geometry-independent kinetic plots, 2.7 μm SPP and 5 μm FPP based
columns were assessed for their kinetic performance and the maximal number of plates
each column can generate in a given analysis time. The 2.7 μm SPP based column
showed remarkable performance improvements in speed and efficiency as indicated by
the kinetic plots.

5.2 Introduction

The separation of enantiomers is among the more challenging chromatographic
separations due to the fact that conventional strategies employed to separate achiral
analytes are ineffective when applied to enantiomers. Researchers have devised new

113

and improved chiral selectors with differing enantiomeric selectivity over the years.[9,10,12-14,17,18,20,25,212,213] As the introduction of effective, new classes of chiral selectors has slowed, other important factors such as efficiency and analysis speed have started to garner attention from the chromatography community.[45,52,62-64,127,184,214,215] For the past few decades, unprecedented growth in analyses of chiral analytes as potential small molecule drug candidates in the pharmaceutical industry has spurred the development of techniques that increase the throughput in chiral separations.[45] Researchers have explored various column screening methods to reduce method development time, and they utilized smaller particle sizes of fully porous particles (FPPs) and superficially porous particles (SPPs) to improve efficiencies and analysis times, which is a typical constraint in enantiomeric separations.[22,52,59,63,64,71,127,184,215-219] Both a parallel column screening approach for rapid method development and use of injector programming to increase throughput have been reported.[214,216] Short columns also have been utilized in sub/supercritical fluid chromatography (SFC) with gradient methods for fast screening of analytes.[22,71]

Since their introduction in 2007, the latest generation of 2.7 μm SPPs have shown notable performance for achiral separations and have shown efficiencies comparable to sub-2 μm FPPs, at a reduced backpressure.[49,220] Lindner and coworkers reported the first use of this morphology in chiral separations by preparing a quinidine based stationary phase on 3 μm SPPs.[64] Thereafter, researchers attempted to use SPPs for coated polysaccharides and bonding with a cyclic oligosaccharide to gain efficiency and reduce analysis times.[53,65,66] Efforts to achieve high efficiencies and short analysis times in chiral analysis remained confined typically to a few example separations, until Patel et al. reported ultrafast chiral separations in liquid chromatography of more than 60 enantiomers in less than 40 seconds.[52] Combination of high selectivity chiral selectors

114

(macrocyclic glycopeptides and cyclic oligosaccharides), short high-efficiency columns, and instrument optimizations led to several separations under 10 seconds, with the shortest being 5 seconds.[52] Compared to the analogous 5 µm FPP commercial columns, a 3-4 fold improvement in theoretical plates/meter (N/m) and a reduced plate height (h) as low as 1.6 was achieved with 2.7 µm SPP based CSPs.[52] The efficiency gain of SPPs come from a decrease in contribution to band broadening from longitudinal dispersion, resistance to mass transfer, and particularly eddy dispersion.[221] This decline in eddy dispersion contribution is caused by improved packing homogeneity.[58] Recently, Wahab et. al demonstrated sub-second chiral, achiral, and HILIC separations using 0.5 x 0.46 cm i.d. columns packed with 2.7 µm SPP phases.[184] In retrospect, bonding a high selectivity chiral selector to SPPs to exploit their high efficiencies, reduced backpressures, and shorter analyte retention times is the most promising approach to achieve ultrafast separations.[52,184,215] A recently published comprehensive review highlights the current advances in high-throughput and high-efficiency chiral liquid chromatography.[45] Some researchers have noted their tribulations in attempting to obtain high-efficiency packed beds with polar SPPs.[46,222] We do not share these difficulties in our work with 2.7 µm SPPs. Next few chapters will document the science behind slurry packing and our approach to obtaining high-efficiency packed beds with modern sub-2 µm FPPs and 2.7 µm SPPs.[47,48]

Quinine derivatized with a *tert*-butyl carbamate moiety shows enantiomeric selectivity towards a wide range of acidic analytes, especially N-blocked amino acids.[16,17,223] Quinine and quinidine based CSPs can sometimes offer opposite elution orders which are beneficial in trace analysis and preparative applications.[16,17] Providing chiral separations in polar organic and reversed phase HPLC modes make this selector amenable to use with mass spectrometry (MS). Owing to quinine's strong interactions

with acidic solutes, use of counterions in the form of strong additives/buffers is necessary to reduce retention of analytes and improve the peak shapes. High concentration of buffers, however, are not compatible with certain MS sources such as electrospray ionization (ESI). It is expected that chromatographic performance of quinine phases can benefit from being bonded 2.7 μm SPPs.[45,184,224]

In this work, we have bonded tert-butyl carbamoylated quinine on 2.7 μm SPPs via two different linkage types to prepare high-efficiency anion-exchange CSPs. This work is the first report of high-efficiency 2.7 μm SPP based quinine CSPs, and they are compared with a 5 μm FPP based commercial column in UHPLC and SFC. We also report ultrafast chiral separations using 2.7 μm SPP based CSPs in UHPLC and SFC. Further, benefits of enhanced efficiencies and reduced retention times afforded by 2.7 μm SPPs were assessed for improving chiral LC-MS compatible methods. A comparison between the 5 μm FPP and 2.7 μm SPP based quinine columns is shown with use of van Deemter and kinetic plots, depicting the clear advantage of 2.7 μm SPPs for chiral separations where efficiency and speed are concerned.

5.3 Experimental

5.3.1 Materials

All solvents, reagents, and analytes including HPLC grade methanol (MeOH), formic acid (FA), ammonium formate (HCOONH$_4$), ammonium acetate (NH$_4$OAc), *tert*-butyl isocyanate, (3-mercaptopropyl)trimethoxysilane, triethylamine, and triethoxysilane were purchased from Sigma-Aldrich (St. Louis, MO, US), unless otherwise stated. (8*S*, 9*R*)-quinine was purchased from Alfa Aesar (Ward Hill, MA, US). Chiralpak QNAX column (15 x 0.46 cm i.d.) packed with *tert*-butyl carbamoylated quinine (attached to 5 μm FPPs via mercaptopropyl silane linkage) was provided by Chiral Technologies Europe (Illkirch, France). Agilent Technologies (Santa Clara, CA, US) provided the SPP

116

silica with 2.7 μm particle diameter, surface area of 120 m^2/g, and pore size of 120 Å. The core of the SPP is 1.7 μm in diameter and the surrounding shell thickness is 0.5 μm. SFC grade CO_2 was supplied by Airgas (Radnor, PA, US). Distilled water was further purified to 18.2 MΩ.cm using a Milli-Q purification system (EMD Millipore, Billerica, MA, US).

5.3.2 Synthesis of Chiral Selectors

All synthesis procedures were carried out under a dry argon atmosphere using anhydrous solvents, when possible. SPP silica was dried in an oven before use. (8*S*, 9*R*)-quinine was derivatized with *tert*-butyl isocyanate to form *tert*-butyl carbamoylated quinine (tBu-quinine) as reported previously.[16] It is crucial to use a chiral selector with the highest optical purity available. The smallest amount of chiral impurity can have detrimental effect on enantiomeric selectivity.[225] Figure 5-1 provides the structures and abbreviations of chiral selectors, QML SPP and QHS SPP, synthesized and bonded to 2.7 μm SPPs *via* mercaptopropyl silane linkage and hydrosilation, respectively. The 2.7 μm SPP silica was derivatized with (3-mercaptopropyl)trimethoxysilane to create silica with mercaptopropyl linkage based on work reported previously.[17,226] The tBu-quinine was bonded to silica with mercaptopropyl linkage to create quinine-mercapto linker (QML) SPP CSP (see Figure 5-1A).[17] To hydrosilate tBu-quinine, it was reacted with excess triethoxysilane in presence of ~5 mg of H_2PtCl_6 catalyst in anhydrous ethanol. Unreacted triethoxysilane was removed by washing the product mixture with *n*-hexanes. The tBu-quinine attached to triethoxysilane was then bonded to 2.7 μm SPPs to create quinine-hydrosilated (QHS) SPP CSP (see Figure 5-1B).

It is noted that the commercial column Chiralpak QNAX packed with 5 μm FPPs, used in this study for comparison purposes, has the same chiral selector (bonded via the

same chemistry) as the QML 2.7 µm SPP. The elemental analysis data and surface

coverage of chiral selectors on 2.7 µm SPPs are provided in Table 5-1 (data not available

for commercial column from manufacturer). Although, the SPPs typically have lower

overall surface area than FPPs, and consequently a lower absolute amount of the

bonded chiral selector, it is the relative surface coverage of the selector that governs the

enantiomeric selectivity, as shown previously.[52,53] A notably higher surface coverage was

obtained on QML 2.7 µm SPP (1.61 µmol/m^2) compared to QHS 2.7 µm SPP (0.54

µmol/m^2), which led to better enantiomeric selectivity on QML 2.7 µm SPP in most cases.

Indifferent to numerous attempts, QHS 2.7 µm SPP could not be prepared with higher

selector coverage, a limitation to the hydrosilation bonding approach for this CSP.

tert-butyl carbamoylated Quinine
(mercapto linker, QML)

tert-butyl carbamoylated Quinine
(hydrosilated, QHS)
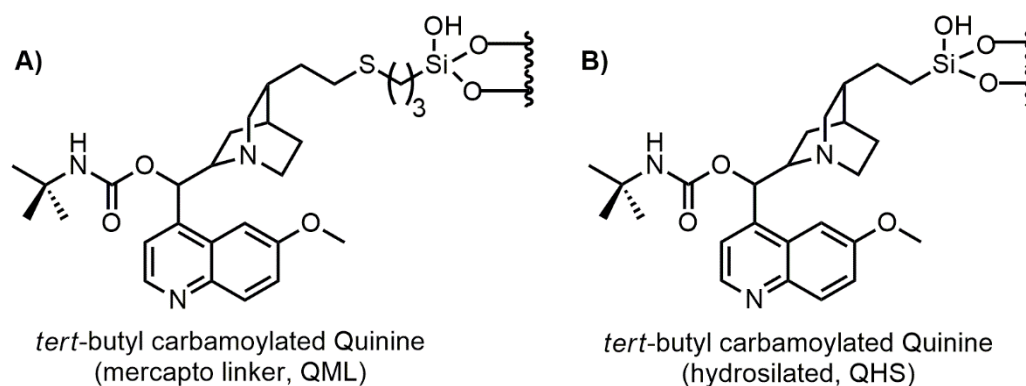
Figure 5-1. Structures of both variants of the quinine based chiral stationary phases prepared in this study. The tert-butyl carbamoylated quinine was bonded to 2.7 µm superficially porous particles (SPPs) via A) mercaptopropyl silane linkage (same chemistry as 5 µm FPP commercial Chiralpak QNAX) and B) hydrosilation with triethoxysilane.

Table 5-1. Properties of chiral stationary phases compared in this study.

Chiral Stationary Phase (CSP)	quinine mercapto linker (QML)	quinine hydrosilated (QHS)	Chiralpak QNAX
Silica particle size	2.7 µm SPP	2.7 µm SPP	5 µm FPP
Dimensions (cm)	5 x 0.46	5 x 0.46	15 x 0.46
%C[a]	6.97	2.26	-[b]
%N[a]	0.73	0.17	-[b]
Surface coverage from %C (µmol/m^2)	1.61	0.54	-[b]
Surface coverage from %N (µmol/m^2)	1.45	0.34	-[b]

Theoretical plates N/m (achiral probe)[C]	182,000	180,000	86,600
Reduced plate height h (achiral probe)[C]	2.0	2.1	2.3
Theoretical plates N/m (chiral probe)[D]	136,000	136,000	46,000
Reduced plate height h (chiral probe)[D]	2.7	2.7	4.3
Specific column permeability K_V (m^2)	2.87×10^{-15}	2.16×10^{-15}	1.03×10^{-14}
Column permeability K_{V0} (m^2)	4.69×10^{-15}	3.60×10^{-15}	1.42×10^{-14}

[a]Data obtained from elemental analysis of chiral stationary phase [b]Data not available from manufacturer
[C]Analyte: 1,3-dinitrobenzene, UHPLC method: 70/30 heptane/EtOH, 1.0 mL/min.
[D]Analyte: dichlorprop, UHPLC Method: 80/20 MeOH/100 mM NH_4OAc (pHa 6.0), 1.0 mL/min. Agilent 1290 UHPLC instrument was used for efficiency comparison with configuration as detailed in the Experimental section.

5.3.3 Column Packing

All CSPs were washed with diethyl ether, MeOH, acetonitrile, dichloromethane, and acetone to remove any materials adsorbed onto CSP. The silica fines were removed by suspending the CSPs in a solvent and removing the supernatant during sedimentation process. CSPs were dried in a vacuum oven. A slurry system was optimized for each CSP using methods described previously.[52,57] These 2.7 µm SPP CSP slurries were packed in 5 x 0.46 cm i.d. and 3 x 0.46 cm i.d. analytical columns (IDEX Health and Science, Oak Harbor, WA) using a pneumatically driven pump at constant pressures. A 0.5 x 0.46 cm i.d. C18 guard column (Agilent Technologies) was emptied to be used as a 0.5 cm column, packed as described in previous statement. The 0.5 x 0.46 cm i.d. column featured a 0.5 cm long barrel with a built-in frit at the outlet end attached to a 3 cm x 127 µm i.d. stainless steel extension fitted with a ferrule and a 1/16'' fitting.

5.3.4 Instrumentation

5.3.4.1 Liquid Chromatography System

Liquid chromatography was performed on an Agilent 1290 Infinity series UHPLC system (Agilent Technologies, Santa Clara, CA, US) equipped with a quaternary pump with a built-in-degasser, a high-performance autosampler, and a diode array detector. A 2

μm inlet filter was attached to all mobile phase lines. The UHPLC system was optimized to reduce extra-column volume using a low volume autosampler needle and needle seat (Agilent Ultralow Dispersion Kit P/N 5067-5189), a detector flow cell with a volume standard deviation of 1.0 μL, and Agilent A-Line fittings with stainless steel tubing (75 μm i.d.). The thermostated column compartment and 6-port column-switching valve were bypassed to further reduce the extra-column volume. The detector data collection rate was set to 160 Hz with a response time of 0.016 s for all separations to minimize the instrumental artifacts and avoid peak distortion.[52,105] Note that using a very high detector frequency with longer analysis times significantly increases the data file size and the computer workload. A 3 x 0.46 cm pre-column packed with 50 μm native silica particles (M.S. Gel from AGC Si-Tech Co., Ltd, Exton, PA, US) was connected between the pump and autosampler to saturate the mobile phase with silicic acid to prevent damaging the analytical column. The instrument was controlled by OpenLAB CDS ChemStation software (Rev. C.01.06 [61], Agilent Technologies 2001−2014) in Microsoft Windows 8.1. Details on retention parameters and data analysis are provided below.

For the sub-second separation in Figure 5-3C, the autosampler and column thermostat were bypassed and the pre-column was connected to a Rheodyne 7520 manual injector (Rheodyne LLC, Rohnert Park, CA, US) which included a 1.0 μL internal sample loop. The manual injector was connected to a 7 cm x 75 μm i.d. NanoViper tubing from ThermoFisher Scientific (Waltham, MA, US) attached to the 0.5 x 0.46 cm i.d. column which was directly connected to the inlet of the detector flow cell.

5.3.4.2 Sub/Supercritical Fluid Chromatography System

Sub/supercritical fluid chromatography was performed on a Jasco (Easton, MD, US) SFC-2000-7 instrument equipped with a Jasco LC-Net II controller, a Julabo

(Allentown, PA, US) FL601 CO_2 chiller (set at -10 °C), a CO_2 tank, a CO_2 pump (PU-2086 plus), a modifier pump (PU-2086 plus), a Jasco LV-2080-03 solvent selection unit, an auto-sampler (AS-2059-SF plus), a high-pressure compatible UV detector (UV-2075 plus), a backpressure regulator (BP-2080 plus) with a heat controller (HC-2068-01), a 6-valve changing unit (SCF-VCH-BP), and a make-up pump (PU-2080 plus) to supply additional liquid to the backpressure regulator. The SFC system was modified to reduce extra-column volume by using a 2 µL sample loop and 75 µm i.d. tubing to connect the autosampler to the column inlet and the column outlet to the detector. For ultrafast separations shown in Figure 5-3, 254 µm i.d. connection tubing was utilized. The column oven was bypassed to further reduce extra-column volume, and separations were performed at ambient temperature. The backpressure regulator was maintained at 80 bar, unless otherwise stated. Time accumulation (moving average) filter was used in UV detector setting along with a 100 Hz data collection rate with a 0.0005 min response time to minimize instrumental artifacts and avoid peak distortion. The SFC system was controlled using ChromNAV software (ver 1.17.01 [build 8] Copyright 2003-2011 Jasco Corp.) in Microsoft Windows xP. Details on retention parameters and data analysis are provided below.

5.3.4.3 Instrument Optimizations

Extra-column band broadening can adversely affect the chromatography and reduce the efficiency of the peaks, especially in case of short columns packed with small particle size silica, as was applied in this work. It is important to use an instrument that is optimized with low extra-column volume to realize the intrinsic efficiencies of these highly efficient columns. Thus, all chromatography performed in this work was done so on an instrument optimized for low-extra column volume. Extra-column band dispersion can be

121

drastically reduced by using the small injection volumes, a narrow i.d. autosampler injection needle and needle seat, shortest possible connection tubing with narrow i.d., and a low volume detector flow cell.[52,227] Using the right fittings to connect tubing that can form a zero dead-volume seal is equally important.[228] It is also necessary to optimize the detector settings for ultrafast separations by using smaller response times and higher sampling frequency, where available. Many researchers have suggested using detector frequency that provides 20 points per peak, however, as recent studies have shown this may not be enough when it comes to very narrow peaks in case of high-efficiency columns and ultrafast separations.[52,105] It was recommended to use a minimum of 40 Hz detector sampling frequency and a maximum response time of 0.13 s to prevent deleterious effects on chromatographic peak shapes.[52,105] Collecting data at the highest detector sampling frequency is recommended so long as it provides adequate signal-to-noise ratio for the analysis. The manufacturing of improved instruments with lower extra-column volume, higher detector sampling frequency, and lower response times can further help in making these separations even faster.

5.3.5 Chromatography

The reported chromatographic parameters for UHPLC and SFC were obtained from their respective chromatographic data systems listed in the Instrumentation section. Resolution (R_S) was obtained using half height method $\left(R_S = \frac{2.35(t_{R_2} - t_{R_1})}{2(W_{0.5,1} + W_{0.5,2})}\right)$; where t_R = retention time and $W_{0.5}$ = peak width at half height. The theoretical plates (N) were calculated by half height method $N = 5.545\left(\frac{t_R}{W_{0.5}}\right)^2$. For assessing peak asymmetry, USP tailing factor (T) is used. $T = \frac{W_{0.05}}{2f_{0.05}}$; where $W_{0.05}$ = peak width at 5% peak height and $f_{0.05}$ = distance from leading edge of the peak to the peak maximum at 5% peak height. A T

122

value of 1 indicates symmetric/Gaussian peak, T> 1 indicates tailing peak, and T < 1 indicates fronting peaks. For the sub-second separation shown in Figure 5-3C, peak fitting as exponentially modified Gaussians (EMG) was performed with PeakFit software v4.12. See recent work by Wahab et al. for more information.[184] All mobile phases were degassed using sonication under vacuum and filtered using a 0.2 μm porous filter to remove particulates before use. All solvent mixtures are given in (v/v), and separations were performed at room temperature, unless otherwise stated. The pH_a reported for mobile phases is the apparent pH. For all comparison analyses, identical sample concentration and volumes were injected on 2.7 μm SPP and 5 μm FPP based columns on the same instrument. For comparison in SFC (Table 5-3), 60% CO_2 - 40% 100/0.4/0.35 MeOH/FA/HCOONH$_4$ (v/v/w) was used as mobile phase at flow rate of 4.0 mL/min. Backpressure regulator was maintained at 80 bar and the temperature was ambient. In order to increase the elution strength of the mobile phase, formic acid (FA) and ammonium formate (HCOONH$_4$) are added to MeOH modifier (without adjusting pH_a) in this study. For ultrafast SFC separations (Figure 5-3D-F), 25% MeOH was used as modifier with 0.6/0.5 FA/HCOONH$_4$ (v/w) as additives to increase the elution strength of the mobile phase with backpressure regulator at 78 bar. The flow rate used was 20.0 mL/min. For van Deemter and kinetic plots, each analysis was performed 3 times to determine the average and the deviation. For each flow rate, columns were allowed to thermally equilibrate for 10 minutes prior to the analysis to stabilize frictional heating. For kinetic plots, mobile phase viscosity was assumed to be constant through all flow rates.

5.4 Results and Discussion

The column permeability governs the flow of mobile phase at a given pressure. It is desirable to have higher column permeability in order to use higher flow rates. The specific column permeability was calculated using the Darcy's law,

$$K_V = \left(\frac{\eta L}{\Delta P} u\right)$$ (5-1)

where K_V is the specific column permeability (m^2), η = mobile phase viscosity (Pa.s), L = column length (m), ΔP = pressure drop across the column (Pa), and u = superficial linear velocity (m/s) obtained by dividing the volumetric flow rate (m^3/s) by the cross sectional area (m^2) of the column. As expected, compared to the commercial CSP that uses 5 μm diameter FPPs, the specific column permeability of QML 2.7 μm SPP and QHS 2.7 μm SPP columns are 4 and 5 times lower, respectively (Table 5-1). However, the reduction in specific permeability for 2.7 μm SPPs is far less than a 10-fold reduction reported previously for a π-complex sub-2 μm CSP compared to its 5 μm FPP counterpart.[63] With relatively high permeability compared to sub-2 μm FPPs, high-efficiency of 2.7 μm SPP based columns can be achieved on typical HPLCs (~400-600 bar limit) which are more ubiquitous in analytical labs. Substituting the linear velocity u_0 for superficial linear velocity u in equation 3-1 provides column permeability K_{V0} which is also provided in Table 5-1. A similar trend, described for specific column permeability K_V, is observed for K_{V0}.

5.4.1 2.7 μm SPP vs. 5 μm FPP comparison

Dichlorprop and 1,3-dinitrobenzene were used to compare the chiral and achiral efficiencies, respectively, of QML 2.7 μm SPP, QHS 2.7 μm SPP, and the commercial 5 μm Chiralpak QNAX columns in UHPLC (Table 5-1). In both cases, 2.7 μm SPP columns show improvement of nearly 100,000 N/m over the QNAX column and reduced plate

124

heights of 2.0-2.1 for 1,3-dinitrobenzene. The shorter 2.7 µm SPP based columns provide

higher efficiencies with a similar or better peak asymmetry values (Table 5-1), despite

short columns being more difficult to pack.[158]

5.4.1.1 Liquid Chromatography

A comparison of analysis times (t_{R_2}), enantiomeric selectivity (α), and resolutions

(R_S) for a range of acidic analytes separated on all quinine based columns in UHPLC is

provided in Table 5-2. For simplicity, t_{R_2} is assumed as the analysis time. Since the

purpose of this table is to compare the chromatographic performance of all columns,

separations were performed using identical mobile phase conditions. According to Table

5-2, QML 2.7 µm SPP provides resolution and selectivity values similar to QNAX in most

cases with significantly reduced analysis time for the 2.7 µm SPP based column. Figure

5-2B vs C shows the separation of dichlorprop on these two columns with the QML 2.7

µm SPP exhibiting reduced analysis time with an improvement of 90,000 N/m, which is a

3-fold increase. Comparing Figure 5-2A vs 2B where both columns show same efficiency

(Table 5-1) and similar selectivity (Table 5-2), QML 2.7 µm SPP shows improved

resolution due to a higher retention factor. As seen in Table 5-2, QML 2.7 µm SPP,

attributed to its overall higher chiral selector surface coverage (Table 5-1), provides

higher selectivity and resolution values compared to QHS 2.7 µm SPP in most cases. It is

interesting that, even in cases where the selectivity of QHS 2.7 µm SPP and QML 2.7 µm

SPP are similar, the hydrosilated variant provides significantly lower (74% on average)

retention times (Table 5-2). When compared to the QNAX column, the QHS 2.7 µm SPP

column is able to provide, on average, 93% lower retention times, with several

separations demonstrating total analysis time shorter than the dead time on the 5 µm

FPP column (Table 5-2). Figure 5-2A vs. B-C shows this phenomenon for dichlorprop. It

is clear that the high efficiencies of 2.7 µm SPPs is the driving force behind their improved performance as seen in Figure 5-2. The 2.7 µm SPPs used to prepare these columns have a core to particle diameter ratio (ρ) of 0.63 which is within the range to yield optimum performance.[229] Note that the selectivity of quinine based columns can be heavily influenced by the mobile phase aqueous to organic ratio, pH_a (apparent pH), and the buffer/counterion type and its concentrations.

Table 5-2. UHPLC comparison of retention time (t_{R_2}), selectivity (α), and resolution (RS) for acidic analytes on quinine hydrosilated SPP (QHS SPP), quinine mercapto-linker SPP (QML SPP), and the commercial Chiralpak QNAX (QNAX FPP) columns. See footnotes for details.

Analytes	MP[b]	QML 2.7 µm SPP (5 cm x 0.46 cm			QHS 2.7 µm SPP (5 cm x 0.46 cm)			QNAX 5 µm FPP (15 cm x 0.46 cm)		
		t_{R_2}[C] min	α	R_S	t_{R_2}[C] min	α	R_S	t_{R_2}[C] min	α	R_S
Dichlorprop	A	5.5	1.20	3.4	1.4	1.22	2.6	25.7	1.20	3.5
FMOC-DL-ala	A	8.9	1.47	6.7	1.4	1.64	4.1	37.5	1.56	7.7
1,1'-binaphthyl-2-diylhydrogenphosphate	A	18.4	1.39	5.6	1.6	1.37	2.4	63.8	1.46	6.6
Dansyl-α-N-butyric acid	A	9.5	1.23	3.7	1.3	1.25	1.9	33.6	1.25	3.9
Benzoyl-DL-valine	A	5.3	2.23	13.4	1.5	2.38	7.2	23.2	2.41	14.4
DNB-DL-phenylglycine	C	8.0	4.18	19.4	3.1	6.85	13.8	29.6	5.58	20.9
DNB-DL-leucine	C	12.0	8.84	25.5	4.7	14.5	12.9	48.7	12.92	26.3
Z-DL-phenylalanine	C	1.8	1.15	1.3	1.0	1.30	2.0	8.4	1.20	2.0
Acetyl-DL-valine	A	2.3	1.56	6.8	1.1	1.46	2.9	7.9	1.59	3.8
Dansyl-DL-serine	A	9.2	1.29	4.5	2.0	1.40	3.3	39.7	1.32	4.8
3-oxo-1-indan carboxylic acid	B	4.4	1.08	1.5	-	1.0	-	16.6	1.10	1.8
Phosphonic acid[a]	A	4.1	1.06	1.0	-	1.0	-	13.9	1.11	1.7

[a]2-hydroxy-4-(2-methoxyphenyl)-5,5-dimethyl-1,3,2-dioxaphosphorinane [b]Method A = 80/20 MeOH/100 mM NH$_4$OAc (pH$_a$ 6.0), flow rate = 1.0 mL/min. Method B = 80/20 MeOH/100 mM NH$_4$OAc (pH$_a$ 6.0), flow rate = 0.8 mL/min. Method C = 80/20 MeOH/100 mM NH$_4$OAc (pH$_a$ 7.0), flow rate = 1.0 mL/min. [C]Retention of 2nd eluted peak in minutes.

UHPLC
Analyte: Dichlorprop

SFC
Analyte: Dansyl-Serine

A
Rs = 2.6
N/m = 137,000

quinine hydrosilated SPP
(QHS SPP)
5 x 0.46 cm i.d.
2.7 μm SPP

D
Rs = 3.0
N/m = 60,000

B
Rs = 3.5
N/m = 136,000

quinine mercapto linker SPP
(QML SPP)
5 x 0.46 cm i.d.
2.7 μm SPP

E
Rs = 2.5
N/m = 66,000

C
Rs = 3.5
N/m = 46,000

Chiralpak QNAX (QNAX)
15 x 0.46 cm i.d.
5 μm FPP

F
Rs = 3.5
N/m = 22,000
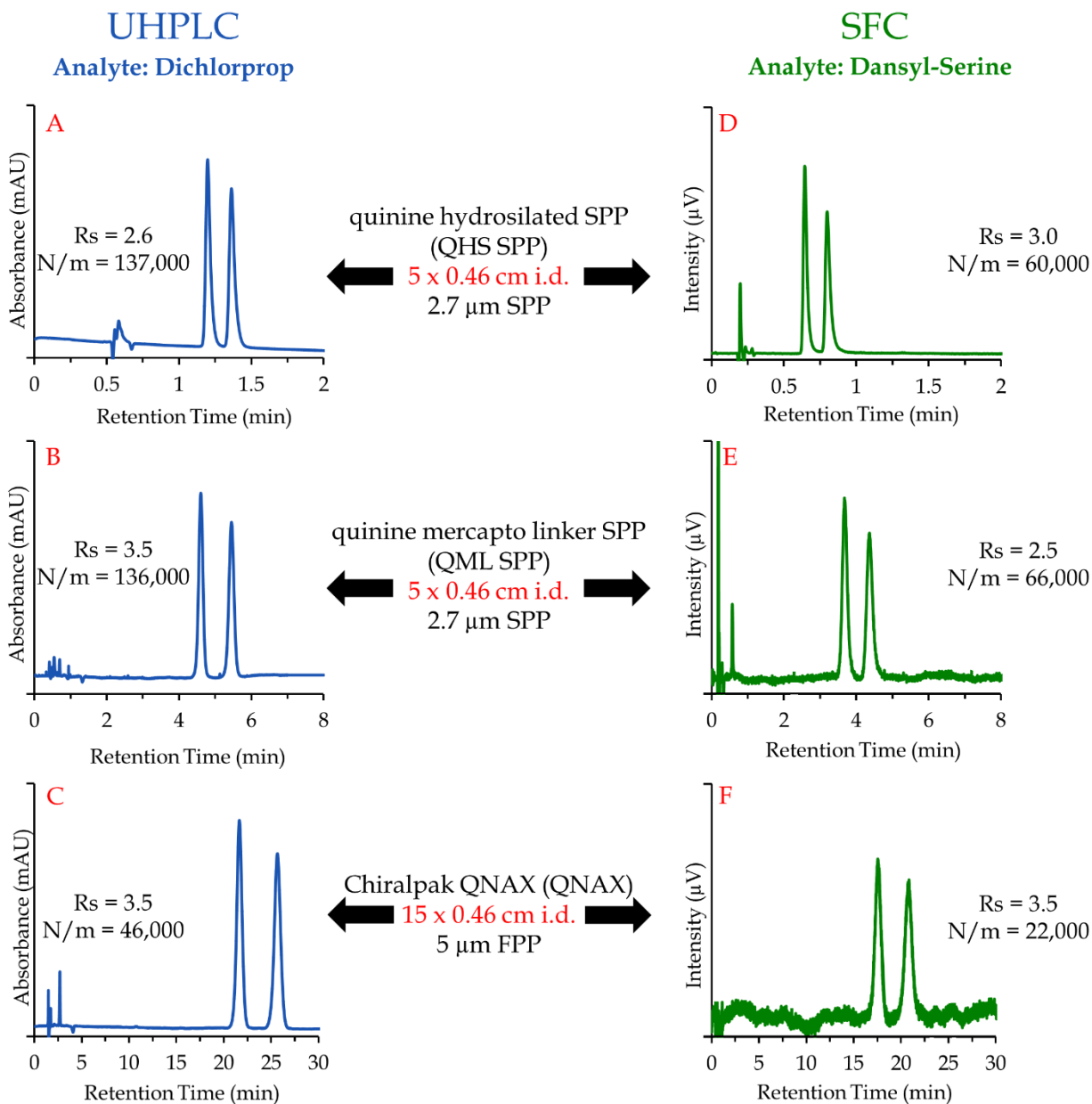
Figure 5-2. A comparison of two 2.7 μm SPP based columns prepared in this study with commercial 5 μm FPP Chiralpak QNAX on UHPLC and SFC under typical chromatographic conditions. UHPLC separations (A-C) were performed using analyte dichlorprop with the mobile phase 80/20 MeOH/100 mM NH_4OAc (pH_a 6.0) at 1.0 mL/min flow rate. SFC separations (D-F) were performed using analyte dansyl-serine with the mobile phase 60% CO_2 – 40% 100/0.4/0.35 MeOH/FA/$HCOONH_4$ (v/v/w) at 4.0 mL/min.

127

Backpressure regulator was maintained at 80 bar and temperature was ambient. See Experimental section for details on N/m and R_S.

3.4.1.2 Sub/Supercritical Fluid Chromatography

Table 5-3 shows retention parameters for several analytes separated on three quinine columns in SFC. QML 2.7 µm SPP showed similar selectivity compared to the QNAX column and comparable resolution values even though it was 3 times shorter. Interestingly, QHS showed equal or better selectivity compared to QML 2.7 µm SPP and QNAX in most cases while providing all separations under a minute. Despite that, due to low retention of analytes, and consequently larger contribution from extra-column dispersion, QHS 2.7 µm SPP showed slightly lower resolution values compared to QML 2.7 µm SPP (Table 5-3). Figure 5-2D-F show separation of dansyl-serine. Both 2.7 µm SPP based columns, QHS SPP and QML SPP, show nearly 3 times the efficiency (60,000 N/m) compared to the commercial 5 µm FPP column QNAX (22,000 N/m). The 2.7 µm SPP columns also showed 4-20 times faster analysis compared to the 5 µm FPP based column.

Table 5-3. Subcritical fluid chromatography (SubFC) comparison of retention time (t_{R_2}), selectivity (α), and resolution (R_S) for acidic analytes on quinine hydrosilated SPP (QHS SPP), quinine mercapto-linker SPP (QML SPP), and the commercial Chiralpak QNAX (QNAX) FPP columns. See footnotes for details.

	QML 2.7 µm SPP (5 x 0.46 cm)			QHS 2.7 µm SPP (5 x 0.46 cm)			QNAX 5 µm FPP (15 x 0.46 cm)		
Analyte	t_{R_2}	α	R_S	t_{R_2}	α	R_S	t_{R_2}	α	R_S
FMOC-alanine	1.0	1.5	4.5	0.4	1.7	2.9	5.0	1.5	5.3
benzoyl-valine	0.9	2.3	9.2	0.4	2.8	6.0	3.2	2.3	14.8
FMOC-leu	0.8	1.7	5.7	0.3	2.1	2.2	4.3	1.8	7.2
Dichlorprop	1.0	1.1	1.9	0.4	1.3	1.6	3.9	1.2	2.4
dansyl-serine	4.3	1.2	2.5	0.8	1.3	3.0	20.8	1.1	3.5
Z-phenylalanine	0.9	1.2	1.8	0.3	1.3	1.7	3.3	1.1	1.7
dansyl leucine	1.5	1.1	1.2	0.4	1.1	-[a]	8.5	1.1	1.3
3-oxo-1-indan-carboxylic acid	0.6	1.1	1.4	-	1.0	-	2.4	1.2	2.1

Mobile phase: 60% CO2 - 40% 100/0.4/0.35 MeOH/FA/HCOONH4 (v/v/w), flow rate: 4.0 mL/min. Backpressure regulator was maintained at 80 bar and the temperature was ambient. [a]Resolution could not be determined

5.4.2 Ultrafast Separations in HPLC and SFC

The current acceptable time limit for a separation to be considered "ultrafast" is ≤ 60 seconds.[52,224] Figure 5-3 shows three UHPLC and 3 SFC ultrafast chiral separations performed on QHS 2.7 µm SPP columns with the longest separation at 12 seconds and the shortest being under 1 second. Figure 5-3A shows a 12 sec separation of benzoyl valine with a resolution of 4.7 on a 3 cm QHS 2.7 µm SPP column on an optimized UHPLC instrument at 4.5 mL/min. In order obtain even faster separations, a 0.5 x 0.46 cm i.d. column was prepared (See Experimental), and DNB-leucine was separated within 4 seconds (Figure 5-3B). To further reduce the extra-column volume, UHPLC instrument was modified (See Experimental) to separate DNB-phenylglycine in just under a second (Figure 5-3C). Further developments regarding sub-second separation, including peak fitting used to obtain the chromatogram, are described elsewhere.[184] Figure 5-3D-F show ultrafast separations of FMOC-blocked amino acids performed in SFC operating at 20.0 mL/min using a 3 x 0.46 cm i.d. column packed with QHS 2.7 µm SPP. These are only representative examples to showcase the capability of this 2.7 µm SPP CSP and most of the analytes from Table 5-2 can be optimized to separate under a minute using QHS 2.7 µm SPP as well as QML 2.7 µm SPP.[52] Note that all separations on QHS 2.7 µm SPP in SFC were under a minute (Table 5-3). See Experimental for the instrument optimizations.
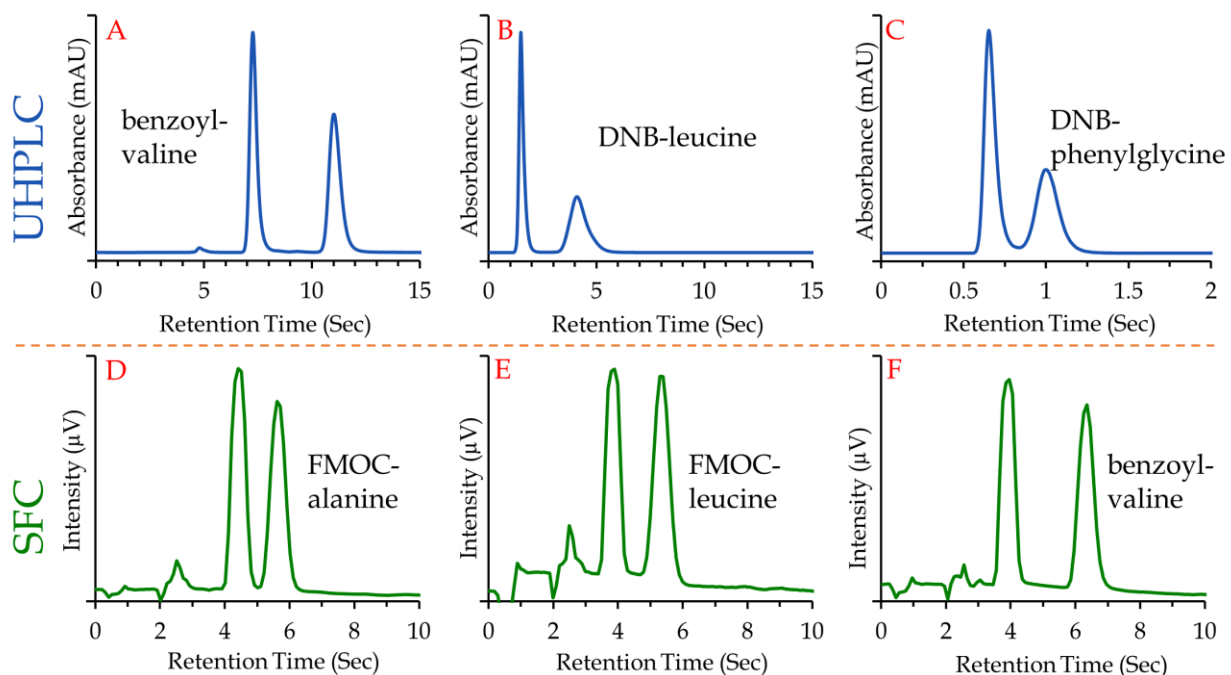
Figure 5-3. Ultrafast separations of *N*-blocked amino acids performed with the hydrosilated quinine (QHS) column packed with 2.7 µm SPPs in UHPLC and SFC. A) benzoyl-valine on QHS SPP column (3 x 0.46 cm i.d.), mobile phase: 90/10 MeOH/100 mM NH_4OAc (pHa 7.0) at 4.5 mL/min flow rate. B) DNB-leucine on QHS SPP column (0.5 x 0.46 cm i.d.), mobile phase: 100/0.5/1.8 MeOH/FA/TEA (v/v/v) at 5.0 mL/min flow rate. C) DNB-phenylglycine on QHS SPP column (0.5 x 0.46 cm i.d.) using a modified UHPLC (as described in the Experimental section), mobile phase: 70/30 ACN/20 mM NH_4OAc at 5.0 mL/min flow rate. SFC separations of D) FMOC-alanine, E) FMOC-leucine, and F) benzoyl-valine were performed using a QHS SPP column (3 x 0.46 cm i.d.), mobile phase: 75% CO_2 – 25% 100/0.6/0.5 MeOH/FA/$HCOONH_4$ (v/v/w) at 20.0 mL/min flow rate. Backpressure regulator was maintained at 78 bar and temperature was ambient.

The combination of high selectivity selectors, high-efficiency columns, reduced retention of 2.7 µm SPPs, and instrumental optimizations allow such ultrafast separations.[45,52,184] These columns can be of use for fast screening, provide increased productivity, and a fast 2nd dimension in 2D-LC that enables separation within seconds to avoid the wrap-around effect. With high selectivity for N-blocked amino acids, these CSPs can be of use in high-throughput analysis of biological samples where separation of amino acids is of critical interest.[2,230] For the commercial 5 µm FPP QNAX column, the

130

manufacturer lists maximum flow rate of 2.0 mL/min and maximum backpressure of 180

bar. In comparison, 2.7 μm SPP based columns prepared in this study showed no signs

of instability or performance degradation at 5 mL/min flow rate with backpressures up to

800 bar.

5.4.3 LC-MS Compatible Methods

   For separation of chiral acids with MS detection, quinine based CSPs are

attractive due to their high selectivity, and their operation in polar organic and reserved

phase LC modes. The question is, can 2.7 μm SPP based columns alleviate issues

pertaining to high counterion concentrations (20-100 mM) which are incompatible with

certain MS sources such as ESI (Figure 5-4). Furthermore, the analysis time increases

considerably with the use of low flow rates necessary for LC-MS methods. Figure 5-4

shows the separation of dansyl-α-N-butyric acid performed at 1.0 mL/min on Chiralpak

QNAX (15 x 0.46 cm i.d.) and QML 2.7 μm SPP (5 x 0.46 cm i.d.) using two different

buffer concentrations in the mobile phase. One mobile phase contained 80% MeOH-20%

100 mM NH_4OAc aqueous buffer (20 mM overall), while the other mobile phase

contained 80% MeOH-20% 10 mM NH_4OAc aqueous buffer (2 mM overall). The pH_a was

kept at 6.0 for both mobile phases. In all cases, the shorter high-efficiency QML 2.7 μm

SPP column is able to provide the same resolution as QNAX with the analysis being

more than 3 times faster (Figure 5-4). With the use of a 10 mM buffer for QML 2.7 μm

SPP (Figure 5-4A), the analysis is completed within 17 min, which is 2 times faster than

analysis time of the 5 μm FPP based column with 100 mM buffer (Figure 5-4D).

Moreover, observing the tailing factors and peak shapes in Figure 5-4, it is apparent that

reducing the buffer concentration leads to slight fronting. Clearly, 2.7 μm SPP based

column are the superior choice for developing LC-MS compatible methods that provides

faster analysis. Higher efficiency also leads to improved signal-to-noise (S/N) ratio which can help with quantitation as well as detection of trace level analytes. Researchers using other buffers such as ammonium formate for MS compatible methods can expect results similar to those shown in Figure 5-4.
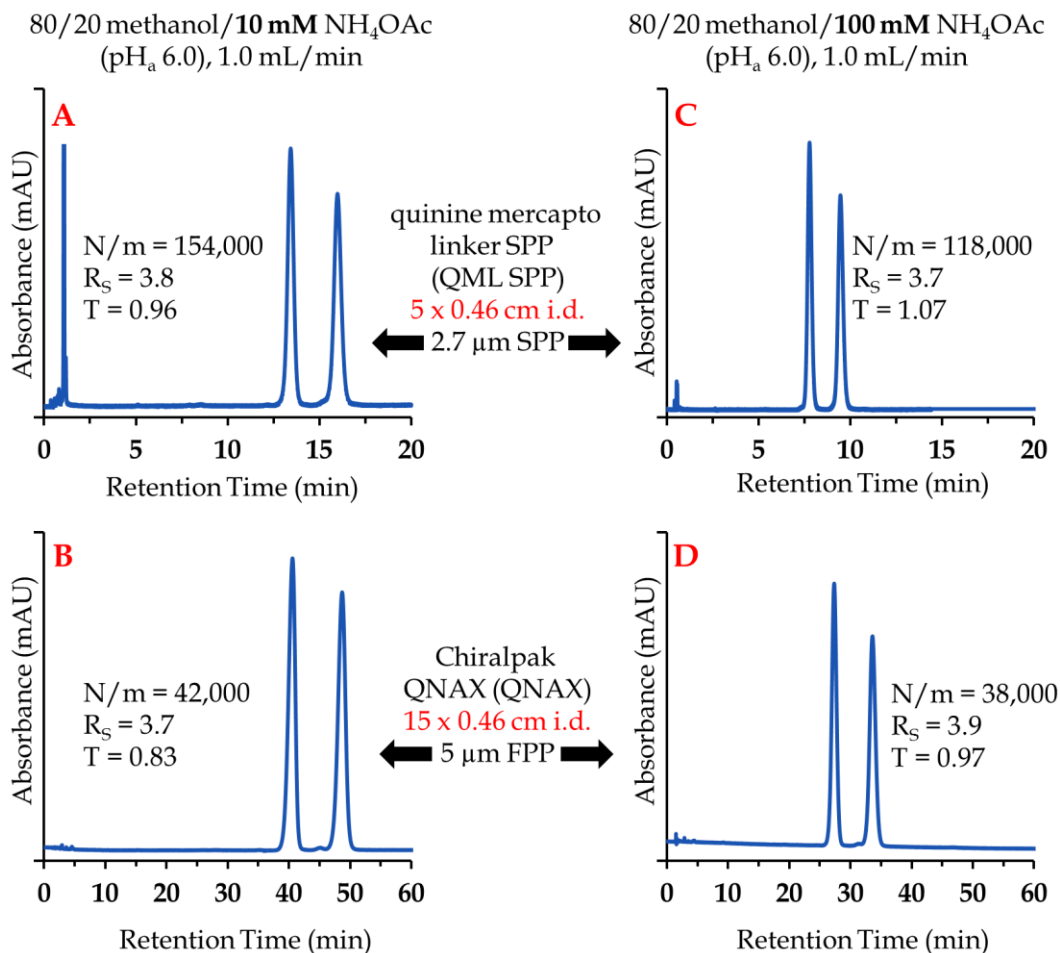
Figure 5-4. Effect of reduced buffer concentration in the mobile phase on column performance for better MS compatible methods. Dansyl-α-N-butyric acid was analyzed on the quinine mercapto linker SPP (QML 2.7 μm SPP) (A and C) and 5 μm FPP Chiralpak QNAX (B and D) at flow rate of 1.0 mL/min with two different buffer concentrations in mobile phase. Mobile phase for A and B: 80/20 MeOH/10 mM NH4OAc (pHa = 6.0). Mobile phase for C and D: 80/20 MeOH/100 mM NH4OAc (pHa = 6.0). See Experimental section for details on N/m, RS, and T.

5.4.4 van Deemter Plots

Figure 5-5 shows van Deemter plots of reduced plate height (h) vs. linear velocity u_0 (mm/s) generated on QNAX (blue square, ■), QHS 2.7 μm SPP (orange circle, ●), and QML 2.7 μm SPP (green triangle, ▲) columns in UHPLC using benzoyl-valine (Figure 5-5A) and SFC using FMOC-alanine (Figure 5-5B). The 2.7 μm SPPs are expected to provide higher theoretical plates (N) or lower plate height (H) values compared to 5 μm FPPs due to their smaller particle size. However, since the reduced plate height h is independent of particle size, any improvement seen in Figure 5-5 for 2.7 μm SPP columns is solely due to improved packing homogeneity and performance of 2.7 μm SPPs. Also apparent is the lower h_{min} (h at the lowest point on the curve) and higher $u_{0,opt}$ (u_0 at the lowest point on the curve) for 2.7 μm SPP columns. Columns packed with 2.7 μm SPPs show an increase in efficiency advantage at higher flow rates, which is essential for ultrafast separations. Despite showing almost identical reduced plate heights for achiral and chiral probe analyte in Table 5-1, QHS 2.7 μm SPP does show slightly higher reduced plate height in Figure 5-5 compared to QML 2.7 μm SPP. A possible explanation for this behavior could be the increased contribution of extra-column band broadening at low retentions, typically observed on the QHS 2.7 μm SPP column.
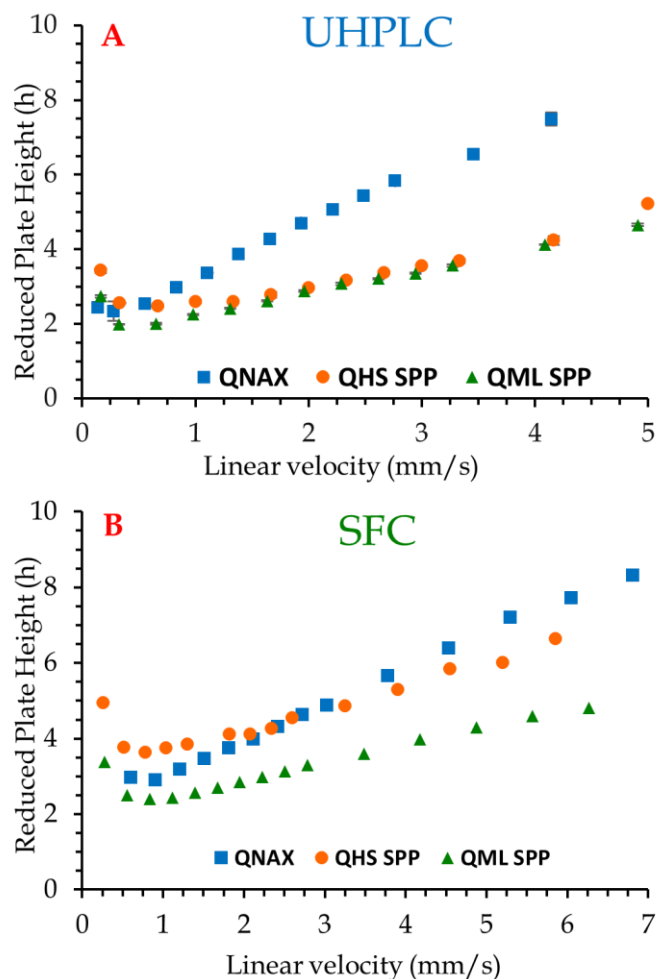
Figure 5-5. The van Deemter plots showing reduced plate height (h) against linear velocity u_0 (mm/s) for chiral analytes in SFC and UHPLC on quinine mercapto linker SPP (QML SPP, 5 x 0.46 cm i.d., 2.7 μm SPP, green triangle, ▲), quinine hydrosilated SPP (QHS SPP, 5 x 0.46 cm i.d., 2.7 μm SPP, orange circle, ●), and Chiralpak QNAX (QNAX, 15 x 0.46 cm i.d., 5 μm FPP, blue square, ■). A) UHPLC van Deemter with analyte: benzoyl-valine, mobile phase: 90/10 MeOH/100 mM NH_4OAc (pH_a 7.5), 254 nm B) SFC van Deemter with analyte: FMOC-alanine (1st enantiomer), mobile phase: 60% CO2 – 40% 100/0.6/0.5 MeOH/FA/$HCOONH_4$ (v/v/w), 254 nm. Backpressure regulator maintained at 78 bar and temperature was ambient.

5.4.5 Kinetic Plots

The van Deemter plots (Figure 5-5) provide useful data such as minimum

reduced plate height, optimum linear velocity, and a visual representation of contributions

from A, B, and C terms to band broadening. It however does not account for column

permeability or backpressure generated, differences in particle morphology (e.g. FPPs

vs. SPPs), or analysis time. A better and more fair comparison of these factors can be

made with the use of kinetic plots (Figure 5-6). The idea of kinetic plots was explored

decades ago by investigators such as Giddings, Knox, Poppe, and recently by Desmet

and co-workers.[231-234] Although there's many different types of kinetic plots, the analysis

time vs. N and column length vs. N plots chosen for this study have been considered the

most useful for chromatography practitioners.[233,234] These plots account for particle size,

silica morphology, permeability, and column lengths. Comparing the columns using these

geometry-independent plots can allow unbiased comparison of their intrinsic kinetic

performance. Using experimentally determined specific column permeability and plate

height vs. linear velocity data from the van Deemter plot, dead time and maximum

theoretical plates can be calculated when columns are operated at maximum system

pressure (ΔP_{max}) with equation 3-2 and 3-3.

$$N = \left(\frac{\Delta P_{max}}{\eta}\right)\left(\frac{K_S}{u_0 H}\right)_{exp} \tag{5-2}$$

$$t_0 = \left(\frac{\Delta P_{max}}{\eta}\right)\left(\frac{K_S}{u_0^2}\right)_{exp} \tag{5-3}$$

where ΔP_{max} = maximum possible system pressure (Pa), H = theoretical plate

height (m), η = mobile phase viscosity (Pa.s), u_0 = linear velocity (m/s), K_V = specific

column permeability, and the subscript exp denotes experimentally obtained data.

Analysis time at ΔP_{max} was calculated by using $t_{R_2} = t_0(1 + k_2)$ and the column length

using L = N x H_{exp}. The literature viscosity value of 90/10 MeOH/H2O mixture[235] is used

as η (effect of buffer is assumed negligible), and it is used as a constant value through all

flow rates.

Figure 5-6 shows the kinetic plots prepared using the above equations for QML 2.7 μm SPP and 5 μm QNAX columns at ΔP_{max} of 1200 bar and 600 bar to compare their kinetic performance under UHPLC and HPLC system pressures, respectively. In each comparison, lower y-axis and higher x-axis values correlate to better performance. The QHS 2.7 μm SPP CSP was omitted from this comparison due to different bonding chemistry of the selector which led to drastically different retention times in comparison to the other two CSPs that use traditional bonding (Table 5-2). With ΔP_{max} of 600 bars, Figure 5-6A shows the QML 2.7 μm SPP column (blue circle, ●) being advantageous compared to QNAX column (yellow diamond, ♦) for up to 50 min analysis times and 90,000 plates on HPLC systems. The 2.7 μm SPP based column generates greater number of maximum plates compared to 5 μm FPP based column for the same analysis time making it possible to achieve greater resolution of analytes under HPLC pressures. Similarly, for a desired number of plates, relatively lower analysis times can be achieved when using 2.7 μm SPP based column under HPLC pressures. Gasparrini and coworkers compared a sub-2 μm FPP pi-complex CSP with a 5 μm FPP CSP and concluded that the sub-2 μm FPP was in fact not advantageous at HPLC pressures.[63] The performance improvement of 2.7 μm SPP columns are even more impressive when compared at ΔP_{max} of 1200 bar, a UHPLC system pressure. The QML 2.7 μm SPP column (green square, ■) far outperforms the QNAX column (red triangle, ▲) and remains advantageous till the last point on its curve at 507 min analysis time and 285,000 plates (See Figure 5-6A). For practical usage, typical analysis times are expected to be less than 1 hour, and thus 2.7 μm SPP based CSP provides greater performance than 5 μm FPP CSP in HPLC and UHPLC for most analyses. Kinetic plot numbers such as $t_{R,1k}$ (time needed to generate 1000 plates) have been suggested as a better metrics compared to h_{min} or $u_{0,min}$ for direct comparison of columns.[233] To avoid adding uncertainty

136

from extrapolation, the $t_{R,1k}$ value has been omitted in favor of $t_{R,10k}$ and $t_{R,25k,}$ provided in

Table 5-4. It is clear that, regardless of the ΔP_{max}, QML 2.7 µm SPP reaches the 10,000

and 25,000 plates mark much faster than QNAX in each case proving that its

performance far exceeds that of the 5 µm FPP based column. With use equation 3-4,[7]

one can calculate plates (N) required to achieve a particular resolution (R_S) value, and

determine the necessary analyte retention to achieve the corresponding value based on

Figure 5-6A.

$$R_S = \frac{\sqrt{N}}{4}\left(\frac{\alpha-1}{\alpha}\right)\left(\frac{k_2}{1+k_2}\right)$$ (5-4)

Table 5-4. Kinetic plot values for QML SPP and QNAX columns.

CSPs	ΔP_{max} (bars)	$t_{R,10k}$ (min)[a]	$t_{R,25k}$ (min)	L_{10k} (m)[b]	L_{25k} (m)
QNAX 5 µm FPP	1200	5.5	14	0.45	0.7
QNAX 5 µm FPP	600	2.7	8.5	0.27	0.46
QML 2.7 µm SPP	600	1.5	6.3	0.09	0.18
QML 2.7 µm SPP	1200	1.2	4.2	0.11	0.21

[a]$t_{R,10k}$ = analysis time needed to generate 10,000 plates on each column
[b]L_{10k} = column length corresponding to 10,000 plates value

Further, if an analysis needs to be completed within a certain timeframe for

applications such as second dimension in 2D-LC or real-time monitoring of reactions, the

corresponding plates generated on each column for the analysis time can be calculated

and used to determine the expected resolution value from equation 3-4. Figure 5-6B

provides column length L vs N plots which show the maximum number of plates

generated for various column lengths at ΔP_{max} of 1200 and 600 bar. It is apparent that for

each ΔP_{max}, 2.7 µm SPP based column generates significantly greater number of plates

compared to 5 µm FPP based column for any given column length. Clearly, for any

number of desired plates, a relatively shorter 2.7 µm SPP column could provide the

needed performance resulting in a faster analysis (Figure 5-6B). Similar to $t_{R,10k}$ values,

L_{10k} (length of column necessary to generate 10,000 plates) and L_{25k} values were also

137

calculated to find that 2.7 μm SPP columns can theoretically reach these plate numbers with much shorter column in comparison to QNAX regardless of the ΔP_{max} (Table 5-4). Using these kinetic plots, fine-tuned methods can be developed with desired resolution values and analysis times by choosing the correct particle morphology and column length. These results show that 2.7 μm SPPs provide a number of benefits in terms of speed and efficiency over a 5 μm FPP based column.
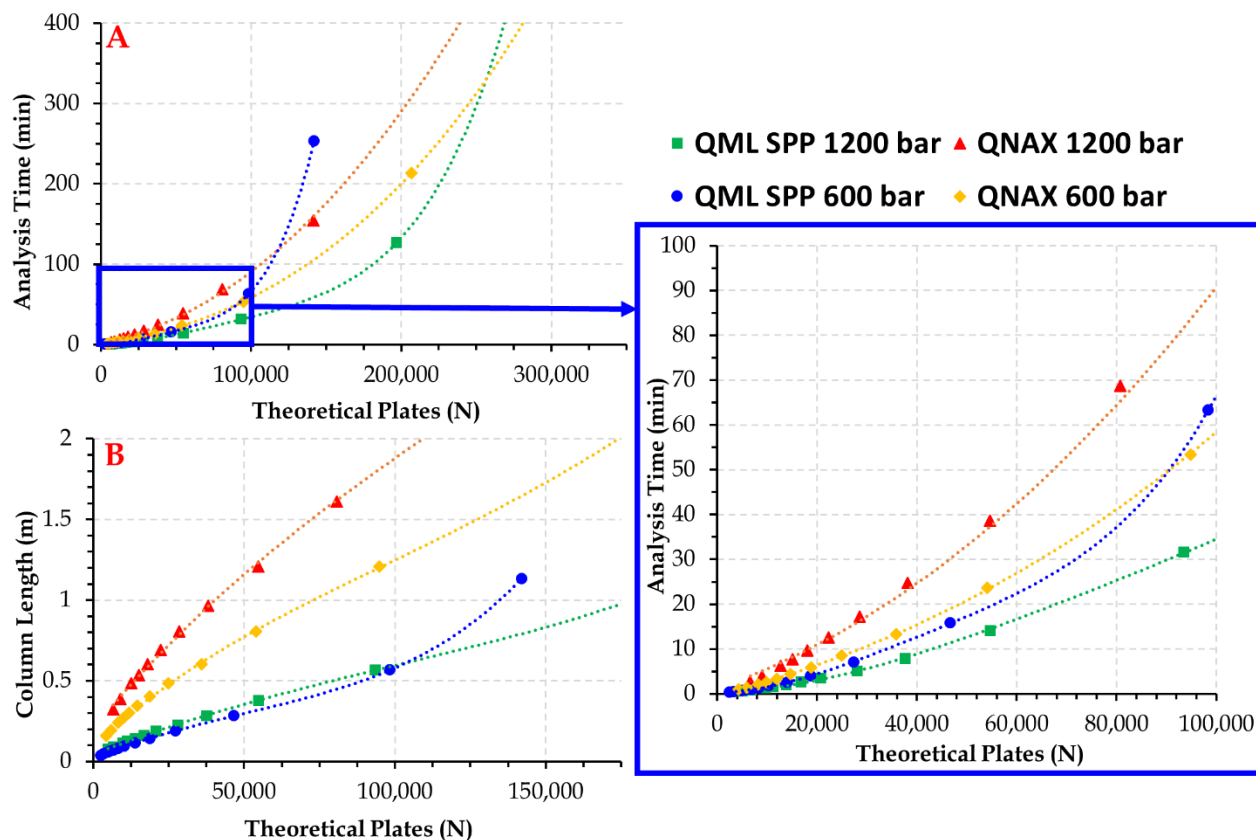
Figure 5-6. Kinetic plots A) Analysis time or t_{R2} (min) vs. N. and B) column length L (m) vs. N for QML SPP (2.7 μm SPP) and QNAX (5 μm FPP) columns comparing the intrinsic performance of different particle size and morphology for benzoyl-valine. Mobile phase: 90/10 MeOH/100 mM NH₄OAc (pHa 7.5), 254 nm. Plots are generated at ΔP_{max} of 600 bar (HPLC) for QML SPP (blue circle, ●) and QNAX (yellow diamond, ♦) as well as 1200 bar for QML SPP (green square, ■) and QNAX (red triangle, ▲) columns.

5.5 Conclusion

Two new high-selectivity quinine based chiral selectors were bonded to 2.7 μm SPPs to create high-efficiency CSPs that were extensively characterized and compared with the analogous commercial 5 μm FPP based column in UHPLC and SFC. 2.7 μm SPP based quinine CSPs have significantly higher efficiencies and provide remarkably faster analysis times than the traditional 5 μm FPP based columns. High selectivity, high-efficiency, and low retentions on the QHS 2.7 μm SPP CSP were exploited to obtain several rapid separations that are on the order of a few seconds which can dramatically improve the productivity in routine analyses. 2.7 μm SPP based columns were also shown to provide rapid analysis even with reduced counterion concentrations which can enable fast LC-MS analysis with ESI compatible mobile phases. Improved efficiencies also result in better signal-to-noise ratios which can make it possible to achieve lower LOD and LOQ values for biological samples analyzing N-blocked amino acids. 2.7 μm SPPs have relatively higher column permeability than sub-2 μm particles making it possible to take advantage of their performance in HPLC as well as UHPLC. Geometry independent kinetic plots and van Deemter plots showed the improved performance of 2.7 μm SPPs over traditional 5 μm FPPs in HPLC and UHPLC conditions.

Chapter 6

Gone in Seconds: Praxis, Performance, and Peculiarities of Ultrafast Chiral Liquid

Chromatography with Superficially Porous Particles

6.1 Abstract

A variety of brush-type chiral stationary phases (CSPs) were developed using superficially porous particles (SPPs). Given their high efficiencies and relatively low back pressures, columns containing these particles were particularly advantageous for ultrafast "chiral" separations in the 4–40 s range. Further, they were used in all mobile phase modes and with high flow rates and pressures to separate over 60 pairs of enantiomers. When operating under these conditions, both instrumentation and column packing must be modified or optimized so as not to limit separation performance and quality. Further, frictional heating results in axial thermal gradients of up to 16 °C and radial temperature gradients up to 8 °C, which can produce interesting secondary effects in enantiomeric separations. It is shown that the kinetic behavior of various CSPs can differ from one another as much as they differ from the well-studied C18 reversed phase media. Three additional interesting aspects of this work are (a) the first kinetic evidence of two different chiral recognition mechanisms, (b) a demonstration of increased efficiencies at higher flow rates for specific separations, and (c) the lowest reduced plate height yet reported for a CSP.

6.2 Introduction

For much of three decades, the development and study of chromatographic enantiomeric separations have been dominated by investigations focused on selectivity. This is not surprising given the unique position of chiral separations in chromatography where conventional strategies used for all other molecules are completely ineffective for

140

enantiomers. Hence, the highest impact studies involved conceiving, understanding, and optimizing the use of new and better chiral selectors.[9-14,17,19,25,27,30,212,213,236-242] Numerous thermodynamic and mechanistic studies as well as evaluations of solvent and additive effects continue even today.[243-246]

As the field of "chiral separations" has matured, it has focused on other, more typical chromatographic concerns including speed, efficiency, and kinetic effects. While "chiral separations" are ultimately affected by the same parameters as achiral separations, they can have some idiosyncrasies (vide infra) as compared to the most extensively studied systems which typically involve reversed phase liquid chromatography on C18 or analogous stationary phases.

The demand for fast and efficient achiral separations provided the impetus for researchers to explore new avenues to increase throughput of chiral screening and analysis. Welch et al. first used multi-parallel chiral screening and method development systems that provided method development times of ~1 h.[216] The 8-channel microfluidic HPLC system utilized microbore (0.3 mm i.d.) columns packed with traditional 5 µm fully porous particles (FPPs) and provided chiral method development times of around 1 hour.[216,247] Hamman et al. used supercritical fluid chromatography (SFC) at high flow rates, short columns, and a gradient to obtain a 2.5 min screening method.[22] Guillarme, et al. used sub-2 µm achiral columns with a chiral derivatizing agent to produce fast (2-5 min) enantiomeric separations of amphetamine and β-blockers.[44] Shortly after, Ai and co-workers developed a bonded sub-1 µm mesoporous silica based cyclodextrin chiral column and published a few 1–6 min enantiomeric separations.[59] Concurrently, Gasparrini et al. studied a bonded brush-type (pi-complex) phase using sub-2 µm fully porous particles (FPPs) and demonstrated a few normal phase enantiomeric separations in the 15–40 s range.[63]

141

More recently, superficially porous particles (SPPs) for achiral separations have allowed for column efficiencies comparable to sub-2 µm FPPs while using conventional HPLCs and column hardware.[49] There have been numerous empirical and theoretical comparisons of these approaches when used in a reversed phase (C18) format.[43,50,220,221] SPPs are able to decrease all contributions to band broadening (i.e., longitudinal diffusion, eddy dispersion, and stationary phase mass transfer contributions).[221] Initially it was thought that better packing of SPPs was due to their having narrower particle size distributions than FPPs, but it was later shown that better packing homogeneity across the column (i.e., from wall to center of the bed) is largely responsible for the decreased eddy dispersion contribution.[58,144] Since, SPP columns are generally better packed than FPP columns, they can yield reduced plate heights of 1.3–1.5 for columns packed with conventional achiral stationary phases, whereas FPP based columns typically have reduced plate heights greater than 2.0.[43] Also, the shell thickness of SPPs leads to a shorter trans-particle path length which can decrease mass transfer contributions to band broadening for large molecules with small diffusion coefficients and smaller molecules that have slow adsorption–desorption kinetics.[49,51,53] This is particularly important at higher flow rates.

The possible benefits of SPPs in other important but more specialized areas of LC are less explored. Chankvetadze compared a polysaccharide based chiral selector coated on FPPs and SPPs in both nano-LC and HPLC.[65,66] In the latter, an obvious decrease in enantiomeric selectivity was noted for the SPP based material. Gritti and Guiochon's theoretical treatment of the same polysaccharide based chiral selector indicated that a 10% gain in resolution (Rs) could be possible due to the decreased plate heights afforded by the SPPs.[229] However, this estimated value was based on an assumption that the SPP based polysaccharide column would have a similar

enantiomeric selectivity value as the analogous FPP based column which, as noted, has not been obtainable to date. Most recently, Spudeit et al. presented the first successful and practical SPP CSP.[53] This work showed that brush-type chiral selectors (i.e., isopropylcarbamated cyclofructan 6) have a higher chiral selector load (per surface area). This plus the observed increase in column efficiency for the SPP based CSP resulted in improved enantiomeric separations, while maintaining the same enantiomeric selectivity as FPP based CSPs.[53] Further, the SPP CSP maintained this performance with 50–75% lower retentions. When comparing constant retention modes, the Rs values obtained using the SPP column were far greater than the FPP columns. It was also noted that as flow rates increased (e.g., to 3 mL/min), the resolution per analysis time greatly improved for the SPP column (by 18–67%) meaning that high-throughput screening would benefit from such columns.[53]

In this work, a broad range of analyte types and polarities including pharmaceuticals, catalysts, peptides, amino acids, primary amines, and biaryls among others were baseline separated on a variety of SPP brush type CSPs that are very effective for ultrafast chiral separations (~4–40 s range). It is demonstrated that they can be performed in any mobile phase conditions or mode, i.e., reversed phase, normal phase, polar organic, and HILIC. Finally, the practice of ultrafast chiral LC often produces interesting and unusual consequences that must be recognized, dealt with, and/or properly understood for optimal performance.

6.3 Experimental

6.3.1 Materials

All HPLC solvents and reagents for reactions were purchased from Sigma-Aldrich (St. Louis, MO). Cyclofructan-6 (CF6) and cylcofructan-7 (CF7) derivatized with

isopropyl carbamate and dimethylphenyl carbamate groups, respectively, were synthesized by AZYP LLC (Arlington, TX). The 2.7 μm superficially porous silica particles with a surface area of 120 m^2/g and pore size of 120 Å were provided by Agilent Technologies (Wilmington, DE). The core is 1.7 μm in diameter and the surrounding shell thickness is 0.5 μm. The fully porous 2.1 and 3 μm silica particles were purchased from Daiso (Tokyo, Japan) and Glantreo (Cork, Ireland), respectively. The 2.1 μm fully porous particles have a surface area of 479 m^2/g and pore size of 91 Å, whereas the 3 μm fully porous particles have a surface area of 300 m^2/g and pore size of 100 Å. Tröger's bases were obtained as indicated in the literature.[248]

6.3.2 Synthesis of Stationary Phases

All reactions were carried out in anhydrous solvents under a dry argon atmosphere. The synthetic procedures for the six stationary phases employed in this work have already been published.[9,10,239,240,249] The first chiral stationary phases explored were cyclofructan based as they have recently proven to be unique chiral selectors.[9,29,98,99,250-252] The cyclofructan-6 derivatized isopropyl carbamate (CF6-P) and cyclofructan-7 dimethylphenyl carbamate (CF7-DMP) were bonded to silica particles under anhydrous conditions as described previously.[9] The 2-hydroxypropyl-β-cyclodextrin bonded silica (CD-HP) was synthesized via a proprietary bonding procedure.[239,249] Macrocyclic antibiotics vancomycin, teicoplanin, and teicoplanin aglycone were covalently attached to silica surface as described by Armstrong et al.[10,240] Each of the above chiral selectors were bonded to 2.7 μm SPPs. The 2.1 and 3 μm fully porous particles were functionalized with CF6-P. The CHN analyses of the phases and chiral selector coverage per surface are provided in Table 6-1 below.

144

Table 6-1. Elemental analysis and the surface coverage for the SPP based chiral stationary phases.

Stationary phase	%C	%N	Surface coverage µmol/m^2	Selector loading %
CF6-P	6.2	0.88	0.88	13.1
CF7-DMP	3.05	0.21	0.11	5.0
teicoplanin	4.73	0.57	0.34	8.8
vancomycin	5.32	0.94	0.48	10.0
hydroxypropyl-β cyclodextrin	4.17	Not detected	0.50	8.5
teicoplanin aglycone[a]	8.34	1.74	N/A	N/A

[a]The details required to calculate surface coverage values for this stationary phase are unavailable.

Each stationary phase was slurry packed with a pneumatically driven Haskel pump (DSTV-122) into 10 cm × 0.46 cm i.d., 5 cm × 0.46 cm i.d., and 3 cm × 0.46 cm i.d. stainless steel columns (IDEX Health and Science, Oak Harbor, WA). See the next sub-section for the packing method. Commercial LARIHC CF6-P, LARIHC CF7-DMP, Chirobiotic V, Chirobiotic T, Chirobiotic TAG, and Cyclobond I 2000 HP-RSP columns (fully porous 5 µm particles, 25 cm × 0.46 cm i.d.) which were used for comparative purposes were provided by AZYP LLC, Astec, and Supelco/Sigma-Aldrich.

6.3.3 Column Packing

Each stationary phase was slurry packed with a pneumatically driven Haskel pump (DSTV-122) into 10 x 0.46, 5 x 0.46 and 3 x 0.46 cm i.d. stainless steel columns (IDEX Health and Science, Oak Harbor, WA). The slurry optimization procedures, such as reduction of shear thickening, optical microscopy, and settling vial tests were conducted for several organic solvents before packing.[57] A 2 µm frit cap (IDEX) was used to cap the column ends quickly after the packing procedure. The column specific permeability (Ks) was determined by plotting the pressure drop against the linear mobile phase velocity (discussed later).

6.3.4 Instrumentation

All ultrafast separations were performed on an Agilent 1290 Infinity series UHPLC system (Agilent Technologies, Santa Clara, CA) equipped with a quaternary pump, an auto-sampler, and a diode array detector. Routine separations were performed on an Agilent 1260 HPLC equipped with a quaternary pump, an auto-sampler, and a diode array detector. An inlet filter was installed between the pump outlet and the auto-sampler injection valve to prevent clogging of 75 μm tubings. For fast separations, the data collection rate was set at 160 Hz with a response time of 0.016 s, unless otherwise stated. The thermostated column compartment and the column switching 6-port valve were bypassed to minimize the length of connection tubings. The instrument was further optimized to reduce extra-column effects by using an ultralow dispersion kit from Agilent (P/N 5067-5189). The kit consists of an ultralow dispersion needle and needle seat, two 75 μm i.d. stainless steel connection tubings, and a detector flow cell with a volume standard deviation V(σ) of 0.6 μL. Alternatively, 75 μm i.d. polyether ether ketone (PEEK) nanoViper connection tubings (Thermo Fisher Scientific, MA) were also employed. The instrument was controlled by OpenLAB CDS ChemStation software (Rev. C.01.06 [61], Agilent Technologies 2001–2014) in Microsoft Windows 8.1. The reported percentages of mobile phases (m.p.) are listed as volume/volume (v/v).

6.3.5 Chromatography Peak Parameters

The reported theoretical plates (N, by half height method), peak asymmetry factors (USP tailing factor $T = \frac{W_{0.05}}{2f}$; where $W_{0.05}$ = peak width at 5% peak height, f = distance from the leading edge of the peak to the peak maximum at 5% peak height), peak variance σ^2 (by tangent method), and retention times (t_R) were obtained from

146

OpenLAB CDS ChemStation software. Resolutions $\left(R_S = \frac{2.35\,(t_{R_2} - t_{R_1})}{2\,(W_{0.5,1} + W_{0.5,2})} \right)$ were calculated

using the half-height method. To assess the extra-column contribution to the observed

plate heights, the column was removed and the tubings were connected by a zero dead

volume union. See later section for calculations.

6.3.6 Axial Temperature Gradient in Mobile Viscous Frictional Heating

The effect of viscous frictional heating of the mobile phases in the SPP columns

was studied by wrapping the column in an insulating sheet (at room temperature) and

inserting a Mastech thermocouple MS8222H (Pittsburgh, PA) inside the column outlet

with the help of a screw cap. The flow rate was varied and the resulting temperature was

monitored after 10 min of equilibration.

6.4 Results and Discussion

Figure 6-1A provides comparisons of different particle size fully porous particles

(FPPs) and superficially porous particles (SPPs) which have the same bonded chiral

selector (via the same chemistry) and with the same mobile phase. These

chromatograms were generated using conventional HPLCs with conventional conditions

and column sizes (i.e., 1.0 mL/min flow rate and 5 cm × 0.46 cm i.d. columns). Clearly

using the same mobile phase, the SPP-based CSP provided both the greatest efficiency

and shortest analysis time as compared to all FPPs, including the 2.1 μm particles

(Figure 6-1A). However, according to Gritti and Guiochon, a better comparison of such

columns is realized when resolutions (RS) are compared at constant retention (Figure

6-1B).[229] They also indicated that a SPP's core to particle diameter ratio (ρ) can be

related to its gain in resolution. Specifically ρ values between 0.5 and 0.95 at constant

retention factor (k) can slightly improve the resolution. Interestingly, recent work on a

brush-type CSP showed a resolution increase of 20%.[53] In Figure 6-1B, the increase in resolution of the SPP-CSP over both 3 and 2.1 μm FPPs is ~30%, which is quite impressive. The SPP-CSP used here had a ρ value of 0.63 (see Experimental Section), which is within the optimal range (vide supra).[229] A direct comparison of the efficiencies, reduced plate heights, and tailing factors of current commercial columns (5 μm particles) and the analogous CSPs on 2.7 μm SPPs is given in Table 6-2. The 3–4-fold increase in efficiencies is impressive but not totally unexpected given the smaller SPP particle diameter. However, the reduced plate heights of the SPPs also are up to 2 times smaller and with comparable or better peak symmetries. The reduced plate height (h) of 1.6 for the CF7-DMP SPP is the smallest reported for any CSP on any particle to date. Given these results, it is clear that SPP based CSPs should be particularly advantageous for ultrafast chiral separations.

Table 6-2. Comparison of theoretical plates/meter (N/m), reduced plate height (h), and USP tailing factor using a standard achiral probe 1,3-dinitrobenzene with 70:30 heptane: ethanol at reduced velocity of 4.5 (1 mL/min for 2.7 μm SPP, 0.6 mL/min for 5 μm FPP).

Stationary phase	N/m[a]	h	Tailing factor[b]
Stationary phases bonded to 2.7 μm SPP			
CF6-P[c]	172,000	2.2	1.1
CF7-DMP[d]	221,000	1.6	1.2
teicoplanin[d]	165,000	2.3	1.0
teicoplanin aglycone[C]	133,000	2.8	1.3
vancomycin[C]	173,000	2.1	0.9
hydroxypropyl-β-cyclodextrin[d]	181,000	2.0	1.3
Commercial columns packed with 5.0 μm FPP (25 x 0.46 cm)			
LARIHC CF6-P	70,000	2.9	1.1
LARIHC CF7-DMP	59,000	3.4	1.2
Chirobiotic-T	54,000	3.7	0.9
Chirobiotic-TAG	50,000	4.0	1.1
Chirobiotic-V	57,000	3.5	0.9
Cyclobond I 2000 HP-RSP	37,000	5.4	1.1

[a]N/m calculated by half height method.

148

[b]USP tailing factor $T = \frac{W_{0.05}}{2f}$. (Where $W_{0.05}$ = peak width at 5% peak height, f = distance from the leading edge of the peak to the peak maximum at 5% peak height.

[c]dimensions of these columns were 10 x 0.46 cm.

[d]dimensions of these columns were 5 x 0.46 cm.
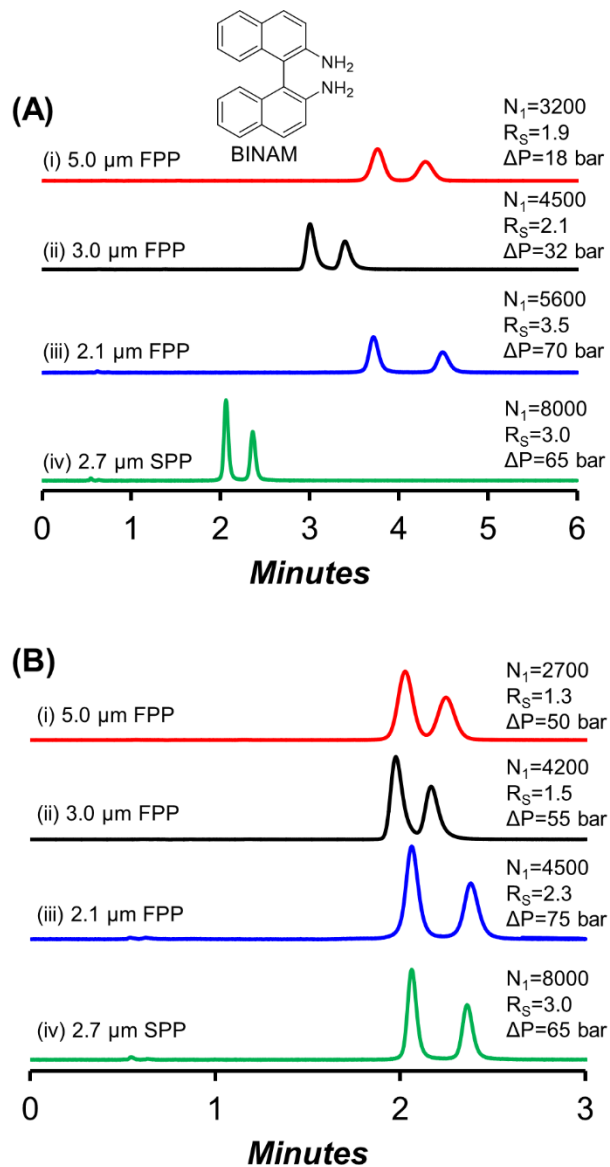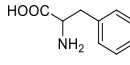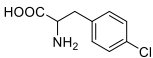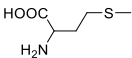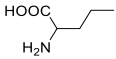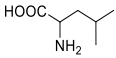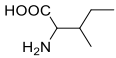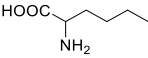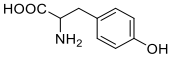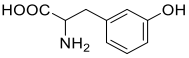
Figure 6-1. Enantiomeric separations of BINAM on CF6-P bonded to SPPs and FPPs at 1.0 mL/min, Tcol = 25 °C. All columns were 5 cm × 0.46 cm in dimensions. (A) Constant MP mode, MP = 92:8 heptane−ethanol. (B) Constant retention mode, MP = (i) 82:18

149

heptane−ethanol, (ii) 85:15 heptane−ethanol, (iii) 82:18 heptane−ethanol, and (iv) 92:8 heptane−ethanol.

In the literature, the current accepted time limit for being labeled as an ultrafast chromatographic separation seems to be ~1 min.[224,253] This is probably a reasonable choice since typical HPLC autoinjectors cycle at ~1 injection per min (or down to 0.5 min for UHPLC). Hence in ultrafast LC, the chromatographic separations can be completed more quickly than new samples can be injected (by conventional injection devices). Figure 6-2 and Table 6-3 show over 60 such baseline enantiomeric separations. The table covers a wide structural variety of enantiomers. Most separations are <40 s and almost a quarter of those are on the order of 10 or fewer seconds. Furthermore, these are accomplished in all mobile phase modes, i.e., normal phase, reversed phase, and polar organic modes and on a variety of bonded CSPs. Theoretically, we could screen ~90 to 360 chiral analytes per hour which could use less solvent than any other current method. However, this is restricted to ~60 to, at most, 120 samples/hour because of instrumental autoinjector limitations. Certainly, this is not the first nor the only example of chromatographic potential being limited by instrumental deficiencies.[224,254] Indeed, as discussed in the following paragraphs, the separations shown in Figure 6-2 and listed in Table 6-3 cannot be achieved under standard HPLC conditions used for Figure 6-1.
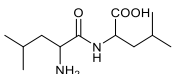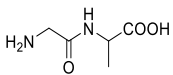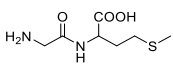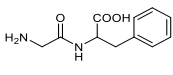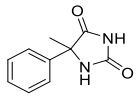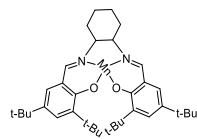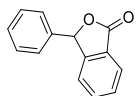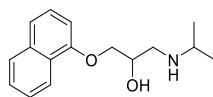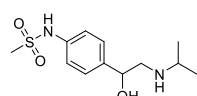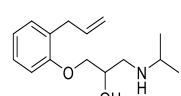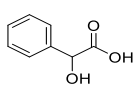
Table 6-3. Chromatographic data for optimized ultrafast chiral separations on six different chiral stationary phases (CSPs) bonded to 2.7 μm superficially porous silica.[1]
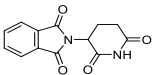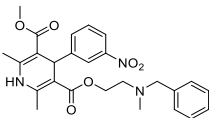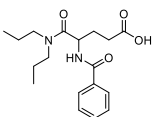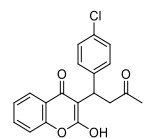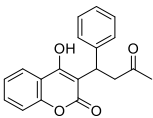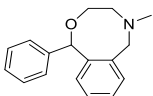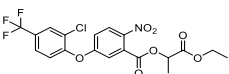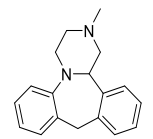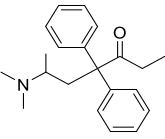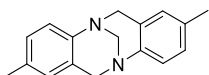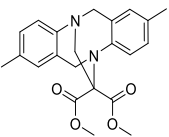
#	Analyte	Structure	CSP[2]	mobile phase; flow rate	t_{R_1} sec	t_{R_2} sec	R_S[1]
1	Alanine	HOOC H_2N	T	25 water:75 MeOH; 3.1 mL/min	12	18	3.2
			TAG	70 water:30 MeOH; 2.5 mL/min	10	13	2.2
2	Phenylalanine	HOOC NH_2	T	25 water:75 MeOH; 2.5 mL/min	15	21	2.2
			TAG		15	22	2.1

150
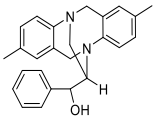
#	Analyte	Structure	CSP[2]	mobile phase; flow rate	t_{R_1} sec	t_{R_2} sec	R_S[1]
3	4-Chlorophenylalanine		TAG	40 water:60 MeOH; 2.5 mL/min 40 water:60 MeOH; 2.5 mL/min	17	26	1.9
4	Threonine		T	10 water:90 MeOH; 2.9 mL/min	13	17	1.6
			TAG	25 water:75 MeOH; 2.5 mL/min	11	15	2.6
5	Methionine		T	90 water:10 MeOH; 3.7 mL/min	8	9	1.5
			TAG	90 water:10 MeOH; 3.3 mL/min	9	12	2.3
6	Valine		T	25 water:75 MeOH; 2.5 mL/min	10	15	2.6
			TAG	90 water:10 MeOH; 2.2 mL/min	11	14	1.6
7	Norvaline		T	80 water:20 MeOH; 3.0 mL/min	8	10	1.5
			TAG	80 water:20 MeOH; 3.0 mL/min	8	13	2.1
8	Leucine		T	10 water:90 MeOH; 2.9 mL/min	13	23	3.2
			TAG	90 water:10EtOH; 3.0 mL/min	9	12	1.9
9	Isoleucine		T	60 water:40 MeOH; 2.5 mL/min	11	14	1.7
			TAG	90 water:10 MeOH; 2.5 mL/min	11	14	1.6
10	Norleucine		T	60 water:40 MeOH; 2.5 mL/min	11	15	2.3
			TAG	60 water:40 MeOH; 2.5 mL/min	13	17	1.7
11	Tyrosine		T	25 water:75 MeOH; 2.5 mL/min	14	18	2.0
			TAG	60 water:40 MeOH; 2.5 mL/min	13	18	1.7
12	m-Tyrosine		T	90 water:10EtOH; 3.7 mL/min	9	12	1.9
			TAG	99 water:1 MeOH; 3.7 mL/min	10	31	2.5

#	Analyte	Structure	CSP[2]	mobile phase; flow rate	t_{R_1} sec	t_{R_2} sec	R_S[1]
13	o-Tyrosine		TAG	15 water:85 MeOH; 3.0 mL/min	16	23	1.6
14	Homophenylalanine		T	90 water:10 MeOH; 3.5 mL/min	12	18	2.7
			TAG	60 water:40 MeOH; 2.2 mL/min	17	39	3.1
15	Homoserine		TAG	50 water:50 MeOH; 2.5 mL/min	10	13	1.5
16	Proline		T	90 water:10 MeOH; 3.7 mL/min	8	13	3.6
			TAG	90 water:10 MeOH; 3.0 mL/min	10	17	2.5
17	2-Phenylglycine		T	90 water:10 MeOH; 3.5 mL/min	9	15	3.3
			TAG	30 water:70 MeOH; 2.7 mL/min	7	14	3.7
18	6-methyl-Tryptophan		T	25 water:75 MeOH; 2.5 mL/min	17	23	1.9
19	3-(1-Napthyl)alanine		T	25 water:75 MeOH; 2.5 mL/min	19	26	1.8
20	3,5-DNB-Tryptophan methyl ester		CF7-DMP	70:30:0.1 heptane:EtOH:TFA, 3.0 mL/min	38	44	1.9
21	BINAM		CF7-DMP	90:10:0.1 heptane:EtOH, 4.8 mL/min	10	12	1.9
22	NOBIN		CF7-DMP	98:2:0.1 heptane:EtOH, 4.5 mL/min	17	22	2.5
23	Vanol		CF6-LP[3]	98.5:1.5 heptane:EtOH, 3.5 mL/min	29	33	1.7
24	2-Amino-1,2-diphenylethanol		CF6-LP[4]	70:30:0.3:0.2 ACN:MeOH:TFA:TEA, 4.0 mL/min	18	20	1.8
25	2-Amino-1-(4-nitrophenyl)-1,3-propanediol		CF6-LP[4]	80:20:0.3:0.2 ACN:MeOH:TFA:TEA, 4.0 mL/min	28	30	1.6

152

#	Analyte	Structure	CSP[2]	mobile phase; flow rate	t_{R_1} sec	t_{R_2} sec	R_S[1]
26	2,4-Dichloro-α-phenethylamine		CF6-LP[3]	90:10:0.3:0.2 ACN:MeOH:TFA:TEA, 5.0 mL/min	12	14	1.8
27	2-Chloro-indan-1-ylamine hydrochloride		CF6-LP[3]	90:10:0.3:0.2 ACN:MeOH:TFA:TEA, 4.5 mL/min	12	14	1.6
28	1(1-naphthyl)ethylamine		CF6-LP[4]	80:20:0.3:0.2 ACN:MeOH:TFA:TEA, 4.5 mL/min	23	25	1.9
29	(1S.2S/1R,2R) trans-1-Amino-2-indanol		CF6-LP[3]	92:8:0.3:0.2 ACN:MeOH:TFA:TEA, 5.0 mL/min	20	26	1.8
30	α-Ethylbenzylamine		CF6-LP[4]	80:20:0.3:0.2 ACN:MeOH:TFA:TEA, 4.0 mL/min	30	32	1.6
31	1-biphenyl-4-yl-ethylamine		CF6-LP[4]	80:20:0.3:0.2 ACN:MeOH:TFA:TEA, 3.0 mL/min	38	40	1.5
32	Norphenylephrine hydrochloride		CF6-LP[4]	75:25:0.3:0.2 ACN:MeOH:TFA:TEA, 3.7 mL/min	36	39	1.5
33	Normetanephrine hydrochloride		CF6-LP[4]	75:25:0.3:0.2 ACN:MeOH:TFA:TEA, 3.6 mL/min	34	37	1.5
34	2-Amino-1-(4-nitrophenyl)-1,3-propanediol		CF6-LP[4]	80:20:0.3:0.2 ACN:MeOH:TFA:TEA, 4.0 mL/min	28	30	1.6
35	Tryptophanol		CF6-LP[4]	80:20:0.3:0.2 ACN:MeOH:TFA:TEA, 4.0 mL/min	27	30	1.5
36	DL-Ala-DL-Ala[5]		T	40:60 water:MeOH, 3.3 mL/min	18	26	2.5
37	DL-Leu-DL-Ala[5]		T	40:60 water:MeOH, 3.0 mL/min	20	25	2.4

153

#	Analyte	Structure	CSP[2]	mobile phase; flow rate	t_{R_1} sec	t_{R_2} sec	R_S[1]
38	DL-Leu-DL-Leu[5]		T	40:60 water:MeOH, 3.3 mL/min	18	27	2.5
39	Gly-DL-Ala		T	40:60 water:MeOH, 3.3 mL/min	20	49	5.8
40	Gly-DL-Met		T	40:60 water:MeOH, 3.3 mL/min	19	55	6.4
41	Gly-DL-Phe		T	40:60 water:MeOH, 3.3 mL/min	21	49	5.0
42	5-Methyl-5-phenylhydantoin		T[6] TAG[6] V	MeOH, 4.7 mL/min MeOH, 4.7 mL/min 90:10 1% TEAA pH 7:ACN, 3.0 mL/min	5 5 15	5 6 17	1.5 2.4 1.7
43	Jacobsen's catalyst		CD-HP[3,6]	97:3:0.3:0.2 ACN:MeOH:TFA:TEA, 4.75 mL/min	8	9	1.8
44	3-Phenylphthalide		T	50:50 1% TEAA pH 4.1:MeOH, 2.6 mL/min	15	20	1.9
45	Propanolol		T	70:30:0.3:0.2 ACN:MeOH:AA:TEA, 4.0 mL/min	29	33	1.6
46	Sotalol		T[3]	60:40:0.3:0.2 ACN:MeOH:AA:TEA, 4.0 mL/min	20	22	1.5
47	Alprenolol		T[3]	65:35:0.3:0.2 ACN:MeOH:AA:TEA, 4.0 mL/min	21	24	1.5
48	Mandelic Acid		T	50:50 1% TEAA pH 4.1:MeOH, 2.4 mL/min	6	8	1.9

154

#	Analyte	Structure	CSP[2]	mobile phase; flow rate	t_{R_1} sec	t_{R_2} sec	R_S[1]
49	Thalidomide		V[6]	MeOH, 4.95 mL/min	5	6	2.7
50	Nicardipine		V	100:0.1 mM MeOH:NH₄TFA, 1.0 mL/min	29	34	1.7
51	Proglumide		V	80:20 1% TEAA pH 4.1:ACN, 4.0 mL/min	15	18	1.5
52	Coumachlor		V	80:20 1% TEAA pH 4.1:ACN, 4.5 mL/min	30	38	1.7
53	Warfarin		V	85:15 1% TEAA pH 4.1:ACN, 4.0 mL/min	29	36	1.5
54	Nefopam		CD-HP[3]	65:35 20 mM NH₄OAc:ACN, 2.5 mL/min	35	40	2.1
55	Lactofen		CF7-DMP[3]	98:2:0.1 heptane:IPA:TFA, 2.0 mL/min	31	34	1.8
56	Mianserin		V	100:0.15:0.05 MeOH:AA:TEA, 4.0 mL/min	15	19	1.7
57	Methadone		CD-HP[3]	78:22 0.1% AA:ACN,3.7 mL/min	26	30	1.6
58	Tröger's base		CF7-DMP[3]	70:30 heptane:EtOH, 2.5 mL/min	18	20	1.8
59	*Ethano*-bridged Tröger's base 1		CD-HP[3]	57:43 20 mM NH₄OAc pH 4.1:EtOH, 1.3 mL/min	31	38	1.6

155

#	Analyte	Structure	CSP[2]	mobile phase; flow rate	t_{R_1} sec	t_{R_2} sec	R_S[1]
60	*Ethano*-bridged Tröger's base 2		CD-HP[3]	55:45 20 mM NH$_4$OAc pH 4.1:ACN, 2.0 mL/min	24	28	1.6

[1]All separations were performed on an Agilent 1290 UHPLC instrument optimized for low extra column volume. See Experimental Section for more information on R$_S$. Column dimensions for all separations were 3 x 0.46 cm and column temperature was ambient (~ 22 °C), unless otherwise stated.

[2]T = teicoplanin, TAG = teicoplanin aglycone, CF7-DMP = Cyclofructan-7 dimethylphenyl carbamate, CF6-P = Cyclofructan-6 isopropyl carbamate, V = vancomycin, CD-HP = hydroxypropyl-β-cyclodextrin.

[3]dimensions of column = 5 x 0.46 cm

[4]dimensions of column = 10 x 0.46 cm

[5]Data for the first eluted pair of enantiomers

[6]T$_{col}$ = 60 °C
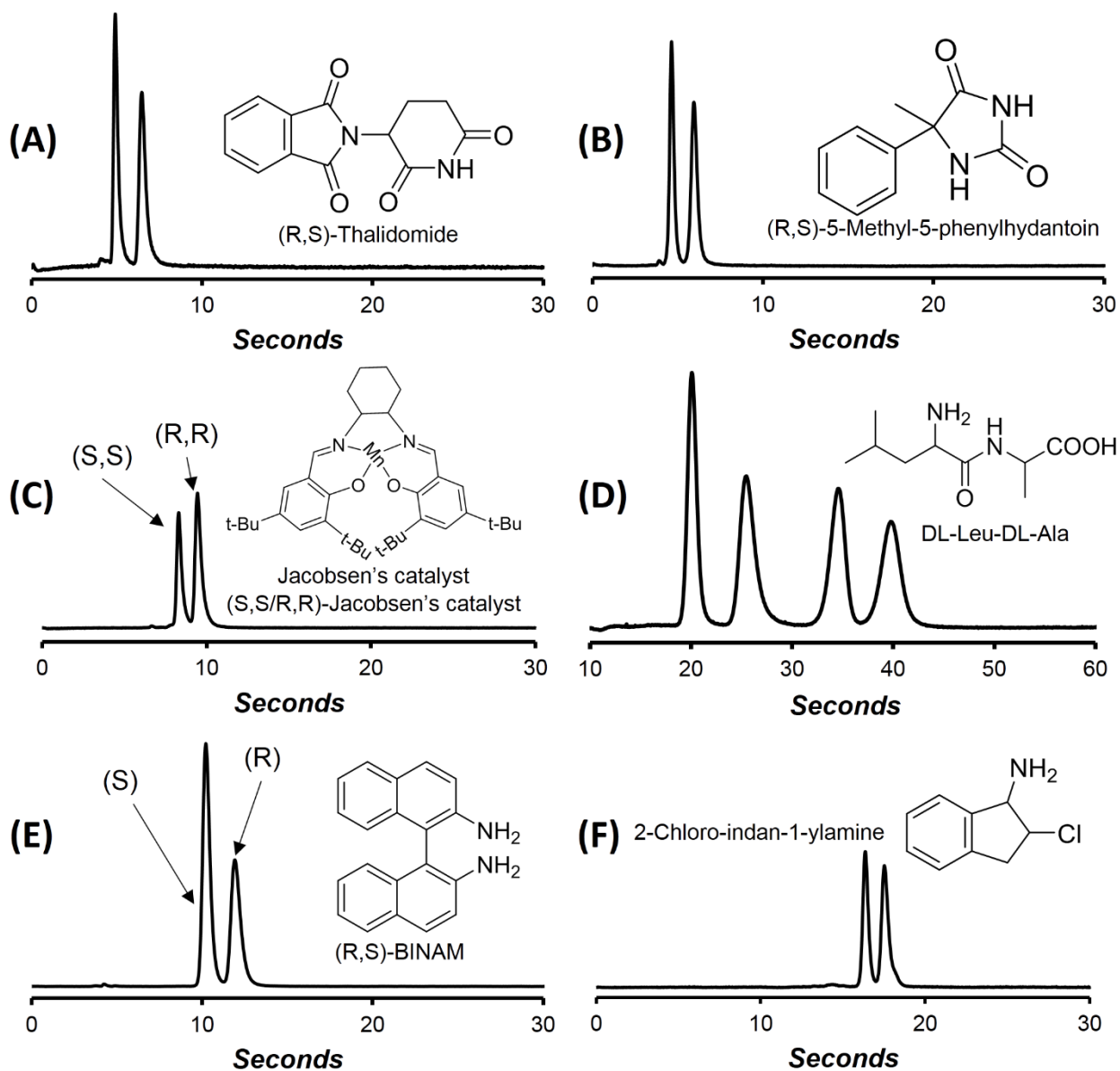
Figure 6-2. Representative ultrafast enantiomeric separations on each of 6 chiral stationary phases: (A) vancomycin SPP (3 cm × 0.46 cm), MP = methanol, 4.95 mL/min, T_{col} = 60 °C; (B) teicoplanin aglycone SPP (3 cm × 0.46 cm), MP = methanol, 4.70 mL/min, T_{col} = 60 °C; (C) hydroxylpropyl-β-cyclodextrin SPP (5 cm × 0.46 cm), MP = 97:3:0.3:0.2 acetonitrile–methanol–TFA–TEA, 4.75 mL/min, T_{col} = 60 °C; (D) teicoplanin SPP (3 cm × 0.46 cm), MP = 40:60 water–methanol, 3.00 mL/min, T_{col} = 22 °C; (E) CF7-DMP SPP (3 cm × 0.46 cm), MP = 90:10 heptane–ethanol, 4.80 mL/min, T_{col} = 22 °C; (F) CF6-P SPP (10 cm × 0.46 cm), MP = 70:30:0.3:0.2 acetonitrile–methanol–TFA–TEA, 4.50 mL/min, T_{col} = 22 °C.

157

6.4.1 Effect of Packing on Columns Used for Ultrafast Chiral LC

One of the useful tests for assessing the quality of packed beds is to calculate the specific permeability of the chromatographic column using the Darcy's law for pressure drop across a porous medium. Accomplishing ultrafast separations in HPLC generally requires higher flow rates, higher pressures, and shorter columns. Consequently, both the column packing quality and permeability are important. A detailed analysis of column quality parameters is presented in the classic work by Bristow and John H. Knox.[146] According to Darcy's law:

$$\Delta P = \frac{u\eta L}{K_s} \tag{6-1}$$

where ΔP is the pressure drop across the column (Pa), u is the superficial linear velocity (m/s) calculated by dividing the volumetric flow rate (m^3/s) by the cross sectional area of the cylindrical column (m^2), η is the viscosity of the mobile phase (Pa.s), L is the length of the column (m), and K_s is the specific permeability (m^2). From the slope of pressure drop vs. linear velocity, the specific permeability of the packed bed can be obtained (Figure 6-3). To accomplish ultrafast separations, enantiomeric selectivity must be sufficient and column efficiencies must be as high as possible. The quality of the column packing affects all these parameters except enantiomeric selectivity. It is well known that unique packing procedures are often needed for different stationary phases as well as for the same stationary phase packed into columns of different dimensions.[55] For commercial columns, these procedures are usually treated as trade secrets. In a recent academic study on packing of SPPs, Jorgenson, et al. indicated that the best packed capillary column used a slurry of agglomerated particles.[56] For the SPP-CSPs in this study, the opposite was found. Figure 6-4 shows the difference in performance of two identically packed columns where the only difference was in the slurry medium. The "well

158

dispersed" slurry (Figure 6-4B) produced a column with > 2.3x higher efficiencies and with more symmetrical peaks. The permeability of the column from the agglomerated suspension and the dispersed suspension were $4.64 \times 10^{-15}\,m^2$ and $4.33 \times 10^{-15}\,m^2$, respectively. As expected, both permeabilities are significantly greater (~ 63% to ~ 67%) than values reported for 1.7 µm FPP-CSP.[63]
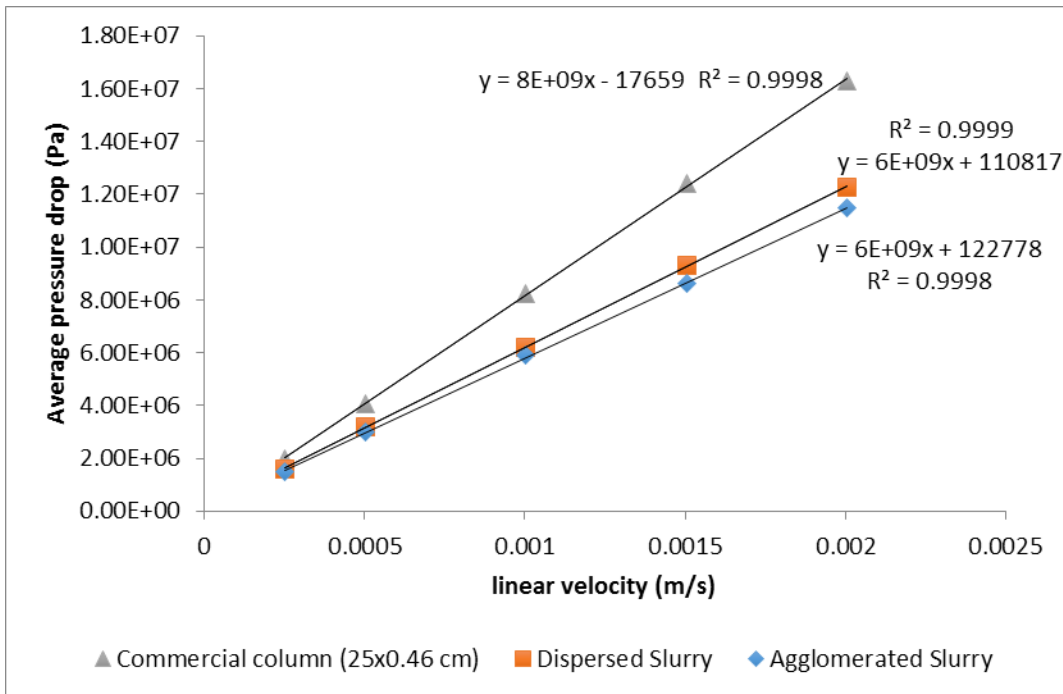
Figure 6-3. Comparison of specific permeability of commercial CF7-DMP column (5 µm FPP, 25 cm x 0.46 cm i.d.) vs. SPP CF7-DMP (2.7 µm SPP, 5 cm x 0.46 cm i.d.). Mobile phase: 70% Heptane-30% Ethanol.
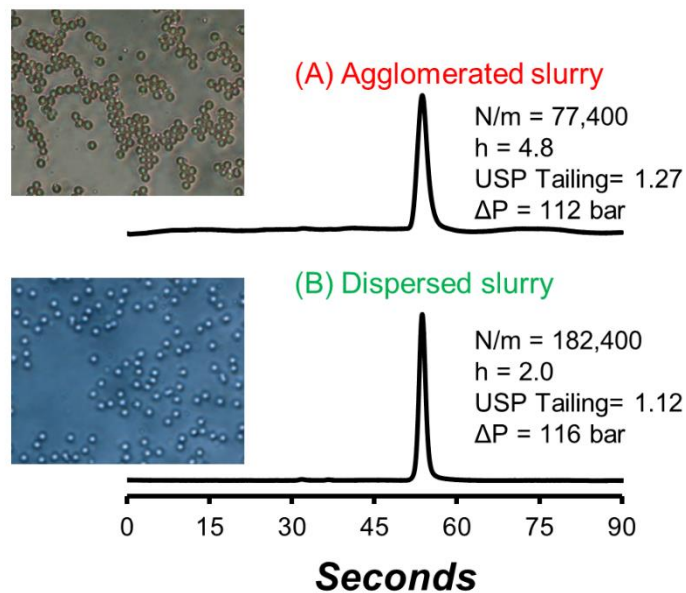
Figure 6-4. Comparison of the efficiency of 2.7 µm CF7-DMP SPPs packed using different slurry solvents. Conditions: 5% (w/v) slurry packed in 5 x 0.46 cm columns using constant pressure mode; pushing solvent: methanol. Both columns were packed at the same pressure and conditioned equally. Probe: 1,3-dinitrobenzene, m.p. = 70:30 heptane:ethanol, 1.0 mL/min, 230 nm. Top (A) shows the appearance of agglomerated suspension and (B) shows a dispersed suspension under an optical microscope at 500x magnification.

6.4.2 Detector Sampling Rates and Response Times

The detector sampling rate (also known as sampling frequency, data acquisition frequency or rate, etc.) and the detector response time become increasingly important for rapidly eluting analytes and highly efficient separations as demonstrated with SPPs. Under certain circumstances, peak shapes, peak width, and baseline noise can vary considerably as a result of detector settings. There is some debate as to the exact cause and nature of these effects.[255] We will address this debate in a subsequent communication but will only present the empirical results, as it impacts enantiomeric separations herein. Figure 6-5 shows the effect of detector sampling rate and response time (for an Agilent 1290 UHPLC) on the efficiency (N), resolution (RS), and baseline noise for six ultrafast enantiomeric separations performed under otherwise identical

160

conditions. Note that with Agilent ChemStation software, the detector sampling rate and response times are coupled and the operator cannot independently change or "unpair" these two parameters. The observed effects are the combined result of these two parameters. At the lowest sampling rate and longest response time (bottom curve, Figure 6-5), the separation is not discernible, the apparent efficiency and resolution is poor, but there is little baseline noise. The separation parameters improve tremendously as the sampling rate increases and the coupled time constant decreases up to about the 80 Hz curve. Concurrently the noise level increases (see 80× zoom in Figure 6-5). The default setting on this instrument is 2.5 Hz. It should be noted that with other instruments (Dionex and Shimadzu, for example) the operator can independently set these detector settings which could relate in an array of unwanted or suboptimal combinations. It is apparent that to maintain high efficiency and good resolution when doing ultrafast separations that detector coupled sampling rates should be ≥40 Hz and response time ≤0.13 s (Figure 6-5). For enantiomeric separations <10 s, even higher rates and lower times are needed. If one is simply screening samples and concentration is not a factor, the choice of detector settings are straightforward (e.g., 80 or 160 Hz). However, if is examining either very low amounts of an analyte or enantiomeric purities, the higher baseline noise (top curve in Figure 6-5) can obscure low level enantiomeric impurities (e.g., <1% and especially <0.1%) and decrease the accuracy and precision of the measurement.
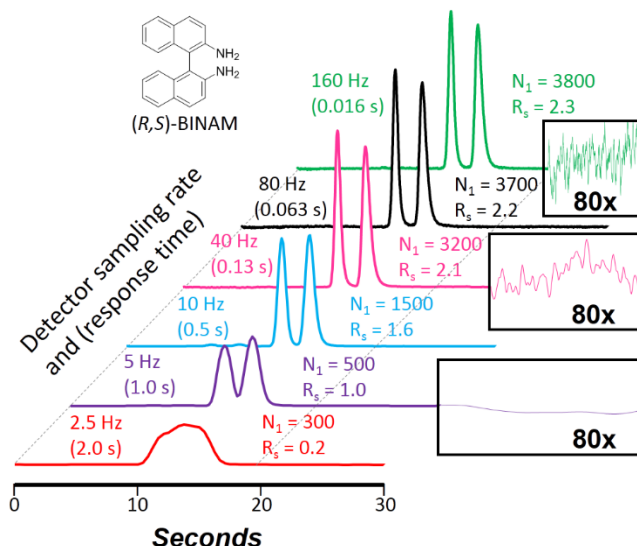
Figure 6-5. Effect of detector sampling rate and response time on efficiency (*N*) and resolution (*R*s) in ultrafast chromatographic separations. BINAM analyzed on CF7-DMP SPP (3 cm × 0.46 cm), MP = 90:10 heptane–ethanol, 4.0 mL/min, T_{col} = 22 °C; 1 Hz = 1 s^{-1}.

6.4.3 Extra Column Band Broadening Effects on Ultrafast Separations

The efficiency of a chromatographic (Gaussian and non-Gaussian) peak is defined as:

$$N_{obs} = \frac{t_R^2}{\sigma_{obs}^2}$$

(6-2)

where N_{obs} is the apparent efficiency, t_R is the mean time of the peak and σ_{obs}^2 is the observed peak variance. The observed peak variance includes the band broadening contribution from the column and other components from the injector port to the detector flow cell. For any true measurement of the efficiency and high efficiency separations, extra-column effects should be minimized in the chromatography system. Assuming Gaussian peaks, the extra-column band broadening can be estimated by removing the column and connecting the injection port directly to the detector by a zero-dead volume

162

union using the same tubing connections. The peak widths at the baseline (4σ) can be determined by tangent method and converted into σ (in unit time) by dividing by 4. Thus, width at the base w = 4σ. The widths at the base (4σ) for first peak in Figure 6-6A and Figure 6-6B are 0.01677 min and 0.01310 min, respectively. When the column was removed and the tubings were connected by a zero-dead volume union, the peak widths were 0.00719 min and 0.00298 min for Figure 6-6A and Figure 6-6B configuration, respectively. This approach gives a simple way of estimating the variance. It is desirable that the ratio of the variance of the system and the peak variance (σ_{ratio}^2) observed with a column and the system be kept as small as possible.

$$\sigma_{ratio}^2 = \frac{\sigma_{system}^2}{\sigma_{column+system}^2} \tag{6-3}$$

In this study, the moment analysis was used to account for the exact peak shapes of retained peaks and the peak without any column. By using moment analysis, same intrinsic efficiencies were obtained. The Agilent Chemstation Software calculates the second moment by the following relation:

$$\sigma^2 = M2 = \frac{d_t^2}{X}\sum_{i=1}^{N}\left(\left(i - 1 - \frac{Y}{X}\right)^2 A_i\right) \tag{6-4}$$

where N = number of area slices, A_i = value of area slice indexed by I, $\sum_{i=1}^{N}$ = sum of starting index 1 to final index N for discrete observations, d_t = time interval between adjacent area slices, t_0 = time of first area slice, $X = \sum_{i=1}^{N} A_i$, $Y = \sum_{i=1}^{N}((i-1)A_i)$. It is desirable that the ratio σ_{ratio}^2 of the variance of the system and the peak variance observed with a column and the system should be kept as small as possible. The corrected peak variance was calculated as follows:

$$\sigma^2{}_{intrinsic} = \sigma^2{}_{obs} - \sigma^2{}_{extra} \tag{6-5}$$

163

Finally, $N_{intrinsic}$ was calculated using the $\sigma^2_{intrinsic}$ in the efficiency equation as follows:

$$N_{intrinsic} = \frac{t_R^2}{\sigma^2_{intrinsic}}$$ (6-6)

It is well established that extra column band broadening is a concern when using short and/or narrow-bore columns that often are packed with smaller diameter particles, as in UHPLC.[227] In this regard, chiral separations are no different, especially when doing ultrafast separations where it is essential to maintain high efficiencies. Figure 6-6 illustrates this assessment. A "stock" UHPLC was tested (top chromatogram, Figure 6-6) and then the "extra column parts" of the instrument were replaced with smaller volume versions. Using the variance (σ^2) calculated from second moment analysis, intrinsic column efficiencies were calculated in each case, reflecting the true column efficiency of 4750 plates for a 20 s separation. The σ_{ratio}^2 was also calculated using the relationship $\sigma_{ratio}^2 = \sigma_{system}^2/\sigma_{column+system}^2$. As can be seen, a complete system optimization produced a decrease in the extra column variance ratio from 26% to 3% and this resulted in an ultrafast enantiomeric separation that went from ~71 000 plates/m and a resolution of 1.4 to ~94 000 plates/m and a resolution of 1.7.

164
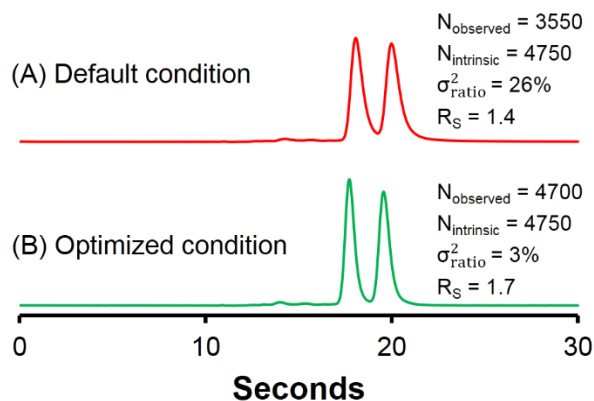
Figure 6-6. Optimization of Agilent 1290 UHPLC for ultrafast separations by replacing stock parts with low extra column volume alternatives. Tröger's base analyzed on CF7-DMP SPP (5 cm × 0.46 cm), MP = 70:30 heptane–ethanol, 2.5 mL/min, T_{col} = 22 °C. Percent extra column contribution is expressed as $\sigma_{ratio}^2 = \sigma_{system}^2/\sigma_{column+system}^2$. (A) Stock condition: stock injection needle and needle seat, 170 μm i.d. connection tubing (22 cm total) with IDEX 10-32 finger tight fittings, and a 1.0 μL detector flow cell. (B) Optimized conditions: ultralow dispersion needle and needle seat, 75 μm i.d. nanoViper connection tubing (22 cm total), 0.6 μL detector flow cell.

6.4.4 Kinetic and Thermal (Frictional) Considerations

Both the general topic of column efficiency and the more specific issue of frictional heating have been considered for columns containing small particles (e.g., <2 μm diameter) and for narrow bore columns.[256] Most of these studies focused on reversed phase C18 based column formats.[257-261] There are few kinetic studies on small particle and SPP chiral stationary phases (CSPs) and none on the effect of frictional heating on these CSPs.[65,66,229] As stated previously, CSPs are subject to the same thermodynamic and kinetic constraints as other column types. However, the manifestation of these kinetic terms can differ as much from one CSP to another as they do from conventional C18 or silica gel stationary phases. Likewise, the effect of frictional heating and column temperature gradients has been evaluated and discussed for C18 reversed phase

165

columns.[257,259,261] For SPP-based CSPs, differences as well as any peculiarities can be revealed by any of the related kinetic plots (van Deemter, reduced van Deemter, or Knox).[256] For the purpose of this discussion, we will use the standard Giddings' coupled van Deemter equation of:

$$H = \frac{B}{u} + C_S u + C_{SM} + \left(\frac{1}{A} + \frac{1}{C_M u}\right)^{-1} \qquad (\ 6\text{-}7\ )$$

where H is the height equivalent to a theoretical plate, A is the eddy dispersion term, B is the longitudinal diffusion term, C_S is stationary phase mass transfer, C_{SM} is mass transfer in the stagnant mobile phase (sometime treated as "short range" eddy dispersion), C_M is the moving mobile phase mass transfer term, and u is the linear velocity (m/s) of the mobile phase.[6]

Figure 6-7 shows four unique sets of van Deemter plots done in the (A) polar organic mode, (B) normal phase mode, and (C and D) in the reversed phase mode under two different temperature conditions. Each set of curves contains one pair of enantiomers and at least one achiral test molecule. The experimental conditions are given in the legend. The solvent temperature at the column outlet was measured at different linear velocities and mobile phase modes (see the Experimental Section and Appendix A).

166
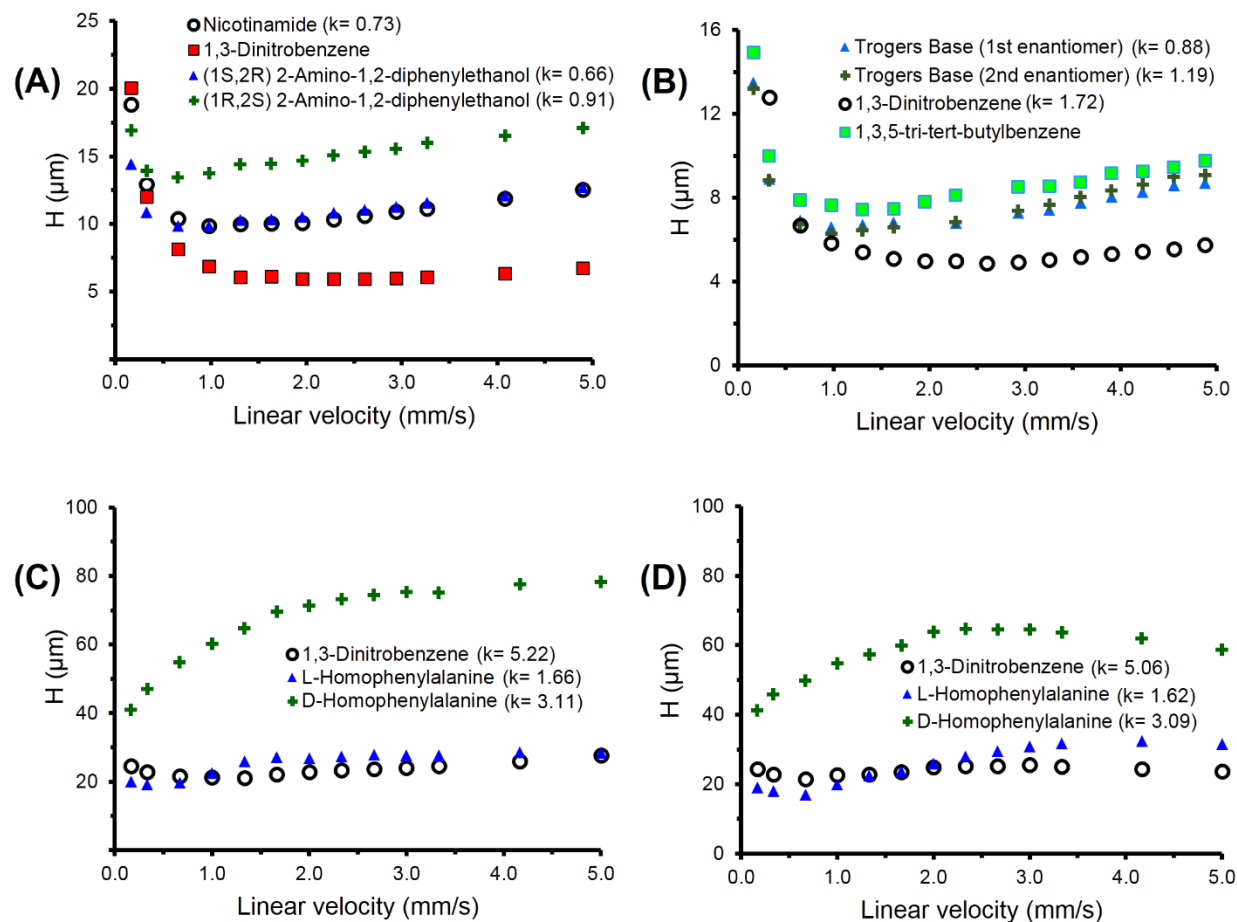
Figure 6-7. van Deemter plots for chiral and achiral analytes in polar organic mode, normal phase, and reversed phase on 2.7 µm SPP CSPs. (A) CF6-P SPP (10 cm × 0.46 cm i.d.), MP = 80:20:0.3:0.2 acetonitrile–methanol–TFA–TEA, T_{col} = 25 °C (thermostated). (B) CF7-DMP SPP (10 cm × 0.46 cm), MP = 90:10 heptane–ethanol, T_{col} = 25 °C (thermostated). (C) Teicoplanin bonded SPP (5 cm × 0.46 cm), MP = 90:10 water–methanol, T_{col} = 25 °C (thermostated). (D) T_{col} = 22 °C (not thermostated), other conditions were identical to part C. See the Appendix A for temperature effects on selectivities. The k values reported are for a flow rate of 1 mL/min.

The "polar organic" plots in Figure 6-7A indicate what some would consider to be a normal "well behaved" system. The achiral void volume marker (1,3-dinitrobenzene) has the lowest H at all linear velocities above ~0.5 mm/s and the flattest rise at higher velocities. The least retained (first eluted) enantiomer and a retained achiral analyte

167

(nicotinamide) had almost identical efficiencies at all linear velocities and similar, slightly greater slopes at higher linear velocities. The most retained enantiomer is generally thought to have the greatest resistance to stationary phase mass transfer as it is subject to a greater number of associative stereochemical interactions and often reorientation of the enantiomer.[244,262] This appears to be so as the H_{min} is at a slightly lower linear velocity for the second enantiomer compared to the first enantiomer and the achiral probe, indicating an increase in the C_S term.

Figure 6-7B shows the analogous plots for the enantiomers of Tröger's base as well as retained and unretained achiral probe molecules in the normal phase mode. The relative kinetic behaviors of these molecules are quite different than those in Figure 6-7A. The plots of the enantiomers are almost identical at all linear velocities. However, this behavior is believed to be related to two different things, one of which relates to the stereochemical recognition mechanism while the other is related to general column properties. The similar kinetic behaviors of the two enantiomers indicate that chiral recognition is likely due to the presence of repulsive (steric) interactions rather than multiple associative interactions with one of the enantiomers. For example, the minimum 3-point of interaction needed for chiral recognition could come from one associative interaction plus 2 steric interactions with one of the enantiomers. The only requirement of this model is that the total energy of association be greater than that of the combined steric repulsive interactions. Such systems have been proposed previously, but this is the first time kinetic data has been used to support such a scenario.[244,262]

Also important is the relative behavior of the retained and unretained achiral analytes in Figure 6-7B which is opposite to that in Figure 6-7A. The unretained void volume marker (1,3,5-tri-*tert*-butylbenzene) has worst efficiency at all linear velocities but a flatter rise than the enantiomers at higher linear velocities. The retained achiral

168

molecule (1,3-dinitrobenzene) exhibited the highest efficiency at all linear velocities and had the flattest rise at higher linear velocities. This type of behavior has been reported previously in a few instances for well packed, high efficiency columns.[227,263] The van Deemter curves in Figure 6-7B were produced using a standard HPLC with a conventional injector, tubings, column compartment, and detector flow cell. When the extra column effects were minimized (Figure 6-6), the observed efficiencies of the 1,3,5-tri-*tert*-butylbenzene and 1,3-dinitrobenzene were nearly identical. This clearly illustrates the pronounced effects of extra column band broadening on observed efficiencies in such van Deemter curves. Indeed, the highest efficiency column (CF7-DMP with a reduced plate height (h = 1.6)) was chosen for this example in an ultrafast format. Under these conditions, one must be aware at all times of extra column effects and how they can generate apparent anomalous behaviors.[256]

Figure 6-7C,D is for the same reversed phase enantiomeric separation and the same retained achiral analyte (1,3-dinitrobenzene). The only difference in these two series of experiments was that the column in Figure 6-7C was in a thermostated, temperature controlled, "still air device" set at 25 °C, while for Figure 6-7D the column was in ambient conditions (22 °C). It is well-known that teicoplanin chiral selectors strongly and selectively bind D-amino acid enantiomers and that this leads to greater resistance to mass transfer and broader peaks. This is confirmed by the upper plots for the more retained D-homophenylalanine in Figure 6-7C,D. Indeed no H minima vs linear velocity can be identified from these plots and the efficiencies are lower than those in the other mobile phase modes. It should be noted that such efficiencies can be greatly improved by judicious use of specific additives, but that is not the subject of this work. As in the polar organic mode, the curves for the first eluted (least retained) enantiomer and

169

the achiral retained analyte (1,3-dinitrobenzene) are quite similar to one another and both show minima in the 0.5–1 mm/s region.

Perhaps the most striking aspect of these plots is the trend shown in Figure 6-7D. At linear velocities higher than ~2.5 mm/s, the efficiencies of both enantiomers and 1,3-dinitrobenzene begin to improve significantly. This effect is most pronounced for the more retained D-homophenylalanine. It is well documented that two types of temperature gradients develop (axial and radial) when there is significant frictional heating.[257,259,261,264] Eluents with the heat capacity and density of mobile phases used in Figure 6-7 (acetonitrile, heptane, and water) and operating pressures above 300 bar can easily generate axial temperature differentials of 10 °C.[261] In fact, when the flow averaged temperature was measured at the column outlet at various linear velocities in three different modes, the axial temperature differences ranged from 11 to 16 °C (see the measured values in Appendix A). This axial variation in fast separations does not contribute to an increase in peak width. On the other hand, the peak efficiency is significantly affected by radial temperature gradients which change local viscosities, velocity profiles, and diffusion coefficients of analytes.[261,264] A first order "approximation" of the maximum radial temperature difference ΔT_R which can develop between the column center and the column wall is given by

$$\Delta T_R = \frac{u\left(\frac{dP}{dz}\right)R^2}{4\lambda_{rad}}$$

(6-8)

where u is the superficial flow velocity in m/s (obtained by dividing the volumetric flow rate by the total cross sectional area of the column), dP/dz the change in pressure in the direction of the column axis (z) per unit length in N/m³, R the column radius in m, and λ_{rad} is the approximate thermal conductivity of the mobile phase in the radial direction in W/m °C.[264]

For example, in the normal phase mode (Figure 6-7B), the thermal conductivity

of the heptane–ethanol mixture is approximately 0.13 W/m°C.[265] At low linear velocities,

(1.67 mm/s or 1 mL/min, ΔP = 80 bar), the magnitude of the maximum radial temperature

difference is 1 °C; however, as the linear velocity is increased to 5 mm/s (3 mL/min), the

pressure drop is significant (250 bar), and the calculated maximal radial temperature

gradient is 8 °C. Note that equation (2 – 8) is generally used for first order

approximations, it has been shown that the calculated radial temperature gradients can

overestimate the observed radial gradients because it ignores the compressibility of the

eluent. Consequently the actual energy generated in the column is reduced by a factor of

2/3.[259] On the other hand, as in Figure 6-7D, when a water-rich mobile phase is in use

(thermal conductivity of 0.55 W/m°C), a linear velocity of 1.67 mm/s (1 mL/min)

generated a back pressure of 112 bar due to higher viscosity. The calculated value of

ΔT_R is only 1 °C, and at higher linear velocities, e.g., 5 mm/s (3 mL/min), a radial

temperature difference of only 4 °C is developed. Also note than the axial temperature

difference in Figure 6-7B,D was similar (~12 °C). However, the data used in Figure 6-7B

was from a thermostated column (walls ~25 °C) while Figure 6-7D was not thermostated.

Though, since heptane (Figure 6-7B) is far more compressible than water (Figure 6-7D),

the energy produced is reduced by $^2/_3$. However, it is clear from Figure 6-7D, that there

are other factors, as in some chiral separations when resistance to mass transfer effects

are more pronounced. In these interesting cases, such as a high thermal conductivity

water rich mobile phase, the gain in efficiency from an improvement in mass transfer at

higher axial temperature gradients is enough to visibly counter any smaller losses in

efficiency due to radial temperature gradients and eddy dispersion. This possibility was

noted early on by Halász[261] and is apparent in Figure 6-7D. See the Appendix A for

detailed temperature measurements and calculations. It should be considered that this increase in column temperature from frictional heat also leads to reduced selectivity (See Table 6-4), as is expected.

Table 6-4. Selectivity values for Figure 6-7 van Deemter Plots

	Selectivity α	
van Deemter plot	At 0.2 mL/min	At 3 mL/min
Figure 5A (CF6-P, 10cm SPP, thermostated at 25 °C)	1.37	1.36
Figure 5B (CF7-DMP, 10cm SPP, thermostated at 25 °C)	1.35	1.32
Figure 5C (teicoplanin, 5cm SPP, thermostated at 25 °C)	1.95	1.82
Figure 5D (teicoplanin, 5cm SPP, non thermostated)	1.93	1.77

6.5 Conclusions

The results of this study, indicate that (1) SPPs are advantageous for ultrafast and high efficiency chiral separations, (2) enantiomeric separations on the order of few seconds are now feasible in all mobile phases with bonded brush type CSPs, (3) kinetic behaviors can sometimes be used to shed light on chiral recognition mechanisms, (4) CSPs can show quite different kinetic profiles from each other and from achiral systems, (5) ultrafast chiral separations require optimized detection and minimization of extra column effects, (6) frictional heating effects must be accounted for in ultrafast separations as they can manifest themselves in disparate ways and to different degrees for various CSPs and mobile phase modes, (7) efficiencies and separation speeds for chiral analytes can now exceed those in capillary electrophoresis. Also it is feasible to expect that (8) SPPs may be advantageous for preparative separations when their high efficiencies, faster analyses times, and reduced solvent consumption compensate for lower chiral selector loading, (9) ultrafast SPP-CSPs may be attractive as the second dimension in

2D-LC because of their greater selectivity and orthogonality to conventional achiral stationary phases, and (10) real-time monitoring of product formation in asymmetric synthesis is possible with ultrafast chiral separations.

Chapter 7

Salient Sub-Second Separations Approaching the Speed of Sensors

7.1 Abstract

Sub-second liquid chromatography in very short packed beds is demonstrated as a broad proof of concept for chiral, achiral, and HILIC separations of biologically important molecules. Superficially porous particles (SPP, 2.7 µm) of different surface chemistries, namely, teicoplanin, cyclofructan, silica, and quinine, were packed in 0.5-cm long columns for separating different classes of compounds. Several issues must be addressed to obtain the maximum performance of 0.5 cm columns with reduced plate heights of 2.6 to 3.0. Modified UHPLC hardware can be used to obtain sub-second separations provided extra-column dispersion is minimized and sufficient data acquisition rates are used. Further, hardware improvements will be needed to take full advantage of faster separations. The utility of power transform, which is already employed in certain chromatography detectors, is shown to be advantageous for sub-second chromatography. This approach could prove to be beneficial in fast screening and two-dimensional liquid chromatography.

7.2 Introduction

One of the basic tenets of separation science is to achieve adequate resolution in the shortest possible time. Not surprisingly, the relative meaning of "shortest possible time" has evolved over five decades, where early separation of biological molecules in 30–60 min was once considered fast liquid chromatography.[34,266] By current standards, ultrafast liquid chromatography is usually considered as sub-minute separations— although the lower limit will continue to decrease with developments in smaller particle synthesis, improved packing technologies, design of the column hardware, and peak

174

detection methods.[52,105] Recently, researchers have shown unprecedented separation speeds of 4–5 s in packed beds by using high efficiency particles for both achiral and chiral separations in liquid chromatography as well as supercritical fluid chromatography.[45,52,70,127,215,267] It is not uncommon to obtain plate heights $H < 2d_p$ (d_p = particle diameter) with superficially porous particles (SPP) or fully porous sub-2-μm particles with exceptionally narrow size distribution.[268] The excellent performance of the former arises from lower contributions to eddy dispersion in the band broadening processes.[269] These efficiencies are providing an impetus to separation scientists to push the boundaries of analysis speed by utilizing very short columns. Ultrafast liquid chromatography is a very promising approach for high throughput screening methods[270] or in two-dimensional chromatography of complex samples where it is necessary to have high speed separations in the second dimension. [271-273]

To date, ultrahigh speed separations of a few seconds or as low as milliseconds have been achieved in special electrophoretic microchip plates or in capillary zone electrophoresis. [274-277] Other approaches such as shear driven chromatography and wide bore hydrodynamic separations have also shown some promise in this regard.[278,279] Special detection technologies were employed such as on-column detection followed by image processing to extract the peak profile.[275,280] Handling of rapidly eluting peaks in the domain of conventional liquid chromatography is currently hindered by extra-column dispersion and even the data sampling rates on many commercial UHPLCs. The ideal chromatographic output from extremely high efficiency columns and fast eluting peaks is convoluted by several factors. The shape of the injector pulse, the cup-flow distribution pattern of the inlet and outlet frits, diffusion and mixing in plumbing unions, flow profiles in the tubings, data sampling rate, and embedded noise suppressing algorithms in any chromatographic setup all affect the true peak shape in deleterious ways.[105,281] Second,

175

in the majority of UHPLCs, the maximum flow rate is limited to 2–5 mL/min, which is another factor limiting separation speed.

The aim of this work is to analyze the conceptual and practical aspects of sub-second separations on state of the art ultrahigh performance instruments using 0.5 cm packed columns with 2.7 μm SPP particles. We discuss and propose simple instrumental modifications and simple mathematical approaches allowing chromatographers to circumvent the challenges in ultrafast LC (*vide supra*) and obtain sub-second separations. The shortest possible analytical column dimensions available commercially (0.5 × 0.46 cm i.d.) are used with four different chemistries (silica, cyclofructan-6, teicoplanin, and quinine bonded phases). These column chemistries are compatible with normal, reversed phase, HILIC, and polar organic/ionic modes and are used for a broad proof of concept. The polar organic mode uses ACN as a major component of the mobile phase, while MeOH is used to adjust the retention time with small amounts of acid/base additives to modify the selectivity.

7.3 Experimental

7.3.1 Materials

All HPLC solvents, buffers, and analytes were obtained from Sigma-Aldrich (St. Louis, MO). The 2.7 μm superficially porous particles with 1.7 μm core diameter and 0.5 μm shell thickness were provided by Agilent Technologies (Wilmington, DE). Surface area of the particles is 120 m^2/g, and pore diameter is 120 Å. Mobile phase compositions are given as volume/volume (v/v). The pH and mobile phase additive concentrations are given for the aqueous portion of the mobile phase before mixing with an organic modifier, and all experiments were conducted at room temperature.

7.3.2 Stationary Phases

The stationary phase materials were synthesized by AZYP LLC (Arlington, TX). Teicoplanin, cyclofructan-6, and quinine-based stationary phases were prepared according to the reported methods.[10,16,94] The stationary phase material was either packed into 0.5 cm × 4.6 mm i.d. empty guard columns by Agilent Technologies, (Wilmington, DE) or packed in our laboratory using dispersed slurry techniques and pneumatic pumps. Superficially porous silica (2.7 µm) guard columns were purchased from Agilent Technologies. As reported earlier,[52] it was found that dispersed suspensions of core–shell particles produced optimum results with pressures of 10 000 psi. These pressures were necessary to stabilize the bed against high flow rates (5 mL/min max on the UHPLC) for sub-second chromatography. For further characterization of the column volume (and to estimate the dead times), pycnometry was performed using the density difference method with water and methanol ($n = 3$).[16] The dead volumes of the column were found to be 75, 69, and 75 µL for SPP silica, SPP teicoplanin, and SPP quinine, respectively. Therefore, at 5 mL/min, the average dead time of the SPP guard column (in Agilent's hardware) would be 0.83 to 0.89 s. These dead times are consistent with the elution time of acetone under HILIC mode conditions.

7.3.3 Instrumentation

The Agilent 1290 UHPLC is equipped with a degasser, quaternary pump, autosampler, temperature controlled column compartment, and diode array detector. The instrument was controlled by OpenLabs CDS ChemStation software (Rev. C.01.06 [61], Agilent Technologies 20012014) under Microsoft Windows 8.1. In order to operate the instrument at the highest flow rate possible (5.0 mL/min, without pressure restriction), the in-line filter was removed. The pump outlet was directly connected to a presaturator

177

column (5 × 0.46 cm i.d.) filled with silica (M.S. Gel, D-50-120A, AGC SciTech Co., Ltd.). This column has two roles (a) to act as a filter and (b) to saturate the incoming mobile phase with dissolved silica before it hits the analytical column. This process ensures the long life of a column without any back-pressure. The autosampler and the column oven were bypassed. The presaturator column outlet was then connected to a Rheodyne 7520 manual injector (Rheodyne LLC, Rohnert Park, CA) with an internal loop size of 1 µL. Full loop injections were made. The Rheodyne was connected to the column via 7 cm × 75 µm Nanoviper tubing and the column outlet was directly inserted into the UHPLC detector flow cell. The column consists of a 0.5-cm-long barrel with a permanently sealed frit at one end followed by a 3 cm × 120 µm stainless steel extension. The detector has a dispersion volume $V(\sigma)$ of 1 µL (G4212–60008). Although smaller flow cells are available (0.6 µL dispersion), there is potential of bursting the flow cell with compressible mobile phases at high flow rates. The retention times were determined with respect to the pressure pulse generated by manual injection.

7.3.4 Data Processing

Peak deconvolution and fitting of the peaks as exponentially modified Gaussians (EMG) and moment analysis were performed on PeakFit software v4.12.

7.4 Results and Discussion

7.4.1 Preparation and Characterization of Short 0.5 cm x 0.46 cm i.d. Columns

In order to achieve sub-second liquid chromatography, short 0.5 cm columns were chosen. There is a question of which column diameter is best. Potentially, the narrow i.d. columns (0.21 or 0.30 cm i.d.) would provide very high superficial linear velocities at the maximum flow rates in the UHPLC; e.g., at 5 mL/min the superficial linear velocities in 0.46, 0.30, and 0.21 cm i.d. columns would be 0.501, 1.17, and 2.40

178

cm/s, respectively. It might appear that the 0.21 cm i.d. format would be the most suitable

diameter for ultrafast separations. Unfortunately, the practical difficulties encountered in

packing a 0.21 cm i.d. column and minimizing the extra-column effects override the

benefits of narrow bore columns currently. Even in the long column format for

superficially porous particles, the 0.21 cm i.d. columns achieve about 60% of the plates of

the 0.46 cm i.d. format. For further work, 0.5 cm × 0.46 cm i.d. columns were chosen for

slurry packing, since the wall effects are virtually negligible in 0.46 cm i.d. columns.

7.4.2 Is the Sampling Frequency Available for Sub-Second Chromatography?

For sub-second chromatography, it was necessary to simulate the separation

and assess the required sampling frequency based on the efficiencies observed in the

0.5 cm columns. Shannon's theorem dictates that in order to accurately capture the

analytical signal, the minimum sampling frequency must be equal to twice the maximum

frequency components in the signal being acquired.[282] In Figure 7-1A, we simulate two

sub-second Gaussian peaks in the presence of root-mean-square noise of ±0.06 units.

This is the typical noise expected in a modern UV UHPLC detector. The plate counts of

0.5 cm column (150–200 per second) were set on the basis of realistic numbers obtained

under very high flow rates (~5 mL/min). In order to extract the frequency components of

such signals, Fourier transform (FT) of this simulated chromatogram was done. As the FT

shows, >95% of the useful chromatographic information is under 15 Hz. Shannon's

theorem guides us to sample the data at a minimum of 2 × 15 Hz; therefore, 40 and 1000

Hz should be sufficient as shown in Figure 7-1C and D. Note the number of points is less

than 20 points per peak in the 40 Hz chromatogram. Two modern UHPLCs can sample

the data up to 160 to 250 Hz, respectively. In the near future, ever higher efficiencies are

likely in very short columns, and then even these sampling frequencies and response

times may be insufficient in sub-second chromatography. The Agilent's UHPLC employed here couples the sampling frequency with a rather sophisticated undisclosed digital filter which behaves very closely to a centered moving average with Gaussian weights.[105]
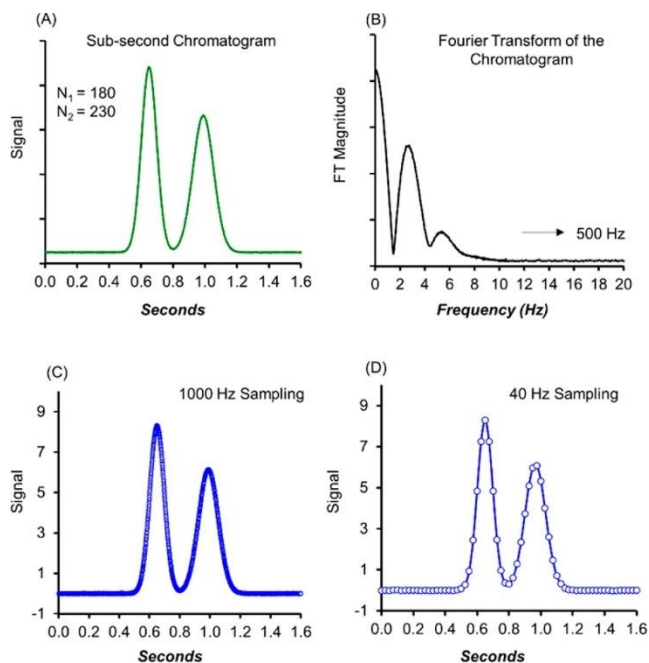
Figure 7-1. Computer simulation of a sub-second separation with RMS noise of ±0.06 under a second in (A) time domain, (B) frequency domain via Fourier analysis, (C) time domain signal at 1000 Hz of sampling frequency, and (D) time domain signal at 40 Hz of sampling frequency. Computer simulations are done with OriginPro 2015 (Origin Lab Corporation, MA).

7.4.3 Hardware Considerations in Sub-Second Chromatography

To achieve ultrafast separations in packed 0.5 × 0.46 cm i.d. columns, packing approaches and extra-column dispersion of UHPLC needed extensive optimization. The most convenient approach to making very short columns is to pack the superficially porous particles in available (empty) guard columns using dispersed slurry techniques.[57] On the basis of the previously optimized hardware[52] (low dispersion UHPLC autosampler, 25 cm × 75 μm tubing, and 1 μL detector), 600–700 plates at optimum flow rates (0.8 mL/min) were considered as well-packed columns. This efficiency (*N*) corresponds to *H* ~

2.3d_p to 3.0d_p without subtracting any source of dispersion. For column lengths of 0.5 cm, the extra-column dispersions on any state of the art UHPLC cannot be ignored.[266] Assuming all the extra-column volumes behaved as a perfect mixer,[266] the extra-column variances were estimated to be 2.2 µL^2. The second moment analysis also confirmed that the extra-column variance was only ~11% of the chromatographic peak variance at low flow rates. Despite this ultralow dispersion, there is an additional fundamental challenge with very short connection tubings (3 and 7 cm) employed in this work. Indeed, the Aris-Taylor Gaussian dispersion breaks down because of short residence time of the analyte in the tubings.[283] The eluting peaks (in the absence of column) were observed to produce non-Gaussian tailing profiles, as predicted by Golay along with a "foot" at the tailing end.[283] The "foot" or the hump is marked with an arrow in Figure 7-2C. It is interesting that this peak shape fits neither an exponentially modified Gaussian (EMG) nor other empirical versions of peak fitting software (PeakFit v 4.12) such as the "Half Gaussian Modified Gaussian (GMG)" models or their hybrids (EMG-GMG). Obviously, even those relatively poor fit models ($R^2 \sim 0.98$) show that the second moment is higher in terms of square microliters than the second moment at low flow rates (0.8 mL/min). Similar peak shapes with a "foot" in the tailing region without columns were reported by Gritti et al.[284] The tailing envelope may be superimposed on the band profile eluting from very short columns. A simple but elegant approach for overcoming such fundamental challenges in sub-second chromatography is outlined in the last section of this article.
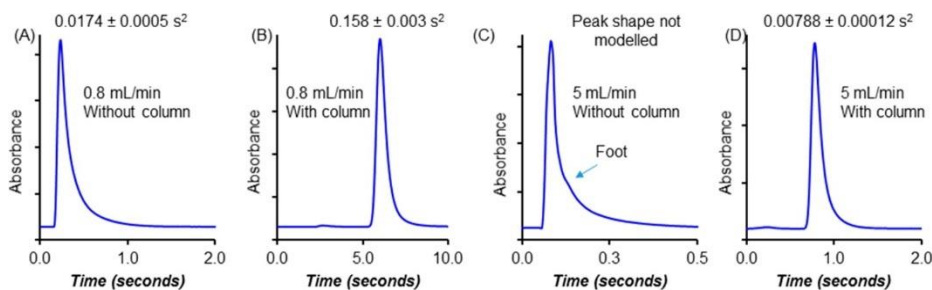
Figure 7-2. Demonstration of effect of extra column effect originating from short connection tubing. Chromatographic conditions: column, 0.5 cm × 4.6 mm i.d. 2.7 μm core–shell silica guard column (Agilent Technologies); mobile phase, ACN/water (80:20); analyte, thymine; connection tubing, 70 mm × 75 μm i.d. NanoViper (A) at 0.8 mL/min without the column, (B) at 0.8 mL/min with the column, (C) at 5.0 mL/min without the column, and (D) 5.0 mL/min with the column (second moments are given with the corresponding peak).

7.4.4 Examples of Sub-Second Chromatography

Examples of several different chiral and nonchiral sub-second separations in various chromatographic modes are given in Figure 7-3. Baseline sub-second separations are more easily achieved when the first analyte elutes before the dead time, e.g., due to Donnan exclusion. The separation window becomes small between the dead time and 1 s. However, this upper 1 s limit is arbitrary in this work, and ultrafast separations can be readily achieved in a few seconds.[52] Using a flow rate of 5 mL/min, the dead time is estimated to be ~0.8 s from pycnometric measurements on the silica column. Figure 7-3A shows the enantiomeric separation of N-(3,5-dinitrobenzoyl)-DL leucine on a SPP quinine phase. In Figure 7-3B, a HILIC mode separation of mellitic acid from benzamide is shown. Note that mellitic acid is repelled from the stationary phase. Similarly two dipeptides, Glu-Asp and Gly-βAla, are baseline separated on the teicoplanin bonded SPP column (Figure 7-3C). In Figure 7-3D, we show that it is possible to perform ultrafast screening by resolving three peaks (two sulfonic acids and a derivatized amino acid) under a second using the methods outlined in the next section. A doubly charged sulfonic acid is repelled from the stationary phase like mellitic acid. It is also important to

182

have retention time reproducibility for sub-second separations. Using the HILIC mode, six injections were made and retention times calculated for mellitic acid and 4-aminosalicylic acid. The percent RSD for the retention time of both peaks was found to be <2%.
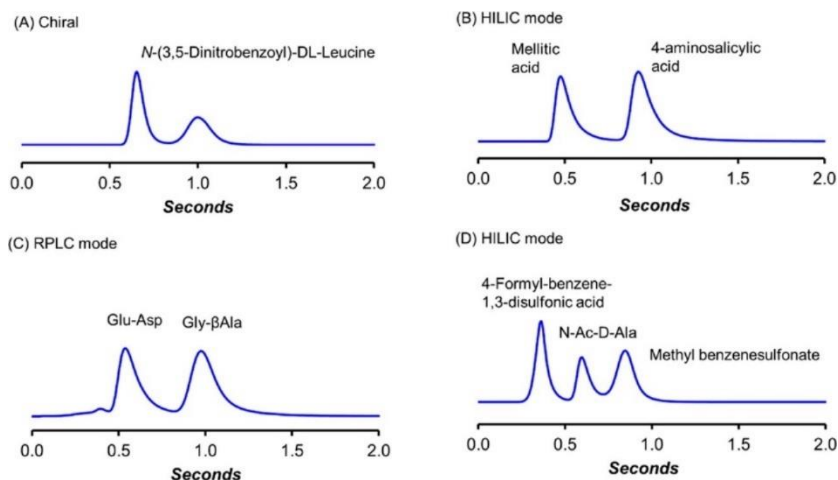
Figure 7-3. Sub-second chromatography on various stationary phases using 0.5 x 0.46 cm i.d. columns (A) SPP Quinine, 70:30 (ACN/20 mM NH4CO2H), 5 mL/min; (B) SPP silica, 94:6 (ACN/15 mM NH4CH3CO2), 5 mL/min; (C) SPP Teicoplanin, 42:58 (ACN/20 mM NH4CO2H), 5 mL/min; (D) SPP Teicoplanin, 70:30 (ACN/water), 5 mL/min. Data sampling rate 160 Hz. For parts A and D, see next section on power transforms.

7.4.5 The Effect of "Power Transform" in Sub-Second Chromatography

It can be noted that under ultrafast separations and short columns, the peaks are non-Gaussian (tailed) due to trans-column velocity biases in the tubings and frits as well as the particulate bed (*vide supra*). Additionally, if the peaks are eluting before the dead time (due to Donnan exclusion), the efficiencies of such peaks can be compromised. Under the highest flow rates available on the UHPLC (5 mL/min), the 0.5 cm SPP columns provided about 150 to 200 plates. Using the simplest expression for peak capacity in the isocratic mode, and where there is a possibility of a peak eluting before the dead time, we can write the peak capacity (*P*) for a sub-second separation in a time span of 0.4 to 1.0 s, with a chromatographic resolution of 1 as[285]

$$P = 1 + \int_{0.4}^{1.0} \frac{\sqrt{200}}{4t} \, dt = 1 + \left(\frac{\sqrt{200}}{4} \right) (\ln 1.0 - \ln 0.4) \approx 4$$

Using the same approach for the peak capacity for analogous higher efficiency separations, it is determined that for $N = 500$, $P = 6$, and for $N = 1200$, $P = 9$. In Figure 7-4, we demonstrate the full potential of fitting three peaks under a second in the HILIC mode. The resolution (~0.6) is a result of the extra-column tailing effect alluded to above. The chromatographic profile of peaks can be deconvoluted into three exponentially modified Gaussians at 0.48, 0.68, and 0.93 s as shown in Figure 7-4B. It is clear from the peak fitting model that tailing is causing this lowered resolution. It is known that raising Gaussian functions to any power ($n > 0$) still maintains them as Gaussian functions with an effect of reducing their standard deviations. Thus, squaring or cubing the output signal yields a peak at the *identical retention time* but with a narrower width (See Figure 7-4). It can be shown mathematically that for Gaussian peaks, the efficiency directly scales as the power n and the resolution scales as $\sqrt{n}$.[286] Such an approach is already embedded in some commercial detectors such as the evaporative light scattering detector without the user's control.[287] Recently, Thermo launched a UHPLC that allows the chromatographer to choose the power "n" to transform the chromatograms.
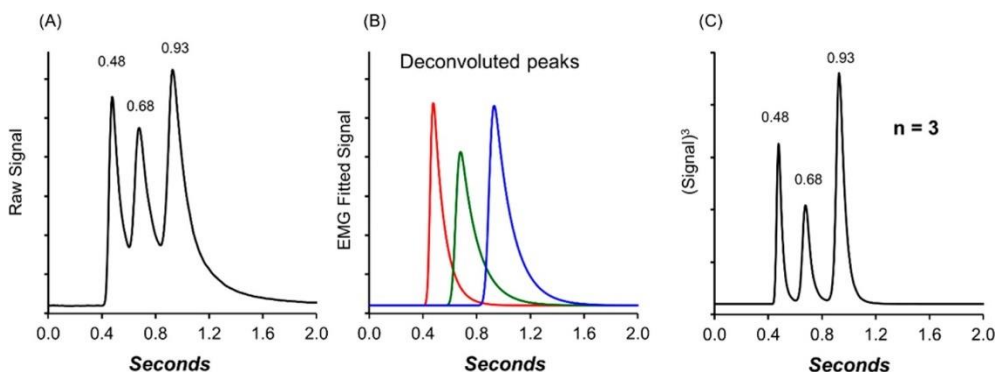
Figure 7-4. Application of power transforms in sub-second chromatography of three components (mellitic acid, 2,3-dihydroxybenzoic acid, and 4-aminosalicylic acid). (A) The original sub-second chromatogram. (B) Deconvoluted chromatogram into three exponentially modified Gaussian peaks. (C) Power transform with cubic of the original data. Column, 0.5 cm × 4.6 mm i.d. 2.7 µm SPP silica; mobile phase, ACN/15 mM ammonium acetate = 94:6 (v/v), 5 mL/min at 220 nm.

Figure 7-4C shows that if the same chromatographic data (y ordinate) is raised to a power of 3, the same separation can now be baseline resolved into three components. This approach is a very powerful method for extracting information for ultrafast screening purposes from a low resolution chromatogram, which is indeed the main purpose of sub-second chromatography. There is a caveat, however, in that the peak areas change in this power transformation as $A_{pt} = Y_{max}{}^n[\sigma\sqrt{(\pi/n)}]$, where A_{pt} is the peak area after applying the power n, Y_{max} is the maximum amplitude, and σ is the standard deviation of the peak.[286] Calibration curves constructed can be nonlinear if quantitation is desired.

7.4.6 Optimal Column Geometries of Sub-Second Separations

Performing ultrafast and sub-second separations requires the most optimized components in all aspects of chromatography from instrumentation, high-selectivity selectors, high-efficiency columns, and appropriate methods of separation. As the stationary phase or the column is the heart of any separation, it is crucial to determine the optimal column geometries that are beneficial for sub-second separations. A study was performed using 2.7 µm bare SPP silica packed in short columns of various geometries.

These columns were evaluated using van Deemter plot using cytosine as probe molecule in HILIC mode (Figure 7-5). The van Deemter plot showed an interesting observation in that the 0.3 cm i.d. columns performed ahead of the 0.46 cm i.d. columns as well as 0.21 cm i.d. columns. Using a narrower diameter can offer higher linear velocities and opportunity to further reduce analysis times to obtain the sub-second separations. Note that reduce plate heights of 1.7-1.8 are obtained for 1.0 x 0.3 cm i.d. column which are exceptional for such short columns for bare silica.
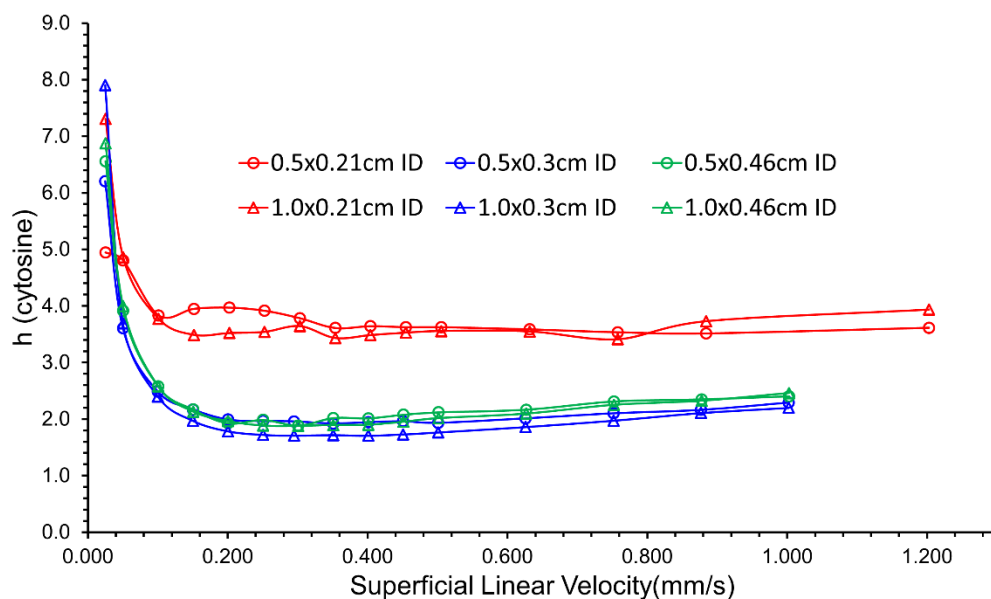
Figure 7-5. A van Deemter plot comparison of different column geometries packed with 2.7 μm bare SPP silica operating under a HILIC mode. Mobile phase: 90/10 ACN/100 mM NH$_4$OAc, 254 nm. Column equilibrated at each flow rate for 3 min before injection.

7.4.7 Applications of Sub-Second Separations

The studies and examples discussed so far have involved probe molecules and analytes that are well behaved to demonstrate the proof-of-concept of the ultrahigh performance chromatography. To evaluate the practical applicability of sub-second separations, structurally and functionally related molecules also were separated. As the 1.0 x 0.3 cm i.d. column geometry provided an optimal combination of efficiency and high

186

linear velocity, it was used with bare silica of 1.9 µm in size to obtain sub-second

separation of nucleosides, plant hormones – cytokinins, plant hormones – auxins, and

salicylic acid and derivatives (Figure 7-6). This is the first reported instance of multiple

baseline separated analytes under a second in traditional liquid chromatography. Note

that no resolution enhancement or peak treatment methods have been used in this figure

and the separations are reported as obtained from the chromatograph. These ultrahigh

performance columns can fill the great void that currently exists for suitable columns in

2nd dimension in 2DLC or in on-line liquid chromatography where very fast separations

are needed.
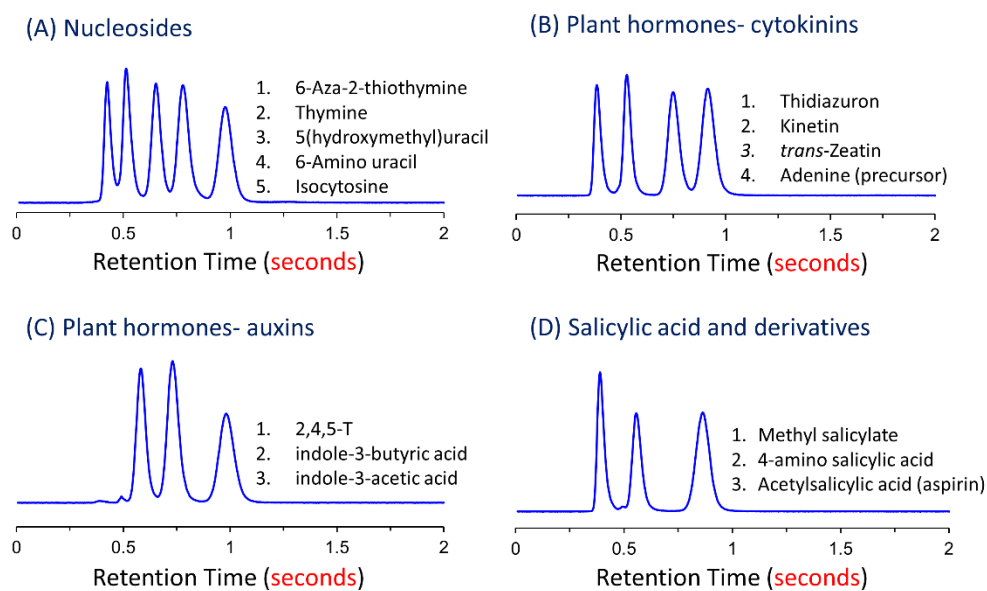
Figure 7-6. Sub-second HILIC separations of structurally and functionally related analytes on bare 1.9 µm SPP silica packed in 1.0 x 0.3 cm i.d. columns. (A) nucleosides, 8.0 mL/min flow rate, (B) plant hormones – cytokinins, 7.9 mL/min flow rate, (C) plant hormones – auxins, 7.9 mL/min flow rate, (D) salicylic acid and derivatives, 7.9 mL/min flow rate. Method: 90/10 ACN/100mM NH$_4$OAc mobile phase, 254 nm UV, 250 Hz sampling frequency, 0.0 s detector response time.

The sub-second chiral separations also were performed using teicoplanin and

quinine based stationary phases packed in 1.0 x 0.3 cm i.d. columns (Figure 7-7). The

187

ultrahigh efficiencies obtained from optimal column packing and very high selectivities of

quinine based chiral selector offered the opportunity to further perform a sub-second

separation of two chiral analytes (Figure 7-7E-F). With high peak capacity, sub-second

separations can be practical to use in cases of samples contaminated with impurities or

have solvent peaks and yet have baseline resolved separation of species of interest.
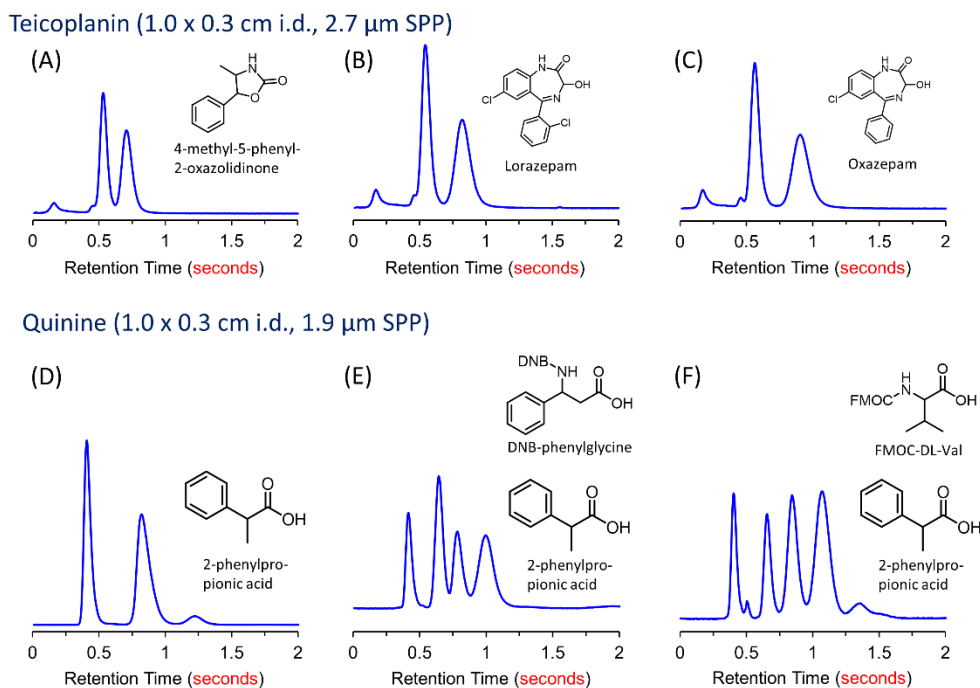
Figure 7-7. Sub-second chiral separations on teicoplanin and quinine chiral selectors. The top row (A) 4-methyl-5-phenyl-2-oxazolidinone, (B) Lorazepam, and (C) Oxazepam were separated on teicoplanin bonded to 2.7 µm SPP packed n 1.0 x 0.3 cm i.d. column. Method: mobile phase - methanol, 7.5 mL/min flow rate, 220 nm. The bottom row (D) 2-phenylpropionic acid, 90/10 ACN/100 mM HCOONH4 mobile phase, 7.85 mL/min, (E) DNB-phenylglycine and 2-phenylpropionic acid, 90/10 ACN/100 mM HCOONH4 pHa 7.4 mobile phase, 7.7 mL/min, (F) FMOC-Val and 2-phenylpropionic acid, 90/10 ACN/200 mM HCOONH4 pHa 6.8 mobile phase, 7.85 mL/min. 254 nm UV, 250 Hz sampling frequency, 0.0 s detector response time.

To further explore the ultimate capability of these ultrahigh performance columns,

a sub-second separation of 10 analytes was performed (Figure 7-8). This separation

represents the potential for high-throughput separations where complex samples can be

188

analyzed in real-time. Figure 7-8A shows the 10 peak separation with extra-column band broadening effects removed using Fourier Transform deconvolution. This is the highest number of compounds to have been separated under sub-second regime in traditional liquid chromatography. When operating in such extreme conditions, it is important to note that the high detection frequency (250 Hz) and low detector sampling time become crucial to collect the intrinsic peak profiles. The high linear velocities offered by narrower diameter columns can truly be harnessed when paired with high flow rate UHPLC with low extra-column volumes to realize remarkable separations as seen below.
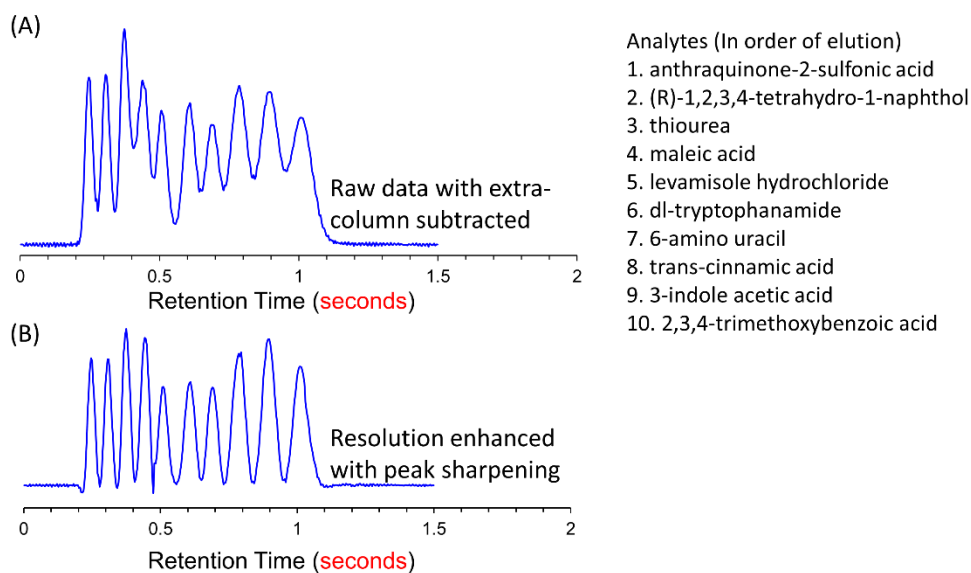
Figure 7-8. A sub-second separation of 10 analytes in HILIC mode performed on 1.9 µm bare SPP silica packed in 1.0 x 0.3 cm i.d. column. (A) the apparent chromatogram from the analysis with extra-column band broadening removed using Fourier Transform deconvolution, (B) the apparent chromatogram sharpened with resolution enhancing technique of segmented sharpen based on derivatives. Mobile phase: 90/10 ACN/100 mM NH_4OAc, 8.0 mL/min flow rate, 254 nm UV, 250 Hz sampling frequency, 0.0 s detector response time.

As the analytes are not baseline separated, a resolution enhancement technique was developed which is based on the derivatives and enhances the resolution of species

while keeping the peak properties intact (Figure 7-8B). The so called "segmented peak sharpening" method retains the retention time and peak are of the original chromatogram. Application of this resolution enhancement technique improves the resolution of all species to near baseline. Briefly, taking the 2nd derivative and 4th derivative of the chromatogram, multiplying them with certain arbitrarily chosen cofactors, and subtracting the new values from the original chromatogram results in a transformation with enhanced resolution of species. The cofactors are further optimized to obtain the desired chromatogram. Taking this concept further, the chromatogram can be divided in 10-20 different segments with different cofactors applied on each segment, allowing a very fine-tuned resolution enhancement that prevent peak distortion while retaining the peak areas and the retention time. This new resolution enhancement method will be covered in depth elsewhere.

7.5 Conclusions

The foundations of performing sub-second chromatography in small packed beds using superficially porous particles are outlined. Various modes of chromatography were demonstrated including reversed phase, HILIC, and chiral separations as a proof of concept. Detection and hardware challenges need to be further addressed. Although the sampling frequencies are adequate for the current efficiencies achievable in ultrafast chromatography, they may not be for future improved columns. The bigger challenge so far is the peak shapes due to non-Gaussian dispersion in short tubings, which can be circumvented by on-column injection and on-column detection technologies as is done in electrophoretic methods. Modern UHPLCs are limited to 2–5 mL/min flow rates at higher pressures (>500 bar), and this is less than desirable for these separations. Using power transforms on exponential functions (as those used for modeling peak shapes) is a very

190

simple way to improve peak shapes, reduce variances, and decrease noise in sub-

second screening.

Chapter 8

General Summary

8.1 Chapter 2

New chiral HPLC methods were presented for the enantiomeric separation of a variety of biaryl atropisomers using heptane with ethanol as a polar modifier. The primary mechanism of retention is likely dipolarity/polarizability interactions between the 2,2′ functionalities of the biaryls and polar groups present on the derivatized cyclofructans. Selectivity was observed for 24 out of 30 probe analytes with 17 baseline separations using three different CSP's. The CF6-P CSP was the most successful with 15 baseline separations using simple mobile phases without the need for additives. When ethanol was used as a polar modifier, high efficiencies and good peak symmetries were observed. When propanol and butanol were used, selectivity was improved but band broadening and peak tailing were increased. All probes studied showed enthalpy-driven patterns and the trend in absolute enthalpies of the second eluting enantiomer matched the trend in selectivities observed for the three types of 2′,2-binapthyls. Future work will involve determining the energy barriers to racemization as well as modeling studies to determine the effects of different substituents on molecular hybridization and chiral recognition.

8.2 Chapter 3

Simple objective means to analyze total peak shapes and their departure from symmetry and Gaussian profile are proposed. An Excel™ template is provided which automates the entire analysis. Assessment of peak shapes by single valued descriptors of peak shape such as USP tailing, skew, or kurtosis are inadequate because they do not give a complete picture of the overall peak shape. The derivative test is based on the

192

concept that if a peak is symmetric, their inflection points will be mirror images. The derivative test is a very sensitive test for the "presence" of asymmetry on *any* peak shape, even when the data is sampled at very high sampling rates up to 200 Hz. The signal to noise ratio should be high for the proposed tests (as is usually the case). The Gaussian test superimposes a Gaussian model on a normalized peak with its set of constraints and shows the problematic regions of the peak. The standard deviation is extracted from the upper section of the peak rather than the conventional half height approach. The proposed methods will be useful for researchers engaged in stationary phase development, column packing, or hardware design to achieve better peak shapes. The approach used in the Gaussian test is general and, in fact, can be used for testing the departure of any peak shape from the expected mathematical model.

8.3 Chapter 4

Herein a unified approach toward the science of making high efficiency reproducible packed columns was presented. Theoretical considerations and non-Newtonian properties of suspensions were shown. The nonlinear viscosity behavior of suspensions can govern the nature of the packed bed (e.g., jammed state, shear thickened state etc.). Therefore, column packing can be considered as an ultrahigh pressure filtration process of a non-Newtonian suspension. After gaining experience from a range of nonpolar to polar stationary phases with modern SPP and FPP of narrow particle size distribution, a flowchart was developed to provide a logical progression of packing stationary phases of any chemistry. Illustrative examples were shown showing different packing phenomena and suspension properties. Results indicate that relatively concentrated nonaggregating suspensions usually produce better packed analytical and narrow bore columns regardless of the stationary phase chemistry. The best packed

193

reversed phase capillaries usually require aggregating solvents. More studies are needed for capillary columns using different stationary phases to generalize this phenomenon. New directions in colloidal crystals, 3D printing are laid out and the use of nonconventional approaches such as 3D printing and active-flow management are highlighted. Future work on quantitative suspension rheology is needed to understand and model the dynamics of the column packing process, a technology which will continue to evolve for several decades to come.

8.4 Chapter 5

Two new high-selectivity quinine based chiral selectors were bonded to 2.7 μm SPPs to create high-efficiency CSPs that were extensively characterized and compared with the analogous commercial 5 μm FPP based column in UHPLC and SFC. 2.7 μm SPP based quinine CSPs have significantly higher efficiencies and provide remarkably faster analysis times than the traditional 5 μm FPP based columns. High selectivity, high-efficiency, and low retentions on the QHS 2.7 μm SPP CSP were exploited to obtain several rapid separations that are on the order of a few seconds which can dramatically improve the productivity in routine analyses. 2.7 μm SPP based columns were also shown to provide rapid analysis even with reduced counterion concentrations which can enable fast LC-MS analysis with ESI compatible mobile phases. Improved efficiencies also result in better signal-to-noise ratios which can make it possible to achieve lower LOD and LOQ values for biological samples analyzing N-blocked amino acids. 2.7 μm SPPs have relatively higher column permeability than sub-2 μm particles making it possible to take advantage of their performance in HPLC as well as UHPLC. Geometry independent kinetic plots and van Deemter plots showed the improved performance of 2.7 μm SPPs over traditional 5 μm FPPs in HPLC and UHPLC conditions.

194

8.5 Chapter 6

The results of this study, indicate that (1) SPPs are advantageous for ultrafast and high efficiency chiral separations, (2) enantiomeric separations on the order of few seconds are now feasible in all mobile phases with bonded brush type CSPs, (3) kinetic behaviors can sometimes be used to shed light on chiral recognition mechanisms, (4) CSPs can show quite different kinetic profiles from each other and from achiral systems, (5) ultrafast chiral separations require optimized detection and minimization of extra column effects, (6) frictional heating effects must be accounted for in ultrafast separations as they can manifest themselves in disparate ways and to different degrees for various CSPs and mobile phase modes, (7) efficiencies and separation speeds for chiral analytes can now exceed those in capillary electrophoresis. Also it is feasible to expect that (8) SPPs may be advantageous for preparative separations when their high efficiencies, faster analyses times, and reduced solvent consumption compensate for lower chiral selector loading, (9) ultrafast SPP-CSPs may be attractive as the second dimension in 2D-LC because of their greater selectivity and orthogonality to conventional achiral stationary phases, and (10) real-time monitoring of product formation in asymmetric synthesis is possible with ultrafast chiral separations.

8.6 Chapter 7

The foundations of performing sub-second chromatography in small packed beds using superficially porous particles are outlined. Various modes of chromatography were demonstrated including reversed phase, HILIC, and chiral separations as a proof of concept. Detection and hardware challenges need to be further addressed. Although the sampling frequencies are adequate for the current efficiencies achievable in ultrafast chromatography, they may not be for future improved columns. The bigger challenge so

195

far is the peak shapes due to non-Gaussian dispersion in short tubings, which can be

circumvented by on-column injection and on-column detection technologies as is done in

electrophoretic methods. Modern UHPLCs are limited to 2–5 mL/min flow rates at higher

pressures (>500 bar), and this is less than desirable for these separations. Using power

transforms on exponential functions (as those used for modeling peak shapes) is a very

simple way to improve peak shapes, reduce variances, and decrease noise in sub-

second screening.

Appendix A

Supporting Information for Chapter 6

A1. Sizes of components on UHPLC instrument

Table A 1. Instrumental parts that contribute to extra-column band broadening and their dimensions

Parts	Dimensions
Agilent 1290 UHPLC stock needle	6.5 cm x 130 µm
Agilent 1290 UHPLC stock needle seat	11 cm x 130 µm
Agilent ultralow dispersion kit needle	6.5 cm x 75 µm
Agilent ultralow dispersion kit needle seat	11 cm x 75 µm
Stock steel tubings (total)	22 cm x 170 µm
nanoViper capillaries (total)	22 cm x 75 µm
Detector flow cell	0.6 µL

A2. Temperature Measurements Data for Viscous Frictional Heating

Table A 2. CF6-P (10 x 0.46 cm) packed with 2.7 µm SPP. Mobile phase = 80/20/0.3/0.2 ACN/MeOH/TFA/TEA. Temperature measured at the column outlet (flow averaged temperature). Inlet temperature (~ 22 °C) was the same as ambient temperature in each case.

Flow rate mL/min	Pressure (bar) of the System	Temperature (°C) of the Eluent at the Outlet
0.5	45	23
1.0	97	24
1.5	151	26
2.0	209	27
2.5	271	29
3.0	336	31
3.5	408	32
4.0	497	35
4.5	582	37
5.0	668	39

Table A 3. CF7-DMP (10 x 0.46 cm) packed with 2.7 µm SPP. Mobile phase = 90 Heptane-10 EtOH. Temperature measured at the column outlet (flow averaged temperature). Inlet temperature (~ 22 °C) was the same as ambient temperature in each case.

Flow rate mL/min	Pressure (bar) of the System	Temperature (°C) of the Eluent at the Outlet
3.0	354	34
3.5	426	36

Table A 4. Teicoplanin (5 x 0.46 cm) packed with 2.7 µm SPP. Mobile phase = 90/10 Water/MeOH. Temperature measured at the column outlet (flow averaged temperature). Inlet temperature (~ 22 °C) was the same as ambient temperature in each case.

Flow rate mL/min	Pressure (bar) of the System	Temperature (°C) of the Eluent at the Outlet
0.5	109	25

1.0	226	27
1.5	346	28
2.0	468	30
2.5	579	32
3.0	681	34
3.5	780	36
4.0	> More than packing pressure	N/A

A2. First Order Approximation for Radial Temperature Gradient

$$\Delta T_R = \frac{u\left(\frac{dP}{dz}\right)R^2}{4\lambda_{rad}}$$ (A - 1)

where u is the superficial flow velocity in m/s (obtained by dividing the volumetric flow rate by the total cross sectional area of the column), dP/dz the change in pressure in the direction of the column axis per unit length in N/m³, R the column radius in m and λ_{rad} is the approximate thermal conductivity of the mobile phase in the radial direction in W/m°C. The equation (A - 1) can also be written as the following[259]

$$\Delta T_R = \frac{F_v \Delta P}{4\pi\lambda_{rad}L}$$ (A - 2)

Table A 5. First Order Approximation for Radial Temperature Gradient for Normal Phase

Flow rate		P (sys+col),	P(sys),	P (col),	P(col),	Length	Thermal Cond[265]	
mL/min	m³/s	bar	bar	bar	Pa	m	(W/m °C)	T Max (°C)
1.0	1.67E-08	105	25	80	8000000	0.1	0.1253	1
2.0	3.33E-08	225	61	164	16400000	0.1	0.1253	3
3.0	5.00E-08	364	107	257	25700000	0.1	0.1253	8
3.5	5.83E-08	433	136	297	29700000	0.1	0.1253	11

Mobile phase (v/v): 90 Heptane – 10 Ethanol. Column: CF7-DMP SPP. Dimensions: 10 cm x 0.46 cm i.d.

Table A 6. First Order Approximation for Radial Temperature Gradient for Reversed Phase

Flow rate		P (sys+col), bar	P(sys), bar	P (col), bar	P(col), Pa	Length m	Thermal Cond[265] (W/m °C)	T Max (°C)
mL/min	m³/s							
1.0	1.67E-08	178	66	112	11200000	0.05	0.555	1
2.0	3.33E-08	348	140	208	20800000	0.05	0.555	2
3.0	5.00E-08	517	221	296	29600000	0.05	0.555	4
3.5	5.83E-08	601	266	335	33500000	0.05	0.555	6

Mobile phase (v/v): 90 Water – 10 Methanol. Column: Teicoplanin bonded SPP. Dimensions: 5 cm x 0.46 cm i.d.

Appendix B

Publication Information for Chapters 2-7

and Daniel W. Armstrong. 2016, 88, 8821-8826. Copyright 2017 with permission from

American Chemical Society. ACS AuthorChoice License.

References

(1) Patel, D. C.; Breitbach, Z. S.; Woods, R. M.; Lim, Y.; Wang, A.; Jr, F. W. F.; Armstrong, D. W., *The Journal of Organic Chemistry* **2016,** *81*, 1295-1299.

(2) Weatherly, C. A.; Du, S.; Parpia, C.; Santos, P. T.; Hartman, A. L.; Armstrong, D. W., *ACS Chemical Neuroscience* **2017**.

(3) Mitra, S.; Chopra, P., *Indian Journal of Anaesthesia* **2011,** *55*, 556-562.

(4) Lin, G.-Q.; You, Q.-D.; Cheng, J.-F., *Chiral Drugs: Chemistry and Biological Action*. Wiley: 2011.

(5) Rahman, A.; Khanum, S.; Turcu, S., *J Allergy Ther* **2012,** *3*.

(6) Giddings, J. C., *Dynamics of Chromatography: Principles and Theory*. 1 ed.; CRC Press: 2002.

(7) Foley, J. P., *Analyst* **1991,** *116*, 1275-1279.

(8) Sandra, P.; David, F., Selectivity tuning in capillary gas chromatography. In *Multidimensional Chromatography*, Cortes, H. J., Ed. Marcel Dekker: New York, 1990; Vol. 50, p 424.

(9) Sun, P.; Wang, C. L.; Breitbach, Z. S.; Zhang, Y.; Armstrong, D. W., *Analytical Chemistry* **2009,** *81*, 10215-10226.

(10) Armstrong, D. W.; Tang, Y.; Chen, S.; Zhou, Y.; Bagwill, C.; Chen, J.-R., *Analytical Chemistry* **1994,** *66*, 1473-84.

(11) Armstrong, D. W.; Stalcup, A. M.; Hilton, M. L.; Duncan, J. D.; Faulkner, J. R., Jr.; Chang, S. C., *Anal. Chem.* **1990,** *62*, 1610-15.

(12) Armstrong, D. W.; Ward, T. J.; Armstrong, R. D.; Beesley, T. E., *Science* **1986,** *232*, 1132-5.

(13) Armstrong, D. W.; DeMond, W., *Journal of Chromatographic Science* **1984,** *22*, 411-415.

(14) Pirkle, W. H.; Welch, C. J.; Lamm, B., *J. Org. Chem.* **1992,** *57*, 3854-60.

(15) Pirkle, W. H.; Hyun, M. H., *Journal of Chromatography A* **1985,** *322*, 309-320.

(16) Mandl, A.; Nicoletti, L.; Lämmerhofer, M.; Lindner, W., *Journal of Chromatography A* **1999,** *858*, 1-11.

(17) Laemmerhofer, M.; Lindner, W., *J. Chromatogr. A* **1996,** *741*, 33-48.

(18) Uray, G.; Lindner, W., *Chromatographia* **1990,** *30*, 323-327.

(19) Okamoto, Y.; Kawashima, M.; Yamamoto, K.; Hatada, K., *Chem. Lett.* **1984**, 739-42.

(20) Ichida, A.; Shibata, T.; Okamoto, I.; Yuki, Y.; Namikoshi, H.; Toga, Y., *Chromatographia* **1984,** *19*, 280-284.

(21) Beesley, T. E.; Scott, R. P. W., *Chiral Chromatography*. 1 ed.; Wiley: 1999.

(22) Hamman, C.; Wong, M.; Aliagas, I.; Ortwine, D. F.; Pease, J.; Schmidt Jr, D. E.; Victorino, J., *Journal of Chromatography A* **2013,** *1305*, 310-319.

(23) Sogah, G. D. Y.; Cram, D. J., *Journal of the American Chemical Society* **1979,** *101*, 3035-3042.

(24) Newcomb, M.; Toner, J. L.; Helgeson, R. C.; Cram, D. J., *Journal of the American Chemical Society* **1979,** *101*, 4941-4947.

(25) Pirkle, W. H.; Finn, J. M., *Journal of Organic Chemistry* **1981,** *46*, 2935-2938.

(26) Hermansson, J., *Journal of Chromatography A* **1983,** *269*, 71-80.

(27) Allenmark, S.; Bomgren, B.; Borén, H., *Journal of Chromatography A* **1983,** *264*, 63-68.

(28) Armstrong, D. W.; Rundlett, K. L.; Chen, J.-R., *Chirality* **1994,** *6*, 496-509.

(29) Zhang, Y.; Breitbach, Z. S.; Wang, C. L.; Armstrong, D. W., *Analyst* **2010,** *135*, 1076-1083.

(30) Sun, P.; Armstrong, D. W., *J. Chromatogr. A* **2010,** *1217*, 4904-4918.

(31) Gao, H.; Ess, D. H.; Yousufuddin, M.; Kürti, L., *Journal of the American Chemical Society* **2013,** *135*, 7086-7089.
(32) Li, G.-Q.; Gao, H.; Keene, C.; Devonas, M.; Ess, D. H.; Kürti, L., *Journal of the American Chemical Society* **2013,** *135*, 7414-7417.
(33) Kirkland, J. J., Superficially porous supports for chromatography. Google Patents: 1970.
(34) Horvath, C. G.; Preiss, B. A.; Lipsky, S. R., *Analytical Chemistry* **1967,** *39*, 1422-1428.
(35) Verzele, M., *Journal of Chromatography A* **1984,** *295*, 81-87.
(36) Kirkland, J. J., *Analytical Chemistry* **1992,** *64*, 1239-1245.
(37) Schafer, W.; Bu, X.; Gong, X.; Joyce, L. A.; Welch, C. J., 9.02 High-Throughput Analysis for High-Throughput Experimentation in Organic Chemistry A2 - Knochel, Paul. In *Comprehensive Organic Synthesis II (Second Edition)*, Elsevier: Amsterdam, 2014; pp 28-53.
(38) Collins, K. D.; Gensch, T.; Glorius, F., *Nat Chem* **2014,** *6*, 859-871.
(39) Robbins, D. W.; Hartwig, J. F., *Science* **2011,** *333*, 1423-1427.
(40) Beeler, A. B.; Schaus, S. E.; Porco Jr, J. A., *Current Opinion in Chemical Biology* **2005,** *9*, 277-284.
(41) McNally, A.; Prier, C. K.; MacMillan, D. W. C., *Science* **2011,** *334*, 1114-1117.
(42) Buitrago Santanilla, A.; Regalado, E. L.; Pereira, T.; Shevlin, M.; Bateman, K.; Campeau, L.-C.; Schneeweis, J.; Berritt, S.; Shi, Z.-C.; Nantermet, P.; Liu, Y.; Helmy, R.; Welch, C. J.; Vachal, P.; Davies, I. W.; Cernak, T.; Dreher, S. D., *Science* **2015,** *347*, 49-53.
(43) DeStefano, J. J.; Langlois, T. J.; Kirkland, J. J., *Journal of Chromatographic Science* **2008,** *46*, 254-260.
(44) Guillarme, D.; Bonvin, G.; Badoud, F.; Schappler, J.; Rudaz, S.; Veuthey, J.-L., *Chirality* **2010,** *22*, 320-330.
(45) Patel, D. C.; Wahab, M. F.; Armstrong, D. W.; Breitbach, Z. S., *Journal of Chromatography A* **2016,** *1467*, 2-18.
(46) Catani, M.; Ismail, O. H.; Gasparrini, F.; Antonelli, M.; Pasti, L.; Marchetti, N.; Felletti, S.; Cavazzini, A., *Analyst* **2017,** *142*, 555-566.
(47) Wahab, M. F.; Patel, D. C.; Wimalasinghe, R. M.; Armstrong, D. W., *Analytical Chemistry* **2017,** *In Press*.
(48) Wahab, M. F.; Patel, D. C.; Armstrong, D. W., *Journal of Chromatography A* **2017,** *1509*, 163-170.
(49) Gritti, F.; Guiochon, G., *LC-GC North America* **2012**, 586-597.
(50) Gritti, F., *LC-GC North America* **2014**, 928-940.
(51) Dolzan, M. D.; Spudeit, D. A.; Breitbach, Z. S.; Barber, W. E.; Micke, G. A.; Armstrong, D. W., *Journal of Chromatography A* **2014,** *1365*, 124-130.
(52) Patel, D. C.; Breitbach, Z. S.; Wahab, M. F.; Barhate, C. L.; Armstrong, D. W., *Analytical Chemistry* **2015,** *87*, 9137-9148.
(53) Spudeit, D. A.; Dolzan, M. D.; Breitbach, Z. S.; Barber, W. E.; Micke, G. A.; Armstrong, D. W., *Journal of Chromatography A* **2014,** *1363*, 89-95.
(54) Spudeit, D. A.; Breitbach, Z. S.; Dolzan, M. D.; Micke, G. A.; Armstrong, D. W., *Chirality* **2015,** *27*, 788-794.
(55) Kirkland, J. J.; DeStefano, J. J., *Journal of Chromatography A* **2006,** *1126*, 50-57.
(56) Blue, L. E.; Jorgenson, J. W., *Journal of Chromatography A* **2015,** *1380*, 71-80.
(57) Wahab, M. F.; Pohl, C. A.; Lucy, C. A., *Journal of Chromatography A* **2012,** *1270*, 139-146.

(58) Bruns, S.; Stoeckel, D.; Smarsly, B. M.; Tallarek, U., *Journal of Chromatography A* **2012,** *1268*, 53-63.

(59) Ai, F.; Li, L.; Ng, S.-C.; Tan, T. T. Y., *Journal of Chromatography A* **2010,** *1217*, 7502-7506.

(60) Xiao, Y.; Tan, T. T. Y.; Ng, S.-C., *Analyst* **2011,** *136*, 1433-1439.

(61) Min, Y.; Sui, Z.; Liang, Z.; Zhang, L.; Zhang, Y., *Journal of Pharmaceutical and Biomedical Analysis* **2015,** *114*, 247-253.

(62) Cancelliere, G.; Ciogli, A.; D'Acquarica, I.; Gasparrini, F.; Kocergin, J.; Misiti, D.; Pierini, M.; Ritchie, H.; Simone, P.; Villani, C., *Journal of Chromatography A* **2010,** *1217*, 990-999.

(63) Kotoni, D.; Ciogli, A.; Molinaro, C.; D'Acquarica, I.; Kocergin, J.; Szczerba, T.; Ritchie, H.; Villani, C.; Gasparrini, F., *Analytical Chemistry* **2012,** *84*, 6805-6813.

(64) Reischl, R. J.; Hartmanova, L.; Carrozzo, M.; Huszar, M.; Frühauf, P.; Lindner, W., *Journal of Chromatography A* **2011,** *1218*, 8379-8387.

(65) Fanali, S.; D'Orazio, G.; Farkas, T.; Chankvetadze, B., *Journal of Chromatography A* **2012,** *1269*, 136-142.

(66) Lomsadze, K.; Jibuti, G.; Farkas, T.; Chankvetadze, B., *Journal of Chromatography A* **2012,** *1234*, 50-55.

(67) Maftouh, M.; Granier-Loyaux, C.; Chavana, E.; Marini, J.; Pradines, A.; Heyden, Y. V.; Picard, C., *Journal of Chromatography A* **2005,** *1088*, 67-81.

(68) Miller, L., *Journal of Chromatography A* **2012,** *1250*, 250-255.

(69) Grand-Guillaume Perrenoud, A.; Veuthey, J.-L.; Guillarme, D., *Journal of Chromatography A* **2012,** *1266*, 158-167.

(70) Regalado, E. L.; Welch, C. J., *Journal of Separation Science* **2015,** *38*, 2826-2832.

(71) Sciascera, L.; Ismail, O.; Ciogli, A.; Kotoni, D.; Cavazzini, A.; Botta, L.; Szczerba, T.; Kocergin, J.; Villani, C.; Gasparrini, F., *Journal of Chromatography A* **2015,** *1383*, 160-168.

(72) Pu, L., *Chemical Reviews* **1998,** *98*, 2405-2494.

(73) Kuiling, D.; Xin, L.; Baoming, J.; Hongchao, G.; Masato, K., *Current Organic Synthesis* **2005,** *2*, 499-545.

(74) Guillena, G.; Hita, M. d. C.; Nájera, C.; Viózquez, S. F., *The Journal of Organic Chemistry* **2008,** *73*, 5933-5943.

(75) Aleman, J.; Cabrera, S., *Chemical Society Reviews* **2013,** *42*, 774-793.

(76) Liao, J.; Sun, X.; Cui, X.; Yu, K.; Zhu, J.; Deng, J., *Chemistry – A European Journal* **2003,** *9*, 2611-2615.

(77) Horton, D. A.; Bourne, G. T.; Smythe, M. L., *Chemical Reviews* **2003,** *103*, 893-930.

(78) Patchett, A. A.; Nargund, R. P., *Annual Reports in Medicinal Chemistry* **2000,** *35*, 289-298.

(79) Bringmann, G.; Gulder, T.; Gulder, T. A. M.; Breuning, M., *Chemical Reviews* **2011,** *111*, 563-639.

(80) Gübitz, G., *Chromatographia* **1990,** *30*, 555-564.

(81) Qiu, H.; Padivitage, N. L. T.; Frink, L. A.; Armstrong, D. W., *Tetrahedron: Asymmetry* **2013,** *24*, 1134-1141.

(82) Huang, K.; Breitbach, Z. S.; Armstrong, D. W., *Tetrahedron: Asymmetry* **2006,** *17*, 2821-2832.

(83) Armstrong, D. W.; He, L.; Yu, T.; Lee, J. T.; Liu, Y.-s., *Tetrahedron: Asymmetry* **1999,** *10*, 37-60.

(84) Armstrong, D. W.; Lee, J. T.; Chang, L. W., *Tetrahedron: Asymmetry* **1998,** *9*, 2043-2064.

(85) Nelson, T. D.; Welch, C. J.; Rosen, J. D.; Smitrovich, J. H.; Huffman, M. A.; McNamara, J. M.; Mathre, D. J., *Chirality* **2004,** *16*, 609-613.

(86) Lipka, E.; Yous, S.; Furman, C.; Carato, P.; Deghaye, C.; Bonte, J.-P.; Vaccher, C., *Chromatographia* **2012,** *75*, 337-345.

(87) Loukotková, L.; Rambousková, M.; Bosáková, Z.; Tesařová, E., *Chirality* **2008,** *20*, 900-909.

(88) Armstrong, D. W.; Ward, T. J.; Czech, A.; Czech, B. P.; Bartsch, R. A., *The Journal of Organic Chemistry* **1985,** *50*, 5556-5559.

(89) Iuliano, A.; Pieroni, E.; Salvadori, P., *Journal of Chromatography A* **1997,** *786*, 355-360.

(90) Záruba, K.; Král, V. r., *Tetrahedron: Asymmetry* **2002,** *13*, 2567-2570.

(91) Kalíková, K.; Janečková, L.; Armstrong, D. W.; Tesařová, E., *Journal of Chromatography A* **2011,** *1218*, 1393-1398.

(92) Smuts, J. P.; Hao, X.-Q.; Han, Z.; Parpia, C.; Krische, M. J.; Armstrong, D. W., *Analytical Chemistry* **2014,** *86*, 1282-1290.

(93) Weng, W.; Guo, H.; Zhan, F.; Fang, H.; Wang, Q.; Yao, B.; Li, S., *Journal of Chromatography A* **2008,** *1210*, 178-184.

(94) Sun, P.; Wang, C.; Breitbach, Z. S.; Zhang, Y.; Armstrong, D. W., *Analytical Chemistry* **2009,** *81*, 10215-10226.

(95) Sun, P.; Wang, C.; Padivitage, N. L. T.; Nanayakkara, Y. S.; Perera, S.; Qiu, H.; Zhang, Y.; Armstrong, D. W., *Analyst* **2011,** *136*, 787-800.

(96) Gondová, T.; Petrovaj, J.; Kutschy, P.; Armstrong, D. W., *Journal of Chromatography A* **2013,** *1272*, 100-105.

(97) Janečková, L.; Kalíková, K.; Vozka, J.; Armstrong, D. W.; Bosáková, Z.; Tesařová, E., *Journal of Separation Science* **2011,** *34*, 2639-2644.

(98) Padivitage, N. L. T.; Dodbiba, E.; Breitbach, Z. S.; Armstrong, D. W., *Drug Test Anal* **2014,** *6*, 542-551.

(99) Perera, S.; Na, Y.-C.; Doundoulakis, T.; Ngo, V. J.; Feng, Q.; Breitbach, Z. S.; Lovely, C. J.; Armstrong, D. W., *Chirality* **2013,** *25*, 133-140.

(100) Grushka, E., Chromatographic Peak Shape Analysis. In *Methods of Protein Separation*, Catsimpoolas, N., Ed. Springer US: Boston, MA, 1975; pp 161-192.

(101) Pap, T. L.; Pápai, Z., *Journal of Chromatography A* **2001,** *930*, 53-60.

(102) Di Marco, V. B.; Bombi, G. G., *Journal of Chromatography A* **2001,** *931*, 1-30.

(103) Forbes, C.; Evans, M.; Hastings, N.; Peacock, B., *Statistical Distribution*. 4th ed.; Wiley-Interscience: Hoboken, NJ, 2010.

(104) Baeza-Baeza, J. J.; García-Álvarez-Coque, M. C., *Journal of Chromatography A* **2011,** *1218*, 5166-5174.

(105) Wahab, M. F.; Dasgupta, P. K.; Kadjo, A. F.; Armstrong, D. W., *Analytica Chimica Acta* **2016,** *907*, 31-44.

(106) Miyabe, K.; Guiochon, G., *Journal of Chromatography A* **1999,** *857*, 69-87.

(107) Shalliker, R. A.; Broyles, B. S.; Guiochon, G., *Journal of Chromatography A* **2000,** *888*, 1-12.

(108) Ghasemi, A.; Zahediasl, S., *Int J Endocrinol Metab* **2012,** *10*, 486-489.

(109) Schulz-Trieglaff, O.; Machtejevas, E.; Reinert, K.; Schlüter, H.; Thiemann, J.; Unger, K., *BioData Mining* **2009,** *2*, 4.

(110) Rix, H., *Journal of Chromatography A* **1981,** *204*, 163-165.

(111) Dondi, F., *Analytical Chemistry* **1982,** *54*, 473-477.

(112) Felinger, A., *Data Analysis and Signal Processing in Chromatography*. 1st ed.; Elsevier Science: Netherlands, 1998.

(113) Brychkov, Y. A., *Handbook of Special Functions: Derivatives, Integrals, Series and Other Formulas*. Chapman and Hall/CRC: 2008.

(114) Pearson, K., *Philosophical Transactions of the Royal Society of London. (A.)* **1895,** *186*, 343-414.

(115) Inc., S. S. *PeakFit Software*, 4.12; San Jose, CA, 2017.

(116) Hetzel, T.; Loeker, D.; Teutenberg, T.; Schmidt, T. C., *Journal of Separation Science* **2016,** *39*, 3889-3897.

(117) Guillarme, D.; Veuthey, J.-L. *UHPLC in Life Sciences*; 2012; p 145.

(118) Kadjo, A. F.; Dasgupta, P. K.; Su, J.; Liu, S.; Kraiczek, K. G., *Analytical Chemistry* **2017,** *89*, 3884-3892.

(119) Kurganov, A.; Trüdinger, U.; Isaeva, T.; Unger, K., *Chromatographia* **1996,** *42*, 217-222.

(120) Nawrocki, J.; Dunlap, C.; McCormick, A.; Carr, P. W., *Journal of Chromatography A* **2004,** *1028*, 1-30.

(121) Weber, T. P.; Jackson, P. T.; Carr, P. W., *Analytical Chemistry* **1995,** *67*, 3042-3050.

(122) Paek, C.; Huang, Y.; Filgueira, M. R.; McCormick, A. V.; Carr, P. W., *Journal of Chromatography A* **2012,** *1229*, 129-139.

(123) Paek, C.; McCormick, A. V.; Carr, P. W., *Journal of Chromatography A* **2011,** *1218*, 1359-1366.

(124) Muna, G. W.; Swope, V. M.; Swain, G. M.; Porter, M. D., *Journal of Chromatography A* **2008,** *1210*, 154-159.

(125) West, C.; Elfakir, C.; Lafosse, M., *Journal of Chromatography A* **2010,** *1217*, 3201-3216.

(126) Knox, J. H.; Kaur, B.; Millward, G. R., *Journal of Chromatography A* **1986,** *352*, 3-25.

(127) Barhate, C. L.; Wahab, M. F.; Breitbach, Z. S.; Bell, D. S.; Armstrong, D. W., *Analytica Chimica Acta* **2015,** *898*, 128-137.

(128) Patel, D. C.; Breitbach, Z. S.; Yu, J.; Nguyen, K. A.; Armstrong, D. W., *Analytica Chimica Acta* **2017,** *963*, 164-174.

(129) Wang, Y.; Wahab, M. F.; Breitbach, Z. S.; Armstrong, D. W., *Analytical Methods* **2016,** *8*, 6038-6045.

(130) Wahab, M. F.; Pohl, C. A.; Lucy, C. A., *Analyst* **2011,** *136*, 3113-3120.

(131) Wahab, M. F.; Ibrahim, M. E.; Lucy, C. A., *Analytical Chemistry* **2013,** *85*, 5684-5691.

(132) Shalliker, R. A.; Broyles, B. S.; Guiochon, G., *Journal of Chromatography A* **2000,** *878*, 153-163.

(133) Koh, J.-H.; Broyles, B. S.; Guan-Sajonz, H.; Hu, M. Z. C.; Guiochon, G., *Journal of Chromatography A* **1998,** *813*, 223-238.

(134) Verzele M., D., *LC-GC* **1986,** *4(7)*, 616-618.

(135) Wu, Y.; Ching, C., *Chromatographia* **2003,** *57*, 329-337.

(136) Godinho, J. M.; Reising, A. E.; Tallarek, U.; Jorgenson, J. W., *Journal of Chromatography A* **2016,** *1462*, 165-169.

(137) Jorgenson, J.; Pohl, C.; Gritti, F.; Wahab, M. F., *Personal Communication* **2017**.

(138) Cheong, W. J., *Journal of Separation Science* **2014,** *37*, 603-617.

(139) Spain, I. L.; Paauwe, J., *High pressure technology Volume I,* . Dekker: New York, N.Y., 1977.

(140) Gritti, F.; Bell, D. S.; Guiochon, G., *Journal of Chromatography A* **2014,** *1355*, 179-192.

(141) Catani, M.; Ismail, O. H.; Cavazzini, A.; Ciogli, A.; Villani, C.; Pasti, L.; Bergantin, C.; Cabooter, D.; Desmet, G.; Gasparrini, F.; Bell, D. S., *Journal of Chromatography A* **2016,** *1454*, 78-85.

(142) Billen, J.; Guillarme, D.; Rudaz, S.; Veuthey, J.-L.; Ritchie, H.; Grady, B.; Desmet, G., *Journal of Chromatography A* **2007,** *1161*, 224-233.

(143) Cabooter, D.; Billen, J.; Terryn, H.; Lynen, F.; Sandra, P.; Desmet, G., *Journal of Chromatography A* **2008,** *1204*, 1-10.

(144) Gritti, F.; Farkas, T.; Heng, J.; Guiochon, G., *Journal of Chromatography A* **2011,** *1218*, 8209-8221.

(145) Zats, J. L., *Journal of the Society of Cosmetic Chemists* **1985,** *36*, 393-411.

(146) Bristow, P. A.; Knox, J. H., *Chromatographia* **1977,** *10*, 279-289.

(147) Kromasil, *https://*www.kromasil.com/support/dac_packing.php *(Jan 19, 2017).*

(148) Broquaire, M., *Journal of Chromatography A* **1979,** *170*, 43-52.

(149) Domagalska, D. E.; Loscombe, C. R., *Chromatographia* **1982,** *15*, 657-659.

(150) Karapetyan, S. A.; Yakushina, L. M.; Vasiyarov, G. G.; Brazhnikov, V. V., *Journal of High Resolution Chromatography* **1983,** *6*, 440-441.

(151) Szumski, M.; Buszewski, B., *Critical Reviews in Analytical Chemistry* **2002,** *32*, 1-46.

(152) Zimina, T.; Smith, R. M.; Highfield, J. C.; Myers, P.; King, B. W., *Journal of Chromatography A* **1996,** *728*, 33-45.

(153) Zimina, T. M.; Smith, R. M.; Myers, P.; King, B. W., *Chromatographia* **1995,** *40*, 662-668.

(154) Reed, G. D.; Loscombe, C. R., *Chromatographia* **1984,** *18*, 695-697.

(155) Roumeliotis, P.; Chatziathanassiou, M.; Unger, K. K., *Chromatographia* **1984,** *19*, 145-150.

(156) Avery, N. C.; Light, N., *Journal of Chromatography A* **1985,** *328*, 347-352.

(157) Giesche, H.; Unger, K. K.; Esser, U.; Eray, B.; Trüdinger, U.; Kinkel, J. N., *J. Chromatogr. A* **1989,** *465*, 39-57.

(158) Wong, V.; Shalliker, R. A.; Guiochon, G., *Analytical Chemistry* **2004,** *76*, 2601-2608.

(159) *Knauer Wissenschaftliche Geräte GmbH, High Pressure Column Packing Device Manual* **2007**, 19.

(160) Karapetyan, S. A.; Yakushina, L. M.; Vasijarov, G. G.; Brazhnikov, V. V., *Journal of High Resolution Chromatography* **1985,** *8*, 148-149.

(161) Vissers, J. P. C.; Hoeben, M. A.; Laven, J.; Claessens, H. A.; Cramers, C. A., *Journal of Chromatography A* **2000,** *883*, 11-25.

(162) MacNair, J. E.; Patel, K. D.; Jorgenson, J. W., *Analytical Chemistry* **1999,** *71*, 700-708.

(163) Bocian, S.; Nowaczyk, A.; Buszewski, B., *Anal. Bioanal. Chem.* **2012,** *404*, 731-740.

(164) Corradini, C.; Corradini, D.; Huber, C. G.; Bonn, G. K., *Chromatographia* **1995,** *41*, 511-515.

(165) Jewett, D.; Lawless, J. G., *Journal of High Resolution Chromatography* **1980,** *3*, 647-648.

(166) Tyrrell, É.; Hilder, E. F.; Shalliker, R. A.; Dicinoski, G. W.; Shellie, R. A.; Breadmore, M. C.; Pohl, C. A.; Haddad, P. R., *Journal of Chromatography A* **2008,** *1208*, 95-100.

(167) Hou, Y.; Zhang, F.; Liang, X.; Yang, B.; Liu, X.; Dasgupta, P. K., *Analytical Chemistry* **2016,** *88*, 4676-4681.

(168) Gilbert, M. T.; Knox, J. H.; Kaur, B., *Chromatographia* **1982,** *16*, 138-146.

(169) Binks, B. P.; Clint, J. H., *Langmuir* **2002,** *18*, 1270-1273.

(170) Harkins, W. D.; Feldman, A., *Journal of the American Chemical Society* **1922,** *44*, 2665-2685.

(171) Kinloch, A. J., *Adhesion and Adhesives: Science and Technology*. Chapman and Hall, pg. 26-34.: New York, 1987.

(172) Vissers, J. P. C.; Claessens, H. A.; Laven, J.; Cramers, C. A., *Analytical Chemistry* **1995,** *67*, 2103-2109.

(173) Dong, L.; Johnson, D., *Langmuir* **2003,** *19*, 10205-10209.

(174) Mewis, J.; Wagner, N. J., *Colloidal Suspension Rheology*. 1 ed.; Cambridge University Press: 2012.

(175) Shelly, D. C.; Edkins, T. J., *Journal of Chromatography A* **1987,** *411*, 185-199.

(176) Barnes, H., *Journal of Rheology* **1989,** *33*, 329-366.

(177) Gritti, F.; Guiochon, G., *Analytical Chemistry* **2013,** *85*, 3017-3035.

(178) Knox, J. H.; Parcher, J. F., *Analytical Chemistry* **1969,** *41*, 1599-1606.

(179) Benenati, R. F.; Brosilow, C. B., *AIChE Journal* **1962,** *8*, 359-361.

(180) Shalliker, R. A.; Broyles, B. S.; Guiochon, G., *Journal of Chromatography A* **2000,** *888*, 1-12.

(181) Reising, A. E.; Godinho, J. M.; Hormann, K.; Jorgenson, J. W.; Tallarek, U., *Journal of Chromatography A* **2016,** *1436*, 118-132.

(182) Reising, A. E.; Godinho, J. M.; Jorgenson, J. W.; Tallarek, U., *Journal of Chromatography A* **2017,** *1504*, 71-82.

(183) Bröckel, U.; Löffler, F., *Powder Technology* **1991,** *66*, 53-58.

(184) Wahab, M. F.; Wimalasinghe, R. M.; Wang, Y.; Barhate, C. L.; Patel, D. C.; Armstrong, D. W., *Analytical Chemistry* **2016,** *88*, 8821-8826.

(185) Brown, E.; Forman, N. A.; Orellana, C. S.; Zhang, H.; Maynor, B. W.; Betts, D. E.; DeSimone, J. M.; Jaeger, H. M., *Nat Mater* **2010,** *9*, 220-224.

(186) González, B.; Calvar, N.; Gómez, E.; Domínguez, Á., *The Journal of Chemical Thermodynamics* **2007,** *39*, 1578-1588.

(187) Sovilj, M. N., *Journal of Chemical & Engineering Data* **1995,** *40*, 1058-1061.

(188) Wei, I. C.; Rowley, R. L., *Journal of Chemical & Engineering Data* **1984,** *29*, 332-335.

(189) Soliven, A.; Dennis, G. R.; Hilder, E. F.; Andrew Shalliker, R.; Stevenson, P. G., *Chromatographia* **2014,** *77*, 663-671.

(190) MacNair, J. E.; Lewis, K. C.; Jorgenson, J. W., *Analytical Chemistry* **1997,** *69*, 983-989.

(191) Treadway, J. W.; Wyndham, K. D.; Jorgenson, J. W., *Journal of Chromatography A* **2015,** *1422*, 345-349.

(192) Bruns, S.; Franklin, E. G.; Grinias, J. P.; Godinho, J. M.; Jorgenson, J. W.; Tallarek, U., *Journal of Chromatography A* **2013,** *1318*, 189-197.

(193) Patel, K. D.; Jerkovich, A. D.; Link, J. C.; Jorgenson, J. W., *Analytical Chemistry* **2004,** *76*, 5777-5786.

(194) Colón, L. A.; Maloney, T. D.; Fermier, A. M., *Journal of Chromatography A* **2000,** *887*, 43-53.

(195) Shalliker, R. A.; Broyles, B. S.; Guiochon, G., *Analytical Chemistry* **2000,** *72*, 323-332.

(196) Khirevich, S.; Höltzel, A.; Hlushkou, D.; Tallarek, U., *Analytical Chemistry* **2007,** *79*, 9340-9349.

(197) Andreolini, F.; Borra, C.; Novotny, M., *Analytical Chemistry* **1987,** *59*, 2428-2432.

(198) Malik, A.; Li, W.; Lee, M. L., *Journal of Microcolumn Separations* **1993,** *5*, 361-369.

(199) Pieranski, P., *Comptes Rendus Physique* **2016,** *17*, 242-263.

(200) Schure, M. R.; Maier, R. S.; Kroll, D. M.; Ted Davis, H., *Journal of Chromatography A* **2004,** *1031*, 79-86.

(201) Malkin, D. S. An Invesitgation of a Novel Monolithic Chromatography Column, Silica Colloidal Crystal Packed Columns. 2010.

(202) Fee, C.; Nawada, S.; Dimartino, S., *Journal of Chromatography A* **2014,** *1333*, 18-24.

(203) Yin, H.; Brennen, R. A.; Lyster, E.; Slocum, R., **2016 (US Patent 20160231293)**.

(204) De Malsche, W.; Eghbali, H.; Clicq, D.; Vangelooven, J.; Gardeniers, H.; Desmet, G., *Analytical Chemistry* **2007,** *79*, 5915-5926.

(205) Robson, M. M.; Roulin, S.; Shariff, S. M.; Raynor, M. W.; Bartle, K. D.; Clifford, A. A.; Myers, P.; Euerby, M. R.; Johnson, C. M., *Chromatographia* **1996,** *43*, 313-321.

(206) Tong, D.; Bartle, K. D.; Clifford, A. A., *Journal of Microcolumn Separations* **1994,** *6*, 249-255.

(207) Inagaki, M.; Kitagawa, S.; Tsuda, T., *Kuromatogurafi* **1993,** *14*, 55R-60R.

(208) Fermier, A. M., Colón, L. A., In *HPLC 1996 in High Performance Liquid Phase Separations and Related Techniques*, San Francisco, CA, 1996.

(209) Fermier, A. M.; Colón, L. A., *Journal of Microcolumn Separations* **1998,** *10*, 439-447.

(210) McCall, J. P. A Twist on Packing Analytical Columns for Reversed Phase Liquid Chromatography. Florida State University, Florida, 2004.

(211) Camenzuli, M.; Ritchie, H. J.; Ladine, J. R.; Shalliker, R. A., *Analyst* **2011,** *136*, 5127-5130.

(212) Davankov, V. A.; Rogozhin, S. V., *Journal of Chromatography A* **1971,** *60*, 280-283.

(213) Maier, N. M.; Nicoletti, L.; Lammerhofer, M.; Lindner, W., *Chirality* **1999,** *11*, 522-528.

(214) Welch, C. J.; Gong, X.; Schafer, W.; Pratt, E. C.; Brkovic, T.; Pirzada, Z.; Cuff, J. F.; Kosjek, B., *Tetrahedron: Asymmetry* **2010,** *21*, 1674-1681.

(215) Barhate, C. L.; Breitbach, Z. S.; Pinto, E. C.; Regalado, E. L.; Welch, C. J.; Armstrong, D. W., *Journal of Chromatography A* **2015,** *1426*, 241-247.

(216) Sajonz, P.; Schafer, W.; Gong, X.; Shultz, S.; Rosner, T.; Welch, C. J., *Journal of Chromatography A* **2007,** *1145*, 149-154.

(217) Federsel, H.-J., *Chirality* **2003,** *15*, S128-S142.

(218) Maier, N. M.; Franco, P.; Lindner, W., *Journal of Chromatography A* **2001,** *906*, 3-33.

(219) Perrin, C.; Vu, V. A.; Matthijs, N.; Maftouh, M.; Massart, D. L.; Vander Heyden, Y., *Journal of Chromatography A* **2002,** *947*, 69-83.

(220) Omamogho, J. O.; Nesterenko, E.; Connolly, D.; Glennon, J., *LC-GC North America* **2012**, 63-69.

(221) Broeckhoven, K.; Cabooter, D.; Desmet, G., *Journal of Pharmaceutical Analysis* **2013,** *3*, 313-323.

(222) Ismail, O. H.; Pasti, L.; Ciogli, A.; Villani, C.; Kocergin, J.; Anderson, S.; Gasparrini, F.; Cavazzini, A.; Catani, M., *Journal of Chromatography A* **2016,** *1466*, 96-104.

(223) Franco, P.; Zhang, T.; Gargano, A.; Mahut, M.; Lammerhofer, M.; Lindner, W., Enantiomer and topoisomer separation of acidic compounds on anion-exchanger chiral stationary phases by HPLC and SFC. *LC GC Europe* 2012, pp 600-610.

(224) Fekete, S.; Kohler, I.; Rudaz, S.; Guillarme, D., *Journal of Pharmaceutical and Biomedical Analysis* **2014,** *87*, 105-119.

(225) Levkin, P. A.; Maier, N. M.; Schurig, V.; Lindner, W., *Angewandte Chemie International Edition* **2010,** *49*, 7742-7744.

(226) Crudden, C. M.; Sateesh, M.; Lewis, R., *Journal of the American Chemical Society* **2005,** *127*, 10045-10050.
(227) Ma, Y.; Chassy, A. W.; Miyazaki, S.; Motokawa, M.; Morisato, K.; Uzu, H.; Ohira, M.; Furuno, M.; Nakanishi, K.; Minakuchi, H.; Mriziq, K.; Farkas, T.; Fiehn, O.; Tanaka, N., *Journal of Chromatography A* **2015,** *1383*, 47-57.
(228) Majors, R. E., *LC-GC North America* **2014,** *32*, 840-853.
(229) Gritti, F.; Guiochon, G., *Journal of Chromatography A* **2014,** *1348*, 87-96.
(230) Armstrong, D. W.; Gasper, M.; Lee, S. H.; Zukowski, J.; Ercal, N., *Chirality* **1993,** *5*, 375-378.
(231) Giddings, J. C., *Analytical Chemistry* **1965,** *37*, 60-63.
(232) Knox, J. H., *Journal of Chromatographic Science* **1977,** *15*, 352-364.
(233) Desmet, G.; Clicq, D.; Gzil, P., *Analytical Chemistry* **2005,** *77*, 4058-4070.
(234) Desmet, G.; Cabooter, D.; Broeckhoven, K., *Analytical Chemistry* **2015,** *87*, 8593-8602.
(235) Snyder, L. R.; Kirkland, J. J.; Dolan, J. W., *Introduction to Modern Liquid Chromatography*. 3 ed.; Wiley: 2009.
(236) Mikes, F. e.; Boshart, G., *Journal of Chromatography A* **1978,** *149*, 455-464.
(237) Okamoto, Y.; Honda, S.; Okamoto, I.; Yuki, H.; Murata, S.; Noyori, R.; Takaya, H., *Journal of the American Chemical Society* **1981,** *103*, 6971-6973.
(238) Okamoto, Y.; Aburatani, R.; Fukumoto, T.; Hatada, K., *Chem. Lett.* **1987**, 1857-60.
(239) Stalcup, A. M.; Chang, S. C.; Armstrong, D. W.; Pitha, J., *J. Chromatogr. A* **1990,** *513*, 181-94.
(240) Berthod, A.; Chen, X. H.; Kullman, J. P.; Armstrong, D. W.; Gasparrini, F.; D'Acquarica, I.; Villani, C.; Carotti, A., *Analytical Chemistry* **2000,** *72*, 1767-1780.
(241) Gasparrini, F.; Misiti, D.; Rompietti, R.; Villani, C., *J. Chromatogr. A* **2005,** *1064*, 25-38.
(242) Han, X.; He, L.; Zhong, Q.; Beesley, T. E.; Armstrong, D. W., *Chromatographia* **2006,** *63*, 13-23.
(243) Péter, A.; Török, G.; Armstrong, D. W.; Tóth, G.; Tourwé, D., *Journal of Chromatography A* **1998,** *828*, 177-190.
(244) Davankov, V. A., *Chirality* **1997,** *9*, 99-102.
(245) Gasparrini, F.; Misiti, D.; Villani, C., *Chirality* **1992,** *4*, 447-458.
(246) Oberleitner, W. R.; Maier, N. M.; Lindner, W., *Journal of Chromatography A* **2002,** *960*, 97-108.
(247) Sajonz, P.; Gong, X.; Leonard, W. R.; Biba, M.; Welch, C. J., *Chirality* **2006,** *18*, 803-813.
(248) Weatherly, C. A.; Na, Y.-C.; Nanayakkara, Y. S.; Woods, R. M.; Sharma, A.; Lacour, J.; Armstrong, D. W., *Journal of Chromatography B* **2014,** *955–956*, 72-80.
(249) Armstrong, D. W.; Li, W.; Chang, C. D.; Pitha, J., *Analytical Chemistry* **1990,** *62*, 914-923.
(250) Jiang, C. X.; Tong, M. Y.; Breitbach, Z. S.; Armstrong, D. W., *Electrophoresis* **2009,** *30*, 3897-3909.
(251) Woods, R. M.; Patel, D. C.; Lim, Y.; Breitbach, Z. S.; Gao, H. Y.; Keene, C.; Li, G. Q.; Kurti, L.; Armstrong, D. W., *Journal of Chromatography A* **2014,** *1357*, 172-181.
(252) Woods, R. M.; Breitbach, Z. S.; Armstrong, D. W., *Lc Gc N Am* **2014,** *32*, 742-751.
(253) Wang, X.; Carr, P. W.; Stoll, D. R., *Lc Gc N Am* **2010,** *28*, 932-942.
(254) Elgass, H.; Engelhardt, H.; Halász, I., *Z. Anal. Chem.* **1979,** *294*, 97-106.
(255) Guiochon, G.; Sepaniak, M. J., *Analytical Chemistry* **1991,** *63*, 73-73.

(256) Usher, K. M.; Simmons, C. R.; Dorsey, J. G., *Journal of Chromatography A* **2008,** *1200*, 122-128.
(257) de Villiers, A.; Lauer, H.; Szucs, R.; Goodall, S.; Sandra, P., *Journal of Chromatography A* **2006,** *1113*, 84-91.
(258) Fountain, K. J.; Neue, U. D.; Grumbach, E. S.; Diehl, D. M., *Journal of Chromatography A* **2009,** *1216*, 5979-5988.
(259) Gritti, F.; Guiochon, G., *Analytical Chemistry* **2008,** *80*, 5009-5020.
(260) Gritti, F.; Martin, M.; Guiochon, G., *Analytical Chemistry* **2009,** *81*, 3365-3384.
(261) Halász, I.; Endele, R.; Asshauer, J., *Journal of Chromatography A* **1975,** *112*, 37-60.
(262) Boehm, R. E.; Martire, D. E.; Armstrong, D. W., *Analytical Chemistry* **1988,** *60*, 522-528.
(263) Gritti, F.; Guiochon, G., *J. Chromatogr. A* **2010,** *1217*, 6350-6365.
(264) Poppe, H.; Kraak, J. C.; Huber, J. F. K.; van den Berg, J. H. M., *Chromatographia* **1981,** *14*, 515-523.
(265) Qun-Fang, L.; Rui-Sen, L.; Dan-Yan, N.; Yu-Chun, H., *Journal of Chemical & Engineering Data* **1997,** *42*, 971-974.
(266) Hupe, K. P.; Jonker, R. J.; Rozing, G., *Journal of Chromatography A* **1984,** *285*, 253-265.
(267) Ismail, O. H.; Ciogli, A.; Villani, C.; De Martino, M.; Pierini, M.; Cavazzini, A.; Bell, D. S.; Gasparrini, F., *Journal of Chromatography A* **2016,** *1427*, 55-68.
(268) Fekete, S.; Ganzler, K.; Fekete, J., *Journal of Pharmaceutical and Biomedical Analysis* **2011,** *54*, 482-490.
(269) Gritti, F.; Leonardis, I.; Abia, J.; Guiochon, G., *Journal of Chromatography A* **2010,** *1217*, 3819-3843.
(270) Jeong, E. S.; Kim, S.-H.; Cha, E.-J.; Lee, K. M.; Kim, H. J.; Lee, S.-W.; Kwon, O.-S.; Lee, J., *Rapid Communications in Mass Spectrometry* **2015,** *29*, 367-384.
(271) D'Attoma, A.; Heinisch, S., *Journal of Chromatography A* **2013,** *1306*, 27-36.
(272) Gargano, A. F. G.; Duffin, M.; Navarro, P.; Schoenmakers, P. J., *Analytical Chemistry* **2016,** *88*, 1785-1793.
(273) Le Masle, A.; Angot, D.; Gouin, C.; D'Attoma, A.; Ponthus, J.; Quignard, A.; Heinisch, S., *Journal of Chromatography A* **2014,** *1340*, 90-98.
(274) Jacobson, S. C.; Culbertson, C. T.; Daler, J. E.; Ramsey, J. M., *Analytical Chemistry* **1998,** *70*, 3476-3480.
(275) Moore, A. W.; Jorgenson, J. W., *Analytical Chemistry* **1995,** *67*, 3448-3455.
(276) Piehl, N.; Ludwig, M.; Belder, D., *Electrophoresis* **2004,** *25*, 3848-3852.
(277) Guetschow, E. D.; Steyer, D. J.; Kennedy, R. T., *Analytical Chemistry* **2014,** *86*, 10373-10379.
(278) Clicq, D.; Vervoort, N.; Vounckx, R.; Ottevaere, H.; Buijs, J.; Gooijer, C.; Ariese, F.; Baron, G. V.; Desmet, G., *Journal of Chromatography A* **2002,** *979*, 33-42.
(279) Umehara, R.; Harada, M.; Okada, T., *Journal of Separation Science* **2009,** *32*, 472-478.
(280) Vankrunkelsven, S.; Clicq, D.; Cabooter, D.; De Malsche, W.; Gardeniers, J. G. E.; Desmet, G., *Journal of Chromatography A* **2006,** *1102*, 96-103.
(281) Giddings, J. C.; Keller, R. A., *Extracolumn Contribution to Chromatographic Band Broadening*. Marcel Dekker: New York, 1996.
(282) Shannon, C. E., *Proceedings of the IRE* **1949,** *37*, 10-21.
(283) Atwood, J. G.; Golay, M. J. E., *Journal of Chromatography A* **1981,** *218*, 97-122.
(284) Gritti, F.; McDonald, T.; Gilar, M., *Journal of Chromatography A* **2015,** *1410*, 118-128.

(285) Grushka, E., *Analytical Chemistry* **1970,** *42*, 1142-1147.
(286) Dasgupta, P. K.; Chen, Y.; Serrano, C. A.; Guiochon, G.; Liu, H.; Fairchild, J. N.; Shalliker, R. A., *Analytical Chemistry* **2010,** *82*, 10143-10150.
(287) Shock, D.; Dennis, G. R.; Guiochon, G.; Dasgupta, P. K.; Shalliker, R. A., *Analytica Chimica Acta* **2011,** *703*, 245-249.

Biographical Information

Darshan C. Patel obtained his Bachelor of Science in Chemistry with math minor and Bachelor of Science in Biology from University of Texas at Arlington in Spring 2013. He was an undergraduate researcher in laboratory of Professor Daniel W. Armstrong. In Fall 2013, he joined the laboratory of Professor Daniel W. Armstrong as a graduate student and obtained his Doctor of Philosophy degree in Analytical Chemistry in Summer 2017 from University of Texas at Arlington. His graduate research primarily focused on developing new technologies for high-efficiency and high-throughput chiral liquid chromatography. His research interests include stationary phase synthesis, high-efficiency slurry packing, method development and optimization, high-throughput separations, *in silico* resolution enhancing techniques, data visualizations, instrument development, lab automation, and on-line LC.